Recombinant expression of a Protozoan scaffold protein improves Iron-Sulfur biogenesis in *Saccharomyces cerevisiae*.

The School of Biosciences

Ronan M. Egan

A Thesis Submitted to the University of Kent for the degree of PhD. in Cell Biology.

Declaration

No part of this thesis has been submitted in support of any other application for a degree or qualification of the University of Kent or any other University or institution of learning.

All work contained within this thesis is based on my own research conducted over the period of my PhD.

Ronan M. Egan

October 2019

Acknowledgements

This research was funded by University of Kent 50th anniversary GTA studentship, with supporting funds from the Microbiology Society and The Eastern Academic Research Consortium.

I would like to thank my supervisors, Dr. Anastasios Tsaousis and Dr. Tobias von der Haar for their guidance and expertise throughout this project. Biophysical studies on the iron-sulfur cluster of SufCB would not have been possible without the help of Professor Nick Le Brun and Dr. Jason Crack. Members of the KFG provided an extremely friendly and productive work environment and I would like to particularly mention Dr. Dave Beal, Dr. Gemma Staniforth, Dr. Emma Bastow and Dr. Jordan Price for their help, both inside and outside of my Ph.D. Thank you also to my examiners for providing feedback on my finished manuscript. Alan Sims sparked a curiousity in me which, has since become a career and for that I thank him as well. I owe special thanks to my partner, Amber and mother Carmel.

".was *before he left, he went and named me Sue.*"

Cash and Silverstein, 1969.

Table of Contents

Abstract

The creation of microbial cell factories has enabled the production of otherwise fastidious metabolites at industrial scales. By reconstructing metabolic pathways into an easy to grow 'host' chassis, scientists are able to easily scale up processes and greatly increase the metabolite yield, many of which generate extremely high revenues. However, unsurprisingly, the reconstruction of metabolic pathways carries unique problems to overcome. For example, iron-sulfur enzymes have the potential to produce many relevant metabolites with far-reaching applications. However, the exploitation of iron-sulfur enzymes has been hindered by their strong propensity to react with molecular oxygen, resulting in the destruction of the cluster. Therefore, a new method of expressing iron-sulfur proteins is required. In this work, we have shown that heterologous expression of a specialised protozoan (*Blastocystis Nand II*) iron-sulfur chaperone (SufCB) in *Saccharomyces cerevisiae* significantly increased the activity of cytosolic iron-sulfur enzymes within the cell. Mechanistically, we have shown that SufCB genetically, and physically interacts with core members of *S. cerevisiae's* iron-sulfur assembly apparatus. Our system also has the advantage of simplicity, as it requires a single non-codon optimised ORF cloned into a versatile yeast expression vector.

Introduction

1.1 Introduction

The ability to manipulate living things has shaped human society (Bhatia and Bhatia, 2019). One hundred years since the term 'biotechnology' was coined by Karl Ereky (1919), the discipline now encapsulates an ever widening and undeniably crucial life science discipline (Bud, 1989). Although the name is only 100 years old, the concept of biotechnology, i.e., the process of using microbes for useful purposes, is an ancient process dating back to at least 5000 BCE (Reiser and Käppeli, 1989). Whereas ancient civilisations utilized the endogenous capacities of microbes to produce foods and beverages, modern advances in molecular biology has revolutionised this ancient practice and has given 21st century scientists the tools to redesign life itself (Bud, 1989; Reiser and Käppeli, 1989).

Engineering unnatural or 'recombinant' capabilities into a host organism is now a routine process for most laboratories and recombinant platforms boast uses which range from pharmaceuticals, to agriculture and waste removal (Atlas and Hazen, 2011; Jugder et al., 2018; Lopez-Torrejon et al., 2016; Takahashi et al., 2015). For some processes, recombinant expression of a single open reading frame (ORF) is sufficient in order to produce the required product, for others, however, an entire biosynthetic pathway is required (Luo et al., 2019). Due to this the recombinant proteins being expressed should complement the host organism, as the metabolic demand to produce the metabolite can be high or the protein itself can require bespoke post-translational modifications (Huang et al., 2014; Schlesier et al., 2016; Takahashi et al., 2015).

Commonly, the budding yeast *Saccharomyces cerevisiae* is employed to meet these demands, as a robust and simple organism (Huang et al., 2014). Modern figures state that yeast-derived products account for ~20% of all recombinant metabolites, falling slightly behind prokaryotic and mammalian expression systems (Nielsen, 2013). A list of some of these products and their applications are shown in **Table 1.**

Despite taking the lowest share of recombinant products, *S. cerevisiae* has many advantages over prokaryotic and mammalian expression systems (Huang et al., 2014). These include, a sequenced (S288c) genome, inexpensive growth media and maintenance, fast doubling times, and the ability to perform some eukaryotic post-translational modifications (e.g. glycosylation) (Goffeau et al., 1996; Huang et al., 2014). In addition, *S. cerevisiae* cells lack problematic lipopolysaccharide endotoxins as well as the requirement for antibiotic resistance markers thanks to a library of auxotrophic mutants (Duquenne et al., 2013; Pronk, 2002). All of these factors reduce the costs, and increase the attractiveness of developing yeast-based platforms (Magalhães et al., 2011; Peubez et al., 2010).

Table 1. Commercially relevant metabolites produced by *S. cerevisiae* cell factories.

Product	Application	Reference
Bioethanol	Fuels, chemical industry	(Martínez-Alcántar et al., 2019)
Insulin	Treatment of Diabetes	(Thim et al., 1986)
Artemisinic acid	Treatment of Malaria	(Ro et al., 2006)
Resveratrol	Antioxidant	(Sydor et al., 2010)
Cannabinoids	Epilepsy, chronic pain	(Luo et al., 2019)
Ammonia	Agriculture	(Lopez-Torrejon et al., 2016)
Adipic acid	Textiles, chemical industry	(Raj et al., 2018)

The resulting genetically engineered cells can then be viewed as dedicated 'cell factories' which can efficiently produce the required quantities of metabolites according to a regulated, often pre-existing (GMP-compliant) process (Kim et al., 2015). In many cases, these cell factories also offer a much more sustainable and environmentally friendly alternative to 'classical' means of production, e.g. use of nitrogenase instead of the costly Haber process for nitrogen fixation (Chaban and Prezhdo, 2016; Lopez-Torrejon et al., 2016).

1.2 Iron-sulfur enzymes

Each cell factory carries with it a set of requirements which need to be met in order to yield profitable titres of the product (Raj et al., 2018). These can include a requirement for media supplementation or growth under bespoke environmental conditions (Huang et al., 2017; Raj et al., 2018). The latter of these applies for cell factories which express recombinant iron-sulfur enzymes, as the catalytic core of these enzymes is usually destroyed by reaction with oxygen (López-Torrejón et al., 2016). This was recently demonstrated with a yeast cell factory designed to produce the nylon-*6-6* precursor, adipic acid (Raj et al., 2018). Only when grown under anaerobic conditions could the recombinantly expressing cells generate any product, as the enzyme responsible, enoate reductase, was readily inactivated by oxidants (Raj et al., 2018). Whilst *S. cerevisiae* cells are facultative anaerobes, and therefore able to grow under anaerobic conditions, creating these conditions is both costly and requires increased health and safety considerations (use of compressed gases) and extensive operator training (Health and Safety Executive, 1998).

For iron-sulfur enzymes such as, enoate reductase, catalytic iron ions (with oxidation states of II or III) act in concert with sulfide (S^{2-}) within a modular core known as an 'iron-sulfur cluster' (Imlay, 2006). Iron-sulfur clusters are hypothesised to have arisen prior to cellular life, as Archaean deep-sea hydrothermal vents released highly reactive ferrous iron ions (Fe^{2+}) and hydrogen sulfide (H_2S) (Sousa et al., 2018; Wachterhauser, 1988). The reactions between the two not only formed primordial iron-sulfur clusters but are also believed to have catalysed the conversion of atmospheric carbon dioxide into hydrocarbons and, in turn, paved the way for organic life (Wachterhauser, 1988).

1.2.1 Iron-sulfur clusters, their geometries and reactions

Collectively, iron-sulfur enzymes group within a ubiquitous class of metal-binding enzymes, collectively known as metalloproteins (Wang et al., 2019). A recent study of 1371 enzymes with known three-dimensional structures, estimated that 47% associated with metals in any way, whilst 41% of the 1371, bound metal ions directly within their active sites (Andreini et al., 2008). The study also highlighted iron as the third most common protein-binding metal (Andreini et al., 2008). Iron is an excellent redox metal and because of this, iron-binding proteins (including iron-sulfur enzymes) are uniquely capable of catalysing a range of reactions from electron transport to gas-sensing (Crack et al., 2014a; Degli Esposti et al., 1987).

Classically, iron-sulfur cluster enzymes are known to be embedded within electron transport chains (Imlay, 2006; Wu et al., 2002). This is because binding iron-sulfur clusters typically convey lower redox potentials than other prosthetic groups, which is further augmented by the protein environment of the cluster (Capozzi et al., 1998; Imlay, 2006). By placing these enzymes in order of redox potentials, the cell is able to efficiently shuttle high-energy electrons from one iron-sulfur cluster enzyme to another with minimal energy input (Imlay, 2006). Respiration and photosynthesis are two textbook examples of processes which utilise chains of iron-sulfur cluster enzymes as 'biological wires' to generate energy in the form of ATP (Bai et al., 2018). More recently, iron-sulfur cluster enzymes have also been discovered to play crucial roles within amino acid biogenesis, DNA metabolism and translation across all domains of life (Alhebshi et al., 2012; Amorim Franco and Blanchard, 2017; Paul et al., 2015; Rudolf et al., 2006). Due to their essential roles within the cell, deficiencies in iron-sulfur biogenesis have also been attributed to several pathologies, including Friedriech's Ataxia, Myopathy and several mitochondrial dysfunction syndromes (Cai and Markley, 2018).

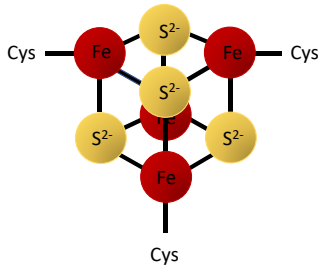

Figure 1. Cartoon of an iron-sulfur cluster of the [4Fe4S] class. Co-ordinating cysteines are also shown (Cys). Iron is represented by red spheres (labelled Fe), sulfide is represented by yellow spheres (S^{2-}). Fourth cysteine is not shown.

In order for a cluster to bind an enzyme, a specific motif must first exist on the accepting apo-protein (Child et al., 2018). For many iron-sulfur enzymes, cysteine residues serve this purpose and co-ordinate the cluster's iron ions via persulfide linkages **(Figure 1)** (Child et al., 2018; Lloyd et al., 2008). Typically, this binding site occurs in a CxxC motif, where the 'C' represents cysteine residues separated by two other amino acids (Child et al., 2018). Because of this, the presence of one or more 'CxxC' motifs within the primary sequence of a protein has been traditionally used to identify candidate iron-sulfur enzymes at the computational level (Bych et al., 2008; Crack et al., 2014a; Yuda et al., 2017).

Whilst cysteine residues serve as the typical coordinating ligand, other amino acid residues have also been observed to bind iron-sulfur clusters (Child et al., 2018), and in some cases this can contribute to the protein's function by altering the cluster's redox properties (Brown et al., 2002; Yuda et al., 2017; Zaugg et al., 1964).

Oxygen-sensitivity is a common feature of iron-sulfur clusters (Crack et al., 2017; Golinelli-Cohen et al., 2016). Whilst the molecular details of these reactions are still being uncovered (Crack et al., 2017), the reason for their sensitivity is due to their intrinsically low redox potentials ($E^{o'}$ -0.4V), compared to other cofactors (Crack et al., 2014a; Imlay, 2006). As the flow of electrons favours movement from a more negative to more positive redox potential, iron-sulfur clusters readily receive electrons provided by oxidants including molecular oxygen (O_2) (Imlay, 2006). This oxidation reaction is damaging to the cell in three ways. First, an oxidation reaction results in the destruction of the cluster and thereby the function of the protein (Alhebshi et al., 2012). Second, cluster oxidation results in the release of iron ions from the cluster which can then react with superoxide to form harmful hydroxyl radicals via the Fenton/Haber Weiss reactions (Crack et al., 2017). Third, the destruction of an iron-sulfur cluster also causes the release of sulfide, which is also toxic to the cell (Crack et al., 2014a). It must be said however, that certain organisms have opted to use iron-sulfur clusters as gas-sensing mechanisms within enzymes, such as FNR and WhiB (Crack et al., 2014a; Kudhair et al., 2017). For other, essential iron-sulfur enzymes however, these reactions are detrimental to the cell and this has been likened to an 'Achilles heel' of aerobic life (Alhebshi et al., 2012).

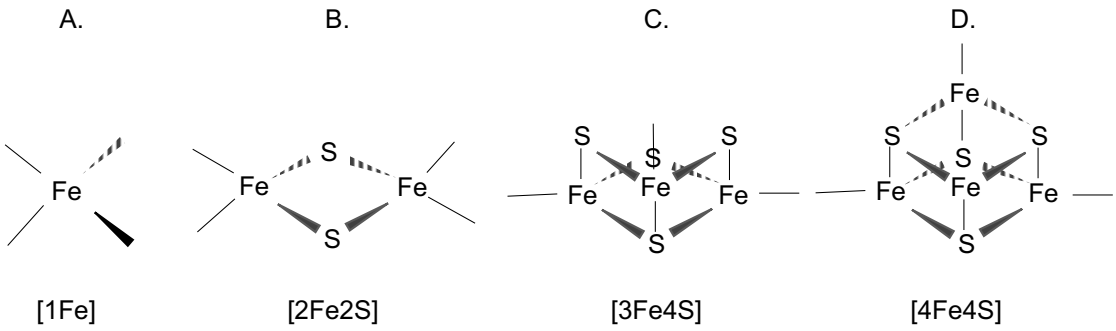

Figure 2. Predominant geometries of iron-sulfur clusters in nature. A) Rubredoxin iron centre, B) [2Fe2S] or Rhomboid cluster. C) [3Fe4S] cluster. D) [4Fe4S] or cuboid cluster.

Various classes or geometries of cluster have been demonstrated in the literature **(Figure 2)** proteins and these range from simple [2Fe2S] clusters to the [FeMo]-co cluster of nitrogenase, which is one of the most complex cofactors known to exist (Shepard et al., 2011; Wollenberg et al., 2003). Although the fine molecular details are still being uncovered, these complex geometries have been observed to form from [2Fe2S] clusters via an enzyme-catalysed reaction termed 'reductive coupling'. (Chandramouli et al., 2007). This process has been observed for several early-acting assembly proteins (IscU and IssA), with reducing equivalents provided by conserved electron transport proteins (Bandyopadhyay et al., 2008; Bernard et al., 2013; Chandramouli et al., 2007; Vaccaro et al., 2017). Aconitase is a prominent example of how a cluster's geometry and ligand

coordination alters its function and relays information regarding iron-status to transcriptional circuitry [(Brown et al., 2002; Narahari et al., 2000). Aconitase is an unusual iron-sulfur protein in such that only three of its four iron-ligands are provided by cysteine leaving the fourth iron ion to bind water (hydroxyl) (Beinert and Kennedy, 1993). This unusual coordination enables the [4Fe4S] cluster of aconitase to transition into a [3Fe4S] cluster and conveys additional properties to enzyme (Brown et al., 2002). In its [4Fe4S]-state, c-aconitase catalyses the interconversion of citrate to isocitrate as part of the Krebs cycle, however as intracellular iron-concentration decreases the [4Fe4S] cluster degrades to a [3Fe4S] wherein c-aconitase becomes an iron-regulatory protein and activates the transcription of iron-uptake genes (Brown et al., 2002; Castro et al., 1994; Roy et al., 2003).

1.3 Cellular methods to counteract the oxidation of iron-sulfur clusters

Iron-sulfur clusters are ancient cofactors which primordial life forms are thought to have quickly become dependent on for otherwise thermodynamically unfavourable metabolic reactions (Imlay, 2006). Iron-sulfur clusters are able to spontaneously form under anaerobic conditions, however, as oxygen accumulated in Earth's previously anaerobic atmosphere, the adverse oxidation of iron-sulfur clusters selected for alternate means of cluster assembly that could be protected from oxygen (Boyd et al., 2014). To answer this, organisms have evolved dedicated pathways to carefully assemble and then delivery iron-sulfur clusters in an aerobic world (Lill et al., 2006). Over the last 20 years, four biosynthetic pathways have been discovered; the iron-sulfur cluster assembly (ISC), the cytosolic iron-sulfur cluster assembly (CIA), the sulfur utilisation pathway (SUF) and the nitrogen fixation (NIF) pathway (Bernard et al., 2013). Whereas ISC, CIA, and SUF have been observed to mature a broad range of iron-sulfur proteins, NIF machinery is typically dedicated to the maturation of nitrogenase in diazotrophs (Pallesen et al., 2013; Tian et al., 2014; Tsujimoto et al., 2018). An exception to this, however, is seen with the archamoeba *Entamoeba histolytica* and *Mastigamoeba balamuthi* which utilise NIF components as a replacement for its housekeeping iron-sulfur assembly pathways (Ali et al., 2004; Nývltová et al., 2013).

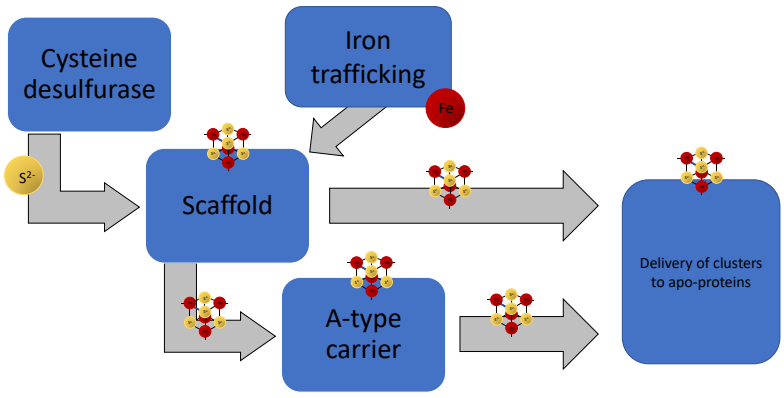

Figure 3. Flow chart of iron-sulfur assembly. Grey arrows indicate the progression of iron-sulfur assembly by the various enzymes (blue boxes). Red and yellow balls indicate iron and sulfide, respectively.

The steps of iron-sulfur assembly are shown in **Figure 3** and illustrates the sequential release of sulfide from cysteine by a cysteine desulfurase (yellow ball), which is accepted by a dedicated scaffold protein 'scaffold' (Braymer et al., 2017; Maio and Rouault, 2015). An iron-trafficking protein also delivers iron (red ball) to the scaffold protein which occurs in parallel or directly after sulfide donation (Chahal et al., 2009; Leidgens et al., 2009). The 'raw' ingredients; iron and sulfide, are then assembled into an iron-sulfur cluster, which may then either pass along to a dedicated carrier protein (A-type carrier) or directly deliver the iron-sulfur cluster to the apo-protein (Lill et al., 2012; Stehling et al., 2018; Tian et al., 2014).

1.3.1 The bacterial SUF pathway is induced under oxidative conditions

Of all the mechanisms that have been described to assemble iron-sulfur clusters, the SUF pathway is predicted to have originated first (Boyd et al., 2014). The SUF machinery **(Figure 4** and **Table 2)** is hypothesised to have been an ancient means of assembling iron-sulfur clusters which may have arisen in response to the challenges (e.g. iron limitation and oxidative stress) posed during the GOE (Boyd et al., 2014). Although SUF components were typically thought to be restricted to plastid-containing organisms and prokaryotes, a growing body of work is starting to unravel a more universal presence of SUF proteins (Stairs et al., 2014; Tsaousis et al., 2012).

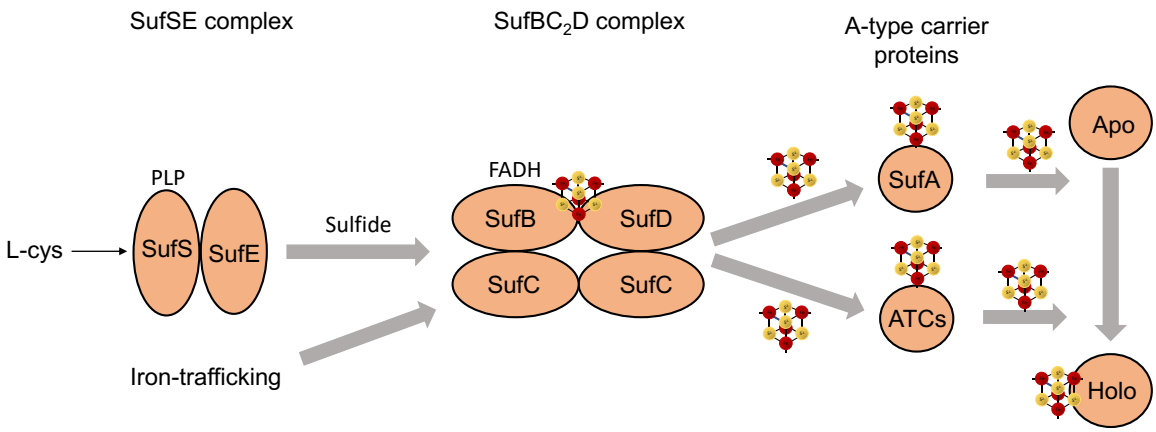

Figure 4. Schematic of the SUF machinery in *E. coli*. Grey arrows indicate the progression of iron-sulfur biogenesis. The three complexes are labelled, and grey arrows indicate the progression of assembly. Abbreviations, L-cys = L-cysteine, PLP = pyridoxal phosphate, ATCs = A-type carriers, Apo = apo-protein, Holo = holo-protein,

Table 2. Summary table of SUF components and their functions, if known. The SUF complexes are also shown in a separate column. SUF fusion proteins not shown.

Protein	Complexes formed	Function	References
SufB	$SufBC_2D$ complex	Scaffold	(Loiseau et al., 2003)
SufC		ATPase	(Kitaoka et al., 2006)
SufD		Potential iron donor	(Saini et al., 2010)
SufS	SufSE complex	Cysteine desulfurase	(Patzer and Hantke, 1999)
SufE		Sulfide shuttle	(Selbach et al., 2013)
SufA	Various	Carrier protein	(Mettert and Kiley, 2014)
SufT		DUF59 protein	(Mashruwala et al., 2016)
SufE1		Chloroplast maturation	(Couturier et al., 2014)
SufE2			(Narayana Murthy et al., 2007)
SufE3			
SufU		Scaffold	(Albrecht et al., 2010)

SUF machinery consists of eleven open reading frames under the control of a single operon (the *suf* operon) (Takahashi and Tokumoto 2002). Five transcriptional regulators have been shown to bind to the *suf* operon in a redox-dependent manner (Mettert et al., 2008) Due to the involvement of Fur, a role for iron-limitation has also been suggested to activate the *suf* operon, but is still debated (Outen et al., 2004; Lee et al., 2008). These are briefly summarised in **Table 3** below.

Under oxidative conditions, each transcriptional regulator undergoes a specific conformational change which modulates its binding affinity to the *suf* operon (Lee et al., 2008). With the exception of IscR, all three proteins also bind at unique non-overlapping sites upstream of the *suf* promoter (Outen et al., 2004). Under non-stressed conditions, the *suf* operon is usually repressed by a Fe^{2+} loaded Fur protein-bound near to the transcription start site (TSS), between base pairs -35 and -10 (Outen et al, 2004). However, under oxidative conditions, Fur is oxidised and consequently, is released from the *suf* operon (Lee et al., 2008). Fur protein also binds with higher affinity to the shared site that IscR which serves to keep SUF at low levels under non-stress conditions (Lee et al., 2008). Upon release from the *suf* operon, Fur protein also activates RhyB which destabilises the transcripts of the *isc* operon, resulting in their degradation (Masse et al., 2005). This mechanism serves to ensure that under oxidative conditions, the SUF machinery is the dominant mode of assembling iron-sulfur clusters (Masse et al., 2005).

Table 3. Transcriptional regulators of the *suf* operon in *E. coli*. Abbreviations: TSS = transcription start site.

Protein	Mechanism	References
IscR	Senses oxidative stress, inhibited by Fur binding	(Mettert and Kiley, 2014)
OxyR	Senses oxidative stress	(Zheng et al., 2001)
IHF	Brings OxyR site into close proximity of the TSS	(Outten et al., 2004)
Fur	Repressor of *suf* senses oxidative stress and iron	(Lee et al., 2008)
NsrR	Nitric oxide sensing	(Vinella et al., 2013)

OxyR has long been known to be involved in the prokaryotic response to oxidative stress (Christman et al., 1989). For the SUF machinery, the oxidation of OxyR causes the formation of an intra-molecular disulphide bond between cysteines 199 and 204, which allows OxyR to bind a site between -244 - -194 on the operon. (Zheng et al., 2001; Outten et al., 2004). However, this site is far away from the *suf* promoter (Outten et al., 2004). The problem of distance is solved via IHF, which binds a site between -164 - -121 and bends the DNA to bring the bound OxyR into close proximity of the *suf* promoter, where it can induce co-operative binding of RNA polymerase (RNAP) to transcribe the *suf* operon (Choi et al., 2001; Lee et al., 2008).

This transcriptional network also serves to overlap the expression of the SUF machinery with that of another iron-sulfur assembly system, the 'ISC' pathway, via IscR (Mettert, et al. 2014). Itself a [2Fe2S] protein, holo-IscR produces a negative feedback loop by repressing the transcription of the housekeeping *isc* operon (Mettert and Kiley, 2014). Under oxidative and iron-limiting conditions, however, apo-Isc predominates over the holo-form and activates transcription of the *suf* operon by binding to the Fur site (Mettert and Kiley, 2014). This is a similar mechanism to the active of *suf* by NsrR, although NsrR specifically responds to nitric oxide via nitrosylation of NsrR's iron-sulfur cluster (either [4Fe4S] or [2Fe2S]) (Vinella et al., 2013).

Purification experiments have shown that the expression of the *sufABCDSE* operon in *E. coli* primarily results in the formation of a multiprotein complex with 1:2:1 ratio between protein SufB, SufC and SufD (Chahal et al., 2009). In addition to the 'SufBC$_2$D' complex, some SufB$_2$C$_2$ also formed but the relevance of the latter complex is yet to be elucidated and is predicted to be artefactual (Saini et al., 2010). As the predominant complex SufBC$_2$D, likely reflects the physiologically relevant state of the SUF machinery and has been shown to bind a [4Fe4S] cluster (Tian et al., 2014; Wollers et al., 2010). This cluster can also be transferred from the SufBC$_2$D complex to aconitase, demonstrating functional relevance in its ability to mature a [4Fe4S] enzyme (Tian et al., 2014). In addition to an iron-sulfur cluster, FADH$_2$ has also been found to bind the SufBC$_2$D complex, demonstrating redox capabilities (Saini et al., 2010; Wollers et al., 2010). Attempts to characterise the relevance of this have shown that flavin is not required for cluster transfer from SufBC$_2$D to apo-proteins but instead may facilitate the reduction of a substrate (e.g. iron) instead (Wollers et al., 2010).

Dissection of SufBC$_2$D into its component proteins reveals that each protein has its own dedicated role to play in iron-sulfur biogenesis by SUF (Layer et al., 2007). SufB acts as the 'core' scaffold and key iron-sulfur ligands have been mapped to SufB's glu434, his433, glu432 and cys405 (Yuda et al., 2017). The geometry of SufB's cluster, however, has been the subject of much uncertainty as the purified protein could be reconstituted with [2Fe2S], [4Fe4S] and [3Fe4S] (Yuda et al. 2017; Layer et al. 2007; Chahal & Wayne Outten 2012) and both [2Fe2S] and [4Fe4S] cluster-loaded SufB proteins were able to mature SufA, ferredoxin and aconitase (Chahal and Wayne Outten, 2012; Chahal et al., 2009; Wollers et al., 2010).

An answer to this problem was recently proposed as SufB's [2Fe2S] cluster was found to be resistant to hydrogen peroxide and EDTA, and could be converted to a [4Fe4S] cluster under reducing conditions (Blanc et al 2014). Given the role of SUF as a stress-responsive system, the stable [2Fe2S] SufB-bound cluster may reflect its physiological form which may then be processed further as needed (Blanc et al., 2014).

SufC acts as the SUF system's ABC ATPase, the activity of which 180-fold when co-incubated with SufB and 5-fold when co-incubated with SufD (Petrovic et al. 2008; Kitaoka et al. 2006; Nachin et al. 2003). In addition, abolishing SufC function also abolishes the activity of the entire SUF system (Loiseau et al., 2003). The relevance of SufCs ATPase has suggested as a means of allosteric regulation of the SUF system (Hirabayashi et al., 2015; Petrovic et al., 2008; Yuda et al., 2017). Fluorescence experiments using ATP-stimulated SufC revealed that stimulating the ATPase activity of SufC (in the $SufBC_2D$ complex) elicited a conformational change in the complex which revealed hydrophobic regions in the SufB-SufD protomer (Hirabayashi et al., 2015; Petrovic et al., 2008). Thiol labelling (DACM) experiments later demonstrated that these exposed sites contained highly conserved cysteine residues (Hirabayashi et al., 2015), one of these sites (cys-405) was later shown to bind an iron-sulfur cluster (Yuda et al., 2017). This work suggests that ATP binding provides an extra layer of allosteric regulation of iron-sulfur biogenesis by SUF and perhaps demonstrates a means by which the SUF system increases its 'aptitude' as a stress-responsive system by tethering intracellular ATP availability to rates of iron-sulfur biogenesis (Hirabayashi et al., 2015).

A dimeric SufSE is responsible for mobilising sulfide (Selbach et al., 2013). Alone, SufS exhibits extremely weak desulfurase activity and requires SufE to function efficiently (Mihara et al. 2000; Layer et al. 2007; Patzer & Hantke 1999). As a desulfurase, SufS mobilises persulfide from L-cysteine using a PLP-cofactor and a conserved cysteine residue, cys364 (Fujishiro et al., 2017). The requirement of SufS for SufE was found to be due to an 11-residue deletion within the active site of SufS (Dai et al., 2015). This deletion prevents SufS from shuttling sulfide to downstream targets, therefore requiring SufE to act as a shuttle instead (Layer et al. 2007; Loiseau et al. 2003). Furthermore, Layer et al. (2007) were able to demonstrate strong interactions between SufE and $SufBC_2D$ which was not dependent on co-incubation of SufE with SufS, demonstrating that SufE acts downstream of SufS and probably trafficks the SufS-liberated cys51-bound sulfide to the $SufBC_2D$ complex (Layer et al. 2007). In addition, SufB must be associated with its partner, SufC in order to bind SufE (Loiseau et al., 2003).

After the cluster is assembled, the SUF system is able to directly or indirectly mature iron-sulfur proteins (Chahal et al., 2009). Indirect cluster transfer occurs via dedicated carrier proteins and the most common amongst these are the A-type carriers (ATCs) (Chahal et al., 2009). The ATC of the SUF system is known as SufA and is a functional homodimer (Wada et al., 2005). SufA delivers nascent clusters to target apoproteins which have been assembled by the $SufBC_2D$ complex by interacting with SufC (Chahal et al., 2009; Wada et al., 2005). Cluster transfer is mediated by the C-terminal of SufA which contains two pairs of essential cysteines, cys114 and cys116, which it uses

to bind its iron-sulfur cluster (Pérard and Ollagnier de Choudens, 2018). Biotin labelling experiments by Chahal et al. (2009), have demonstrated that SufA binds to the $SufBC_2D$ complex at the SufSE binding site, where it receives a its cluster to donate to apo-proteins this also demonstrates mutually exclusive binding between SufSE and SufA and possible a further level of allosteric regulation. SufA's interaction with SufC is also weakened $SufBC_2D$ complex, suggesting a that SufC first recruits SufA before $SufBC_2D$ complex formation facilitates its release (Chahal et al., 2009).

1.3.2 SUF fusion proteins

Since the discovery of the SUF machinery, organisms have been discovered to express SUF machinery as fused-transcripts (Stairs et al., 2014; Tsaousis et al., 2012). The first eukaryotic SUF fusion was discovered within the transcriptome of the microaerophilic stramenophile *Blastocystis sp. ATCC 50177/Nand II* (herein, *Blastocystis* or *Blastocystis Nand II*), which had acquired an ancient *suf* operon and then fused its components into a single ORF (Tsaousis et al., 2012, 2018). It is predicted that this ancient *suf* operon may have originated from a *Methanobacteriales* archaeon, which at the time shared a gut or gut-like environment with *Blastocystis*, thus enabling lateral gene transfer between the two organisms (Tsaousis et al, 2012).

Studies into the biology of the *Blastocystis* SufCB ORF later demonstrated that the fused SufCB transcript could also form a single polypeptide, SufCB, which localised to the cytosol by immunofluorescence (Tsaousis et al., 2012). Purification experiments of recombinant SufCB from *E. coli* cells also demonstrated that the protein is able to bind and transfer a [4Fe4S] cluster by EPR and aconitase maturation, respectively (Tsaousis et al., 2012). Analysis by size exclusion chromatography also demonstrated that the purified SufCB protein existed as both apo-monomeric and holo-dimeric forms **(Figure 5)** (Tsaousis et al., 2012).

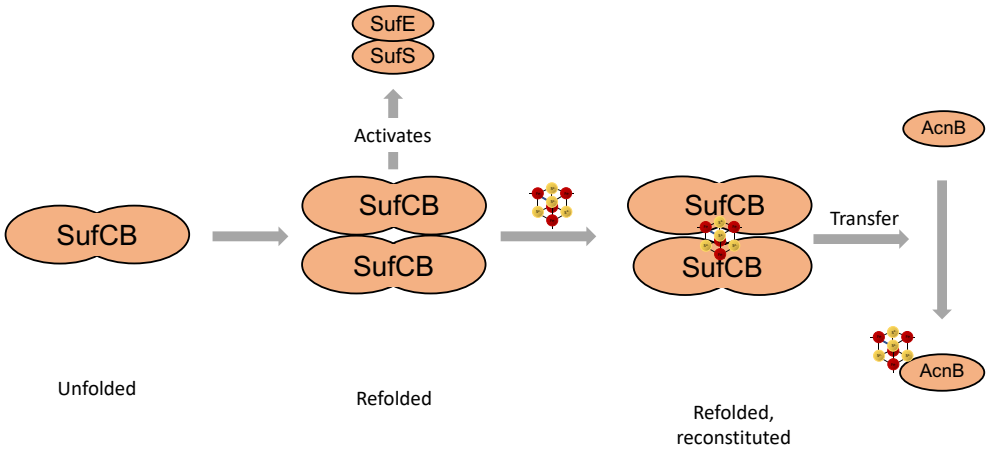

Figure 5. Schematic of the *Blastocystis* SufCB protein as described in Tsaousis et al, (2012). The monomeric inclusion body and homodimeric refolded form are shown. Both the refolded, reconstituted protein containing a [4Fe4S] is shown (red, yellow spheres) and SufCB's ability to transfer its cluster to *E. coli* aconitase (AcnB). Grey arrows indicate how SufCB was processed by the authors.

Given that holo-SufCB could transfer its cluster to a recipient apo-protein (aconitase), it was classified by the authors, as an iron-sulfur cluster scaffold protein (Tsaousis et al., 2012). Moreover, SufCB was also found to stimulate the desulfuration of L-cysteine when co-incubated with SufSE but showed no desulfuration activity itself (Tsaousis et al., 2012). Furthering this, the SufCB protein was found to contain ATPase activity comparable to that of the $SufBC_2D$ complex purified from *E. coli*, but unlike $SufBC_2D$, purified SufCB could not bind $FADH_2$ as indicated by spectroscopy (Tsaousis et al., 2012). The conclusion was then made that the SufCB protein in *Blastocystis* therefore serves a role in iron-sulfur biogenesis in the cytosol of *Blastocystis*. Adding to this work, Stairs et al. (2014) later described two isoforms of SufCB which localise to mitochondrial related organelle and cytosol of the protist, *Pygsuia biforma*. Importantly the *P. biforma* MRO transcriptome indicate the loss of most of its ISC system, apart from homologues of the scaffolds, Nfu1 and Ind1 (Stairs et al., 2014). In addition, a fused SufCB gene was also found to be encoded by *Stygiella incarcerata* (Leger et al. 2016). *S. incarcerata* is a member of the Jakobida, a group of flagellated protists, which are not closely related to either Stramenopiles or Breviata (e.g. *Blastocystis* and *Pygsuia*, respectively) (Leger et al., 2016; Tsaousis et al., 2014) suggesting that SufCB proteins are widespread and likely represent a more common adaptive tool for anaerobes than previously thought (Tsaousis et al., 2012).

All SufCB proteins contain two domains linked together by a loosely conserved 'linker' domain (**Figure 6**) (Tsaousis et al., 2012). The general architecture of SufCB proteins is an N-terminal SufC-like domain, containing domains that align SufCB into the ABC family of ATPases. Their C-terminals encode a SufB-like domain. This domain features heavily conserved regions (between SufCBs and SufB), which may bind SufCB's iron-sulfur cluster (Hirabayashi et al., 2015; Yuda et al., 2017)

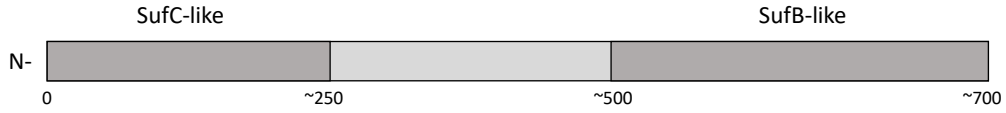

Figure 6. Simplified illustration of a generic SufCB protein. N-terminal SufC-like (residues 0 - ~250) and C-terminal SufB-like (residues ~500 – 700) domains, represented by dark grey rectangles on either terminal of the protein. The light grey middle region has no known alignment or conservation.

Pairwise sequence alignments revealed that SufCBs have maintained high sequence identity to their SUF counterparts, SufC and SufB, demonstrating a possibility for similar functions (Tsaousis et al., 2012). Additional protozoan SufCB sequences provided by A. Tsaousis provided further detail into each SufCB protein and pairwise sequence data is presented (**Appendix 1 - 5**). Despite the respective evolutionary distances, SufCB proteins are well conserved, reflecting important biological functions (Leger et al., 2016; Stairs et al., 2014; Tsaousis et al., 2012). Notably, the presence of SufCB machinery also generally coincides with the loss of canonical iron-sulfur cluster assembly pathways (e.g. ISC), leading to the conclusion that SufCB proteins can functionally replace classic assembly proteins (Leger et al., 2016; Stairs et al., 2014). The three domains of the SufCB proteins are summarised in chapter 1.3.2.1.

1.3.2.1 The SufC-like domain of SufCB proteins

The N-terminal of each SufCB protein (**Figure 7**) is enriched for domains conferring the ABC-ATPase superfamily. The SufC-like portion stretches on average for ~200 residues and displays moderately conserved domains, annotated below:

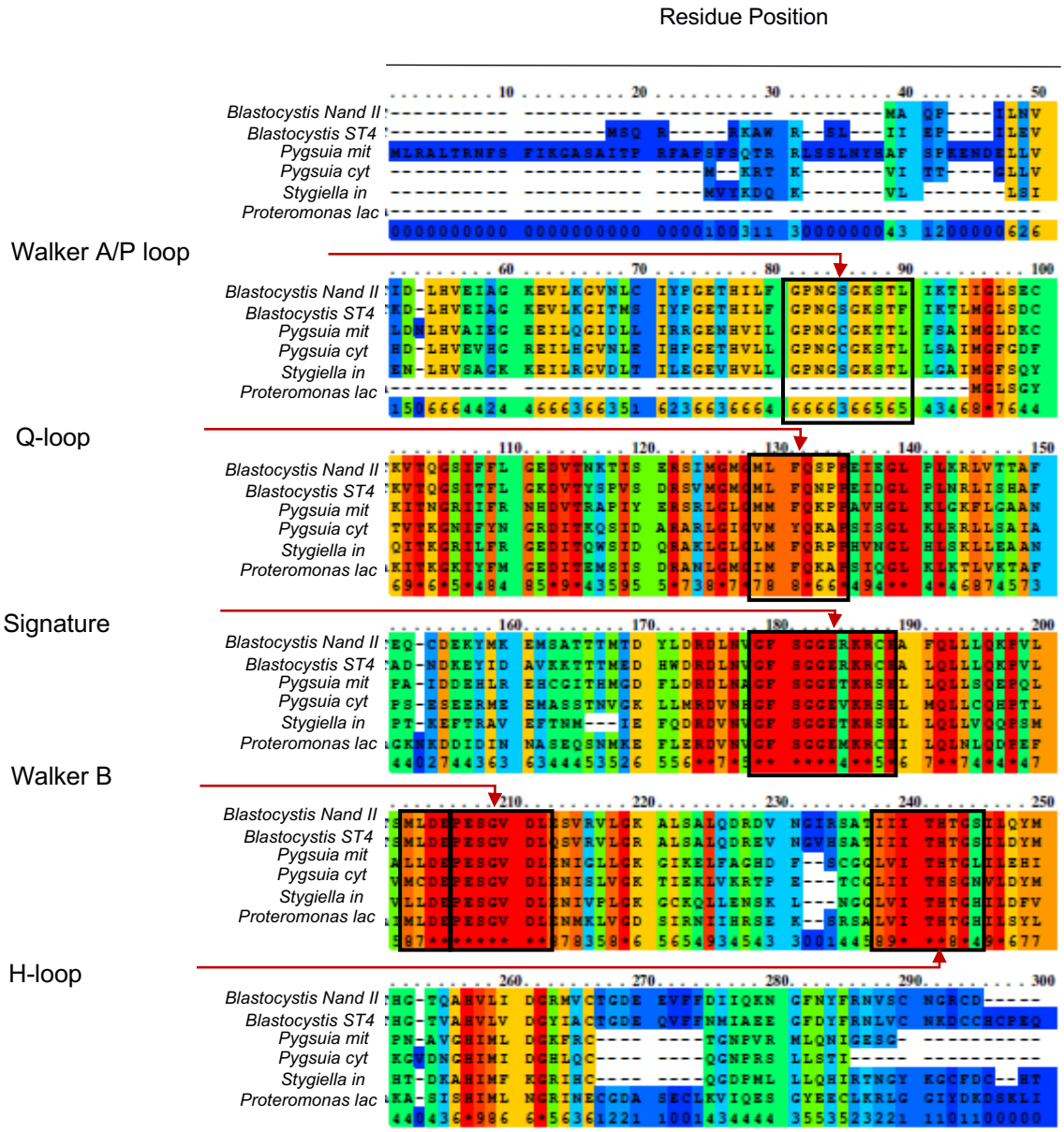

Figure 7. PRALINE Multiple Sequence Alignment of the SufC portion of SufCB proteins, annotated for ATPase domains. Software was used under default settings, http://ibivu.cs.vu.nl/programs/pralinewww/. A heat map is used to infer conservation between residues, blue indicates less conservation, red indicates more conserved regions. Sequences in the order of: *Blastocystis Nand II*, *Blastocystis* subtype 4 , *Pygsuia biforma (mitochondrial SufCB), Pygsuia biforma (cytosolic SufCB), Stygiella incarcerate, Proteromonas lacertae.* Consistency scores (1-10) given along the bottom, scores closest to ten indicates strong conservation.

Annotations of the SufC region using the NCBI conserved domain database (CDD) (**Figure 7**) reveal regions associated with AAA+ ATPase function conserved throughout all SufCB proteins, with a notable exception is seen in *P. lacertae* SufCB, which lacks a walker A motif (**Figure 7**, *P. lacertae*). The similarity above classifies SufCB proteins as P-loop NTPases or Additional Strand Catalytic E (ASCE), this family of proteins are found throughout iron-sulfur biogenesis to mediate and regulate protein-protein interactions and substrate loading/dissociation (Hausmann et al., 2005; Saini et al., 2010; Schwenkert et al., 2010). This subfamily of the AAA+ superfamily contains a characteristic 'core' αβα domain, also termed the nucleotide-binding domain (NBD), which conveys nucleotide-binding activity, and consists of the Walker A, Q-loop, D-loop, H-loop, Signature and Walker B motif (De La Rosa and Nelson, 2011). Crystal structures of ATPases have demonstrated the requirement for all six motifs to constitute an ATP active site (De La Rosa and Nelson, 2011). Given that the *P lacerate* sequence lacks its walker A motif but contains the other five motifs, may suggest a loss of ATPase function or mis-assembly of the gene.

1.3.2.2 The linker-domain

In the 'middle' of each SufCB, between SufC and SufB domains, lies a stretch of ~120 amino acids Figure **8**), which links SufC and SufB-like portions of each protein. This region lacks any major sequence conservation, nor does it align with any superfamily using the NCBI Blast P suite.

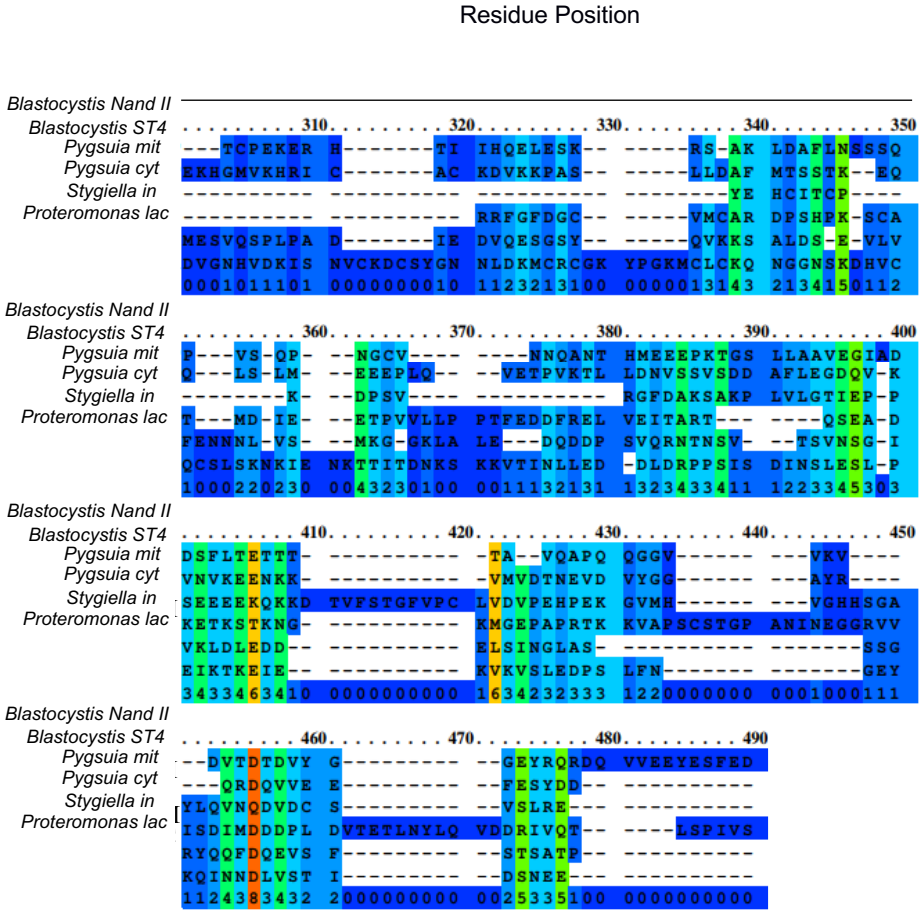

Figure 8. PRALINE Multiple Sequence Alignment of the linker domain of each SufCB sequence, Software was used under default settings, ibivu.cs.vu.nl/programs/pralinewww/. A heat map is used to infer conservation between residues, blue indicates less conservation, red indicates conserved regions. Sequences in the order of: *Blastocystis* Nand II, *Blastocystis* subtype 4 , *Pygsuia biforma (mitochondrial SufCB), Pygsuia biforma (cytosolic SufCB), Stygiella incarcerate, Proteromonas lacertae*. Consistency scores (1-10) given along the bottom, scores closest to ten indicates strong conservation.

Given the lack of conservation amongst SufCB proteins within this domain (**Figure 8**), it was hypothesised that this domain may represent an intrinsically disordered region (IDRs) of the protein. Proteins which contain intrinsically disordered regions (IDRs) are either completely structurally disordered or contain a single disordered region which acts as a flexible 'linker' between two structurally ordered domains (Wright and Dyson, 2015). Proteins with IDRs are mostly found within protein interaction networks to act as a central hub to regulate cellular processes such as signal transduction, translation, transcription and cell cycle control (Berlow et al., 2018).

Intrinsically disordered proteins (IDPs) are characterised by a biased amino acid content which lacks bulky hydrophobic R groups and has a high net charge and this interferes with the formation of stabilising intra-molecular hydrogen bonds (Fernandez et al. 2004; Wright & Dyson 2015). From this sequence bias, the likelihood of a protein to contain an intrinsically disordered region, can therefore be predicted (Dosztányi et al., 2005).

An analysis of the SufCB sequences suggests that the linker domain of SufCB is likely to be intrinsically disordered, with IUPred scores above 0.7 (**Figure 9**). Given its location, this may serve to allow the two SufC-like and SufB-like domains of SufCB to physically interact. By comparison, the SufC and SufB portions of the protein have low IUPRED scores (<0.1 – 0.3) with the SufB portion showing lower disorder (<0.1 – 0.2) scores suggesting that the SufB-like domain is under strong selection to maintain a rigid structure. Of all SufCB proteins, only *P. lacertae* SufCB failed to predict a similarly high likelihood of disorder within this region (**Figure 9**). This could also reflect the lack of a walker A motif, and potential ATPase activity in its SufC-like domain (**Figure 7**).

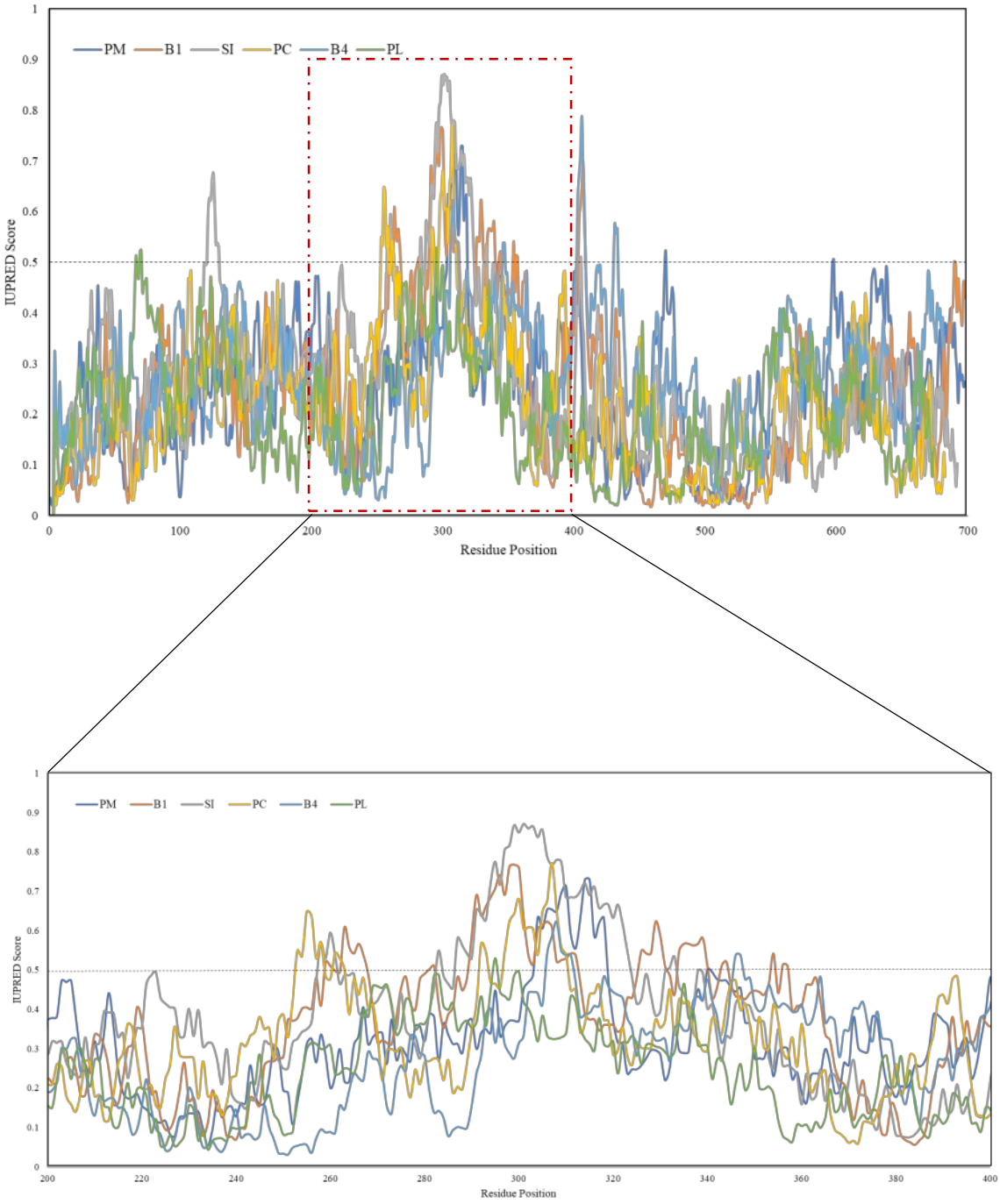

Figure 9. Intrinsically Disordered Region prediction using IUPRED of each SufCB protein. An expanded view of the linker domain is shown in the bottom panel. IUPred software was used under default settings with FASTA SufCB sequences, https://iupred2a.elte.hu. Scores above 0.5 suggest disordered structure. Protein codes are: *Blastocystis hominis*, Subtype 1 = B1, *Blastocystis hominis,* Subtype 4 = B4, *Proteromonas lacertae* = PL*, Pygsuia biforma* (cytosolic variant) = PC, *Pygsuia biforma* (mitochondrial variant) = PM, *Stygiella incarcerate* = *SI.*

1.3.2.3 SufB-like Portion aligns to the UPF0051 superfamily

At their C-terminal, SufCBs contain a 200 residue stretch which aligns into the SufB superfamily (COG0719). This region of SufCB is heavily conserved as indicated by the dark red areas on the heat map **(Figure 10**).

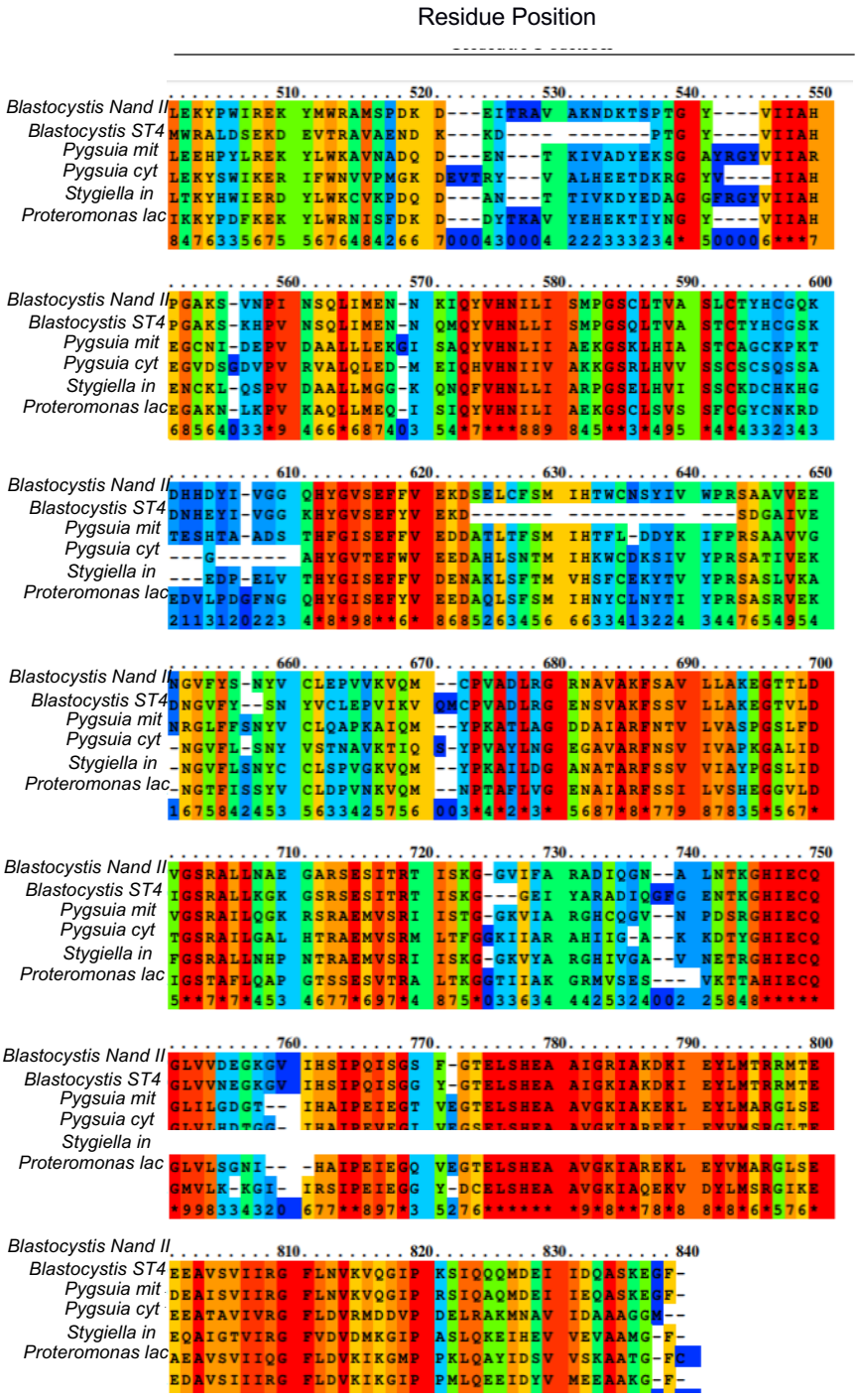

Figure 10. Multiple sequence Analysis of the SufB portion of SufCB. Software was used under default settings, http://ibivu.cs.vu.nl/programs/pralinewww/. A heat map is used to infer conservation between residues, blue indicates less conservation, red indicates conserved regions. Sequences in the order of: *Blastocystis* Nand II, *Blastocystis* subtype 4 , *Pygsuia biforma (mitochondrial SufCB), Pygsuia biforma (cytosolic SufCB), Stygiella incarcerate, Proteromonas lacertae.* Consistency scores (1-10) given along the bottom, scores closest to ten indicates strong conservation.

Examining **figures 7-10** demonstrates that all SufCBs are bidomain proteins which are connected by a likely flexible, disordered linker (**Figure 9**). SufCB proteins are ATPases of the P-loop family and the domains conferring this (Walker A box) are localised to the N-terminals within a SufC-like region (1-235aa) (**Figure 7**). At their C-terminal SufCB proteins contain a heavily conserved region, which aligns to the SufB superfamily (COG0719) and contains SufB scaffold proteins (**Figure 8**). These domains, as well as the protein superfamilies to which they belong, are shown graphically in **Figure 11.**

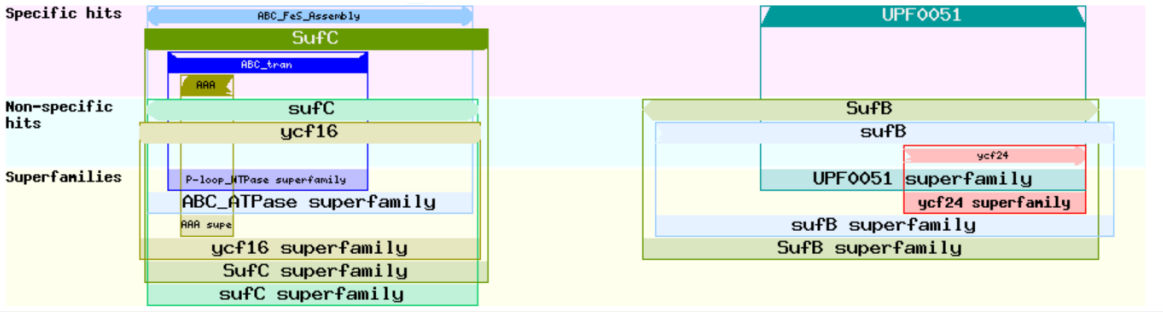

Figure 11. Multiple sequence alignment of SufCB showing SufC and SufB superfamilies at either end of the sequence. The linker domain does not align to any superfamily. NCBI Blast P suite and the Conserved Domain database were used to generate the above graphic, blast.ncbi.nlm.nih.gov/Blast.cgi and hwww.ncbi.nlm.nih.gov/Structure/cdd/. Searches were performed under default settings. A full graphic of the superfamilies is in **Appendix 6,** the highest e-value for a domain hit was 2 x 10^{-3}. The two unlabelled superfamilies, ycf16 and ycf24 belong to ATP transporter and a SufB-like family, respectively.

Initial biochemical data from Tsaousis et al (2012) categorised the *Blastocystis Nand II* SufCB as a scaffold protein. Other protists have since been found to encode a SufCB and transcriptomics have also suggested that these organisms have lost part of, if not the majority of their endogenous iron-sulfur assembly machinery (Stairs et al., 2014; Tsaousis et al., 2014; Leger et al., 2016). It is currently unknown how these protists express their SufCB, but it is expected that oxidative stress plays a role in their expression by an as yet unknown mechanism (Tsaousis et al., 2012). Data to suggest this was collected via RT-qPCR on aerobically prepared *Blastocystis* lysates and demonstrated that SufCB expression was induced under aerobic conditions, within which *Blastocystis* cells experienced oxidative stress (Tsaousis et al., 2012). Given the similarities at both sequence and molecular-levels, *Blastocystis* SufCB likely fulfils a similar protective role to the homologous SUF machinery in prokaryotes (Lee et al., 2008).

It is likely therefore that the SufCB protein enables the microaerophile *Blastocystis* to resist or 'buffer' the stresses of oxygen-exposure during the infectious faecal cyst stage of its life cycle (Tsaousis, et al., 2012). This is but one example of a protective mechanism by *Blastocystis* cells to buffer oxygen stress (Tsaousis et al., 2018). Little is known with regards to other protozoan SufCB proteins, however the high sequence similarities and cell biology data to date suggest that all SufCB proteins serve similar mechanism tailored to their hosts (Stairs et al., 2014; Tsaousis et al., 2014; Leger et al 2016).

1.4 Eukaryotic iron-sulfur cluster biosynthesis

Much like their prokaryotic counterparts, eukaryotes, such as *S. cerevisiae* assemble their iron-sulfur clusters *de novo* using dedicated machinery (Kispal et al., 1999). However, unlike prokaryotes, eukaryotic cells do not express SUF and instead encode compartmentalised biosynthetic machinery (Cai and Markley, 2018). Of these, the cytosolic iron-sulfur assembly (CIA) pathway (**Figure 12 and Table 4**) assembles clusters that are destined for cytosolic and nuclear proteins, and includes proteins involved in translation, DNA repair and amino acid biosynthesis (Alhebshi et al., 2012; Bedekovics et al., 2011; Ito et al., 2010).

Genes encoding CIA proteins are highly conserved throughout eukaryotes, although their respective roles do differ depending on the host organism (e.g. Nbp35 acts alone in *A. thaliana* but the Nbp35-Cfd1 complex is essential in *S. cerevisiae*) (Bych et al, 2008). As with other assembly pathways, the CIA utilises a core scaffold complex which transiently assembles an iron-sulfur cluster before a second late-acting scaffold complex delivers the cluster to an awaiting apo-protein (Netz et al. 2007).

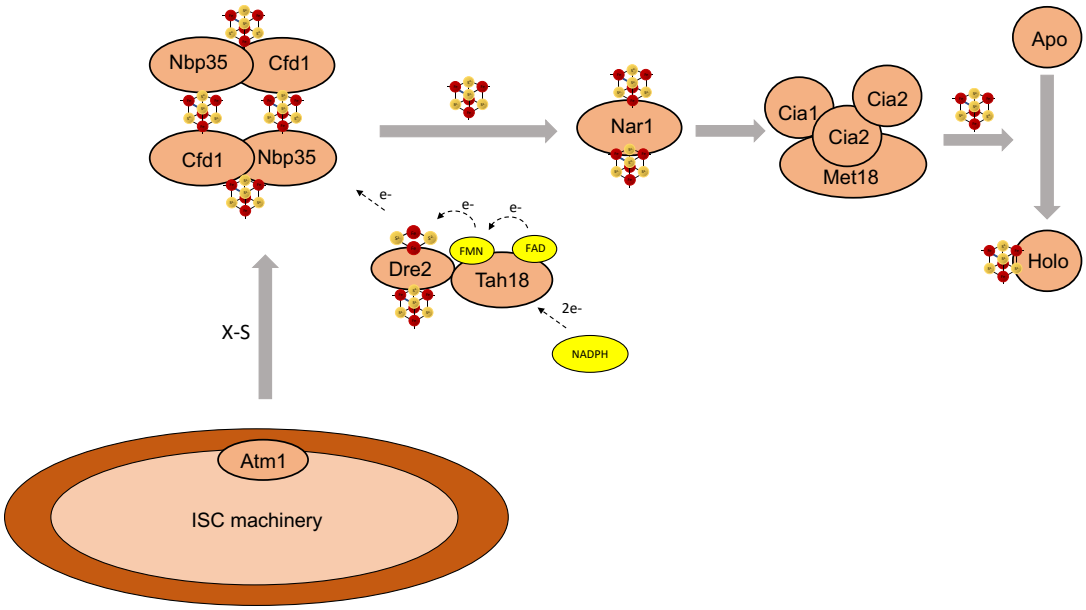

Figure 12. Schematic of the cytosolic iron-sulfur assembly pathway in *S. cerevisiae* which depends upon the export of an unknown sulfide containing compound (X-S) via Atm1. The maturation of apo-proteins to their iron-sulfur loaded holo-form is shown by 'Apo' to 'Holo'. Grey arrows indicate the direction of pathway intermediates, red/yellow spheres are iron-sulfur clusters, e- are electrons, FMN/FAD are flavin cofactors on Tah18.

Table 4. Components of the CIA pathway sorted into their complexes and functions if known.

Protein	Complex	Function	References
Nbp35	Nbp35-Cfd1	Scaffold	(Vitale et al., 1996)
Cfd1	heterotetramer	Scaffold	(Roy et al., 2003)
Dre2	Electron transport chain	Electron carrier	(Netz et al. 2016)
Tah18		Oxidoreductase	(Netz et al. 2010)
Met18		Scaffold	(Wang et al., 2016)
Cia1	CIA targeting complex	Scaffold	(Balk et al., 2005)
Cia2		Scaffold,	(Vo et al., 2017)

1.4.1 The CIA is intimately linked with the mitochondrial machinery

It has been demonstrated that the biogenesis of iron-sulfur clusters by the CIA machinery is dependent upon a functional mitochondrial iron-sulfur pathway (Kispal et al., 1999; Pandey et al., 2019). In yeast, mitochondrial iron-sulfur proteins are synthesised by a series of proteins which are predicted to have been inherited from eubacterial ancestors (Lill et al., 2006). For this reason, the mitochondrial ISC pathway operates in a similar way to the counterpart ISC system of *E. coli*, which like the bacterial ISC system, utilises a cysteine desulfurase, highly U-type scaffolds and a dedicated Hsp70/Hsp40 reaction cycle (Garland et al., 1999; Lill et al., 2006; Uzarska et al., 2013; Webert et al., 2014).

To date, cysteine desulfurase has been identified to operate within the CIA machinery, leading to the assumption that the CIA machinery likely 'outsources' its supply of sulphide to another organelle (Netz et al., 2007; Schaedler et al., 2014). Of these organelles, mitochondria are known to export sulfide-containing molecules for thiouridinylation of tRNAs and the mitochondrial ABC transporter Atm1 is required for cytosolic cluster biosynthesis (Braymer and Winge, 2018; Kispal et al., 1999; Schaedler et al., 2014). Both of these arguments suggest that the CIA obtains its sulfide via an Atm1 dependent mechanism (Kispal et al., 1999).

Several molecules have been put forward as potential sulfide-donors, including an exported iron-sulfur cluster and glutathione (GSH) derivatives (Li and Cowan, 2015; Schaedler et al., 2014). The latter of which (reduced GSH) was found to be tightly associated with crystal structures of the yeast ABC-type transporter Atm1 (Martínez-Pastor et al., 2017; Schaedler et al., 2014). Investigating this further, Schaedler et al., (2014) demonstrated that a radiolabelled (^{35}S) glutathione derivative (glutathione trisulfide, GS-S^0-SG) was selectively transported by yeast and plant (*A. thaliana*) Atm1 homologues using a mix of genetic and molecular techniques. Challenging this, Li and Cowan (2015) proposed that an unusual water-stable glutathione-coordinated [2Fe2S] ([2Fe2S]-$(GS)_4^{2-}$) cluster is instead the Atm1 substrate as it stimulates the ATPase activity of yeast Atm1 and is able to physically bind the yeast ISC machinery. The authors also demonstrated that this cluster could be transported into proteoliposomes by yeast Atm1 (Li and Cowan, 2015). Whilst the evidence suggests that GSH, definitely has a role in the final exported substrate(s), either as a derivative or a coordinating ligand, the exact composition of the compound, termed X-S, remains elusive (Braymer and Winge, 2018; Rocha et al., 2018). Despite the lack of molecular detail, disruption of either Nfs1 or Atm1 has long been known to strongly perturb cytosolic iron-sulfur biogenesis in the yeast system (Kispal et al., 1997, 1999).

1.4.3 Scaffold proteins Nbp35 and Cfd1

The functional core of the CIA pathway is an oligomeric complex consisting of nucleotide-binding proteins Nbp35 and Cfd1 (Stehling et al., 2018). The current model proposes that Nbp35 is the major site of iron-sulfur cluster biosynthesis, whilst Cfd1 promotes cluster transfer and assembly on the Nbp35-Cfd1 heterocomplex (Pallesen et al., 2013). Details on the synthesis of Nbp35-Cfd1's iron-sulfur cluster is largely unknown, however, electron transport provided by the oxidoreductase Tah18 and iron-sulfur protein Dre2 is essential for cluster assembly the Nbp35-Cfd1 and yeast viability (Soler et al., 2011). Current models hypothesise that two flavin-containing molecules (FMN and FAD) on Tah18 are reduced by NADPH which then allows Tah18 to interact with the C-terminal of Dre2, ultimately reducing Dre2's [2Fe2S] cluster (Soler et al., 2011). It has also been demonstrated that the plant Nbp35 (AtNBP35), physically interacts with its Dre2 homologue however whether this is conserved within the yeast system has yet to be demonstrated (Bastow et al., 2017).

Both Cfd1 and Nbp35 are thought to have originated following a genome duplication event as both share a 47.3% sequence identity. Nbp35 and Cfd1 proteins bind to form a tetramer with a bridging [4Fe4S] cluster co-ordinated by a shared C-terminal CPxC motif, **Figure 13** (Vitale et al. 1996b; Stehling et al, 2018). In addition to the conserved cysteine residues, an invariant phenylalanine (F) is also present (**Figure 14, black box**) on both Nbp35 and Cfd1, and is predicted to either help strengthen the bonds between the two proteins (presumed to be via π-stacking) (Pallesen et al., 2013, Stehling et al., 2018).

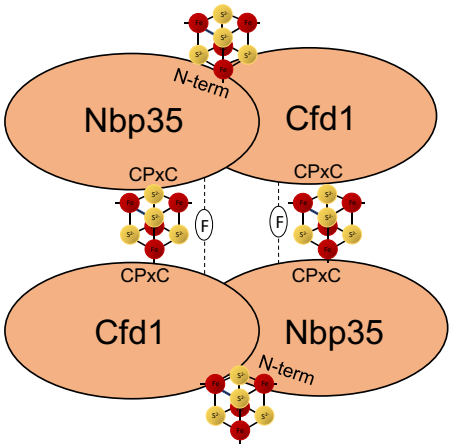

Figure 13. A schematic of the Nbp35-Cfd1 complexes. Both N- and C-terminal cluster binding sites are shown as 'N-term' and 'CPxC', respectively. The stabilising phenylalanine's are shown (F) by dashed lines.

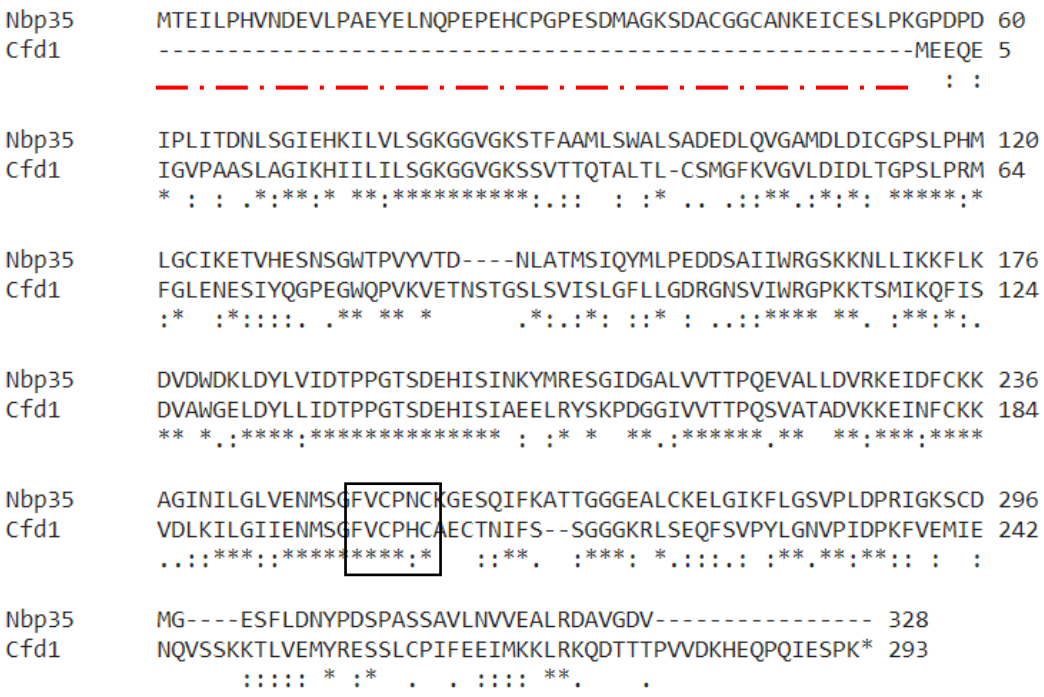

Figure 14. Pairwise sequence alignment of Nbp35 and Cfd1. Sequences were obtained from the Saccharomyces genome database, yeastgenome.org. Alignments using Clustal O (1.2.4), https://www.ebi.ac.uk/Tools/msa/clustalo/. A black box is drawn around the conserved C-terminal binding motif and a dashed red line indicates Nbp35's N-terminal extension.

What differentiates Nbp35 and Cfd1 proteins is the presence of a 52-residue N-terminal extension (**Figure 14, red dashed line**) in Nbp35, which is able to bind a stable [4Fe4S] cluster (Netz, et al., 2007; Bastow et al., 2017). Unlike its labile C-terminal cluster, Nbp35's N-terminal iron-sulfur cluster is predicted to be provide structural support, as the expression of N-terminal (C14A) mutants were found to lead to severely reduced growth and the activity of several iron-sulfur enzymes in *A. thaliana* (Bastow et al., 2017)

Cfd1 proteins contain an invariant C-terminal CPxC motif which is predicted to be the site of a [4Fe4S] cluster (Netz et al. 2007). Whilst no cluster has been found in yeast Cfd1, a much more stable homologue from *C. thermophilum (*ctCfd1*)* revealed a surface exposed [4Fe4S] bridging cluster between homodimeric Cfd1 (Netz et al. 2007; Stehling et al 2018). In addition, the conserved phenylalanine residue two residues upstream of the CPxC motif was shown to stabilise the tertiary structure of the iron-sulfur binding site (Stehling et al., 2018). Based on the sequence conservation of the discovered binding site, it has been proposed that yeast Cfd1 also binds a surface exposed iron-sulfur cluster although this has yet to be experimentally proven (Stehling et al., 2018).

Both Nbp35 and Cfd1 are P-loop NTPases which share specific, 'deviant' walker A motifs **(Figure 15)**, this feature categorises the two proteins into to the distinct signal recognition particle, MinD and BioD (SIMIBI) family of NTPases, which are commonly associated with metal trafficking and iron-sulfur biogenesis (Bych et al., 2008; Camire et al., 2015; Pardoux et al., 2019).

Figure 15. Multiple sequence alignment of Nbp35, Cfd1 and other SIMIBI proteins displaying their deviated walker A motifs (black box). Alignments were performed using Clustal O (1.2.4) under default settings. Sequences for Nbp35 and Cfd1 were sourced from the Saccharomyces genome database, yeastgenome.org. Sequences for NifH from A. vinelandii and MinD from E. coli were sourced from UniProt protein database, uniprot.org. Asterisks underneath residues indicates identical residues, dots and dashes indicates similar residues. SIMIBI lysine (K) residue is indicated by a red arrow.

SIMIBI proteins contain a characteristic walker A motif characterised by a conserved lysine (K) residue in the sequence of GKxxxGKS/T **(Figure 15**, black box**)** (Camire et al., 2015). SIMIBI proteins are typically associated with metal trafficking and examples include the iron-protein of Nitrogenase (NifH) and the arsenic transporter, ArsA (Stehling et al, 2018).

It is unknown at which step in Nbp35-Cfd1 complex and iron-sulfur assembly ATP-binding and hydrolysis takes place (Stehling et al 2018). Other SIMIBI proteins typically couple the binding and hydrolysis of ATP to conformation changes in their structures, which in turn enables them to regulate protein-protein interactions and execute metal transport (Camire et al., 2015). Although both Nbp35 and Cfd1 are known to hydrolyse ATP, much like $SufBC_2D$, the affinity for substrate differs greatly depending on the protein-context **(Table 5**) (Camire et al., 2015; Stehling et al., 2018). For example, homodimeric Nbp35 (Nbp35-Nbp35) and the heterotetrameric (Nbp35-Cfd1-Nbp35-Cfd1) share similar ATP affinities, whereas the ATP affinity of heterodimeric (Nbp35-Cfd1) is 10-fold higher than that of homodimeric Nbp35-Nbp35 (Camire et al., 2015). In addition, Camire et al (2015) were unable to detect any ATPase activity in homodimeric Cfd1.

Table 5. Summary of the ATPase activities within each variant Nbp35, Cfd1 complex. Adapted from Camire et al (2015).

Complex	Stoichiometry	ATPase activity (Y/N)	Relative activity
Homodimeric Nbp35	Nbp35-Nbp35	Y	
Heterotetramer	Nbp35-Cfd1-Nbp35-Cfd1	Y	Similar affinity
Heterodimer	Nbp35-Cfd1	Y	10-fold that of Homodimer
Homodimeric Cfd1	Cfd1-Cfd1	N	-

Point mutations in Nbp35's walker A (lys86) did not significantly affect ATPase activity within homodimeric Nbp35, whereas ATP hydrolysis in the Nbp35-Cfd1 heterotetramer-was reduced below background, without affecting complex formation (Camire et al., 2015). Despite no ATPase activity in dimeric Cfd1, mutating its walker A resulted in markedly decreased activity of Nbp35-Cfd1 heterodimer (Camire et al., 2015). These data **(Table 5)** suggest that allosteric interactions are formed with each new complex and this affects the ATPase active-sites (Camire et al., 2015).

Mammalian Nbp35 and Cfd1 homologues share roughly 50% identity to the yeast proteins, including the N and C-terminal cluster binding sites, respectively (**Appendix 24-25**). Like their yeast counterparts, both proteins (NUBP1 and NUBP2) are indispensable for the assembly of cytosolic and nuclear iron-sulfur clusters (Stehling et al 2018). These authors also demonstrated that human Cfd1 (NUBP2) interacts physically with IOP1 (yeast Cia1 homologue) and this interaction is required to mature IOP1s iron-sulfur cluster (Stehling et al, 2018). Interestingly, a Cfd1-Cia1 fusion gene has been identified in the fission yeast *Schizosaccharomyces pombe* but this fusion hasn't been yet shown at protein level (Balk et al., 2005).

A. thaliana, *C. elegans*, and the SAR supergroup, however, have lost their Cfd1 homologues and instead presumably rely upon conserved (>50% identity, **Appendix 7**) homodimeric Nbp35 to assemble iron-sulfur clusters (Bych et al., 2008; Tsaousis et al., 2014). For *A. thaliana*, two-hybrid experiments demonstrated that Nbp35 (AtNBP35) instead interacts with the oxidoreductase Dre2 (Bastow et al., 2017). AtNBP35 also lost its 'classical' Nbp35-like C-terminal CPxC cluster binding site and instead contains an extended C-terminal motif **(Figure 16**, bottom red arrow**)**, although the relevance of this remains unknown (Bych et al., 2008). It has also been demonstrated by immunofluorescence that *Blastocystis* Nand II also lacks a Cfd1 homologue and it may be such that its Nbp35 (Ind1) or SufCB is able to compensate for this loss (Tsaousis et al., 2014). Both proteins have conserved N-terminal cysteine binding sites (**Figure 16**, top highlighted C's), reinforcing the suggestion that this motif is intrinsic to the stability of Nbp35, rather than the Nbp35-Cfd1 complex (Bastow et al., 2017).

Figure 16. Multiple sequence alignment showing N- and C-terminal iron-sulfur binding sites of Nbp35 homologues, BNbp35 = *Blastocystis* homologue, Nbp35 = *S. cerevisiae* homologue, AtNbp35 = *A. thaliana* homologue. Sequences were obtained from the UniProt protein database, uniprot.org and aligned using Clustal O (1.2.4), under default settings. Conserved cysteine residues are highlighted in yellow. Red box is drawn around the N-terminal cluster binding sites, a black box is drawn around the C-terminal site with a red arrow indicating the conserved C-terminal CPxC motif.

On the mechanism of iron-sulfur assembly by Cfd1-Nbp35, Pallesen et al., (2013) proposed that homodimeric Nbp35 is the functional 'core' of the CIA pathway and that interaction with Cfd1 enhances the binding and release of the newly synthesised Nbp35-bound cluster **(Figure 17)**. Other authors have similarly noted the crucial nature of the complex's ATPase activity for iron-sulfur cluster assembly (Grossman et al., 2018; Pallesen et al., 2013; Stehling et al., 2018). The authors also speculate that the evolution of Cfd1 and its varied presence throughout life may indicate that carrying a Cfd1 may have helped the CIA machinery of these organisms to compete for limiting pools of iron through the maturation of iron-regulatory protein 1 (IRP1) (Pallesen et al., 2013; Sharma et al., 2010).

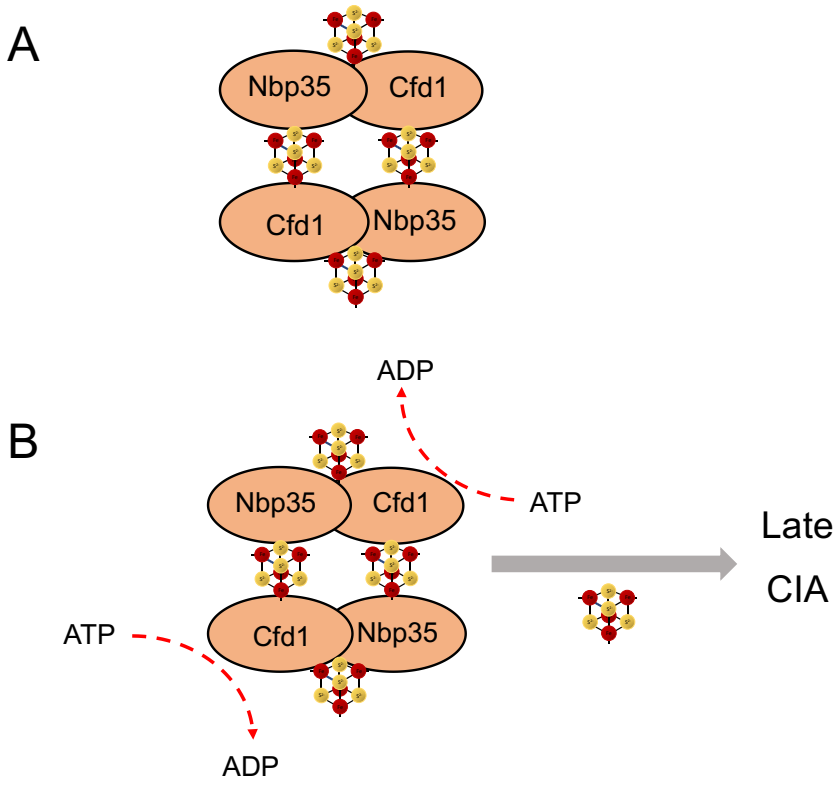

Figure 17. Schematic of the Cfd1 and Nbp35 heterotetramer. (A) The ATPase activity of Cfd1 could drive the release of iron-sulfur clusters from the Nbp35-Cfd1 heterotetramer (B) as described by Pallesen et al, (2013). Grey arrow indicates the transfer of an iron-sulfur cluster to downstream targets.

1.4.4 Late acting CIA scaffolds

In addition to the early acting scaffolds, the CIA system employs a late acting scaffold complex consisting of Cia1, Cia2 and Met18, with the Cia2 protein at the centre to organise complex assembly (**Figure 18**) (Vo et al., 2017). Collectively this complex is known as the 'CIA targeting complex' and data suggest that these proteins tether cluster synthesis by Nbp35-Cfd1 to target proteins (Netz et al., 2014; Upadhyay et al., 2017).

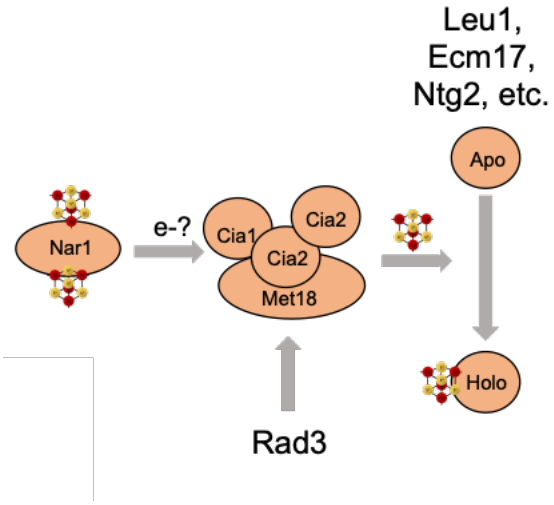

Figure 18. The full CIA targetting complex with associated iron-suflur enzymes. Rad3 is shown to require direct binding Met18, assumed electron transport from Nar1 (e-?) is also shown. Grey arrows dictate movement or recruitment of proteins.

In addition to interacting with the Nbp35-Cfd1 heterotetramer, the CIA targeting complex also interacts with yeast's only iron-hydrogenase, Nar1 (Netz et al., 2012). Nar1 operates at the bridging step between the Nbp35-Cfd1 and CIA targeting complexes and contains two iron-sulfur clusters (Urzica et al., 2009). Although the relevance of the interaction between Nar1 and the CIA targeting complex, remains unknown, it is possible that electrons donated by Nar1's two iron-sulfur clusters may facilitate the reduction of a substrate that is required for delivery of iron-sulfur clusters by the CIA targeting complex (Urzica et al., 2009). In *C. elegans*, Nar1 also serves as a barrier against oxidative stress (presumably to re-reduce oxidised biomolecules) and so Nar1's role within the CIA apparatus in yeast could be to buffer oxidants and prevent damage to the iron-sulfur assembly pathway (Zhao et al., 2014).

As its name suggests, the CIA targeting complex is responsible for directing clusters formed by the CIA machinery towards ~20 target proteins (Paul et al., 2015). The stoichiometry of this complex has long been debated but affinity purifications of the different protein components from Vo et al. (2017) confirmed that two Cia1-$(Cia2)_2$ bind Met18 to form a full CIA targeting complex required to bind iron-sulfur proteins Rad3 and Leu1, respectively (Vo et al., 2017).

Cia1 belongs to the WD40-repeat family and contains seven WD40 beta-propellers. WD40 proteins-typically mediate protein-protein interactions by functioning as docking sites (Srinivasan et al., 2007). Co-immunoprecipitation experiments confirmed the interaction between Nar1 and Cia1, but not Cfd1 or Nbp35 (Balk et al., 2005). In addition, depletion of Cia1 specifically affected the maturation of Leu1, Ecm17 and Rli1 but not Nar1 or Nbp35, thus indicating that Cia1 functions far downstream of the CIA pathway in the maturation of iron-sulfur proteins (Balk et al., 2005). The mammalian Cia1 homologue, MIP18 is protected from proteasomal degradation by binding MMS19, whereas MMS19 is perfectly stable in the absence of MIP18 (Odermatt and Gari, 2017). This interaction is predicted to be a means of limiting the functional transfer of iron-sulfur clusters, as the authors note that unscheduled delivery of iron-sulfur clusters could be potentially detrimental to the cell (Odermatt and Gari, 2017). Human Cia1 (MIP18) has been found to co-purify with several target apo-proteins including DNA polymerase Ɛ, and Viperin, however, this was unable to be replicated in with the yeast system (Moiseeva et al., 2016; Upadhyay et al., 2017).

Met18 is a late acting CIA component which physically interacts with both Cia1 and Cia2 (Vo et al. 2017). Met18 was originally identified in a genetic screen for DNA-alkylation sensitive mutants within *S. cerevisiae* reflecting the roles of iron-sulfur proteins in DNA repair (Prakash and Prakash, 1977). Nonetheless, knockouts are viable and have not been seen to cause a detrimental binding of radiolabelled iron (Fe^{55}) to Nbp35 nor Cfd1, implying Met18 is a late acting CIA component which exerts a redundant function downstream of Nbp35 and Cfd1 (Stehling et al., 2012).

Yeast co-immunoprecipitation experiments demonstrated that Met18 physically interacts with the iron-sulfur enzymes Rad3, Met10, Dna2, Rli1 and Ntg2 (Vo et al., 2017). Therefore it has been suggested that Met18 serves to recruit apo-proteins to the CIA targeting complex and this has been experimentally proven with Rad3 iron-sulfur enzyme, which requires specific motifs on Met18 to receive its iron-sulfur cluster (Vo et al., 2017).

Met18's role as a scaffold protein was first hypothesised by its alignment to the HEAT-repeat family of protein scaffolds (Queimado et al., 2001). All proteins belonging to this family possess two distinct N- and C-terminal domains (**Figure 18**); in yeast, the N-terminal spans residues 1-770 and includes a conserved stretch of amino acids between residues 167-285 (Queimado et al., 2001). This is in comparison to the smaller C-terminal (880-1032), which contains four highly conserved HEAT-repeats (**Figure 18)** (Queimado et al., 2001).

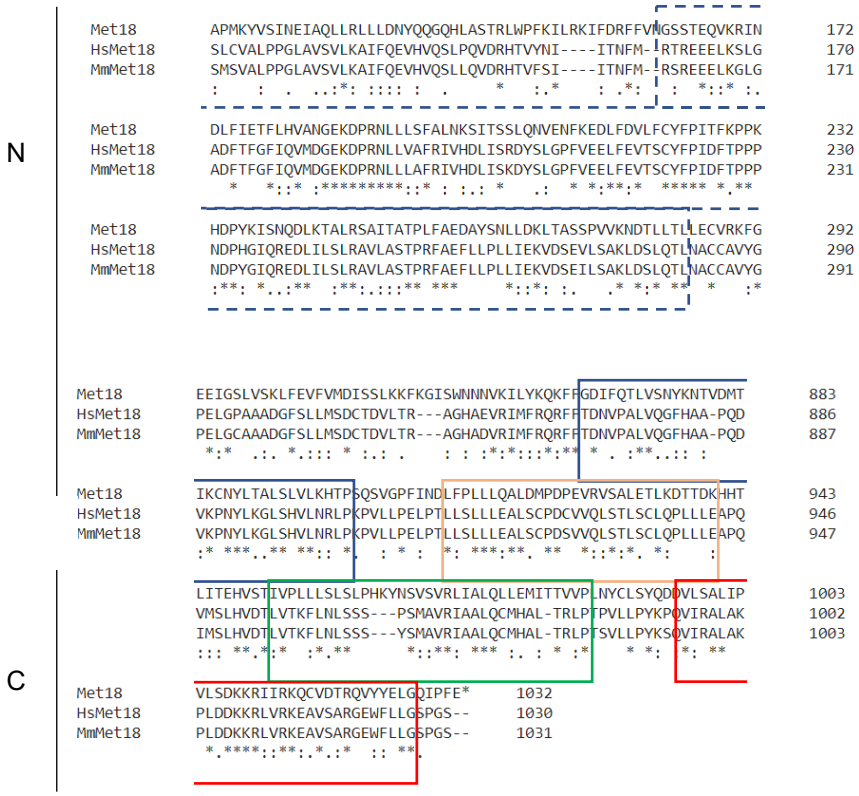

Figure 19. Conservation in Met18 homologues. Truncated multiple sequence alignment of Met18 homologues from *S. cerevisiae*, human and mouse proteins. Sequence alignments were performed in Clustal O (1.2.4) using sequences sourced from UniProt, (Human and Mouse), uniprot.org and the Saccharomyces genome database (*S. cerevisiae*), yeastgenome.org. Sequences are coded as Met18 = *S. cerevisiae*, HsMet18 = *Homo sapiens*, M mMet18 = *Mus musculus*. The conserved N-terminal is boxed in the area labelled 'N'. The four C-terminal HEAT repeats are shown in the area labelled 'C', Motif I – IV are boxed and coloured blue, orange, green and red, respectively. The full untruncated sequence alignment can be found in **Appendix 8.**

The relevance of the HEAT-repeat region of Met18 has been demonstrated to instigate complex assembly within the CIA targeting complex. This was demonstrated by Odermatt & Gary (2017) using mammalian homologues, the authors found that the C-terminal HEAT-repeat region of Met18 was required for assembly of the CIA-targeting complex **(Figure 19)** (Odermatt & Gary 2017). Separate studies have shown both that the iron-sulfur binding site (residues 110 – 196) and an N-terminal domain (residues 438 – 637) of human Rad3 are required to bind CIAO2 and MMS19, respectively (Ito et al., 2010; Vo, A. T. et al., 2017; Van Wietmarschen et al., 2012). As such, it is suggested that the HEAT-repeats of Met18 drive the assembly of Cia1 and Cia2 into a docking site for binding apo-protein targets (Odermatt & Gary 2017; Vo et al. 2017).

Cia2 contains a C-terminal domain of unknown function 59 (DUF59) **(Figure 20)** and although the function of this domain is unknown, its presence is strongly associated with iron-sulfur biogenesis machinery across bacteria and archaea and all eukaryotes encode at least one Cia2 homolog or paralogous pairs with non-redundant functions (Almeida et al., 2005; Mashruwala et al., 2016; Wright & Dyson 2015). Structurally, N-terminal Cia2 proteins contain two conserved regions consisting of an NxNP motif followed by a cluster of highly variant acidic residues, which appears to be intrinsically disordered (Wright and Dyson, 2015). This region was then shown to contribute to the stability of Cia2 protein as Δ*102cia2* deletions yielded significantly less protein product than full-length Cia2 (Wright and Dyson, 2015).

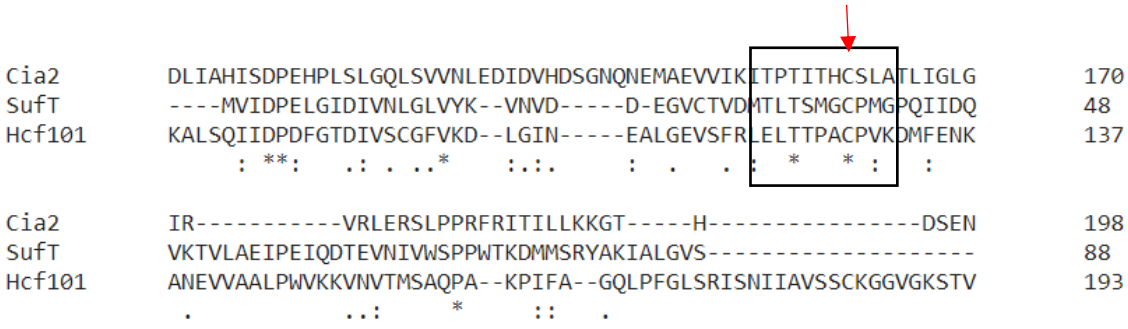

Figure 20. Truncated multiple sequence alignment of DUF59-containing proteins. Cia2's DUF59 domain is aligned with other DUF59-containing proteins, SufT and HCF101. The conserved cysteine residue is shown surrounded by hydrophobic residues.

The C-terminal domain begins with DUF59 domain consisting of two motifs in close vicinity, which potentially forms Cia2's active site (**Figure 20)** (Wright and Dyson, 2015). Several motifs adjacent to the DUF59 domain is missing in bacterial and archaeal proteins indicating that these motifs I, II and V are likely to play a role in mediating protein-protein interactions with the context of the CIA pathway (Wright and Dyson, 2015).

1.4.5 *Blastocystis* iron-sulfur biogenesis apparatus

S. cerevisiae is the model organism for the CIA machinery, however recent work has begun to probe other systems including *Blastocystis Nand II*. It was previously discussed that *Blastocystis Nand II* encodes an unusual cytosolic iron-sulfur scaffold protein, SufCB which localises to the cytosol. This suggests that the SufCB protein functions alongside or in conjunction with *Blastocystis*' native CIA machinery which is largely conserved from the yeast system **(Figure 21**). Notable differences, between the two, however, are a lack of Cfd1 and Dre2 proteins as demonstrated by immunofluorescence (Tsaousis et al., 2014).

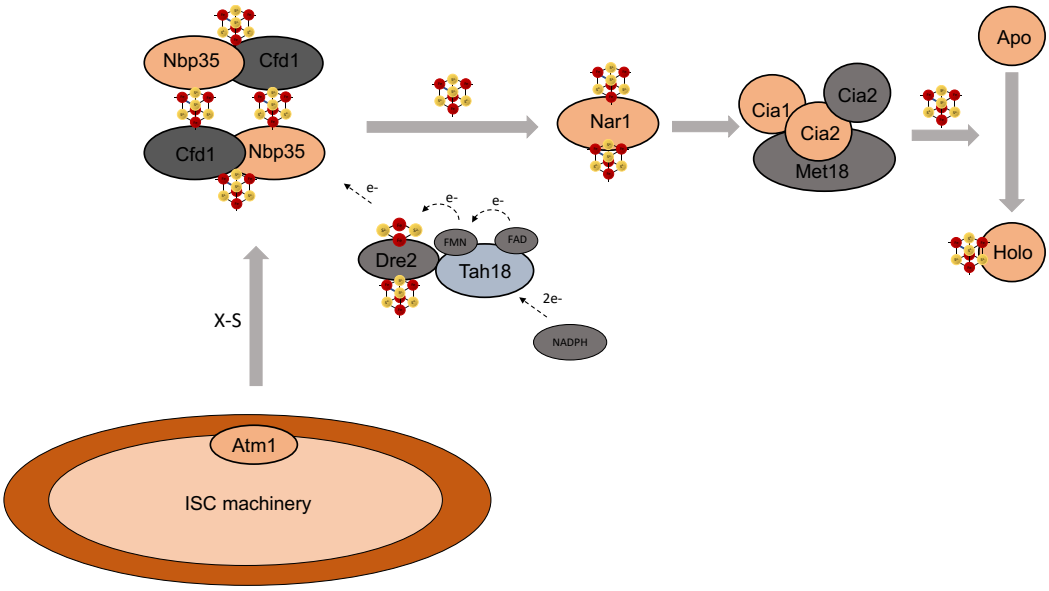

Figure 21. The CIA system as described in *Blastocystis Nand II*. Grey proteins are absent in *Blastocystis*. Tah18 has been coloured light blue as its existence is uncertain. The *Blastocystis* SufCB protein isn't shown. Genomics also revealed a putative Atm1 homologue which has been left orange.

It is unknown how the Nbp35 of *Blastocystis* functions without its Cfd1 partner, however, it is assumed that Nbp35 functions alone as a homodimer, as is presumed in *A. thaliana* which also lacks a Cfd1 (Bastow et al., 2017). It may also be that in the absence of Cfd1, Nbp35 binds with another cytosolic iron-sulfur scaffold, SufCB, but this remains to be experimentally proven **(Figure 22)**. In addition, these data demonstrated that *Blastocystis* may also lack Tah18 whilst cells do contain Met18 protein, its sequence has highly diverged from the yeast counterpart (Tsaousis et al., 2014). Analysis of the Nbp35 sequence reveals that the N-terminal cluster binding extension is conserved from the yeast protein, whereas the C-terminal CPxC cluster binding site is replaced with an extended form, this is similar to the C-terminal of plant Nbp35 **(Figure 16)** (Bastow, et al., 2017). Given that the N-terminal cluster is predicted to be structural, it is likely that the *Blastocystis* Nbp35 homologue binds an N-terminal cluster similar to the yeast protein, whereas the C-terminal cluster remains elusive. Possible Nbp35-complexes in *Blastocystis* are summarised in **Figure 22.** Given that Nbp35 of *A. thaliana* was shown to physically interact with the *A. thaliana* Dre2 in the absence of Cfd1**,** it may also be that Nbp35 functions alongside an unusual partner in the CIA machinery (Dre2 is absent in *Blastocystis*) (Tsaousis et al., 2014, Bastow et al., 2017).

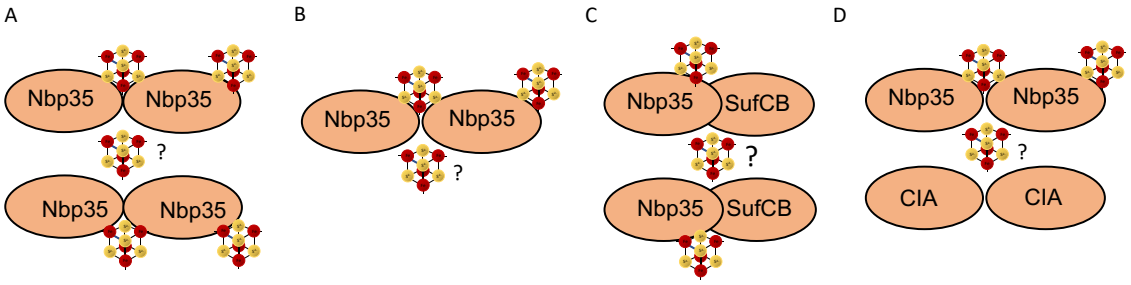

Figure 22. Possible Nbp35 complexes within the Blastocystis CIA machinery. Each Nbp35-complex is predicted to contain an N-terminal [4Fe4S] clusters and a possible C-terminal cluster which is transferred for iron-sulfur assembly similar to the yeast machinery y. A) Nbp35-homotetramer, B) Nbp35-homodimer. C) Nbp35-SufCB heterotetramer, D) Nbp35-CIA component heterotetramer.

In addition to the CIA machinery, the *Blastocystis* genome was also found to contain the open reading frames of ten ISC components: IscS, IscU, Frataxin, Mrs3/4, Ferredoxin, Hsp70, Mge1, Hsp40 and Isa1, which potentially represents a minimal iron-sulfur assembly system (Tsaousis et al., 2012). Immunofluorescence experimented demonstrated that these components (IscS, IscU and frataxin) localised to the *Blastocystis* mitochondria-related organelle (MRO), suggesting that Blastocystis cells have homologous methods of iron-sulfur assembly as other eukaryotes (Tsaousis, et al., 2012). Recombinant expression of these proteins in *Trypanosomes* reveals that these proteins were also able to functionally replace their respective *Trypanosome* knockouts and rescue iron-sulfur biogenesis (Tsaousis et al., 2012). It was also demonstrated that *Blastocystis* expresses a cytosolic SufCB fusion protein, which both functions as an iron-sulfur scaffold and is upregulated under periods of oxygen exposure (Tsaousis et al., 2012). It remains to be seen whether SufCB of *Blastocystis* acts in conjunction as a housekeeping protein within the CIA assembly machinery **(Figure 22)**, or if SufCB serves an auxiliary role to repair iron-sulfur clusters under periods of oxygen-stress (Tsaousis et al., 2012). The latter would place SufCB in line with its SUF homologues in prokaryotic organisms (Tsaousis et al., 2012).

In summary, *Blastocystis* cells assemble their iron-sulfur clusters by minimalised assembly pathways (CIA and ISC), which could either reflect the cell's parasitic and or anaerobic lifestyle. Pallesen et al., (2013), hypothesised that Cfd1 could be the source of iron for the CIA machinery, thus the necessity for Cfd1 could be mitigated if *Blastocystis* could acquire iron from its host (Tsaousis et., 2012). Interestingly, an aspect of *Blastocystis*' lifestyle also enables the cells to assemble iron-sulfur clusters without electron transport from Dre2-Tah18, although the relevance of this complex remains to be seen the yeast homologues are essential for viability and have roles in apoptosis (Netz et al., 2016; Nishimura et al., 2013). This may reflect the cell's anaerobic lifestyle as substrate(s) may arrive in a pre-reduced form to the Nbp35 scaffold in the absence of oxygen (Tsaousis et al., 2012).

1.5 Overexpressing iron-sulfur assembly apparatus improves cluster biogenesis.

The successful overexpression of iron-sulfur proteins was originally shown by Takahashi and Nakamura (1999). These authors demonstrated that overexpressing *ORF1-ORF2-iscS-iscU-iscA-hscB-hscA-fdx-ORF3* led to a dramatically increased maturation of five reporter ferredoxins (Nakamura et al., 1999). The overexpressed operon was later classified as the *isc* operon which serves as the housekeeping iron-sulfur assembly apparatus in *E. coli* (Takahashi and Nakamura, 1999).

Studies since have demonstrated that recombinant expression of the oxygen-responsive *suf* operon can also increase the maturation of Nitrogenase in *E. coli* (Li et al.,. 2016). This utility also appears to have spread throughout nature, as several anaerobic protists have been discovered to encode components of SUF alongside their endogenous iron-sulfur machinery (Tsaousis et al., 2014). The relevance of encoding these auxiliary pathways has yet to be elucidated, however, in some cases, the foreign machinery has partially or completely replaced canonical housekeeping pathways (Leger et al., 2016; Stairs et al., 2014; Tsaousis et al., 2012). For *Blastocystis*, SufCB is predicted to aid survival (e.g. recycling its iron-sulfur clusters) during the infectious stage of its lifecycle, during which the parasite encounters otherwise fatal oxygen-stresses (Tsaousis et al., 2012, 2018).

Recently, Martínez-Alcántar et al., (2019) demonstrated that overexpression of J-domain chaperone Jac1 and Isu1 scaffold led to improved ethanol tolerance in the ethanologenic *S. cerevisiae* strain UMArn3. The authors found that overexpressing both proteins resulted in reduced accumulation of mitochondrial ROS and free Fe^{2+} and hypothesised that these phenotypes resulted from improved recycling of iron-sulfur clusters in the overexpressing strain (Martínez-Alcántar et al., 2019). Similar findings have also been presented by Gakh, Smith IV, and Isaya (2008) as a point mutation in yeast frataxin (Yfh1, Y73A), which results in constitutively active trimeric Yfh1, was shown to coincide with significantly increase aconitase activity and resistance to oxidative damage. The overexpression of the *yfh1* ORF in yeast, however, resulted in decreased aconitase activity, suggesting that the effects of Yfh1 on the cell are context-dependent (Seguin et al., 2009).

.

Aims

The presence of an iron-sulfur cluster greatly increases the functional repertoire of an enzyme (Imlay, 2006). Because of this, iron-sulfur cluster enzymes operate in a variety of useful metabolic pathways. A growing body of literature demonstrates that these products have the potential to provide more efficient and 'greener' sources of raw chemicals for a huge variety of applications (Jugder et al., 2018; Lopez-Torrejon et al., 2016; Raj et al., 2018; Tsujimoto et al., 2018). Attempts to exploit iron-sulfur cluster enzymes for biotechnology, however, often fail due to the incompatibility of iron-sulfur clusters with oxygen (Martínez-Alcántar et al., 2019; Raj et al., 2018). To address this problem, we propose that a new expression platform is required that mitigates the vulnerability of iron-sulfur cluster enzymes to oxidants.

Cell factories offer a means of reconstructing biosynthetic pathways into an easy to grow host organism. For this project, we aim to build a cell factory which recombinantly expresses adaptive iron-sulfur cluster assembly machinery from a microaerophilic protozoan (*Blastocystis*), within an *S. cerevisiae* chassis. Ultimately, we aim to show that the recombinantly expressed protozoan scaffold protein (SufCB) can interact with the iron-sulfur cluster assembly apparatus of *S. cerevisiae* and result in a significantly improved capacity to mature iron-sulfur cluster enzymes.

There are several iron-sulfur enzymes in yeast which produce commercially relevant metabolites such as the antioxidant lipoic acid produced by Lip5 (Schonauer et al., 2009; Williams et al., 2002) and the vitamin supplement, biotin, produced by Bio2 (Ardabilygazir et al., 2018), of which, the latter has also received a patent which detail methods to overexpress the enzyme (Shiuan, 2006). In addition to studying the abundance and activities of endogenous iron-sulfur enzymes, we will also introduce recombinant iron-sulfur enzymes of mammalian origin. Commonly, the [4Fe4S] enzyme, aconitase is used to report on the biogenesis on iron-sulfur clusters in the cell and this protein has been well characterised in the yeast system (Roy et al., 2003). In addition to this, we will also use the [2Fe2S] enzyme, CMAH, which has gained attention recently due to its role in the biogenesis of the immunogenic sialic acid, Neu5Gc (Peri et al., 2018; Takahashi et al., 2015). Sialic acids, such as Neu5Gc, have long been known to modulate immune responses and are promising candidates for carbohydrate-based vaccines (Diaz et al., 2009; Labrada et al., 2018). By creating this 'panel' of iron-sulfur enzymes we will then be able to fully assess whether a SufCB-expressing yeast can be used a microbial cell factory for improved iron-sulfur biogenesis.

In addition, studying the interactions and phenotypes of SufCB-expressing yeast also provides an opportunity to study the iron-sulfur assembly pathways of both yeast and *Blastocystis*, particularly as techniques to genetically manipulate the latter are currently still under development (Li et al., 2019). To date, SUF machinery has been expressed in yeast (*S. cerevisiae*), however, this was purely for localisation studies (Stairs et al., 2014), our work will provide the first instance of a recombinant SufCB fusion protein within the yeast system.

To meet this main project aim, we assigned the following aims to each research chapter:

i. Aim 1: To show that yeast is a suitable host for the SufCB protein.

Using western blotting, fluorescent localisation and microbiological assays (growth rates) we will assess whether the SufCB protein can be expressed in the yeast system, and if so, whether this expression affects the cellular fitness. The latter step will be assessed by quantifying the growth rates of SufCB and non-SufCB expressing yeast.

ii. Aim 2: To show that iron-sulfur cluster assembly is strengthened in the SufCB-expressing yeast system.

Using fluorescence-based reporter systems we will assess whether iron-sulfur cluster enzymes are upregulated in the SufCB-expressing yeast and finally use activity assays (where available) to determine the activity of candidate iron-sulfur cluster enzymes. We will also investigate recombinant iron-sulfur enzymes, aconitase and CMAH, in the yeast SufCB system. In addition, as iron-sulfur enzymes participate in various essential (DNA repair, translation) pathways, we will also investigate stress responses (mixed stressors) in SufCB yeast.

iii. Aim 3: To identify a mechanism for SufCB in yeast and any interacting partners, including whether SufCB can bind an iron-sulfur cluster.

Using yeast genetic tools, we will probe the mechanism of SufCB in yeast and investigate any possible genetic and physical interactions between SufCB and the yeast iron-sulfur cluster assembly machinery. We will also purify SufCB from yeast to investigate whether or not the protein can accommodate an iron-sulfur cluster using reconstitution and anaerobic purification techniques within a partner laboratory.

Materials and Methods

2.1 Health and Safety

All work involving genetically modified organisms and pathogens was performed in a biological safety level 2 laboratory using appropriate PPE and only after carrying out risk and COSSH assessments for all procedures involving hazardous chemicals.

2.2 Data recording and archiving

All data and protocols were recorded in laboratory notebooks.

2.3 Routine cell culture

2.3.1 Preparation of cell culture media

Liquid cell culture media was prepared using the following recipes and routinely made to 200 mL in 250 mL Duran bottles (Fisher Sci, UK). Solid media was prepared in bulk at 400 mL in 500 mL Duran bottles. Recipes for the media used in this study are listed below, solid ingredients were added first and then reverse osmosis double distilled water (RO ddH_2O) added to the meet required final volumes. The full tables of dry ingredients per volume can be found in **Tables 6-13**, below.

Table 6. Media recipe for lysogeny broth.

Lysogeny Broth	Weight (g) required per mL				
Component	100 mL	200 mL	400 mL	800 mL	1000 mL
Sodium Chloride	1 g	2 g	4 g	8 g	10 g
BactoTryptone	1 g	2 g	4 g	16 g	20 g
Yeast Extract	0.5 g	1 g	2 g	4 g	8 g
Agar (if plating)	2 g	4 g	8 g	16 g	20 g

Table 7. Media recipe for YPD.

YPD	Weight (g) required per mL				
Component	100 mL	200 mL	400 mL	800 mL	1000 mL
Glucose	2 g	4 g	8 g	16 g	20 g
Yeast Extract	1 g	2 g	4 g	8 g	10 g
BactoPeptone	2 g	4 g	8 g	16 g	20 g
Agar (if plating)	2 g	4 g	8 g	16 g	20 g

Table 8. Media recipe for synthetic defined minimal media.

SD Minimal media	Weight (g) required per mL				
Component	100 mL	200 mL	400 mL	800 mL	1000 mL
Glucose	2 g	4 g	8 g	16 g	20 g
Yeast Nitrogen Base	0.8 g	1.34 g	2.68 g	5.36 g	6.7 g
Amino acid mix	**See Table 13.**				
Agar	2 g	4 g	8 g	16 g	20 g

Table 9. Media recipe for BiGGY media.

BiGGY Media	Weight (g) required per mL	
Component	200 mL	400 mL
Yeast Extract	1.34 g	2.68 g
Glycine	2 g	4 g
Glucose	2 g	4 g
Sodium Sulphite	0.6 g	1.2 g
Ammonium Bismuth Citrate	1 g	2 g
Agar	2.8 g	4 g

Table 10. Synthetic defined media with non-fermentative carbon sources.

SD Glycerol Media	Weight (g) required per mL				
Component	100 mL	200 mL	400 mL	800 mL	1000 mL
Glycerol	2 mL	4 mL	8 mL	16 mL	20 mL
Yeast Nitrogen Base	1 g	2 g	4 g	8 g	10 g
Amino acid mix	**See Table 13.**				
Agar (if plating)	2 g	4 g	8 g	16 g	20 g

Table 11. Media recipe for sporulation media.

SPOR Media	Weight (g) required per mL				
Component	100 mL	200 mL	400 mL	800 mL	1000 mL
Potassium Acetate	1 g	2 g	4 g	8 g	10 g
Glucose	0.1 g	0.2 g	0.4 g	0.8 g	1 g
Yeast Extract	0.125 g	0.25 g	0.5 g	1.0 g	1.25 g
Agar	2 g	4 g	8 g	16 g	20 g

Table 12. Media recipe for synthetic defined minimal BiGGY media.

SD BiGGY Media	Weight (g) required per mL	
Component	200 mL	400 mL
Yeast Nitrogen Base	1.34 g	2.68 g
Glycine	2 g	4 g
Glucose	2 g	4 g
Sodium Sulphite	0.6 g	1.2 g
Ammonium Bismuth Citrate	1 g	2 g
Amino acid mix	**See Table 13.**	
Agar	2.8 g	4 g

Table 13. Table of amino acid supplements required per media formulation.

Amino acid supplements	Weight (g) required per mL		
Component	100 mL	200 mL	400 mL
Leu dropout mix	0.32 g	0.65 g	1.30 g
Ura dropout mix	0.38 g	0.68 g	1.36 g

2.3.2 Routine sterilisation use and storage of cell culture media.

Before use, all media and buffers were sterilised in a 12 L Bench-top autoclave (Prestige Medical) at +121ºC, 15 lb/square inch for 11 minutes. Media was prepared as required per experiment and not in excess to avoid unnecessary waste and contamination. All media was stored at room temperature for a maximum of 4 weeks, except for media which contained antibiotics, this was stored at +4ºC for a maximum of 1 week after creation. For solid media, 2% w/v granulated agar (BD Difco, UK) was added to each container before autoclaving and gently swirled after removal from the autoclave to solubilise sediment. Solidified plates were stored for a maximum of 2 weeks at +4ºC.

2.3.3 Antibiotic Supplementation

Antibiotic stock solutions were prepared at 1000x required concentration in RO ddH_2O and stored at -20°C for no more than 3 months. Antibiotics were added to the required concentrations (**Table 14**) in each media after sterilising in an autoclave and allowing the bottle to cool to room temperature (**2.3.3**).

Table 14. List antibiotics used. Concentrations are given in µg/mL.

Antibiotic	Concentration (µg/mL)	Supplier
Ampicillin	100	Melford
Chloramphenicol	25	Melford
Geneticin (G418) Disulphate	250	Melford
Doxycycline Hyclate	1-10	Sigma

2.3.4 Glycerol Stocks

Glycerol stocks were made as a suspension of sterile 50% v/v glycerol with an equal volume of overnight culture, placed into 1.5 mL cryotubes and frozen at -80°C.

2.3.5 Culturing *Escherichia coli*

All *E. coli* liquid cultures were incubated at +37ºC, constant shaking at 200 rpm in an INFORS Minitron HT incubator (INFORS, UK). Cultures grown on solid media were incubated in a static incubator at +37ºC.

2.3.5.1 Strain

Table 15. *E. coli* strains used in this study.

Strain	Genotype	Source
DH5α	F–φ80*lac*ZΔM15 Δ(*lac*ZYA-*arg*F)U169 *rec*A1 *end*A1 *hsd*R17(rK–, mK+) *pho*A *sup*E44 λ– *thi*-1 *gyr*A96 *rel*A1	KFG communal Stock

2.3.5.2 Making chemically competent *E. coli* by the CCMB80 method

To prepare competent cells, SOB media (Sigma, UK) was inoculated with one vial of DH5α seed stock (T. von der Haar) and allowed to regrow at +30ºC, until an OD_{600} of 0.3. At this point, the CCMB80 buffer was placed on ice. Revived cells were then harvested in a pre-cooled benchtop centrifuge (Eppendorf, UK) at +4ºC, 3000 rpm for 10 minutes and resuspended in 80 mL of ice-cold CCMB80 buffer. The remaining suspension was then incubated for 20 minutes on ice. Following this, the suspension was harvested again at +4ºC, 3000 rpm for 10 minutes. The supernatant was then discarded before the pellet was resuspended in 10 mL of ice-cold CCMB80 buffer. The OD_{600nm} of the resulting cell suspension was then adjusted to 1.0 - 1.5 for subsequent experiments, before being aliquoted into 1.5 mL microcentrifuge tubes (Eppendorf, UK) and frozen at -80ºC.

2.3.5.3 Transformation of chemically competent *E. coli.*

Competent cells were removed from the -80 freezer and allowed to thaw on ice for 20 minutes, at the same time a sterile 1.5 mL Eppendorf tube (Eppendorf, UK) was also placed on ice. Care was taken throughout to ensure the competent cells were not warmed by the body or ambient temperatures by maintaining on ice throughout. For ligations, 10 µL of the plasmid (half of the ligation reaction) was aliquoted into the pre-chilled 1.5 mL Eppendorf tube and 100 µL of competent *E. coli* was aliquoted on top of the DNA and allowed to incubate on ice for 20 minutes, at the same time a water bath was warmed to +42ºC.

Following 20 minutes on ice, the transformation reaction was heat-shocked for exactly 60 seconds in the pre-warmed water bath before being immediately placed back on ice. 1 mL of LB liquid media was then carefully pipetted on top of the transformation reaction and incubated for 1 hour on a 2 mL thermomixer at +37°C, 800 rpm to partially revive the cells. Cells were then harvested in a benchtop centrifuge for 2 minutes at 2000 rpm, at ambient temperature, 900 µL of supernatant removed. The resulting 100 µL of the supernatant was then used to gently resuspend the cell pellet. This mixture was then plated using a glass rod onto LB agar plates containing the relevant antibiotic. Cultures were then grown in a static plate incubator overnight (16 hours) at +37°C.

2.3.5.4 Extraction of *E. coli* plasmid DNA

Plasmid DNA was purified from an overnight culture grown under selective antibiotic pressure according to the Qiagen spin-column protocol (Qiagen, UK). All steps were carried out according to manufacturer's instructions, albeit with a 70 µL elution at the last step to increase DNA yield (L. Josse advice). If required, the eluate was stored at -20°C until further analysis.

2.3.6 Culturing *Saccharomyces cerevisiae*

All *S. cerevisiae* liquid cultures were incubated at +30°C, constant shaking at 200 rpm in an INFORS HT Minitron incubator (INFORS, UK). Cultures grown on solid media were incubated in a static incubator at +30°C.

2.3.6.1 Strains

Table 16. The communal yeast strain used throughout this study.

Strain	Genotype	Source
BY4741	*MATa his3Δ1 leu2Δ0 met15Δ0 ura3Δ0*	KFG Communal stock

Table 17. *Saccharomyces cerevisiae* deletion strains used in this study, (Winzeler et al., 1999).

Strain	Genotype
BY4741Δ*ftr1*	*MATa his3Δ1 leu2Δ0 met15Δ0 ura3Δ0 ftr1::KANMX*
BY4741Δ*met18*	*MATa his3Δ1 leu2Δ0 met15Δ0 ura3Δ0 met18::KANMX*
BY4741Δ*aft1*	*MATa his3Δ1 leu2Δ0 met15Δ0 ura3Δ0 aft1::KANMX*
BY4741Δ*aft2*	*MATa his3Δ1 leu2Δ0 met15Δ0 ura3Δ0 aft2::KANMX*
BY4741Δ*nfu1*	*MATa his3Δ1 leu2Δ0 met15Δ0 ura3Δ0 nfu1::KANMX*
BY4741Δ*isu1*	*MATa his3Δ1 leu2Δ0 met15Δ0 ura3Δ0 isu1: KANMX*
BY4741Δ*isa1*	*MATa his3Δ1 leu2Δ0 met15Δ0 ura3Δ0 isa1::KANMX*
BY4741Δ*bol3*	*MATa his3Δ1 leu2Δ0 met15Δ0 ura3Δ0 bol3::KANMX*

Table 18. Saccharomyces cerevisiae strains depleted for essential ORFs. Mutants were sourced from the Decreased Abundance by mRNA Perturbation (DAmP) library, (Breslow et al., 2008).

Strain	Genotype
BY4741*nbp35*^{DAmP}	*MATa his3Δ1 leu2Δ0 met15Δ0 ura3Δ0 nbp35*$^{3'UTR}$*::KANMX*
BY4741*cfd1*^{DAmP}	*MATa his3Δ1 leu2Δ0 met15Δ0 ura3Δ0 cfd1*$^{3'UTR}$*::KANMX*
BY4741*dre2*^{DAmP}	*MATa his3Δ1 leu2Δ0 met15Δ0 ura3Δ0 dre2*$^{3'UTR}$*::KANMX*
BY4741*nfs1*^{DAmP}	*MATa his3Δ1 leu2Δ0 met15Δ0 ura3Δ0 nfs1*$^{3'UTR}$*::KANMX*
BY4741*atm1*^{DAmP}	*MATa his3Δ1 leu2Δ0 met15Δ0 ura3Δ0 atm1*$^{3'UTR}$*::KANMX*
BY4741*nar1*^{DAmP}	*MATa his3Δ1 leu2Δ0 met15Δ0 ura3Δ0 nar1*$^{3'UTR}$*::KANMX*
BY4741*cia1*^{DAmP}	*MATa his3Δ1 leu2Δ0 met15Δ0 ura3Δ0 cia1*$^{3'UTR}$*::KANMX*

Table 19. Heterozygous diploid deletion mutant for Cfd1.

Strain	Genotype
BY4743*cfd1*$^{+/-}$	*MATa/MATα:his3Δ1/his3Δ1,leu2Δ0/leu2Δ0, met15Δ0/lys2Δ0, ura3Δ0/ura3Δ0Δcfd1::KANMX*

Table 20. GFP library strains. Yeast containing ORFs with C-terminally tagged with Green Fluorescent Protein (GFP) (Kumar et al., 2002).

GFP Strain	Genotype
BY4741*leu1*^{GFP}	*MATa his3Δ1 leu2Δ0 met15Δ0 ura3Δ0 leu1::leu1*^{GFP}*KANMX*
BY4741*ecm17*^{GFP}	*MATa his3Δ1 leu2Δ0 met15Δ0 ura3Δ0 ecm17::ecm17*^{GFP}*KANMX*
BY4741*rli1*^{GFP}	*MATa his3Δ1 leu2Δ0 met15Δ0 ura3Δ0 rli1::rli1*^{GFP}*KANMX*
BY4741*pol2*^{GFP}	*MATa his3Δ1 leu2Δ0 met15Δ0 ura3Δ0 pol2::pol2*^{GFP}*KANMX*
BY4741*elp3*^{GFP}	*MATa his3Δ1 leu2Δ0 met15Δ0 ura3Δ0 elp3::elp3*^{GFP}*KANMX*
BY4741*ntg2*^{GFP}	*MATa his3Δ1 leu2Δ0 met15Δ0 ura3Δ0 ntg2::ntg2*^{GFP}*KANMX*
BY4741*rad3*^{GFP}	*MATa his3Δ1 leu2Δ0 met15Δ0 ura3Δ0 rad3::rad3*^{GFP}*KANMX*
BY4741*nbp35*^{GFP}	*MATa his3Δ1 leu2Δ0 met15Δ0 ura3Δ0 nbp35::nbp35*^{GFP}*KANMX*
BY4741*sdh2*^{GFP}	*MATa his3Δ1 leu2Δ0 met15Δ0 ura3Δ0 sdh2::sdh2*^{GFP}*KANMX*
BY4741*bio2*^{GFP}	*MATa his3Δ1 leu2Δ0 met15Δ0 ura3Δ0 bio2::bio2*^{GFP}*KANMX*
BY4741*lip5*^{GFP}	*MATa his3Δ1 leu2Δ0 met15Δ0 ura3Δ0 lip5::lip5*^{GFP}*KANMX*
BY4741*act1*^{GFP}	*MATa his3Δ1 leu2Δ0 met15Δ0 ura3Δ0 act1::act1*^{GFP}*KANMX*
BY4741*aft1*^{GFP}	*MATa his3Δ1 leu2Δ0 met15Δ0 ura3Δ0 yap1::yap1*^{GFP}*KANMX*

2.3.6.2 Working Cultures

All yeast experiments were conducted on logarithmic yeast cultures, which had been sub-cultured from overnight growth flasks, prepared according to **2.3.6**. The logarithmic phase was determined by optical density (OD) at OD_{600nm} of 1.0 - 1.5, where the majority of cells could be seen budding. For overnight cultures, 10% of the culture flask's volume was filled with media was inoculated with a roughly 1/10th of a colony (equating to ~10^5 cells), using a sterile 100 µL pipette tip and incubated according to **2.3.6**. Sterility controls were also performed using autoclaved media to ensure that the media and pipette tip remained sterile.

2.4 Molecular cloning

2.4.1 TAE Gel Electrophoresis

DNA was analysed by TAE gel electrophoresis and the gel concentrations (weight per volume, %) varied depending on the molecular weight of the DNA (**Table 21**). For example, a 1% w/v gel was made by dissolving 1 g of Agarose in 100 mL of TAE (40 mM Tris, 20 mM Acetic Acid, 1 mM EDTA, pH 7.0) and boiling the solution in a microwave. To enable visualisation of DNA, intercalating Ethidium bromide (EtBr) was added to the molten agarose in a fume hood to a final concentration of 5 µg/mL. Gels were routinely cast in a 20 mL gel bed and allowed to set on a level surface at room temperature for 1 hour. The gel tank was then filled with 1x TAE buffer and given another 30 minutes to set completely at room temperature. TAE agarose gels were run for 45 minutes at 90 V, 200 mA, the appearance of bubbles indicated successful connections. TAE buffer was not reused due to changes in buffer pH between each electrophoresis run.

Table 21. Table of TAE agarose gel percentages (w/v). A 1% w/v gel was routinely used.

DNA molecular weight (base pairs)	Percentage TAE Gel, %
1000 – 30,000	0.5
800 – 12,000	0.7
500 – 10,000	1.0
200 - 3000	1.5

2.4.2 Oligonucleotides

The cloning of open reading frames was routinely performed by polymerase chain reaction using bespoke oligonucleotides complementary to the genes of interest. To do this, short (~30 bp), nucleotide fragments were designed to be complementary to a region down- and upstream of the start and stop codons, respectively. Sequence lengths were selected based upon the melting temperature (T_m) and overall GC content (%) of the DNA annealing region. Both parameters were between +50-55^{o}C and 45-50%, respectively as determined by an oligonucleotide calculator (Serial Cloner, Fr). The reverse and reverse complements of each DNA sequence were calculated using an online calculator (http://www.bugaco.com/calculators/dna_reverse_complement.php).

Once designed, oligonucleotides (**Table 22**) were synthesised by MWG Eurofins (GmbH) and purified by HPSF to a concentration of 100 pM.

Table 22. Oligonucleotides used in this study. Restriction sites underlined; nucleotide sequences of fusion tags are in bold.

Oligonucleotide Name	Sequence (5'-3')
aco1_F_xba-1	GCCGCTCTAGAATGAGCAACCCATTCGCACACCTTGC
aco1_R_sal-1	GCGGCGTCGACCTACTTGGCCATCTTGCGGATCA
F_sufcb_xma1	GCCGCCCCGGGATGGCGCAGCCTATTTTGAACGTT
R_sufcb_ecor1	GCGCGCGAATTCTCAGAACCCCTCCTTGCTCGC
R_ecor1_sufcb_HIS	GCGGCGAATTCTCA**ATGATGATGATGATGATG**GAACCCCTCCTTGCTCGCC
R_ecor1_sufcb_HA	GCGGCGAATTCTCA**CGCGTAGTCCGGGACGTCGTACGGGTA**GAACCCCTCCTTGCTCGCC
F_cmah	GCCGCGGATCCATGATGGACAGGAAACAGACAGCTG
R_cmah	GCGGCGTCGACCTA**CGCGTAGTCCGGGACGTCGTACGGGTA**ATCACAGTGCATTAGGAACGAC
MatRight	AGTCACATCAAGATCGTTTATGG
MatAlph_HML	GCACGGAATATGGGACTACTTCG
Mata_HML	ACTCCACTTCAAGTAAGAGTTTG

2.4.3 Amplification of DNA by Polymerase Chain Reaction.

All open reading frames were amplified by polymerase chain reaction (PCR). Prior to running the PCR, the reaction cocktail (**Table 23**) was maintained on ice to avoid denaturing the polymerase. After assembling the cocktail, the tubes were briefly centrifuged (5 seconds at 4000 rpm) and placed in a thermocycler (Techne TC312, UK) under the conditions detailed in **Table 24**.

Table 23. PCR Recipe Mix for 100 µL Reaction. Vol. = volume.

Component	Vol. from stock (µL)	Final Concentration
Taq Buffer (10X)	20	1X
dNTPs (10 mM)	10	200 µM
MgCl2 (20 mM)	5	2 mM
Oligonucleotides (100 pM/µL)	1	0.2 µM
Template DNA	1	<50 ng
Taq Polymerase	1	2.5 U
MQ ddH_2O	61	-----

Table 24. Thermocycler settings, denaturing conditions varied with amplicon. Denaturing temperature was adjusted to the melting temperature of the oligonucleotide and increased or decreased, as necessary (e.g. appearance of non-specific bands following PCR). Other parameters were maintained regardless of the cloning template.

Stage	Temperature (^{0}C)	Duration (hr:min:sec)
Preheated Lid	+105	00:05:00
Annealing	+92	00:00:45
Denaturing	+45-55	00:01:00
Extension	+72	1 min/1 kbps
Final Extension	+72	00:10:00
Hold	+20	Indefinite

2.4.4 PCR Clean up

It is a requirement to remove salts and primer dimers from PCR reactions that might otherwise interfere with downstream applications, e.g. ligation. Once the PCR had finished and had been confirmed to be successful by analysing a small aliquot of the total reaction on TAE electrophoresis, the amplified DNA was immediately purified from contaminants using a PCR Clean-up kit (Qiagen, UK), according to manufacturer's instructions.

2.4.5 Gel Extraction

Digests or PCR products were analysed by TAE electrophoresis, and purified using a gel extraction spin column kit (Qiagen, UK). All steps were carried out according to manufacturer's instructions albeit with a 70 µL elution with elution buffer at the final step to increase yield (advice from L. Josse).

2.4.6 Restriction Enzyme Digests

For a 40 µL reaction, the following components were carefully aliquoted in a sterile 1.5mL Eppendorf tube, starting with the smallest volumes first **(Table 25)**. The reaction cocktail was then left to incubate in a pre-heated dry bath (Eppendorf, UK) set to +37°C, for 2 hours shaking at 500 rpm. Before analysing, digests were briefly centrifuged for 5 seconds at 4000 rpm in order to resuspend the condensate and if necessary, stored at -20°C. Restriction enzymes were sourced from New England Biolabs (NEB, UK) and where possible, only High Fidelity (HF) enzymes were used.

Table 25. Recipe for Restriction Enzyme Digest, 40 µL. Although this ratio could be adjusted for larger or smaller volumes. Vol. = volume.

Component	Vol. (µL)
Relevant Buffer (10X)	4
DNA	15
Restriction Enzyme	1 (per enzyme)
MQ ddH_2O	19

2.4.7 Ligation of DNA products

Purified DNA products (pBEVY plasmid and purified amplicon insert) were ligated according to NEB Quick Ligase kit (NEB, UK), following manufacturer's instructions. For routine ligations, an insert: vector, ratios of 0:1 (water control) and 3:1 were routinely used to infer successful reaction. Ligation ratios were calculated using (http://nebiocalculator.neb.com/#!/ligation) and increased if necessary.

2.4.8 Plasmid constructs

The pBEVY plasmid constructs **(Figure 23)** used for this study were obtained from the T. von der Haar communal stock and carried the uracil (*ura3*) and leucine (*leu2*) markers for selection of auxotrophs (Pronk, 2002). Plasmids were stored in a 1.5mL Eppendorf tube (Eppendorf, UK) and dissolved commercial elution buffer (Qiagen, UK) at -20ºC

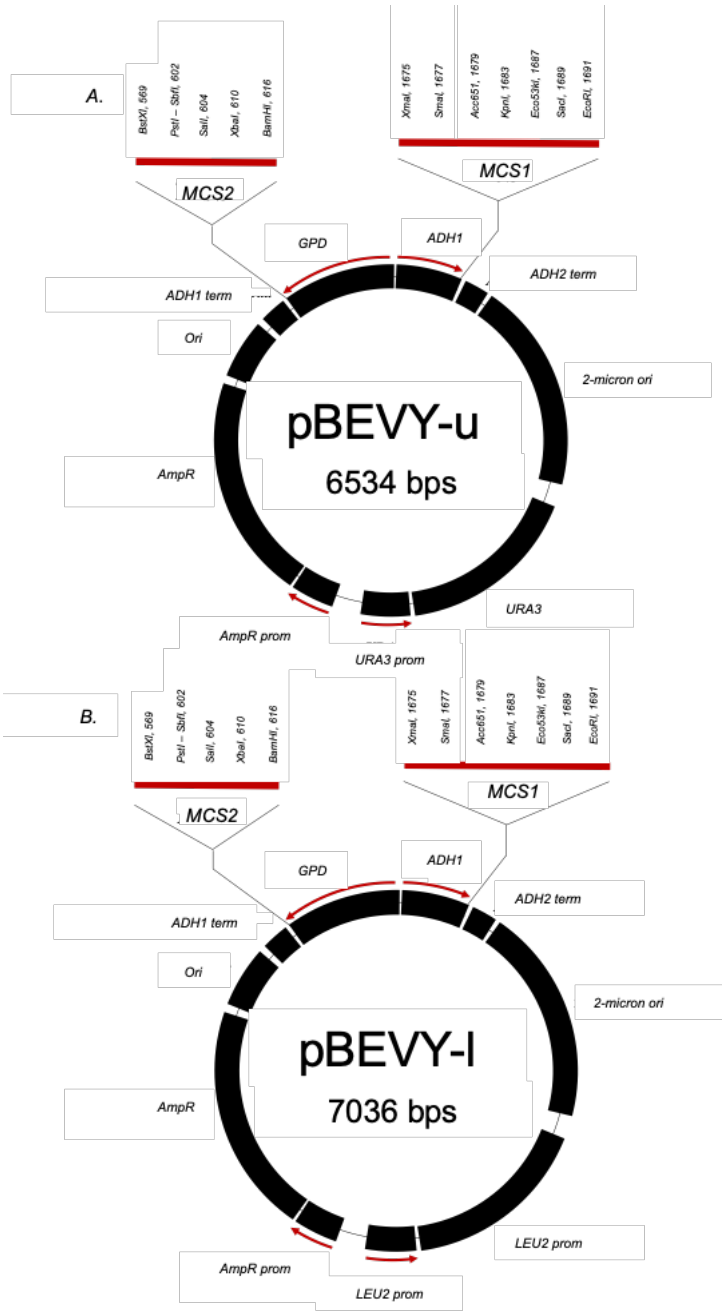

Figure 23. Maps of the multiple-copy (2µ) plasmid constructs used for cloning throughout this study. Multiple cloning sites (designated MCS1/2) on each plasmid which contains all restriction enzymes are shown. The names and molecular weights of the plasmids are shown in the centre, followed by bp (base pairs). The bidirectional promoter (GPD and ADH1) is indicated by a red double-headed arrow on each plasmid.

2.4.9 Quantification of DNA

DNA extracts were quantified by UV spectroscopy on a nanovolume spectrophotometer (NanoDrop 3000, Thermo Fisher) at OD_{260nm}. The quality of the samples was given by a ratio of 260/280 and 260/230, indicative of protein and salt contamination, respectively. The concentrations of DNA were given in ng/µL, MilliQ water and elution buffer were used as blanks as per manufacturer's instructions.

2.4.10 DNA Sequencing of constructs

Sequencing was performed using GATC LightRun (Eurofins Genomics, DE) and pre-printed barcodes. 100 ng of plasmid was mixed 5 µL of commercially available oligonucleotides (M13r and pADH1) in a 10 µL total volume. The tubes were then sealed by parafilm and placed in a 50 mL falcon tube for protection. The sequences were analysed in Serial Cloner software (Serial Basics).

2.5 Yeast molecular biology

2.5.1 Yeast transformations

Plasmids containing genes to be expressed were transformed into BY4741 following the Lithium Acetate/PEG_{4000} transformation method (Ito et al., 1983). Briefly, the components were assembled in a sterile 1.5 mL Eppendorf tube (Eppendorf, UK) according to **Table 26**.

Table 26. Yeast Transformation Cocktail. Values are given for a routine transformation.

Component	Vol. (µL)
Poly-ethylene Glycol 4000 (50% w/v)	240
Lithium Acetate (1M)	36
Single Stranded DNA (1 mg/mL)	10
Beta-mercaptoethanol (14.3M)	2.5
Plasmid	2-5
MQ ddH_2O	69.5-67.5

After assembling the reaction, the tube was left to incubate at ambient temperature for 20 minutes. Following this, the reaction was incubated in a pre-heated water bath (Eppendorf, UK) at +42°C. After incubation, the mix was washed by centrifugation in a benchtop centrifuge for 5 minutes at 4000 rpm, ambient temperature. The supernatant was then discarded completely before the pellet was resuspended in 200 µL sterile RO ddH_20. The cell suspension was then plated onto appropriate drop-out media and incubated for 2-3 days at +30°C until single colonies appeared. For particularly sensitive mutants, heat shock was omitted, instead, the reaction mixture was left at ambient temperature overnight before following through with centrifugation and plating steps.

2.5.2 Yeast Sporulation

Heterozygous deletion mutants were sporulated under starvation conditions on SPOR plates. After five days of incubation at +30°C, the cultures were checked for the appearance of tetrads. The digested cells were dissected as soon as a reasonable number of tetrads could be observed (~50%).

2.5.3 Micromanipulation of Yeast

YPD plates were made 24 hours before and thoroughly dried. One-quarter of the plate was then segmented using a marker. One ‘pin-head’ sized sample of sporulated yeast was then resuspended in 0.5% v/v Zymolyase (0.5 mg/mL, Sigma, UK) and left to incubate at ambient temperature for 5 minutes. 10 µL of the digestion mix was then aliquoted onto the marked off the quarter and spread gently within that quarter using a sterile inoculating loop. Following this, visible tetrads were dissected using a MicroManipulator (Singer Instruments, UK) into the respective spores along the X-axis, with tetrads on the Y-axis. 12 tetrads were dissected for each mutant, to accommodate for poor spore recovery. One well-dried YPD plate was used per mutant or control to be screened. Plates were then sealed with parafilm and allowed to grow in a static +30°C incubator for 5 days.

2.5.4 Colony PCR for Mating Type Determination

A genotype of interest (in this instance mating type) of a colony was assessed using oligonucleotides against a specific locus. Briefly, roughly 1/10th of a colony was aseptically added to 50 µL PCR master mix (Promega, UK). For mating-type determination, haploid/diploid positive controls were included as either BY4741 or heterozygous diploid control (BY4743). Once the reaction had been assembled it was placed in a thermocycler for amplification.

Table 27. Thermocycler settings for mating-type colony PCRs.

Stage	Temperature (^{0}C)	Duration (hr:min:sec)
Preheated Lid	+105	00:05:00
Annealing	+92	00:00:45
Denaturing	+58	00:02:00
Extension	+72	00:02:00
Final Extension	+72	00:10:00
Hold	+20	Indefinite

Bands at 544 bps and 404 bps or 1 band of either size following TAE gel electrophoresis and EtBR straining indicated diploid and haploid strains, respectively.

2.6 Yeast phenotypic assays

2.6.1 Automated growth rate analysis

Growth fitness assays were performed by continually measuring the absorbance of actively growing cultures at an optical density (OD) of OD_{600nm} in a Spectrostar NANO plate reader (BMG Lab tech, UK) using the following settings; double shaking orbital mode, 3 mm diameter shaking width, 1837 second cycle time, 0.5 second positioning delay. The specific growth rate was quantified in Microsoft Excel (Microsoft, US) by applying an exponential trend-line across a three-hour time period and the whole data set was scanned for the highest gradient which also gave the highest R^2 value to ensure accurate depiction of fastest growth rate phase (i.e. flattest gradient). The natural logarithm of 2 was then divided by X, to give doubling time in minutes. The reciprocal of this value was then taken for specific growth rate (Generations per hour, appreviated to Gens/Hr).

2.6.2 Spot plating

Working cultures were resuspended in 90 µL of sterile drop-out media in a sterile flat-bottom 96-well plate (Corning CoStar) and incubated on a microplate shaker (VWR, UK) at +30ºC for 3 hours to allow cells to re-enter logarithmic phase. A second sterile 96-well plate was then used to prepare 5-fold serial dilutions, in which 90 µL of sterilised (autoclaved) 1x PBS (Gibco, UK) was aliquoted using a multichannel pipette (BrandTech Transferpette S-8). 100 µl of culture was then added to the first row before being serially diluted (10 µL culture, in 90 µL of PBS) five-times. An 8 x 6 pin replica plater (Sigma Aldrich, UK) was then sterilised using ethanol and flame, allowed to cool for 10 seconds and placed into diluted cultures, left for 10 seconds to allow attachment, and then quickly and firmly placed upon a dried agar plate. Cultures were incubated at +30ºC for at least 24 hours before colonies were checked. Longer incubation periods were required for certain mutants and assays (Ecm17 assay).

2.7 Protein Work

2.7.1 Denaturing Protein Extraction

If the protein extract was to be loaded straight onto SDS-PAGE, proteins were extracted exactly as described in von der Haar et al., (2007).

2.7.2 Native Protein Extraction using Yeast Protein Extraction Reagent (YPER)

Crude Extracts for enzyme assays, IMAC and coimmunoprecipitation were extracted using Yeast Protein Extraction Reagent (YPER), according to manufacturer's instructions (ThermoFisher, UK).

2.7.3 Native IMAC Purification

5 mL of fast chelating NTA sepharose (GE Healthcare, UK) was loaded into an empty PD10 column (GE Healthcare) and washed with 5 mL MQ ddH_2O which eluted residual ethanol. The sepharose was then charged with 1 column volume of 0.2 M $NiCl_2$ solution. The resin bed was then equilibrated with 10mL binding buffer (300 mM NaCl, 100 mM Tris-HCl, 5 mM imidazole, pH 7.5) and flow-through discarded. Crude protein extract from was then pipetted onto the column and total flow through collected, then placed back through the column. Two millilitres of the second flow-through was then collected in 2mL Eppendorf tubes for later analysis by SDS-PAGE. The resin bed was then washed with 5 column volumes of binding buffer, 5 column volumes of wash buffer I (300 mM NaCl, 100 mM Tris-HCl, 5% v/v Glycerol, 10 mM Imidazole, pH 7.5) and II (300 mM NaCl, 100 mM Tris-HCl, 5% v/v Glycerol 15 mM Imidazole, pH 7.5) in succession. Then eluted with 250 mM Imidazole (300 mM NaCl, 100 mM Tris-HCl, 5% v/v Glycerol, 250 mM Imidazole, pH 7.5).

2.7.4 Denaturing IMAC Purification

Denaturing IMAC was performed in the same fashion as native, albeit with 8 M Urea added to all buffers.

2.7.5 Anaerobic IMAC

Purification of native cluster-bound proteins was performed in an anaerobic workstation (<2ppm [O_2], Belle Technology) using buffers that had been sealed and then bubbled with nitrogen. All buffers were prepared a day in advance and after bubbling with nitrogen, left to degas in a glove box overnight and were prepared to the same recipes in 2.7.3. Lysate was loaded onto on Akta Prime system (GE Healthcare, UK) and a 5 mL HiTrap Ni^{2+}-chelating column (GE Healthcare, UK) was used at a flow rate of 1 mL/min. The passage of coloured material was used to infer successful protein purification. Proteins were eluted by inverting the HiTrap column and using a 12 mL syringe, 10 mL elution buffer was passed through the column, the migration of a visibly brown coloured fraction was used to infer successful elution. The elution step was stopped when all of the coloured fraction had left the column, which could be seen in the now-coloured elution fraction (500 µL). The

darkest fractions were then concentrated using spin concentrators (Amicon, UK), and analysed for cluster binding by UV/Visible spectroscopy (260 – 900 nm) on a JASCO Spectrophotometer (JASCOInc, USA).

2.7.6 Desalting with PD10 columns

Protein fractions were desalted using pre-loaded PD10 columns (GE Healthcare, UK) according to the manufacturer's instructions.

2.7.3 Separation of Proteins by SDS-PAGE

SDS-PAGE was routinely used for the separation of proteins. Routinely, a 10% v/v gel was used, which gave sufficient resolution of high molecular weight products. Resolving gels were cast to roughly 75% of an empty gel cassette (1 mm thickness, Invitrogen, UK) and overlaid with water for a level resolving bed (**Table 28**). Once set, the 10% 'resolving' gel was then overlaid with a 5% v/v 'stacking' gel and comb in order to allow proteins to separate into lanes **(Table 29)**.

Table 28. Recipe for SDS-PAGE resolving Gels. Standard recipe for a 10% v/v acrylamide gel (resolving).

Component	Volumes for 10% v.v
30% v/v Acrylamide	3.6mL
4x Lower Tris, pH 6.8	2.7mL
Deionised Water	4.5mL
APS	40 µL
TEMED	10 µL

Table 29. Recipe for SDS-PAGE stacking Gel. Standard recipe for a 5% v/v acrylamide gel (stacking).

Component	Volumes for 5% v/v
30% v/v Acrylamide	2.7mL
4x Lower Tris, pH 8.8	2.7mL
Deionised Water	5.4mL
APS	40 µL
TEMED	10 µL

2.7.4 Western Blotting

Western blots were used throughout for the detection of target proteins, either directly or via tag (e.g. haemagglutinin, HA). Following separation by SDS-PAGE, the unstained acrylamide gel was removed from its cassette and measured. Following this, one rectangle of polyvinylidene fluoride (PVDF) membrane (Merck, UK) and two rectangles of blotting paper (Whatman, UK) were cut using a guillotine, exactly to the size of the resolving gel being run (roughly 8 cm x 6 cm but exact measurements were taken for each gel). Nitrile gloves were worn and changed regularly avoid protein contamination of PVDF. PVDF was then activated for 30 seconds (until a colour change of PVDF) in >99% v/v analytical grade methanol (Sigma, UK) and quickly placed, with the pre-cut blotting paper (2x) in a clean 200 mL container with 50mL transfer buffer (180 mM Glycine, 20 mM Trisma-base, 2% w/v SDS, pH 7.2) . The SDS-PAGE gel was then placed in the same container to allow all components to equilibrate for 30 minutes at ambient temperature.

Transfer of proteins to PVDF was performed by assembling a sandwich consisting of paper, PVDF, gel, paper and then ran at 9 V for 45 minutes (depending on the size of the target protein and concentration of SDS-PAGE) in a semi-dry blotter. Before running the transfer, the overlay of Gel and PVDF was gently rolled before the whole sandwich was gently purged of air bubbles with the same roller. After transfer, the PVDF was removed and placed in 5% w/v blocking buffer (TBS, 5% w/v milk powder) and blocked, gently rocking, at ambient temperature for 60 minutes. Transfer efficiency was loosely determined by the transfer of coloured marker to PVDF, or for a more precise method, 1x Ponceau stain was used. After blocking, the PVDF membrane was incubated in the primary antibody to the desired concentration. This step was performed either overnight in a cold room or at room temperature, depending on the target protein (anti-GFP was amenable to room temperature incubations).

The primary antibody solution was then carefully decanted into a waste sink and the PVDF was washed in blocking buffer three times before 10 mL of blocking buffer containing secondary antibody was added and the reaction incubated at ambient temperature for 2 hours After this incubation, PVDF was again washed in 20 mL of Tween buffer (TBS, 0.05% v/v Tween-20) three times, placed in 1x PBS and developed used ECL. The PVDF was kept wet throughout.

2.7.5 Enhanced Chemiluminescence Detection (ECL)

ECL was used for the detection of horse-radish peroxidase (HRP) conjugated antibodies. Two solutions (**Table 30**) were made (solution 1 was protected from light with aluminium foil), mixed together on top of the PVDF and incubated at ambient temperature for 2 minutes inside a dark gel doc room. The ECL signal was then quantified using a GeneSys Gel doc (G: Box, Syngene, UK) with accompanying software. The ECL signal was analysed at 10 seconds, 30 seconds, 1 minute, 2 minutes and 5 minutes exposure time.

Table 30. Homemade ECL Solutions. Solutions were dissolved in RO water and solution 2 was protected from light.

Solution	Components (10mL in RO ddH_2O)
Solution 1	100 µL Luminol, 44 µL Coumaric Acid, 1 mL Tris pH 8.5
Solution 2	6.4 µL H_2O_2, 1 mL Tris pH 8.5

2.7.6 Co-immunoprecipitation

Co-immunoprecipitation experiments used commercially available anti-HA magnetic beads (Roche, UK) and HA-tagged fusion protein of interest (SufCB). The beads (25 µL) were used and washed according to manufacturer's instructions in 175 µL of protein buffer (20 mM Tris, 100 mM NaCl, 5 mM MgCl2, 2.5 mM β-ME, pH 7.2). Lysate was added to the beads at a final volume of 1mL, incubated on a rotating platform for at least 45 minutes, and then washed thoroughly in five sets of 2 mL protein buffer to remove non-specific contaminants. Tips were changed each time and care was taken to ensure that samples were not mixed as this could yield false positives. The unbound samples were saved for further analysis. After washing, the protein-bead complexes were eluted by adding 500 µL of protein buffer (above) and then boiling the solution at +95^{o}C for 10 minutes. Samples were stored at -80^{o}C until analysed.

2.7.7 Protein Quantification

2.7.7.1 Quantification by UV-spectroscopy

Protein fractions from IMAC and for iron-sulfur cluster reconstitution were quantified according to absorbance at OD_{280nm}.

2.7.7.2 Quantification by Bradford Reagent (Micro Assay)

Total protein content for enzyme assay was carried out using Bradford Reagent (BioRad, UK), according to manufacturer's instructions in micro (2 mL format).

2.8 Iron-sulfur enzyme activity assays

2.8.1 Sulphite Reductase assay

Two versions of this assay were used. A qualitative plate-based format where yeast was plated until coloured colonies appeared after 5-7 days was used for mutant screening. Alternatively, liquid media was used for quantitative assays in which the bismuth precipitate was measured. After the incubation period at +30^{o}C, 175 rpm, cultures were then harvested by centrifugation at 4000 rpm for 10 minutes and cells lysed to release precipitate using 250 mM NaOH. The precipitate was then quantified by absorbance at OD_{490nm}. Cells were then counted used a haematocytometer to normalise absorbance to the number of cells per sample (expressed as CFU/mL).

2.8.2 Isopropylmalic acid Isomerase (Leu1) activity

Samples were prepared by harvesting (4000 rpm, 15 minutes, +4^{o}C) and then chemically lysing 50 mL of exponential (an OD_{600nm} of 1.0-1.5) cultures using YPER, according to manufacturer's instructions. Supplementation of YPER with 5 mM dithiothreitol (DTT) (Melford, UK) was found to be essential at this stage to maintain Leu1 activity. Lysis was performed by agitating the resuspended pellet on a thermoshaker (Eppendorf, UK) at 600 rpm for 40 minutes at ambient temperature, the resulting lysates were then clarified by centrifugation at 14,300 rpm for 15 minutes, +4^{o}C in a temperature-controlled benchtop centrifuge (Eppendorf, UK). The supernatant generated from this step was then used for all activity assays. To quantify activity, 20 µL of the supernatant was added to a 1 mL UV-cuvette (Sarstedt, UK) and the reaction was initiated by the addition of reducing enzyme buffer (250 mM NaCl, 50 mM, 5 mM DTT Tris-HCl, pH 7.5) supplemented with 1 mM 2-isopropylmalic acid (Sigma, UK) to a final volume of 1mL, this enabled mixing. The spectrophotometer (Eppendorf, UK) was then blanked using the crude mix and the absorbance followed for 15 minutes.

2.8.3 Total aconitase activity assays

For total aconitase activity, samples were prepared in the same manner as for Leu1. However, the enzyme buffer (250 mM NaCl, 50 mM Trisma base, pH 7.2) was supplemented with 1 mM sodium citrate (Sigma, UK) and the absorbance followed in a spectrophotometer (Eppendorf, UK) at OD_{240nm} until a plateau was reached. DTT was omitted from all buffers.

2.8.4 Iron-sulfur cluster reconstitution

The concentration of purified protein quantified by spectroscopy in a reduced volume cuvette at 280nm and then reduced using 5 mM DTT for 30 minutes in a glove box (O_2 < 2 ppm; Belle Technology). The reduced protein (2 mg/mL) was then resuspended in 1mL of reconstitution buffer (300 mM NaCl, 100 mM Tris-HCl, 10% v/v Glycerol, pH 7.5) and incubated with a 4-fold molar excess of iron (III) citrate alongside 1 µL of purified PLP-loaded NifS (0.4 mg/mL, produced by J. Crack) to convert L-cysteine to sulfide. The contents of the cuvette were then mixed by inversion. The screw-lid cuvette was then tightly sealed a and transferred to a JASCO Spectrophotometer (JASCOinc, USA) for wavelength scanning at 260 - 900 nm.

2.8.5 Fluorescence-Activated Cell Sorting (FACS)

FACs assays for GFP intensity were performed using BD FACScaliber Flow Cytometer (BD Biosciences, UK) and used (start-up, usage and shut-down procedures) according to manufacturer's instructions (BD Biosciences). GFP intensity was quantified by histogram under FL-1 channel and compared against non-GFP strain to accommodate for auto-fluorescence. Experiments were routinely performed with four biological replicates on 50 µL of logarithmically growing cells diluted in 3mL of 1x sterile PBS.

2.8.6 Dual-luciferase assay for stop-codon readthrough

The activity of Rli1 was assessed by quantifying stop-codon readthrough of a Firefly/Renilla luciferase fusion. Two constructs were used which either contained a single firefly luciferase ORF or a fused Firefly/Renilla luciferase ORF, separated by a stop codon. The ratio between Firefly to Renilla luciferase could then infer stop-codon readthrough. Transformed yeast were grown for 16 hours in 96-well microplates (100 µL volume) at +30^{o}C and then sub-cultured (1/10) into fresh media and incubated at +30^{o}C for 3 hours, to the allow cells to re-grow into exponential phase. Cells were stressed (if necessary) throughout both incubation periods. Dual-luciferase assays were performed according to a commercially available dual-luciferase kit (Promega, UK) using white opaque microplates. The constructs encoding the fused luciferase proteins (pTH460 and pTH469) were sourced from T. von der Haar stock. Plate measurements were performed using a FluoroStar microplate reader (BMG Labtech) and a pre-set bioluminescence programme (TobiasLuc). Readthrough was calculated by measuring the ratio of bioluminescence of Firefly luciferase to Renilla luciferase after sequentially activating each enzyme. A higher activity of Renilla luciferase indicated more stop codon readthrough.

2.9 Microscopy

2.9.1 Sample Preparation

Working cultures were prepared and re-diluted to OD_{600nm} of 0.1 then allowed to re-enter logarithmic phase (OD_{600nm} >1.0, max of 1.5). 100 µL of culture was then pelleted by gentle centrifugation at 3000 rpm for 2 minutes, washed once with 200 µL 1x sterile PBS, re-harvested and resuspended in 20 µL of sterilised 1x PBS.

2.9.2 Fluorescent Microscopy

Microscopy was performed using an Olympus MT20 fluorescence microscope (Olympus Life Science, UK), connected to a PC running MicroManager software (Edelstein et al., 2010). DAPI stain (Sigma, UK) was used for the detection of nuclei by adding appropriate volume (1 µL per 1 mL) to actively growing cultures and incubating at +30°C for 20 minutes. Incubation time was reduced or prolonged depending on the signal obtained. Nuclei were routinely visualised under filter 1 and excitation of 406 nm. GFP fluorescence was quantified under filter 5, excitation at 490 nm.

2.9.3 Immunofluorescence

To localise SufCB protein in yeast, working cultures were prepared and grown to logarithmic phase to ensure expression of SufCB. Cells were first fixed in 35% v/v formaldehyde (5% v/v) final concentration, for 60 minutes at ambient room temperature (+22-25°C). Cultures were pelleted and washed twice in 1 mL of sterile (autoclaved) immunofluorescence buffer at 3000 rpm for 2 minutes each and finally resuspended in 50 µL of sterile immunofluorescence buffer (100 mM Tris-HCl, 5% sorbitol, pH 7.2), plus 1 µL β-mercaptoethanol (β-ME, Sigma, UK) and 20 µL of 1 mg/mL Zymolyase (Sigma, UK). Resuspended cells were then digested at 37°C for 40 minutes. During this step, 15 µL of 1 mg/mL poly-l-lysine was aliquoted onto a clean microscope slide and allowed to dry at room temperature, before being gently washed off using sterile RO ddH_2O. 15 µL of the washed culture was aliquoted onto the dried PLL spot and allowed to settle for 5 minutes. The excess culture was then gently removed by aspiration using a cut-off blue tip on a p1000 pipette. And 10 µL of 0.1% w/v SDS was added per sample for 30 seconds each and quickly washed again with 20 µL of PBS + 1 mg/mL BSA, ten times. Care was taken from this point on to maintain a damp environment, by placing slides in a plastic container on damp tissue paper. Primary antibody (anti-HA from rabbit, Abcam, UK) was diluted in 1x PBS with 1 mg/mL BSA to 1:2000 dilution and 15 µL added per sample before being left in a damp environment for four hours at room temperature. Following this, samples were gently but thoroughly washed again 10 times using 20 µL 1x PBS + 1 mg/mL BSA before 15 µL of secondary antibody (FITC-conjugated Anti-rabbit) was then aliquoted onto the sample. Slides from this point were in a dark environment to avoid bleaching the fluorophore for 1 hour. A drop of phenylenediamine mounting solution (65 mM in 20% v/v EtOH) containing 1 mg/mL DAPI was placed on top of the cells. A 22mm x 22mm coverslip was then gently but firmly applied to the slide, avoiding air bubbles. Edges were then sealed using nail varnish ready for visualisation.

2.10 Bioinformatics and Data Analysis

2.10.1 Multiple Sequence Analysis using PRALINE

Primary sequences were inputted into PRALINE Multiple sequence alignment software in FASTA format and analysed under default settings. Software was developed by Simossis and Heringa (2005).

2.10.2 Motif Identification using MEME Suite

FASTA sequences were entered into the MEME suite server using all default settings apart from motif search was increased to 50 sites per protein. Software was developed by Bailey et al., (2009).

2.10.3 IUPRED for Intrinsically Disordered Proteins

FASTA sequences were entered into IUPRED using default settings and data downloaded as comma-separated values (.CSV) file. Software was developed by Dosztányi et al., (2005).

2.10.4 BLAST Searching

Homologous protein sequences were identified using NCBI Blast P-suite, searching non-redundant protein sequences, default settings. Software was developed by Johnson et al., (2008).

2.10.5 Data analysis

Raw data was archived and analysed in Microsoft Excel 365 and statistical analysis performed in Minitab 18. Figures were made in vector programs, Paint.net, Veusz and Microsoft PowerPoint.

Introducing the SufCB protein into *S. cerevisiae*.

3.1 Chapter aims

The overarching aim of this research chapter was to demonstrate that yeast is a suitable host for the SufCB protein. As a model organism, the molecular 'toolbox' available for genetically manipulating yeast contains many useful technologies which continue to contribute the advancement of biotechnology (Huang et al., 2014; Nielsen, 2013; Raj et al., 2018). One area that is lacking for yeast-based platforms, however, is a method to highly express recombinant iron-sulfur enzymes.

In this chapter, we describe the procedures that were used to create the SufCB-expressing cell factory. The experimental design for this work included a simple cloning procedure which used restriction enzymes to insert the open reading frame of SufCB into a high copy non-integrating yeast expression vector, pBEVY (Miller et al., 1998). The first sections describe this process and findings therein. To date, no SufCB protein has been expressed within *S. cerevisiae* and so as a novel system, we will also explore phenotypes and begin to characterise the SufCB protein as expressed in yeast.

To achieve this, the following objectives were tasked.

i. To develop a cloning method to insert the SufCB open reading frame into a suitable expression vector.

ii. To develop a western blotting protocol which establishes that SufCB had been expressed as full-length protein and that its molecular weight is comparable to previous descriptions (Tsaousis et al., 2012).

iii. To perform localisation experiments which determine where SufCB may exist *in vivo*.

iv. To perform phenotypic growth assays which determine how expressing SufCB may affect the cell biology of the host yeast.

3.2 Generating a yeast expression vector containing SufCB

The SufCB open reading frame (ORF) was amplified from *Blastocystis* cDNA (A. Tsaousis stock) into the pBEVY-u expression vector (T. von der Haar stock). Analysing the *Blastocystis* SufCB nucleotide sequence in Serial Cloner (SerialBasics, U.S.A.) software enabled us to design oligonucleotides for the initial amplification of SufCB (chapter 2.4.2) and gave an expected molecular weight of SufCB as exactly 2100 base pairs (2.1 kbps). We chose to use the pBEVY series these contain a high-copy number (2μ origin) and a strong bidirectional promoter which has been previously evidenced to produce high levels of recombinant proteins in yeast (Miller et al., 1998). There is also some conflicting evidence that Leu2 markers alter the expression of iron-sulfur enzymes in yeast (Bedekovics et al., 2011), and so a Ura2 marker (pBEVY-u) was used as the base construct instead (Bedekovics et al., 2011). We also designed the oligonucleotides such that each SufCB amplicon contained 'sticky-end' recognition sites for *Xma 1 (5-C^CCGGG-3)* and *EcoR 1 (5-G^GATCC-3)* endonucleases (NEB, UK), which enabled SufCB to be ligated into the alcohol dehydrogenase (*ADH1*) cassette of pBEVY-u. The design of the SufCB construct is shown in **Figure 24**.

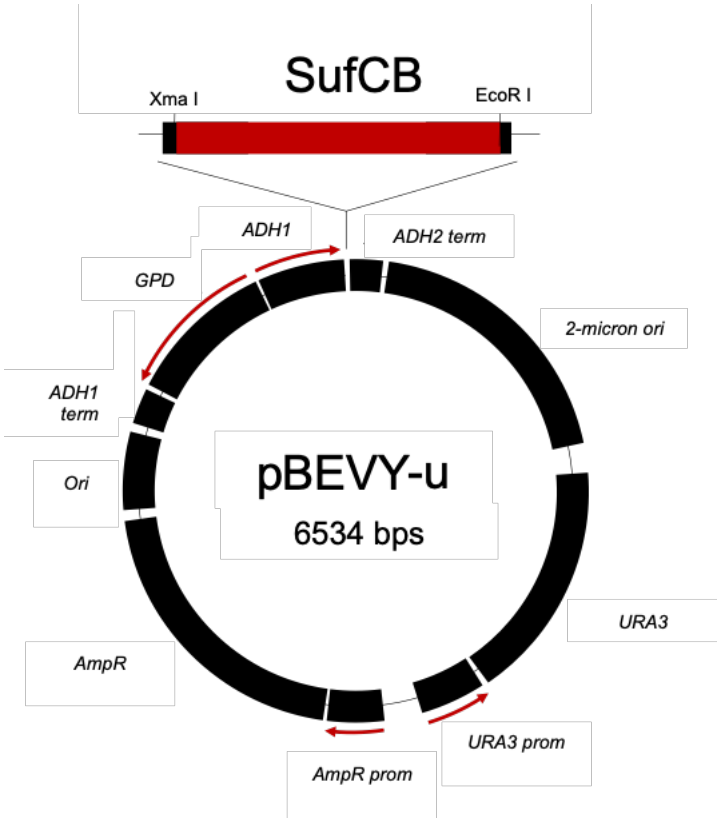

Figure 24. SufCB-construct based on pBEVY-u backbone containing SufCB ligated into the ADH1/ADH2 cassette (red arrow). The open reading frame (ORF) of SufCB is shown by a red bar protruding from pBEVY-u. The size of the SufCB ORF was exactly 2100 base pairs (2.1 kbps). The sequences for Xma1 and EcoR1 recognition sites were obtained from New England Biolabs (NEB), nebcloner.neb.com. The pBEVY-u sequence was obtained from Addgene, addgene.com. Restriction enzymes were chosen using restriction mapper database, restrictionmapper.org.

TAE electrophoresis on the entire (200 µL) PCR reaction was used to confirm a successful amplification of SufCB, and this gave us our starting material. Dense bands at ~2000 base pairs (bps) matching the SufCB ORF (2100 bps) were observed and taken to indicate a successful reaction.

Following the ligation of the purified SufCB amplicon product into pBEVY-u, the entire ligation reaction (10 µL) was transformed into chemically competent *E. coli* (*DH5α*) cells exactly as described in chapter 2.3.5.3, and positive clones (those which had taken up the SufCB-construct) were selected for using LB agar plates supplemented with 100 µg/mL ampicillin disulphate (Melford, UK). After incubating the bacterial transformants for 16 hours at +37°C any colonies which grew on the ampicillin plates were lysed and their plasmids purified using commercially available columns (Qiagen, UK) and analysed for successful integration of SufCB. The results of this are shown across both panels in **Figure 25**. Both gels show that a DNA fragment matching the molecular weight of SufCB (2.1 kbps) can be extracted from the ligated pBEVY-u construct (**Figure 25A**) and moreover the ligated construct can be used to amplify SufCB using the original SufCB oligonucleotides (**Figure 25B**). Both gels demonstrated that SufCB had been successfully integrated into pBEVY-u, and this was later confirmed using GATC lightrun (Eurofins, GmbH) sequencing **(Appendix 9)**. Serial Cloner software demonstrated that the molecular weight of the new SufCB-pBEVY-u construct (pSufCB) was 8.6 kbps.

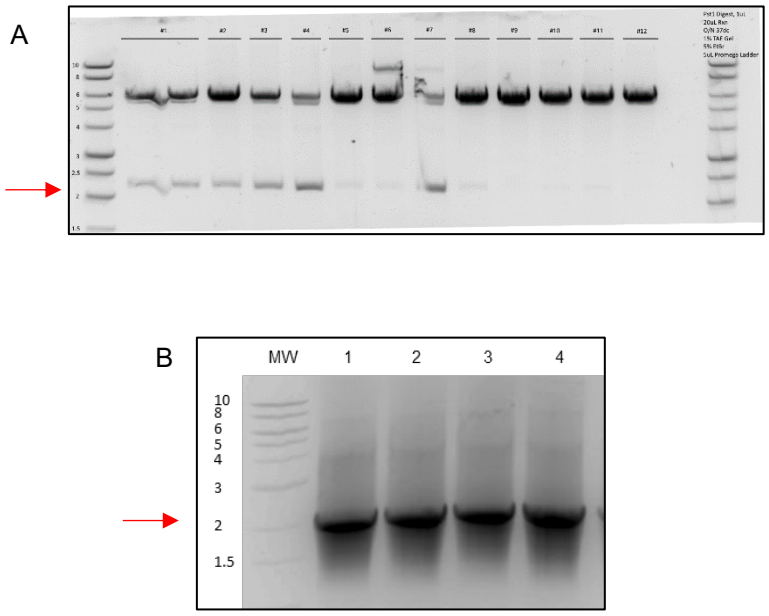

Figure 25. DNA electrophoresis gels (TAE agarose) showing the migration of the SufCB-bearing plasmid. A) After digestion with *EcoR* 1 and *Xma* 1, the numbers at the top of the lanes indicate the identifier of each positive clone, and B) PCR reaction of the construct using the original SufCB oligonucleotides, showing the amplification of SufCB. Both gels indicate that SufCB was successfully incorporated into the pBEVY-u plasmid. Note: Figure 25A used Generuler 1Kb, whereas figure 25B used hyperladder 1Kb. Gel Both gels indicate the presence of SufCB in the final construct. Red arrows indicate the band which matches the SufCB ORF.

3.3 Expression of full-length SufCB protein

Once confirmed to contain SufCB, the construct was then inserted into a commercially available yeast strain, BY4741, using the lithium acetate (LiAc)/PEG method (Ito et al., 1983). Successful transformation of BY4741 cells was confirmed by the growth of yeast colonies on media which lacked uracil (Ura- media, Formedium, UK). Once the SufCB construct had been transformed into the BY4741 yeast, we performed western blotting using a custom-made anti-SufCB antibody (Tsaousis et al., 2012) to confirm the expression of full-length protein.

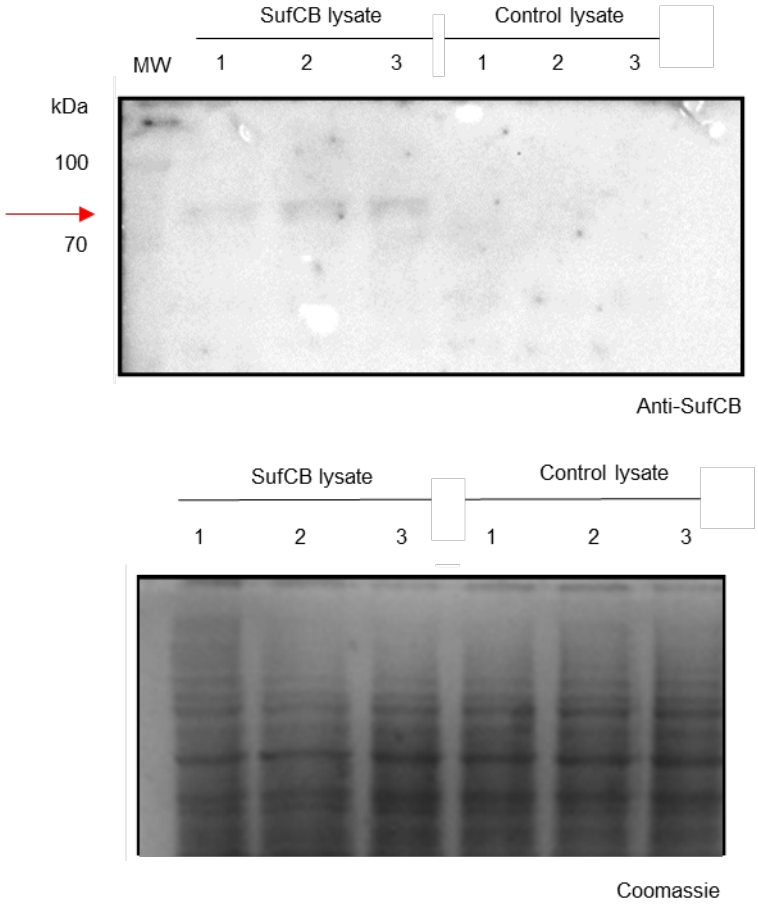

Figure 26. Detecting the SufCB protein in yeast cell-free lysates. A) Anti-SufCB Western Blot for expression of SufCB. B) Coomassie loading control. Proteins were separated using a 10% v/v acrylamide gel and the anti-SufCB antibody was diluted 1:5000. 20 µL of protein was loaded per sample, samples were analysed in biological triplicate. The SufCB protein is indicated by a red arrow. SufCB protein could not be seen on a Coomassie gel.

For this experiment, cell-free lysates were prepared from exponentially growing (OD_{600} of ~1.2) SufCB or control cultures and their proteins separated by SDS-PAGE electrophoresis. SufCB protein was then detected by enhanced chemiluminescence detection (ECL), **Figure 26.** Previous studies demonstrated that that full-length SufCB protein purified from *E. coli* and has a molecular weight of 77 kDa (Tsaousis et al., 2012). From this experiment it was confirmed that the SufCB protein had been successfully incorporated into the open reading frame of pBEVY's *ADH1* cassette. Furthermore, its mass when expressed and translated in *S. cerevisiae*, aligned with previous descriptions (77 kDa), indicating that full-length SufCB exists within the cell (Tsaousis et al., 2012).

3.4 SufCB is primarily localised to the cytosol

Having established that full-length SufCB protein can be translated by *S. cerevisiae* cells, immunofluorescent localisation of the protein was then performed in order to decipher its localisation within the cell. As SufCB localises to the cytosol in its native *Blastocystis* host, it was expected that the recombinant SufCB would also localise to the yeast cytosol, and this could infer that a functional protein was being produced (Tsaousis et al., 2012). For this experiment, a SufCB fusion was created containing a C-terminal haemagglutinin (HA) tag from which we were able to use commercially available anti-HA antibodies (Abcam, UK). Once fixed, cells were also stained with MitoTracker Red and DAPI for visualisation of the mitochondria and nucleus, respectively.

In the samples prepared from SufCB-expressing cells (**Figure 27**), SufCB signal (FITC channel) appeared as diffuse throughout the cell and did not co-localise with either mitochondrial or nuclear fluorescence, suggesting a cytosolic localisation (**Figure 27C-D**). MitoTracker Red dye showed long foci which appear in the centre of the plane of focus, in line with mitochondria (**Figure 27B**). Whereas DAPI staining show a single foci, indicative of nuclei (**Figure 27B**). Lack of fluorescence from either empty vector or SufCB incubated without primary antibody indicated that the high fluorescent intensity observed did originate from antibody cross-linking with the SufCB protein (**Appendix 11**) and not endogenous yeast proteins.

BUSCA (Bologna Unified Subcellular Component Annotator) (http://busca.biocomp.unibo.it/) was used to identify peptide sequences ‘signals’, that may influence where SufCB localises within cells (Savojardo et al., 2018). In addition to the *Blastocystis Nand II* SufCB studied here, we also analysed the five other SufCB’s (**SUF Fusion proteins, 1.3.2**) for the presence of organelle-targeting peptides in order to gain a greater understanding of each protein. Localisation prediction (given in percentage likelihood) was performed against a database of targeting peptides from fungi. Again, with the exception of the *Pygsuia* mitochondrial variant, analysis of these data predicted that SufCBs are likely cytosolic proteins with cytosolic prediction scores of >70% (**Appendix 10**). The three SufCB proteins which originate from the stramenophile lineage, *Blastocystis Nand II*, *Blastocystis* subtype 4 and *P. lactertae* were also predicted by the BUSCA server (>30%) to localise to the nucleus. It is of note that Nbp35 was also originally demonstrated to partially localise to the nucleus in *S. cerevisiae* (Hausmann et al., 2005). It is known that the CIA pathway matures nuclear iron-sulfur proteins, but these are matured within the cytosol and then imported into the nucleus (Stehling et al., 2018).

Overall our data suggest that the SufCB protein expressed in yeast is localised to the cytosol and that this is the default localisation of each SufCB protein, which would enable the SufCB proteins to function alongside or in place of their native CIA machinery.

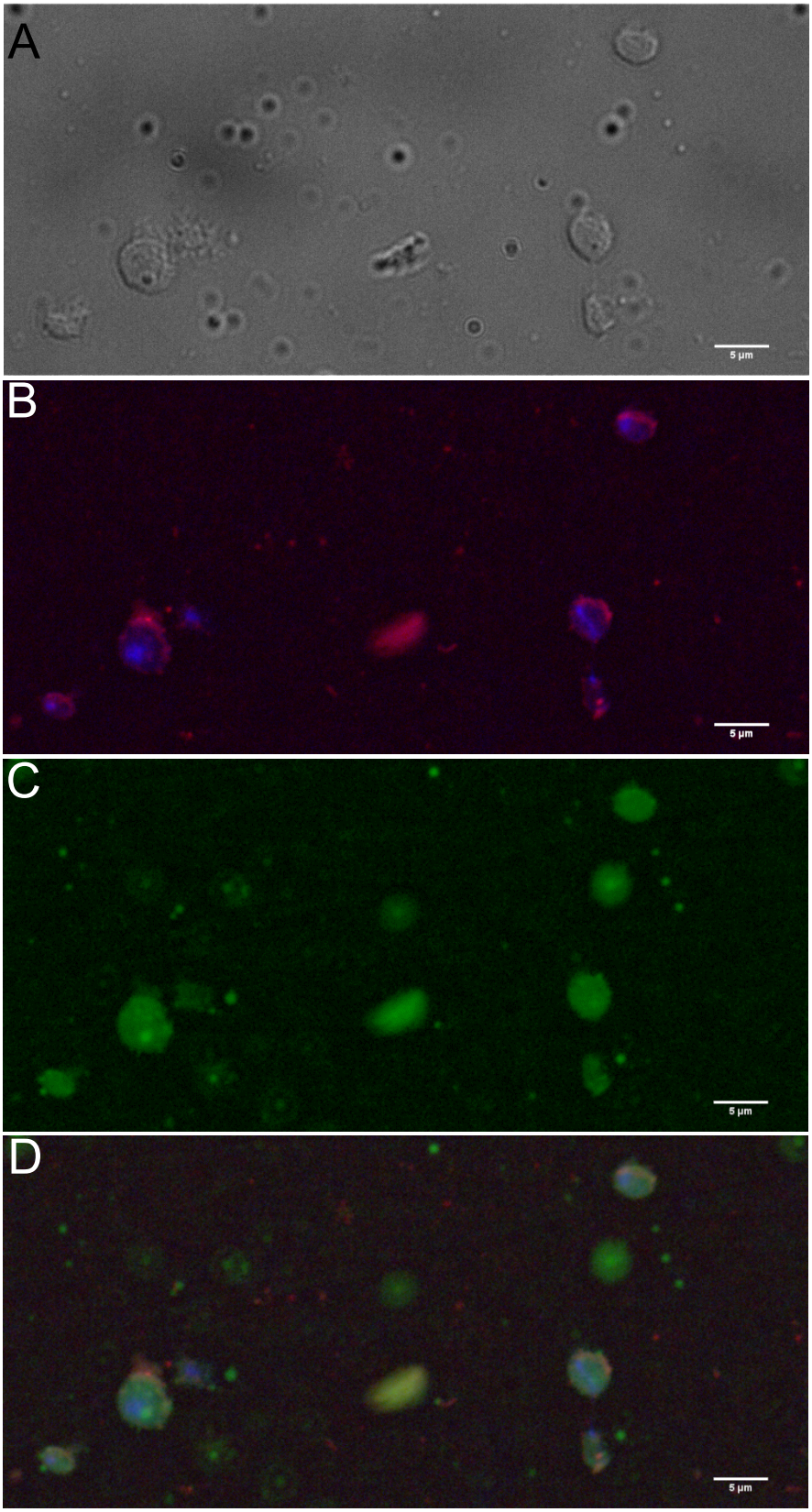

Figure 27. Cytosolic localisation of SufCB protein in yeast. Immunofluorescence of HA-tagged SufCB in fixed *S. cerevisiae* cells, n=5 using anti-HA antibody. A) Brightfield images of 5 µL culture. B) Overlay of MitoTracker Red and DAPI signal, 20ms exposure time. Shows linear mitochondria at the periphery and throughout the cell. C) FITC Signal indicative of SufCB shows diffuse fluorescence throughout the cell, 50 ms exposure. D) Mitochondrial, DAPI and FITC overlay. Image analysis performed in FIJI, background subtraction at 50 px across all images. Scale bar at 5 µm.

3.5 Expressing SufCB does not reduce the fitness of the cell

Specific growth rates were quantified as a measure of the fitness of SufCB-expressing yeast. It was desirable to show that there was no detriment to the growth of yeast when SufCB was expressed under non-stressful conditions. To achieve this, we used high-resolution growth rate analysis was employed and shows no statistically significant difference in the specific growth rates of either SufCB or control cells when grown in minimal media.

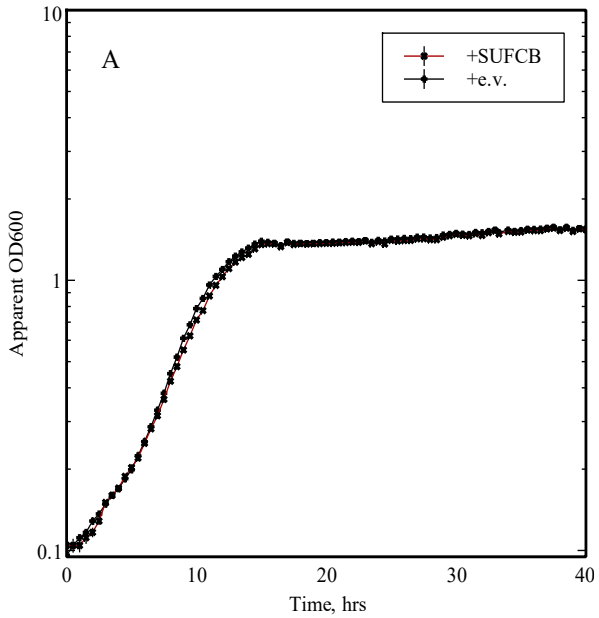

Figure 28. Growth of SufCB expressing yeast compared to control strain. 40-hour growth curve generated from 1mL cultures of SufCB and empty vector transformed *S. cerevisiae* cells grown in minimal media. No difference in growth can be seen between either sample, as seen by overlapping plots. Log^{10} formatted growth curve (Y-axis) and labelled as Apparent OD600 to accommodate for non-standard pathlength on the microplate reader, plus absorbance of the plastic culture plate. Error bars are indicative of standard error of the mean.

Figure 28 demonstrates that the growth of SufCB-expressing cells overlaps that of controls cells and thus, expressing SufCB does not reduce the fitness of its host. Converting these data into specific growth rates, found no statistically significant difference (p=0.460) in the average specific growth rate (**Table 31**).

Table 31. Specific growth rates of SufCB and control yeast cells in minimal media. Data was collected and averaged from all growth experiments. Generations per hour = Gens/Hr, error (±) is SEM. Significance determined from Student's T-test at p<0.05.

Sample	Specific growth rate, Gens/Hr
SufCB	0.39 ± 0.006
Control	0.40 ± 0.02

The observation that no discernible difference in growth rate exists between SufCB yeast and control, demonstrates that expression of SufCB does not affect the fitness of the cell.

3.6 Summary of results

The aim of this chapter was to demonstrate that *S. cerevisiae* was a suitable host within which to express the SufCB protein of *Blastocystis Nand II*.

i. To develop a cloning method to insert the SufCB open reading frame into a suitable expression vector.

The open reading frame of the *Blastocystis* SufCB protein was successfully cloned into a high-copy (2μ) pBEVY-u expression vector under the control of a constitutive promoter. pBEVY-u was chosen for this purpose as a widely used and versatile expression plasmid, which contains two strong promoters; *ADH1* and *GPD*.

ii. To develop a western blotting protocol which establishes that SufCB had been expressed as full-length protein and that its molecular weight is comparable to previous descriptions (Tsaousis et al., 2012).

Following the successful integration of SufCB into pBEVY-u, analysis of cell-free lysates by SDS-PAGE and western blotting with anti-SufCB antibodies confirmed the expression of full-length (77 kDa) SufCB protein which migrated to a similar molecular weight (77 kDa) as previously described by Tsaousis et al., (2012).

iii. To perform localisation experiments on SufCB in yeast cells.

Localisation experiments using immunofluorescence demonstrated a diffuse fluorescent signal arising from commercial antibodies specific to a re-cloned tagged-SufCB. Additional fluorescent markers which localised to organelles (mitochondria and nucleus) were used to confirm localisation. From this experiment, we concluded that SufCB is primarily localised to the cytosol. This was reinforced by localisation prediction software.

iv. To perform phenotypic growth assays which determine how expressing SufCB may affect the cell biology of the host yeast.

The fitness of SufCB expressing yeast was reported by high-resolution growth rate analysis. Comparing these data to a control yeast, which contained pBEVY empty plasmid only it was found that the specific growth rate of SufCB expressing yeast was statistically insignificant ($p=0.460$) from controls. From this, we concluded that expressing SufCB in yeast confers no detrimental effect on cellular fitness under unstressed conditions.

Conclusions

In conclusion, this chapter has provided evidence to demonstrate that yeast cells can accommodate and express the recombinant SufCB protein. In doing so, we have successfully achieved the first aim of this project.

Iron-sulfur enzymes in SufCB expressing yeast.

4.1 Chapter aims

The data gathered in chapter 3, enabled us to progress onto the next aim which assessed whether iron-sulfur cluster assembly is strengthened in the SufCB-expressing yeast system. As organisms that encode SUF machinery do so to protect their iron-sulfur cluster assembly pathways from oxidative damage (Selbach et al., 2013), we hypothesised that a similar protective effect could be conveyed to iron-sulfur clusters produced by SufCB-expressing yeast cells.

Cell factories which use iron-sulfur enzymes have been recorded in the literature with uses ranging from nitrogen fixation to bioremediation (Lopez-Torrejon et al., 2016; Magnuson et al., 2000; Martínez-Alcántar et al., 2019; Raj et al., 2018; Schlesier et al., 2016; Zhai et al., 2014). A selection of these enzymes and their uses are summarised in **Table 32** below. In addition to this, iron-sulfur enzymes have pivotal roles in cell biology (e.g. DNA repair and translation) and so their upregulation may afford the cell with desirable phenotypes, for example, increased resistance to certain stressors (e.g. oxidative stress) which in turn may provide a more useful platform to produce other non-metal containing recombinant proteins (Alhebshi et al., 2012; Martínez-Alcántar et al., 2019; Stehling et al., 2014).

Table 32. Industrial applications of some iron-sulfur cluster enzymes. The enzymes and their purposes are shown in separate columns.

Enzyme	Purpose(s)	Reference
Nitrogenase	Nitrogen fixation, agriculture	(Lopez-Torrejon et al., 2016)
Enoate Reductase	Textiles and adipic acid production	(Raj et al., 2018)
ErpA	Isoprenoid production	(Loiseau et al., 2007)
Jac1/Isu1	Ethanol tolerance	(Martínez-Alcántar et al., 2019)
CMAH	Sialic acid production	(Pearce and Varki, 2010)
Bio2	Biotin production	(Shiuan, 2006)
Rieske protein	C4 photosynthesis	(Ermakova et al., 2019)

To investigate the above aim the following objectives were tasked:

i. To investigate stress responses in SufCB-expressing yeast by using high-resolution growth rate measurements.

ii. To use a panel of fluorescently tagged iron-sulfur proteins in order to assess iron-sulfur biogenesis within a SufCB-expressing cell *in vivo*.

iii. To assess whether any observations arising from ‘ii’ coincide with increased activity of the enzyme(s) identified.

iv. To introduce recombinant mammalian iron-sulfur proteins, aconitase and CMAH, within SufCB yeast and assess its activity compared to control (non-SufCB) strains.

4.2 Analysing the growth rates of SufCB cells under varying conditions

Data in chapter 3.5 demonstrated that expressing SufCB does not confer detrimental phenotypes in yeast when grown in minimal synthetic defined media, compared to controls. Next, we assessed whether expressing SufCB yields a degree of stress resistance to yeast cells, in particular, whether SufCB expression could facilitate the repair of damaged iron-sulfur clusters and whether this could be seen at a phenotypic (cellular fitness) level. High-resolution growth rate analysis to investigate this. Initially, we probed the response to oxidative (hydrogen peroxide) and heavy metal stress (Cu^{2+}) as both are known to strongly destabilise iron-sulfur clusters and the cell at large (Alhebshi et al., 2012; Macomber and Imlay, 2009). We found no effect of SufCB expression on the growth of yeast cells under either of these conditions (**Appendix 12**), until we moved to study the effect of altered iron concentration.

Table 33. Table of specific growth rates (Gens/Hr) of SufCB expressing yeast cells under various iron-stresses. Significance was determined by one-way ANOVA and Tukey's post-hoc test with p=0.05. Iron starvation was achieved by using 0.5 mM ferrozine. Growth rates are shown in generations per hour (Gens/Hr), error (±) is SEM.

Sample			Specific growth rate, Gens/Hr
No stress		SufCB	0.38 ± 0.002
		Control	0.37±0.002
Iron-supplementation	15 mg/mL	SufCB	0.39 ± 0.002
	30 mg/mL	SufCB	0.38±0.002
	15 mg/mL	Control	0.37±0.004
	30 mg/mL	Control	0.35±0.003
Iron-starvation	0.5 mM	SufCB	0.30±0.013
	0.5 mM	Control	0.23±0.009

The data in **Table 33** demonstrates that SufCB expressing yeast cells have a distinct relationship with iron, in such that, SufCB expression cells were seen to be able to tolerate high levels of iron-excess, above that of controls ($p<0.05$). Iron-excess is known to lead to oxidative stress via the Fenton reaction and so these data suggest that SufCB cells can prevent this toxicity by a yet unknown mechanism. In addition to this we also found that SufCB cells are more resistant ($p<0.01$) to iron-starvation by ferrozine (Sigma, UK) than controls. This finding could reflect increased or more efficient iron-storage in SufCB cells. The concentrations of iron to use were taken from a previously reported study (Gaensly et al., 2014).

To probe this further, we assayed the genetic interaction between SufCB and iron-uptake systems in yeast. Ftr1, along with the oxidase, Fet3 forms the primary iron-uptake channel in yeast cells and is transcriptionally upregulated under conditions of iron-starvation (Singh et al., 2006). Expressing SufCB in an Ftr1 knockout (Δ*ftr1*) was found to lead to significant growth rate defects compared to control knockouts expressing empty vector. Furthermore, the growth of SufCB Δ*ftr1* cells could be restored back to values comparable to those of control knockouts upon supplementation of low doses of iron (0.5 – 5 mg/mL).

Table 34. Table of specific growth rates of Δ*ftr1* knockouts expressing SufCB and empty vector and the effect of growth in iron-supplemented media. Iron supplementation was in mg/mL and a wildtype control was used to confirm that the Ftr1 knockout had relatively decreased growth rate. Wildtype control (Control) was included for comparison. Growth rates are shown in generations per hour (Gens/Hr).

Sample		Iron-supplementation, mg/mL	Gens/Hr
Control		0	0.38±0.001
Δ*ftr1*	SufCB	0	0.35±0.002
		0.5	0.37±0.004
		5.0	0.38±0.0006
	Control	0	0.39±0.003
		0.5	0.38±0.003
		5.0	0.37±0.002

The data in Table 34 demonstrates that the growth rates of Ftr1 knockouts (Δ*ftr1*) expressing SufCB show a dose-dependent response to elevated iron-concentration within their growth media. There was a significant difference in the growth rates of cultures without supplementation, where SufCB mutants were found to have significantly worse growth than controls ($p<0.01$). These values then rose upon iron-supplementation to the growth media (synthetic defined). Rising from 0.35 Gens/Hr to 0.38 Gens/Hr with an additional 5 mg/mL of iron, which was found to reach significance ($p<0.05$) from growth in non-supplemented SufCB-cultures. Importantly a similar relationship was not seen ($p>0.05$) in controls in which we saw a decrease in growth rate at higher concentrations (5 mg/mL). At the highest concentration of iron-supplementation (5 mg/mL) we found that the growth of SufCB cells was no longer significantly ($p>0.05$) different to controls, suggesting that these cells (SufCB-Δ*ftr1*) were iron-starved.

4.3 Using GFP-tagged iron-sulfur enzymes to probe abundance changes

A panel of GFP-tagged iron-sulfur enzymes were selected from the genome-wide GFP tag collection (Huh et al., 2003). This panel, roles of each enzyme, and cluster(s) present are listed in **Table 35** below:

Table 35. The panel of GFP-tagged iron-sulfur enzymes used in the following experiment. Information includes the biological role, whether the gene is essential, localisation, and the number/type of clusters present. Information regarding the biological role, the essential status of the ORF, and type of cluster(s) were taken from the Saccharomyces Genome Database (https://www.yeastgenome.org/) and UniProt Protein Database (https://www.uniprot.org/). Localisation abbreviations: Cytosol (Cyt), Nucleus (Nuc), Mitochondrial (Mit) Essential status means knockout mutants are inviable.

Enzyme	Biological role	Essential?	Localisation	Cluster(s) present
Leu1	Leucine Biosynthesis	No	Cyt	[4Fe4S]
Ecm17	Sulphite Reduction	No	Cyt	1x [4Fe4S]
Rli1	Translation Termination	Yes	Cyt	2x [4Fe4S]
Pol2	DNA Replication	Yes	Nuc	1x [4Fe4S]
Ntg2	DNA Repair	No	Nuc	1x [4Fe4S]
Elp3	Translation Initiation	No	Cyt	1x [4Fe4S]
Nbp35*	Iron-sulfur assembly	Yes	Cyt	1.5x [4Fe4S]
Rad3	DNA Repair	Yes	Nuc	1x [4Fe4S]
Bio2	Biosynthesis of biotin	No	Mit	1x [4Fe4S], 1x [2Fe2S]
Lip5	Biosynthesis of lipoic acid	No	Mit	2x [4Fe4S]
Sdh2	Electron transport and TCA cycle	No	Mit	1x [2Fe2S], 1x [3Fe4S], 1x [4Fe4S]
Act1	Actin	No	Universal	None, control

*Nbp35 contains one N-terminal [4Fe4S] cluster and one bridging C-terminal [4Fe4S] cluster and has therefore been denoted as containing 1.5x [4Fe4S] clusters.

A variety of iron-sulfur enzymes were selected for testing in order to yield a more detailed picture of the behaviour of SufCB-expressing cells and any nuances that may exist, for example, preference towards one class or localisation of iron-sulfur cluster enzyme over another. In addition, two negative controls were tested in parallel to each fluorescent protein. These were, Act1 which doesn't contain an iron-sulfur cluster and non-fluorescent (wildtype) yeast cells. These data from this experiment are shown in **Figure 29**.

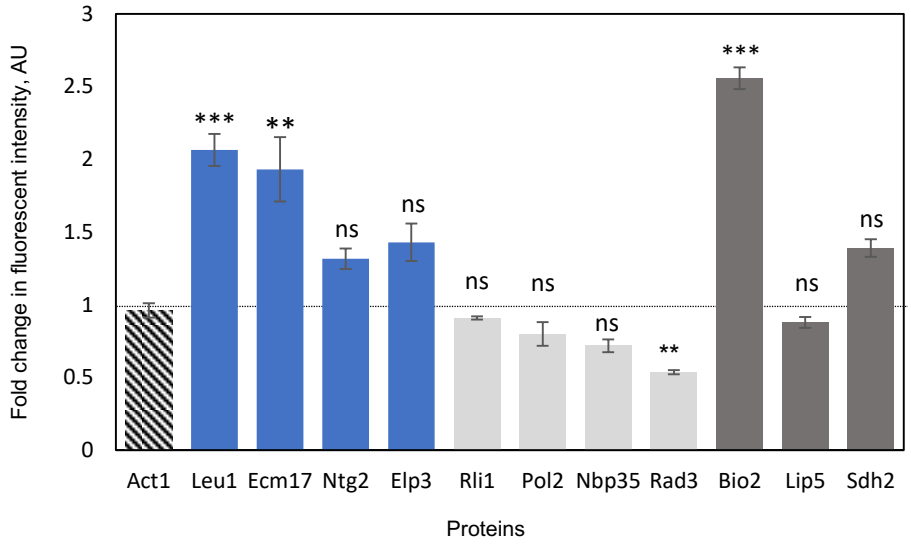

Figure 29. Overexpression of candidate iron-sulfur proteins in SufCB-expressing yeast. Results of probing abundance changes by flow cytometry after removing autofluorescence. These data above represent the average fold-change in abundance of GFP-tagged iron-sulfur enzymes in SufCB expressing yeast compared to expressing empty vector. Significance determined by one-way ANOVA, followed by Tukey's HDS, significance abbreviations: ***=p<0.001, **=p<0.01, ns = non-significance p>0.05. Error bars, +/- the standard error of the mean. Proteins are sorted by essential (blue), non-essential (light grey) and mitochondrial proteins (dark grey). Act1 control is dashed.

Figure 29 illustrates that there are significance fold-changes in the fluorescence of several (n=11) GFP-tagged iron-sulfur proteins between SufCB and control cells, which we took to directly relate to abundance of the enzymes. Significance testing ($p<0.05$) demonstrated that SufCB expression in yeast does resulted in significantly ($p<0.01$) increased abundance of the enzymes, Leu1, Ecm17 and Bio2. Which localise to the cytosol (Leu1, Ecm17) and mitochondria (Bio2), respectively. Further studies into Elp3 and Ntg2 also found a slight, but statistically insignificant ($p>0.05$) increase in fluorescence compared to controls. These data suggest that non-essential genes are targets of SufCB (blue) and can be increased by roughly 2-fold over controls.

Conversely, the abundance of proteins encoded by essential genes, Rad3, Pol2, Nbp35 and Rli1 remained either unaltered or lowered in abundance (Rad3) in SufCB-expressing yeast (light grey). These data also indicate that mitochondria may also be targets of SufCB, as the biotin synthase (Bio2) was found to be upregulated to a similar level as Leu1 and Ecm17. This suggests that the mechanism of SufCB may result in a universal upregulation of iron-sulfur biogenesis.

Data was routinely compared to a GFP-labelled actin ($Act1^{GFP}$) internal control which confirmed that any effects were seen were specific to iron-sulfur biogenesis rather than an increase in translation or GFP released by the cell. Comparing $Act1^{GFP}$ in SufCB and control cells found no statistically significant ($p>0.05$) difference between either sample. In addition to Act1, we also quantified the fluorescence of control yeast expressing empty vector (pBEVY). This auto-fluorescence value was then subtracted from all data sets prior to further processing.

4.4 Relating abundance to activity

The next set of experiments sought to correlate increases in abundance in chapter 4.2 to the activity via enzymatic assays of the proteins, where possible. For these experiments, we assayed the activities of Ecm17, Leu1 and Rli1 (**Appendix 13**).

4.4.1 The sulfite reductase subunit, Ecm17 is hyperactive in SufCB-expressing cells

Ecm17 is a conserved [4Fe4S] enzyme involved in the biogenesis of sulfur-containing amino acids, sulfolipids and coenzymes, and is a widely used reporter for iron-sulfur biogenesis (Brychkova et al., 2012).

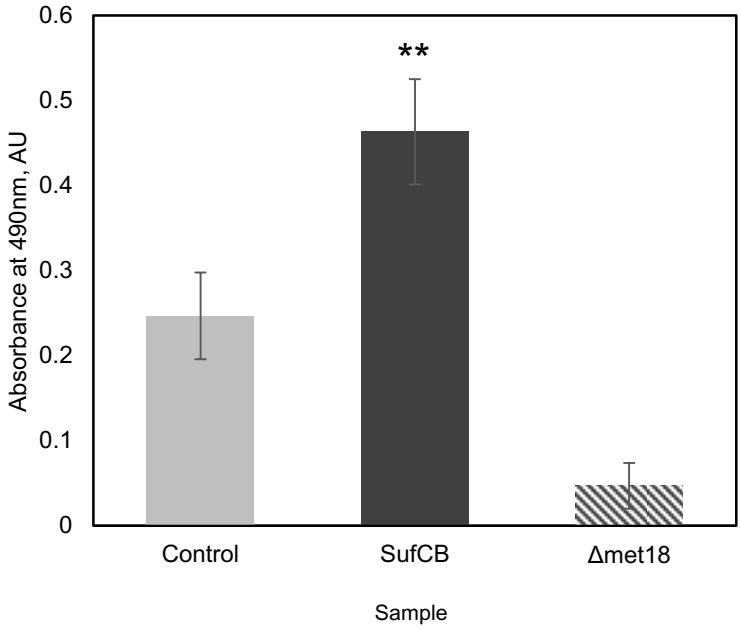

Figure 30. Determining Ecm17 activity by quantification of Bismuth sulfide precipitate at OD_{490nm} in control (Control, light grey) and SufCB-expressing (SufCB, dark grey) cells. Data is mean of three biological replicates in 1 mL cuvettes, after lysis by NaOH, yeast without active Ecm17 (*Δmet18*, not italicised in figure, dashed) was used as a negative control. Absorbances were left unnormalized for cell number. Statistical significance determined by one-way ANOVA, followed by Tukey's HSD, $p<0.05$. Error bars ± standard error of the mean, ** = $p<0.01$.

In yeast, Ecm17 is an essential subunit of the sulfite reductase (SiR) complex which assimilates sulfide. When grown in media containing bismuth sulfite, SiR reduces sulfite to brown sulfide, which can be quantified and related to cytosolic cluster biogenesis (Balk et al., 2005; Yücesoy and Marol, 2003). These data (**Figure 30**) demonstrate that the [4Fe4S] enzyme, Ecm17 is hyperactive in SufCB-expressing cells and this finding aligns with the previously reported abundance data. To confirm the system, a viable CIA mutant, Δ*met18*, was tested in parallel to both samples and showed negligible precipitate after a comparable incubation period. Importantly, cell number was also taken for all data sets to ensure the observed change in precipitation was not due to increase cell number. Viability staining (Phloxine B) indicated no significant difference (ANOVA, $p>0.05$) in cell number between all three mutants (5.31×10^7, 6.39×10^7 and 5.04×10^7 CFU/mL for SufCB-expressing (+*SUFCB*), empty vector and Δ*met18* cultures, respectively). Together our results demonstrate that SufCB upregulated Ecm17, which also increased the activity of the enzyme.

4.4.2 Leu1 retains its activity in aerobic preparations.

The next set of experiments served a dual purpose, The first of which attempted to correlate Leu1 abundance to activity and the second sought to investigate the stability of Leu1's [4Fe4S] cluster in aerobic environments as Leu1 is known to lose most of its activity in the course of a few minutes in aerobic preparations (Hawkes et al., 1993). To accomplish this, we assayed Leu1 activity when purified aerobically from crude cell-free lysates. The activity of Leu1 can be monitored via the production of dimethylcitraconate, which absorbs UV-light at an OD_{235nm} (**Figure 31**) (Hawkes et al., 1993).

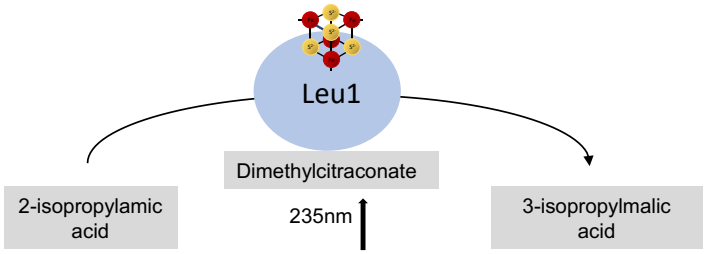

Figure 31. Schematic of the Leu1 assay. The activity of the enzyme can be monitored by a gradual increase in the absorbance at OD_{235nm} when crude extract is incubated with 2-isopropylmalic acid.

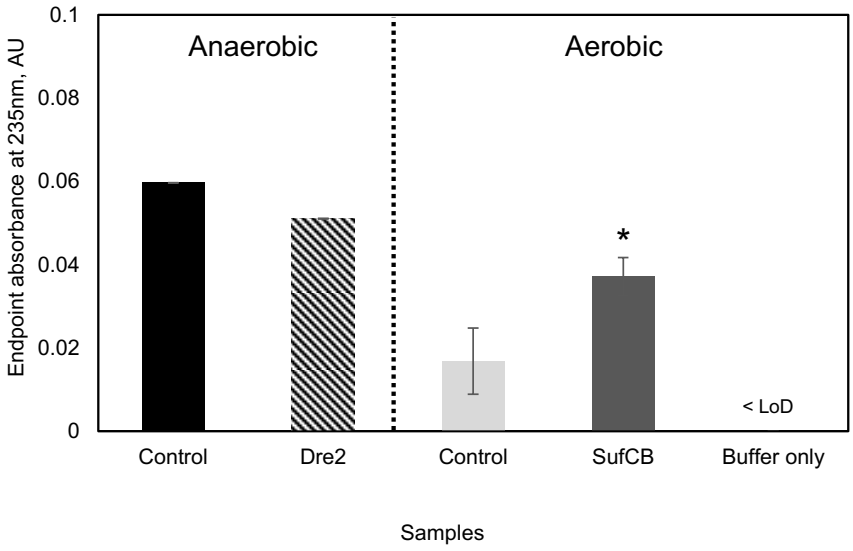

Figure 32. Leu1 activity indicated by increases in absorbance at OD_{235nm} over 15 minutes. Activity persists in expressing yeast, normalised to protein input. SufCB expression protects the activity of Leu1 in air (aerobic). Significance determined by one-way ANOVA, *=p<0.05. Absorbance from the buffer only control was below the limit of detection and cannot be seen on the graph (< LoD), error (±) is SEM.

Due to the unstable nature of Leu1, we performed this assay within (anaerobic) and outside of an anaerobic workstation (aerobic) (**figure 32**). Analysing the Leu1 activity under anaerobic conditions demonstrated that the enzyme was functional in controls and depleted in a Dre2 mutant, and aligns with previously reported data (Zhang et al., 2008). For samples that were lysed outside of the anaerobic workstation (<2ppm [O_2], Belle Technology), very little Leu1 activity could be found in controls. However, this activity could be 'rescued' by SufCB-expression. This data suggests that expressing SufCB increases the resistance of Leu1 to oxidative damage in yeast cell lysates. Given that previous abundance data demonstrated a significantly increased abundance of Leu1 ($Leu1^{GFP}$, **figure 30**), it may be that the persistent Leu1 activity was due to a higher abundance of Leu1 enzyme in extracts.

4.5 SufCB as a host for mammalian iron-sulfur enzymes

4.5.1 Generating an expression construct for Aconitase

We demonstrated in chapter **4.4.2** that although SufCB expression is able to confer some protection to the iron-sulfur clusters of Leu1 in aerobically prepared lysates, the observed effects were only slightly above background and could perhaps be improved upon with a more established assay (**figure 32**).

In order to address this, we investigated the effect of SufCB on a recombinant iron-sulfur enzyme, aconitase (Aco1), which could be designed with high expression. A commercially available aconitase ORF was amplified from cDNA (Source Biosciences, UK**)**. Using restriction enzymes *Sal I* (5' *G^TCGAC* 3') and *Xba 1 (5' T^CTAGA 3')*, following digestion, we then inserted the amplicon into the *ADH1* promoter on pBEVY-l to create the aconitase construct which was then transformed into either SufCB or control yeast (**Appendix 18**).

4.5.2 Growth observations of the co-expressing Aco1 and SufCB cultures.

Before assaying the activity of aconitase in the SufCB-expressing yeast, it was of interest to determine whether there were any observable trends in the fitness of the two mutants. Previous experiments have demonstrated no differences between the growth of SufCB or control yeast, suggesting that the SufCB-cells are able to cope with the overexpressed iron-sulfur enzymes (**Figure 28**). High-resolution growth analysis was used to quantify specific growth rates of Aco1/SufCB-expressing yeast compared to yeast expressing aconitase only. Controls consisted of yeast transformed with empty pBEVY-u and pBEVY-l vectors and were used to accommodate for metabolic stress of maintaining two high-copy plasmids**.**

These results presented in **Table 36** demonstrate that the expression of Aco1 in a SufCB expressing yeast confers a significant reduction in specific growth rate compared to yeast expressing Aco1, only. Whereas expressing Aco1 only, caused a mild, but insignificant (97.09% of control) decrease in specific growth rate compared to control expressing both empty plasmids. However, in a SufCB-expressing background, co-expression of Aco1/SufCB resulted in a statistically significant ($p=0.003$) decrease - when compared with expressing Aco1 only. A property of SufCB expressing yeast, therefore, reduces the cellular fitness when expressing a recombinant iron-sulfur protein, in minimal media.

In addition to this, we were also able to demonstrate that the decrease in growth rate could not be rescued by supplementation of iron salts (0.5 mg/L) to the growth media prior to inoculation. As it was presumed that the growth deficit seen in SufCB/Aco1 cells may have been due to increased expression of aconitase, and therefore depletion of the cell's iron-supply to supply the iron-sulfur clusters. Although, Aco1/SufCB yeast were found to be resistant to iron toxicity at this concentration as seen by a much lower decrease in the growth rate of 4% compared to steeper drops of 7.5% and 7% for cells expressing Aco1 and empty plasmids, respectively.

Table 36. Table of average specific growth rates (in Gen/Hr) before and after supplementing the growth media with iron. Calculated from growth curves of aconitase expressing yeast, Aco1/SufCB = Coexpressing aconitase and SufCB, Aco1 = expressing aconitase only, Empty plasmids = yeast transformed with pBEVY-I and pBEVY-u. Specific growth rates are expressed as mean average with ± standard error of the mean, percentage change calculated from mean values, minus percentages equate to a drop in growth rates. Supp. = supplementation. Error is ± standard error of the mean (SEM).

Strain	Specific Growth Rate before iron supp., Gen/Hr	Specific Growth Rate after iron supp., Gen/Hr	Percentage change with iron supp., %
Aco1/SufCB	0.354 ± 0.005	0.340 ± 0.0028	-4
Aco1	0.378 ± 0.003	0.350 ± 0.0019	-7.5
Empty plasmids	0.390 ± 0.004	0.362 ± 0.002	-7

These data demonstrate two phenotypes from SufCB expressing aconitase cultures. The first being that co-expressing aconitase with SufCB leads to a significant drop in cellular fitness, measured by growth rate. Secondly, we also found specific interactions between the co-expressing SufCB/Aco1 mutant and iron-supplementation, which may reflect an iron regulatory function of aconitase, or a reoccurrence of the iron-dependent functions of SufCB observed in chapter 4.2.

4.5.3 Increased activity of aconitase in SufCB expressing cultures

Activity assays of Aco1/SufCB and Aco1 yeast were performed in order to assess whether SufCB expression could increase the maturation of aconitase. To perform this assay, we quantified the production of cis-aconitate from citrate by aconitase **(Figures 33-34)** in crude cell-free lysates at OD_{240nm} (normalised enzyme activity to input (mg/mL) via Bradford assay). The experimental design was to perform this assay on cultures which co-expressed either SufCB or the empty vector alongside recombinant aconitase, as well as cultures which expressed SufCB or the empty vector only. This enabled us to correct for the endogenous yeast aconitase. This assay was chosen over an isocitrate dehydrogenase-based assay, due to expenses in obtaining purified enzyme. Crude lysate was chosen because we wished to test and compare the total aconitase activity as extracted from either SufCB or control cultures whereas purifying aconitase could call into question the purification yield between either culture. Our method enables us to directly compare the aconitase activity in both cultures.

This design is summarised in the graphic in **Figure 33**. In addition, the controls of substrate only and BSA were used to determine that the activity seen was dependent upon the addition of crude lysate. We also found that DTT (2 – 5 mM) gave false-positive readings such that the substrate only controls appeared to produce cis-aconitate, omitting the DTT removed this observation and DTT was left out of all reaction cocktails therein. Unlike Leu1 assays, aconitase assays did not seem to be dependent upon DTT, possibly reflecting aconitase's stable iron-sulfur cluster.

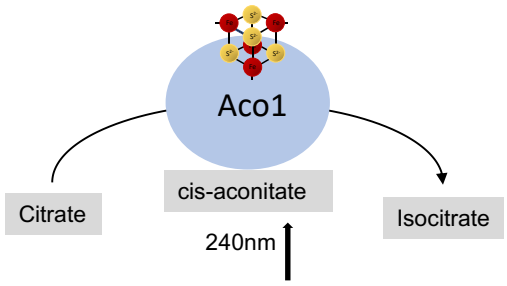

Figure 33. The conversion of citrate to isocitrate via cis-aconitate by aconitase (Aco1). The reaction can be monitored at 240nm by the production of cis-aconitate (shown bound to Aco1).

Following the experiment, the protein content of each crude extract was determined using micro-Bradford assay at 595 nm and absorbances compared to known standards of BSA to quantify the protein content of each crude extract. Absorbances at 240 nm were then normalised to protein input to ensure accurate interpretation of activity measurements. Routinely, aconitase assay gave more consistent results than Leu1 assay and so was performed at four independent biological replicates, in technical triplicate.

The activity was quantified by increases in absorbance at OD_{240nm}. Background aconitase was quantified by performing the aconitase assay on cultures which did not express the recombinant aconitase (shown by dashed grey and blue bars). A slight but insignificant decrease in the endpoint was observed for SufCB cells lacking aconitase. Overall, these data indicate that the maturation of recombinant aconitase is supported in SufCB cells over the course of the reaction and can be seen by a significantly increase endpoint absorbance at OD_{240nm}.

The significantly increased aconitase activity demonstrated in **Figure 34**, also provides a potential explanation for the growth data presented in **Table 36**. This growth detriment may be due to the increased production of recombinant aconitase which places a strain on the protein folding machinery (Čiplys et al., 2011).

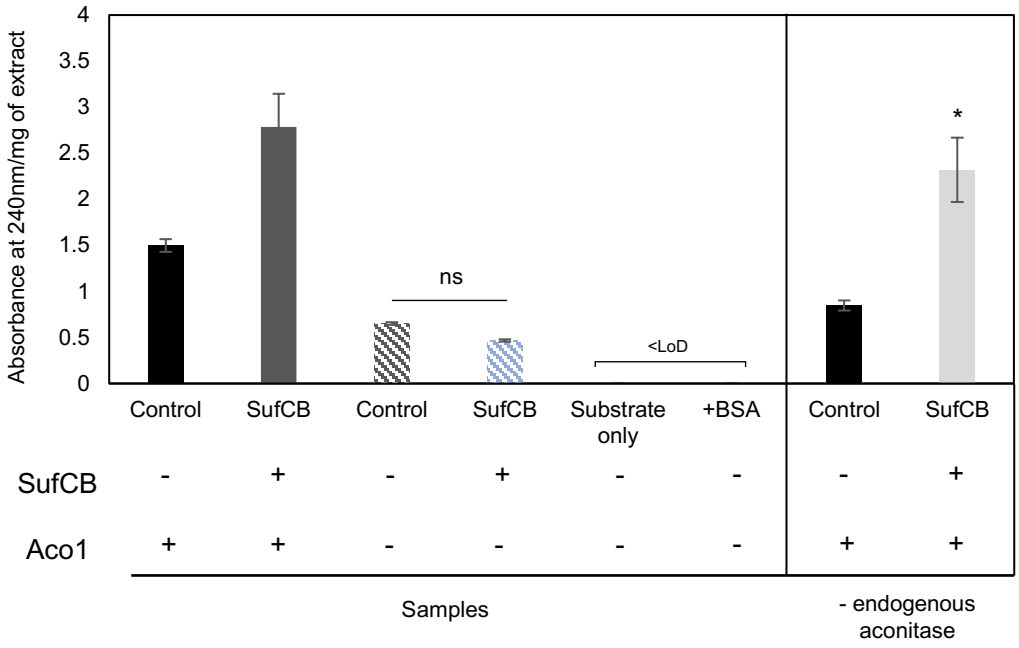

Figure 34. Activity of recombinant aconitase is increased in SufCB expressing cells. The presence or absence of SufCB and aconitase construct is indicated by + or -, respectively. The final two bars represent background aconitase corrected samples. Significance was determined by student's T-test at $p<0.05$. * = $p<0.05$. Where <LoD means that the endpoint absorbance was lower than could be detected on the spectrophotometer. Data was recorded at n=3, triplicate, error bars are SEM.

4.5.4 Assaying an [2Fe2S] enzyme in the SufCB system.

To fully explore the breadth of SufCB's capacity to assemble iron-sulfur clusters, we assayed the abundance of the [2Fe2S] enzyme, cytidine monophospho-N-acetylneuraminic acid hydroxylase (CMAH). Humans lack a functional CMAH gene and so we tested the mouse (*Mus musculus*) homologue. The *CMAH* gene from mice (*Mus musculus*) was cloned into purified pBEVY vector from commercially available cDNA (Source Biosciences) in the exact same manner as with cloning Aco1 (**Appendix 19**). We were unable to source a suitable activity assay and so we relied on relative densitometry to probe whether CMAH was significantly upregulated in abundance in SufCB cultures. To achieve this, we cloned a C-terminal HA tag onto the expression construct which enabled detection of the protein by commercially available anti-HA antibodies (Abcam, UK).

We confirmed the expression of CMAH by western blotting confirmed the appearance of a band corresponding to the molecular weight of CMAH protein, 66 kDa (**Appendix 20**) (Takahashi et al., 2015). Densitometry was performed in Fiji Image Analysis software (Schindelin et al., 2009) and the pixel density (px) was then taken for all lanes by plotting pixel profile and separating bands from the western blot image before taking absolute pixel number per lane. Plot profile was also calibrated against a black line to scale pixel density.

Table 37. The expression of CMAH is slightly but insignificantly higher in SufCB cultures compared to controls. Densitometry was calculated based upon the monomeric 66 kDa band, rather than the high molecular weight band. Error (±) is SEM.

Sample	SufCB	Control
1	4903.104	2788.669
2	4570.447	2056.376
3	3362.446	3208.134
Average (± SEM)	4278.666 ± 468.0663	2684.393px ± 468.0663

Table 37 demonstrates that there is slightly (+59%) higher concentration of CMAH monomer in SufCB expressing cultures compared to controls lacking SufCB. Although this proved statistically insignificant (p=0.051) by densitometry. These data suggest that the SufCB system is specific to the maturation of [4Fe4S] enzymes, although further detailed analyses (quantitative GC/MS for the CMAH product, Neu5Gc) will be required to fully elucidate the effect of SufCB on CMAH expression.

4.6 Summary of results.

The aim of this chapter was to demonstrate that introducing SufCB into yeast can significantly improve the maturation of iron-sulfur enzymes. The research objectives were answered as follows.

i. To investigate stress responses in SufCB-expressing yeast by using high-resolution growth rate measurements.

We assayed whether SufCB confers resistance to oxidative stress, as iron-sulfur clusters are damaged under oxidative conditions and the SUF system is upregulated under oxidative conditions. Although we were unable to conclusively demonstrate that SufCB expression confers an increased resistance (measured by growth rate) to oxidative or copper stressors, our data did demonstrate that SufCB cells have a high metabolic requirement for iron. SufCB cells could resist iron-excess and starvation well above that of controls. We also demonstrate a genetic dependency on iron-uptake within SufCB cells.

ii. To use a panel of fluorescently tagged iron-sulfur proteins in order to assess iron-sulfur biogenesis within a SufCB-expressing cell *in vivo*.

Expressing SufCB within yeast reproducibly coincided with a significant increase in the abundance of iron-sulfur proteins. These data suggest that SufCB affects non-essential proteins, only. Conversely, where tested, essential proteins were found to be either unaffected or in lower abundance in a SufCB-expressing cell. We also demonstrate that this effect is specific to iron-sulfur proteins as the abundance of Act1 was unaffected by expressing SufCB.

iii. To assess whether the observations arising from ‘ii’ coincide with increased activity of the enzyme(s) identified.

The next objective sought to assess whether the increased abundances observed in subchapter 4.2 correlate to enzyme activity within the cell. Leu1 and Ecm17 both gave significantly increased activities in SufCB-expressing cells when compared against controls. In addition, assaying the activity of Rli1 within the cell revealed no change to the activity of this enzyme in a SufCB-expressing cell, also in agreement with the findings in ‘i’, which showed that Rli1 was not upregulated by FACs.

iv. To introduce recombinant mammalian iron-sulfur proteins, aconitase and CMAH, within SufCB yeast and assess its activity compared to control (non-SufCB) strains.

We next tested whether SufCB-expressing cells could act as a host for a model mammalian iron-sulfur protein, aconitase (Aco1). Data revealed that expression of recombinant aconitase in a SufCB yeast leads to reduced cellular fitness, quantified by a decreased growth rate, which can't be rescued by the addition of iron to the growth media. However, the Aco1/SufCB cells were found to be resistant to the detrimental effects on fitness caused by iron excess. Activity assays later showed significantly increased activity of aconitase in an Aco1/SufCB cell as measured by spectroscopy. We also expressed the mouse [2Fe2S] iron-sulfur enzyme, CMAH, however a densitometry approach failed to achieve a significant increase in the concentration of detectable protein by ECL.

Conclusions

In conclusion, chapter 4 explored the phenotypes associated with expressing the SufCB protein in yeast cells. The aim of this chapter was to demonstrate that SufCB expression confers improved maturation of iron-sulfur enzymes in yeast cells and this was achieved by several avenues of research. We began our investigation by studying the effect of various stressors on the growth of SufCB-expressing cells and found that expressing SufCB affords cells with increased or more efficient utilisation or storage of iron. We then found that several endogenous iron-sulfur enzymes were significantly upregulated in SufCB cells and this matched activity measurements, where possible. Notably, mitochondrial enzymes were also found to be upregulated. These observations provide insight into the requirement for iron, as a substrate for iron-sulfur cluster biogenesis and suggests that SufCB expression does place some metabolic burden on yeast cells. One recurrent theme for these measurements was the distinction between essential and non-essential iron-sulfur enzymes. Expression of recombinant (non-essential) enzyme, aconitase, was also found to be upregulated in the SufCB system whereas our data concerning recombinant CMAH failed to reach significance via densitometry. From these data we conclude that non-essential iron-sulfur cluster enzymes are upregulated in the SufCB-expressing yeast and SufCB-yeast may be used a platform for further recombinant iron-sulfur enzymes. Altogether we were successful in achieving each aim and have clearly demonstrated several useful phenotypes of SufCB yeast. However, studies on the expression of the recombinant [2Fe2S] enzyme, CMAH, requires further work to fully investigate whether SufCB is able to boost its activity.

Describing a mechanism for SufCB

5.1 Chapter aims

The process by which eukaryotic cells assemble and deliver their iron-sulfur clusters into recipient proteins consists of dedicated mitochondrial and cytosolic pathways (Cai and Markley, 2018). Studies into the iron-sulfur assembly machinery of SufCB's native *Blastocystis* system have revealed interesting comparisons between how yeast and *Blastocystis* assemble their iron-sulfur clusters (**Table 38**) (Tsaousis et al., 2014). Like yeast cells, *Blastocystis* has been shown to encode a set of compartmentalised iron-sulfur assembly pathways, present in the mitochondrial related organelle (MRO) and cytosol, respectively. However, *Blastocystis* lacks several of the key yeast assembly proteins, such as Cfd1 and a Dre2-Tah18 suggesting that the lifestyle of *Blastocystis* has negated the requirement for these proteins. A breakdown of the differences between the yeast and *Blastocystis* iron-sulfur scaffolds (where they are known) is shown in the Table below, data was taken from Tsaousis et al. (2014).

Table 38. Table comparing the cytosolic iron-sulfur assembly pathway of yeast (*S. cerevisiae*) and *Blastocystis*. Data from Tsaousis et al., (2014). Unknown = possibly highly diverged homologue exists. Data form Tsaousis et al (2014).

S. cerevisiae protein	*Blastocystis*
Atm1	Unknown
Nbp35	Yes, but mutated C-terminal
Cfd1	No
Dre2	No
Tah18	No
Nar1	Yes
Cia1	Yes
Cia2	No
Met18	Unknown
Grx3	Unknown
Grx4	Unknown

Experimental data in chapter 4 demonstrated that expressing *Blastocystis'* iron-sulfur scaffold, SufCB, had a positive effect on the maturation of several iron-sulfur enzymes. Currently, it is not possible to genetically manipulate *Blastocystis*, and this has prevented an understanding of the mechanism of SufCB *in vivo* (Tsaousis et al., 2012). In the following chapter, we attempted to address this knowledge gap by using a wide variety of genetic tools available for the yeast system.

The aim of this chapter was to generate an understanding of how SufCB functions within yeast cells, in order to produce the phenotypes presented in chapter 4.

This took the following forms of enquiry, a molecular genetic approach using knockouts, tetrad dissections and complementation assays. As a complement to this work, we also aimed to purify SufCB from yeast in order to probe whether the purified, yeast-produced, SufCB protein could bind an iron-sulfur cluster. These objectives are summarised as follows:

i. To probe genetic interactions between SufCB and the mitochondrial and cytosolic iron-sulfur pathways.

ii. To replace the yeast CIA machinery with SufCB.

iii. To perform candidate co-immunoprecipitation experiments to identify protein-partners of SufCB in yeast.

iv. To purify SufCB and investigate its chemical properties.

5.2 A genetic screen of iron-sulfur mutants

A genetic screen investigating the effect of expressing SufCB within cells which each lacked a single member of the iron-sulfur assembly apparatus was performed in order to identify any obvious genetic interactors with SufCB. We hypothesised that the major interactions would be with the cytosolic iron-sulfur assembly as SufCB was found to localise to the cytosol of yeast in chapter 3. The genetic screen below (**Figure 35**) was performed by quantifying the specific growth rates of select mutants representing each step in the CIA and core steps in the mitochondrial pathways. For essential genes we used mutants from the DAmP library which had been genetically engineered with greatly reduced transcript levels (Breslow et al., 2008), non-essential genes were studied using knockout mutants library (Horizon Discovery, USA). Ratios were calculated by dividing the specific growth rates (SufCB/control), where a value of >1 indicates that SufCB has a positive effect, ratios of <1 indicates a negative effect and ratio of 1 equals no effect.

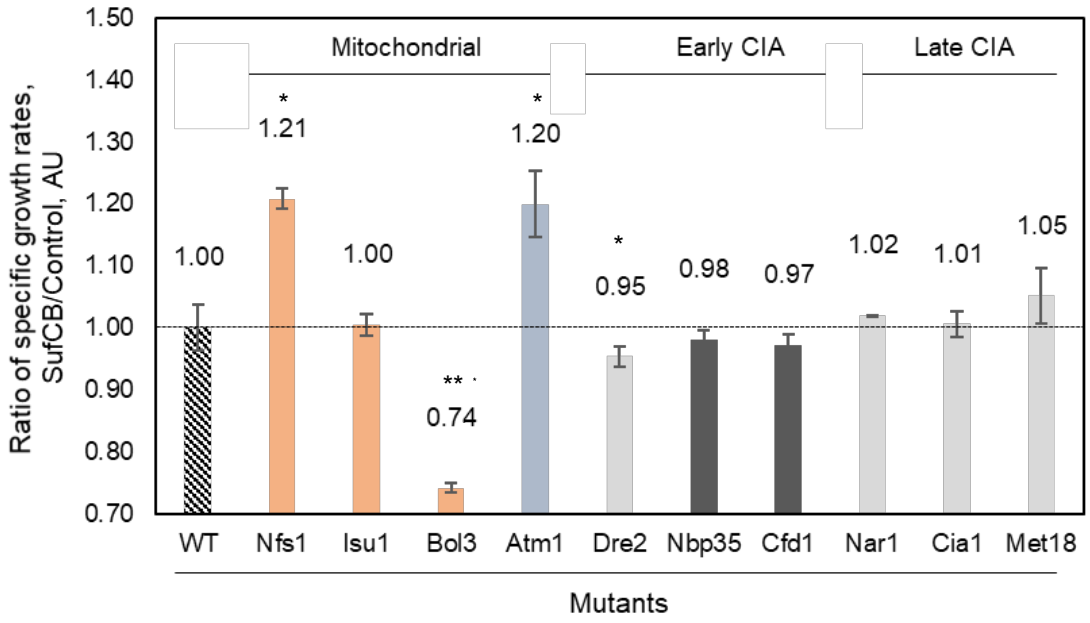

Figure 35. Plot of the ratio of specific growth rates calculated from selected mutants. With the exception of Isu1 and Met18 knockouts, all mutants were DAmP depletion mutants. Colour coding was used to illustrate the localisation and role of each component, orange for mitochondrial proteins, blue for Atm1 (membrane) and shades of grey for CIA proteins. The Nbp35-Cfd1 mutants are shaded a darker grey to highlight its place within the pathway mutants. Abbreviations: WT = wildtype, which expressed a functional iron-sulfur biogenesis pathway (dashed bar). A value of 1 indicates that SufCB has no benefit on the growth. Values less than or higher than one indicates a detrimental and positive effects on the specific growth rate, respectively. Y-axis was truncated to begin at 0.70. Significance was assessed for individual mutants by Student's T-test with a $p<0.05$. ** = $p<0.01$, * = $p<0.05$

The data genetic screen (**Figure 35**) demonstrates that expressing SufCB does have an effect on the growth rate of iron-sulfur assembly mutants. The growth rates of all mutants tested were below that of controls (WT), demonstrating that the cell biology in each mutant had been perturbed. When analysed, the effect of SufCB is focused within the early CIA assembly machinery upstream of the Nbp35-Cfd1 complex (dark grey). Overall, we found no significant ($p>0.05$) interactions between SufCB and CIA targeting complex mutants, both of these observations lead us to believe that SufCB acts early in the CIA pathway.

Strong genetic interactions are demonstrated between SufCB and the mitochondrial proteins Nfs1 and Atm1 and reached significance, $p<0.05$. Both of these proteins are essential for the cluster biogenesis by the CIA machinery and the observed 'rescue' in growth rates suggested that SufCB acts in the earliest stages of the CIA assembly machinery. This effect also appeared to be specific to these proteins as we found no effect of SufCB on a knockout of the core mitochondrial scaffold, Isu1 (**Figure 34**). Data also demonstrated that SufCB-expression elicited significant negative effects on Dre2 and Bol3 mutants. SufCB-expressing Bol3 knockouts conferred a more prominent ($p<0.01$) growth defect than the milder decrease in SufCB-expressing Dre2 mutants ($p<0.05$). The precise function of Bol3 is unknown, but is required for the assembly of [4Fe4S] clusters in yeast mitochondria (Uzarska et al., 2016). Dre2, however, facilitates an essential electron transport step in the CIA apparatus and is required to assemble the clusters of Nbp35 (Netz et al., 2016). Notably, Dre2 is missing in *Blastocystis Nand II* (Tsaousis et al., 2012). Our growth data suggested that SufCB expression is dependent on wildtype concentrations of the Dre2 protein. Unfortunately, we were unable to investigate SufCB's effect on Tah18 mutants, but expect this phenotype would have reflected similarly to Dre2 as the two proteins share a common function within the CIA (Netz et al., 2016; Soler et al., 2011).

Having established two genes which interact with SufCB to affect cellular fitness (in the form of growth rate), we next performed phenotypic assays to further investigate the cell biology of SufCB. Mitochondria are central hubs for the catabolism of non-fermentable carbon sources (e.g. glycerol) in *S. cerevisiae* (Nevoigt and Stahl, 1997; Uzarska et al., 2016). Growth on non-fermentative carbon sources is a widely method to assess the functionality of mitochondria and has been used to study Bol3 and Nfs1 proteins (Rocha et al., 2018; Uzarska et al., 2016). Exponential (OD_{600nm} – 1.0 – 1.5) mutant cultures were spotted on dried glycerol-containing agar plates (YPG) and glucose (YPD) control plates (**Figure 36**). The results of this experiment demonstrated that Nfs1 mutants were able to grow normally when transformed with the SufCB construct, but non-transformed (empty vector) Nfs1 controls failed to grow. A wild-type control (WT) with functional mitochondria was found to grow regardless of the carbon source used.

Interestingly, the opposite effect was found for Bol3 knockouts (**Figure 36**). Although Bol3 knockouts were found to be respiratory competent on non-fermentable carbon sources (**Figure 36B**), expressing SufCB rendered these cells incompetent as the mutants largely failed to grow on glycerol plates (**Figure 36B**). Some growth of SufCB-expressing Bol3 mutants could be observed at the highest dilution (**Figure 36B**), but the effect is still clear. Again wildtype (WT) control could grow on both carbon sources.

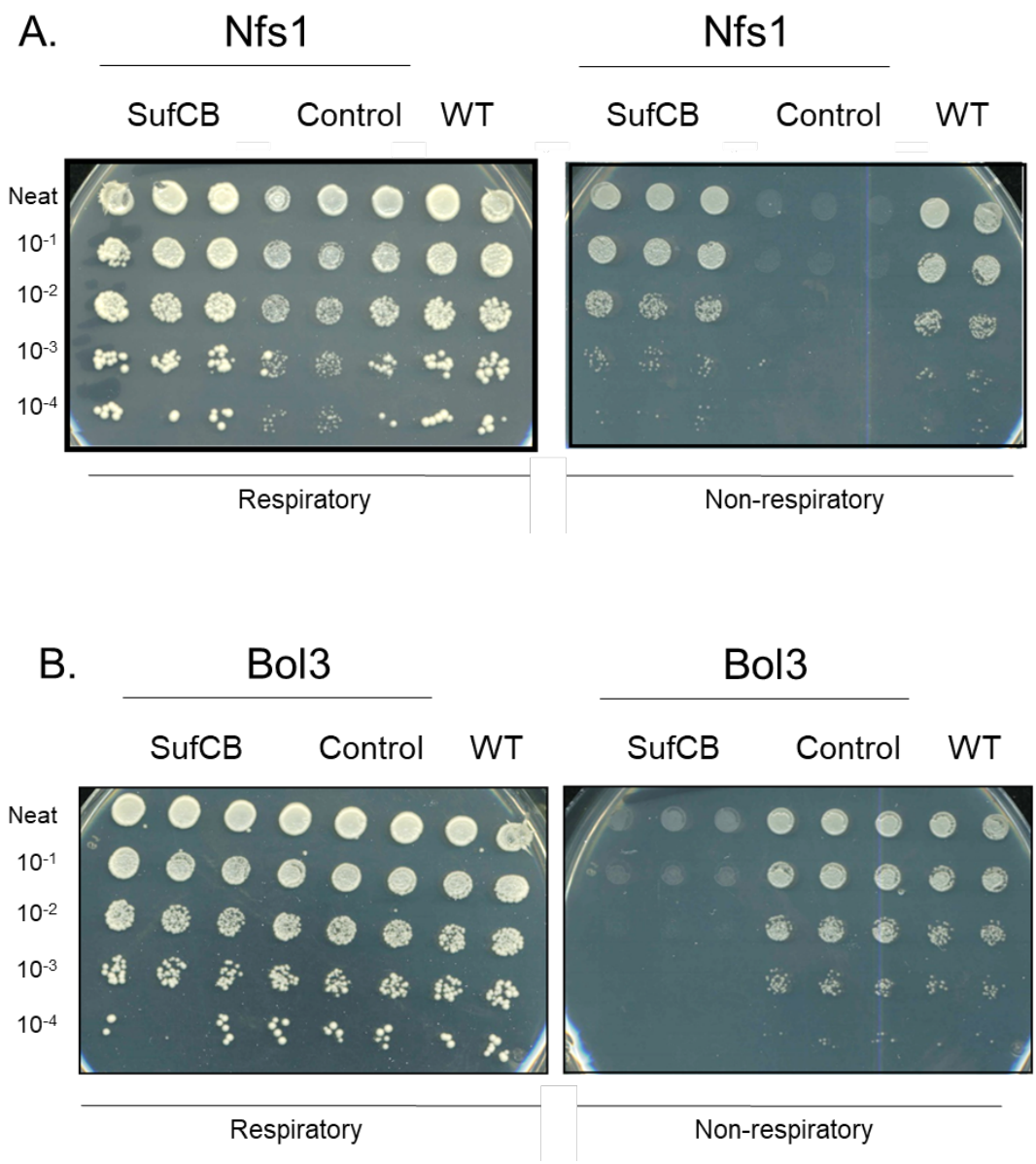

Figure 36A-B. Expressing SufCB has mixed effects on mitochondrial function depending on the genetic background. A) Expressing SufCB in Nfs1 mutants restores respiratory competence, as seen by the growth of SufCB-expressing mutants on non-respiratory carbon source. B) SufCB renders otherwise respiratory competent Bol3 mutants unable to grow on non-respiratory carbon sources. Wildtype (WT) cells were used as respiratory competent control. Experiment were performed at biological triplicate, using glucose and glycerol plates as respiratory and non-respiratory carbon sources, respectively. An 8x6 replica plater was used to plate the cultures and was sterilised by flame before each plating. Plates were incubated in parallel within the same incubator to rule out changing environments as a cause of the growth defects.

Figure 36A-B demonstrates that respiratory competence could be influenced by SufCB within mitochondria mutants and aligns with growth analyses in **Figure 35,** with positive and negative effects on growth rate in Nfs1 and Bol3 mutants, respectively.

For yeast, the mitochondria are the 'hubs' of iron-sulfur biosynthesis and perturbations to the mitochondrial iron-sulfur assembly apparatus have long been known to reverberate throughout the cytosolic iron-sulfur cluster assembly machinery (Kispal et al., 1999). Due to the phenotypes presented in **Figure 36**, it was of interest to assay whether expressing SufCB also rescued cytosolic iron-sulfur assembly in these mitochondrial mutants. This was performed by assaying the activity of the cytosolic iron-sulfur enzyme, Ecm17, in each mutant under 'normal' unstressed conditions (minimal media only) and under iron-starvation (0.5 mM ferrozine).

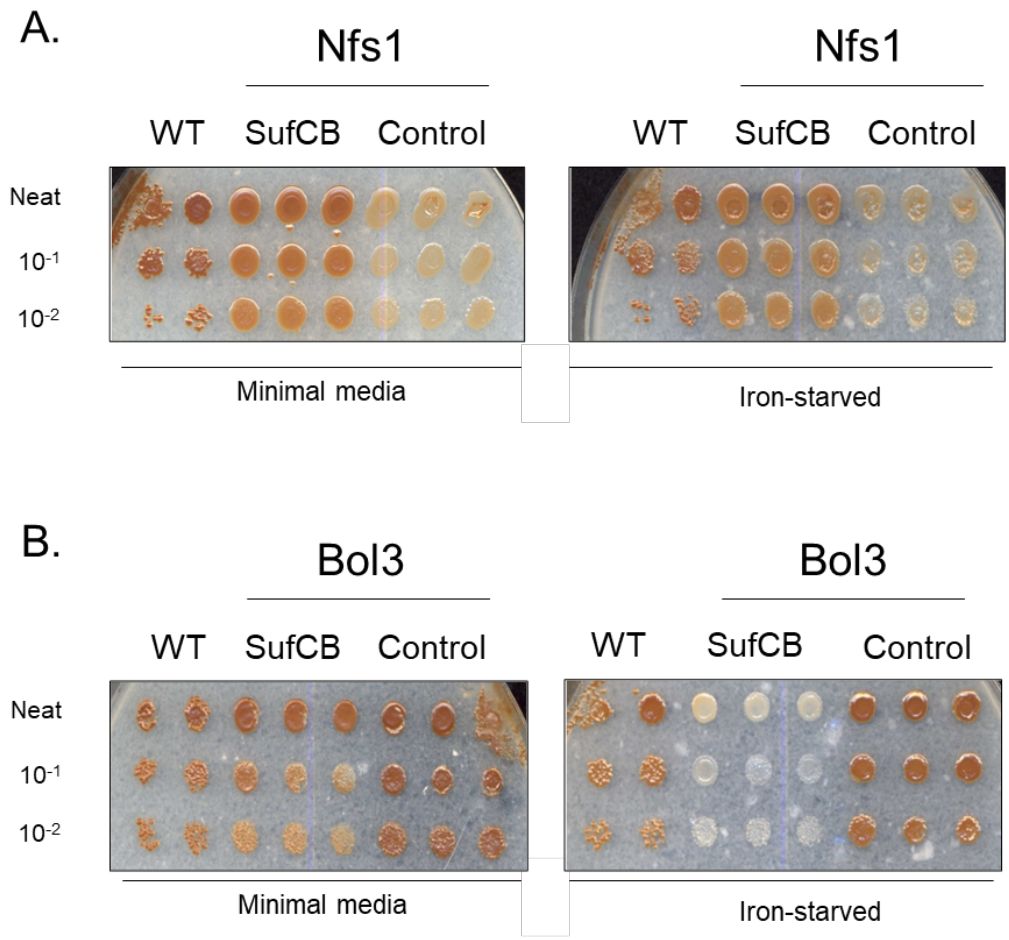

Figure 37. SufCB affects the maturation of cytosolic iron-sulfur protein, Ecm17 in yeast mitochondrial mutants. Ecm17 activity can be assessed by the appearance of bismuth precipitate which leads to dark brown colonies. A) SufCB rescues maturation of Ecm17 in Nfs1 ('SufCB', top panel) under both non-stressed and stressed conditions versus controls which lacked SufCB (controls, top panel). B) Conversely, whereas slightly worsened Ecm17 maturation in a Bol3 knockout seen by pale colonies in SufCB expressing cells ('SufCB', bottom panel), this could however be worsened (paler colonies) by incubating the cells with iron chelator (iron-starved). Wildtype (WT) used as negative control, cells were plated from exponential cultures. Assay was performed in biological triplicate and an 8 x 6 replica plater was used to aseptically transfer cultures and flamed between plating.

Figure 37 demonstrated that the effects of SufCB extend to the maturation of cytosolic iron-sulfur enzyme Ecm17. Again, Nfs1 mutants were rescued under both unstressed and iron-stress conditions (0.5 mM ferrozine) when expressing SufCB. Conversely, this phenotype was found to be reversed in the Bol3 mutant. Slightly paler colonies could be seen in Bol3 mutants expressing SufCB under unstressed conditions, indicating lower Ecm17 activity. This became clearer (worsened) when Bol3 cells were grown on BiGGY media containing ferrozine (0.5 mM), as the SufCB-expressing Bol3 mutants were much paler than Bol3 controls (**Figure 37**). The same spotting experiment was attempted on each of the CIA mutants, but no observable phenotypes were seen.

In summary, data in **figures 35, 36A-B and 37** demonstrated that SufCB genetically interacted with the yeast iron-sulfur assembly apparatus. In particular, interactions appeared to be enriched within the early CIA and mitochondrial proteins. The next set of experiments probed the interaction with CIA proteins further.

5.3 Replacement of Cfd1 with SufCB

A Cfd1 homologue has not been found to be encoded within the *Blastocystis* genome by neither transcriptomic nor immunofluorescence techniques (Tsaousis et al., 2014). Because of this, we hypothesised that SufCB may function in place of Cfd1 within *Blastocystis*, as a Cfd1-like protein.

For this experiment, a Cfd1 heterozygous diploid knockout (n=2, *cfd1*$^{+/-}$, Dharmacon) was used in which one allele of Cfd1 had been replaced with the cassette conveying geneticin resistance (*kanMX*) cassette. The strategy used to perform this replacement is shown in **Figure 38**.

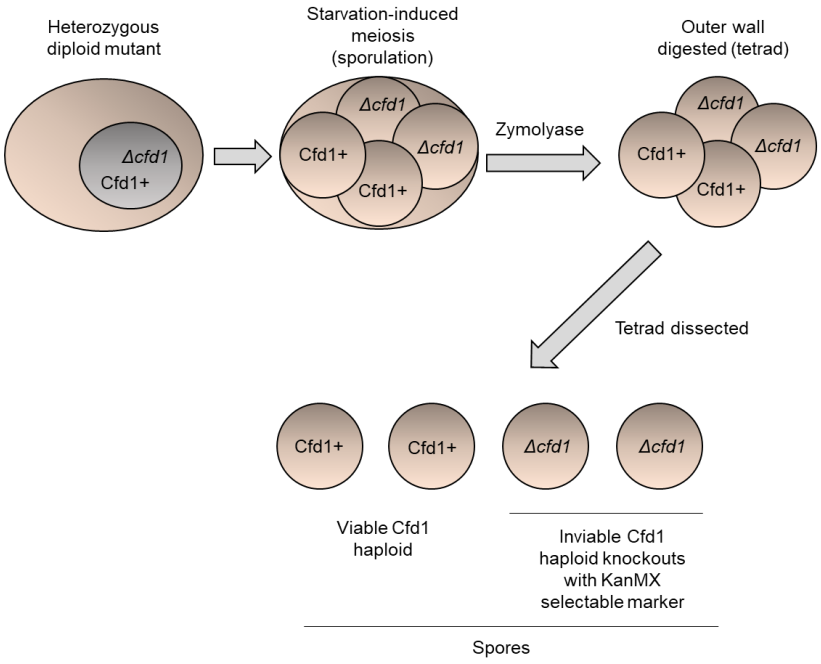

Figure 38. Flow chart of a Cfd1 tetrad dissection. The endpoint of the process yields 4 haploid spores (n=1), of which two contain the essential gene, whilst two are knockouts and are selectable with kanamycin (250 μg/mL). Cells are represented with beige circles, grey circle in the first cell is the nucleus of a diploid mutant (n=2) and contains a single allele of Cfd1.

The parental strain (Cfd1 heterozygous diploid mutant) was transformed with the SufCB construct and cells were struck onto sporulation plates (1% w/v potassium acetate, 0.1% w/v glucose, 0.125% w/v yeast extract, 2% w/v agar, see **chapter 2.3.1, Table 11**). After 5 days of static incubation at +30°C, tetrads could be seen under a light microscope at 40x objective. From here, the procedure followed the tetrad dissection method outlined in **chapter 2.5.3.** Attempts to transform the parental strain with the empty vector (pBEVY-u) consistently failed to yield viable colonies. The parental heterozygous diploid (BY4743) strain was also dissected as a negative control **(Figure 38)**.

Prior to performing the dissection, YPD plates with and without 250 µg/mL geneticin were prepared, thoroughly dried overnight (16 hours) on the benchtop. Following dissection, we expected to see 2 viable spores per tetrad (**figure 39**). After incubating at +30°C for 5 days, the revived spores on each YPD plate were replica plated onto YPD supplemented with geneticin (250 µg/mL) and incubated again at +30°C for another 5 days. Positive growth under geneticin selection was used to indicate that SufCB had successfully replaced Cfd1. After 5 days incubation, two large colonies and one small colony were observed on YPD supplemented with geneticin (**Figure 39B**). From this, we concluded that these spores were viable Cfd1 knockouts which indicated that SufCB had replaced the function of Cfd1.

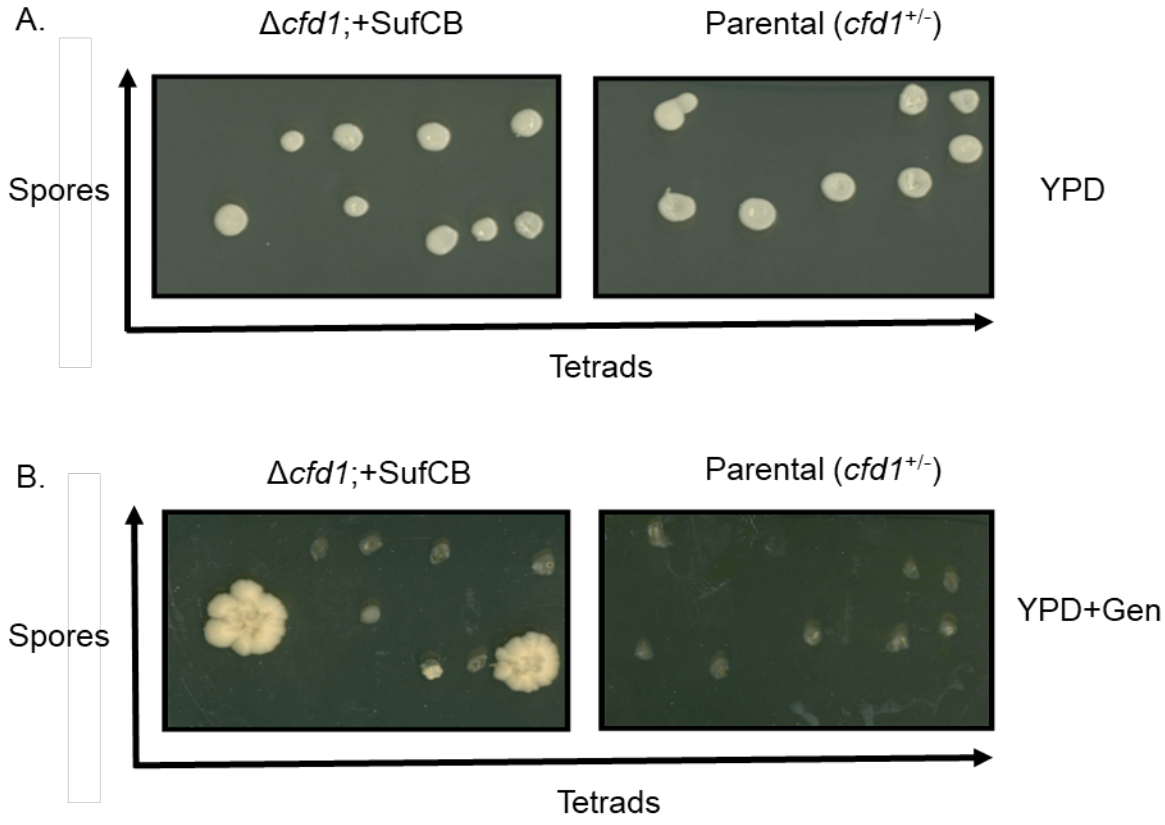

Figure 39. Tetrad dissection of Cfd1. A) Agar plates (YPD) in which dissected tetrads had been separated out in their spores and grown for 3 days from both SufCB transformed and untransformed heterozygous diploid strains. Each tetrad yielded at least one viable spore. B) Spores were replica plated onto plates containing geneticin disulfate (G418, 250µg/mL) to select of the kanamycin resistance marker. Growth on G418 indicates successful replacement of Cfd1 (*cfd1* $^{+/-}$). Tetrads were dissected and plated in a grid pattern where one tetrad (x-axis) was dissected into four spores (y-axis). Plates indicate growth after three days (A) and five days (B).

Although the results of the above experiment suggested that SufCB had functionally replaced Cfd1, further work was required to confirm that these spores were true Cfd1 knockouts. To achieve this, we validated that each geneticin resistant spore was haploid by investigating their mating type via multiplex colony PCR. Following PCR, each sample analysis via TAE agarose electrophoresis. For haploid cells, colony PCR revealed a single band at either 404 bp or 544 bp and a combination of both for diploid cells. Known haploid (BY4741) and diploid (BY4743) strains were used as controls. The results of this investigation are shown in **Figure 40**.

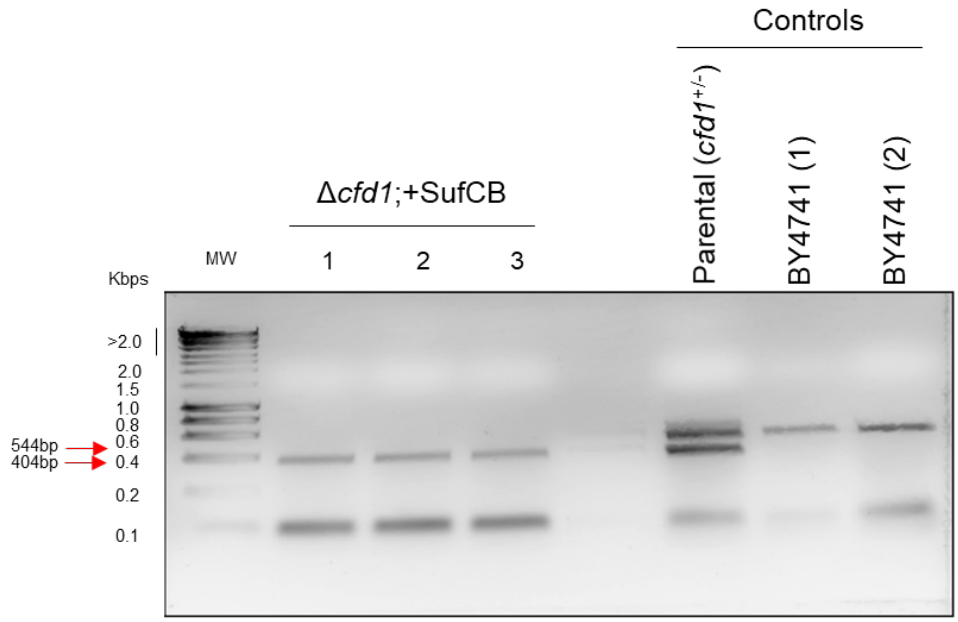

Figure 40. TAE gel indicating that the viable spores observed in Figure 38 were haploid. Mating type colony PCR on G418 resistant spores, parental strain (diploid) and two runs of BY4741 (haploid) were used as controls. 1% TAE Agarose gel, Hyperladder II was used as a standard. Red arrows indicate bands of interest.

The results of this experiment give evidence to suggest that a single viable spore plated in **Figure 39** was haploid and therefore a successful Cfd1-knockout. Three individual PCRs were performed using a small portion (~10%) of each viable genetic-resistant spore (**Figure 39B**). Controls included the parental heterozygous deletion strain (*cfd1*$^{+/-}$) and wildtype (BY4741), as diploid (n=2) and haploid (n=1) controls respectively. After cycling had finished, the entire PCR reaction (50 µL) was analysed by electrophoresis on a 1% w/v TAE agarose gel, which when visualised, revealed a single band at 404bp. The two much larger colonies growing on YPD were found to be diploid by the same method (not shown). In addition, primer dimers can be seen at < 200 bp.

These data in **figures 39** and **40** indicated that our attempts to replace the yeast Cfd1 with SufCB were successful, the resulting mutant was named Δ*cfd1*;+SufCB.

5.4 Supplementing Cfd1 mutants with iron can improve growth rates.

Phenotypically, the SufCB-Cfd1 mutant *(*Δ*cfd1*;+SufCB) was found to be much more slowly growing that than its parental strain, regardless of growth media (rich or minimal media). Quantifying the specific growth rate of Δ*cfd1*;+SufCB in rich YPD media gave an average -52% reduction from the parental heterozygous diploid strain (BY4743) (**Table 39**). Cultures grown in minimal uracil drop-out media similarly displayed a significantly ($p<0.01$) reduced (-62%) growth rate when compared to an uracil prototroph (wildtype expressing empty pBEVY-u). The ability of the Cfd1 knockout mutants to grow in uracil drop out media also further confirmed that the SufCB construct was present in this mutant, as the parental diploid strain was auxotrophic for uracil.

Table 39. Table of specific growth rates in either YPD (rich) or Synthetic defined (minimal) media of either Cfd1 knockouts replaced with SufCB or controls (parental and an uracil prototroph). Growth rates displayed in generations per hour (Gens/Hr), error (±) is SEM.

	Specific Growth Rate, Gens/Hr	
Growth Media	SufCB	Control
YPD	0.245 ± 0.016	0.466 ± 0.004
Minimal media	0.234 ± 0.018	0.374 ± 0.004

To investigate the poor growth of Δ*cfd1*;+SufCB further, we supplemented minimal uracil drop-out media with iron salts at 0.5 mg/L in order to test whether the phenotypes were due to iron deficiencies resulting from the loss of a Cfd1 (Pallesen et al., 2013). T-testing ($p>0.05$) confirmed that this caused a statistically significant ($p<0.01$) increase in growth rate between iron-supplemented and non-iron supplemented cultures of Δ*cfd1*;+SufCB (**Table 40**).

Table 40. Table of specific growth rates of Cfd1 mutants in iron supplemented media. Growth was monitored between SufCB (Cfd1 knockout) and parental diploid strain (control). Growth rates displayed in generations per hour (Gens/Hr), error (±) is SEM.

	Specific Growth Rate, Gens/Hr	
Growth Media	SufCB	Control
Minimal media	0.244 ± 0.016	0.465 ± 0.0039
Minimal media + iron	0.296 ± 0.013	0.468 ± 0.007

When grown in iron supplemented cultures, Δ*cfd1*;+SufCB mutants displayed significantly increased specific growth rates compared to cultures with no iron-supplementation (**Table 41**). Importantly, iron-supplementing parental strain in YPD did not result in similar phenotypes. These data were transformed into ratios and plotted in **Figure 41.**

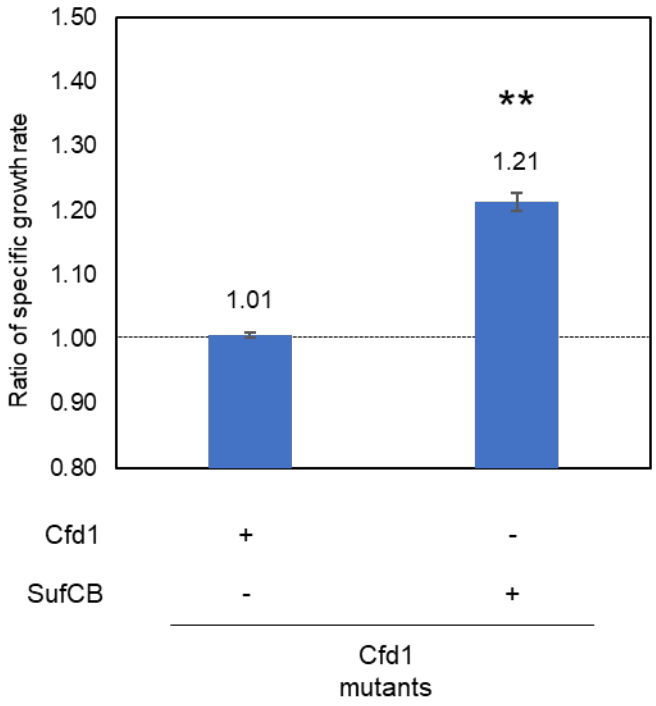

Figure 41. Plot of the ratio of specific growth rates from Δ*cfd1*;+SufCB knockouts and parental strain. Ratio expressed as the iron supplemented growth rate over the growth rate of non-supplemented mutants. A value of 1, indicated no effect of iron supplementation, above 1 indicates an increase in growth rate resulting from iron supplementation of the media. Two-tailed t-testing was used to infer significance using α=0.05, data at n=4, duplicate. Significance codes were p<0.01 = **, error is SEM.

The phenotypic data, therefore, suggest that whilst SufCB could, fundamentally, replace Cfd1 in yeast mutants, the resulting knockouts had poor fitness as evidenced by the growth rate analyses in **Table 40**. This could somewhat be rescued by iron-supplementation which appeared to have a significant and positive effect on the growth rates of the Cfd1 knockouts. In comparison, iron-supplementation had no effect (p>0.05) on the growth of the parental control (**Figure 41**), suggesting that the growth defects that were observed in the SufCB-rescued knockouts were in some part linked to iron-deficiency.

5.5 Iron-sulfur biogenesis in CIA mutants

Results so far have indicated that SufCB may exert its pro-maturation by functioning as an auxiliary Cfd1 protein in *S. cerevisiae* (**figures 39-41**). As our growth data was insufficient to reinforce this hypothesis (**Figure 35**), we moved to look at how SufCB affects the maturation of a reporter iron-sulfur enzyme in CIA mutants. For this, we used the aconitase construct created in **chapter 4.5.1**. We chose to use aconitase as Ecm17 failed to yield any noticeable phenotypes (not shown).

In addition to probing the activity of Aco1 in Nbp35 and Cfd1, we also probed Dre2 mutants. This was because SufCB was shown to aggravate the growth rate of Dre2 mutants, suggesting the dependency of SufCB on wildtype levels of the Dre2 protein. Wildtype yeast which contained these candidate proteins was used as a control. **Table 41** summarises the effects of SufCB expression in each CIA mutant studied so far. Based on these data, biochemical reporter assays we selected the early-CIA members, displayed in **Figure 42**.

Table 41. Summary table of the interactions between CIA machinery and SufCB. The function of each CIA member is also shown.

Protein	Function	Interaction with SufCB
Nbp35	Scaffold	Unknown
Cfd1	Scaffold	Replacement
Dre2	Electron carrier	Possible dependency

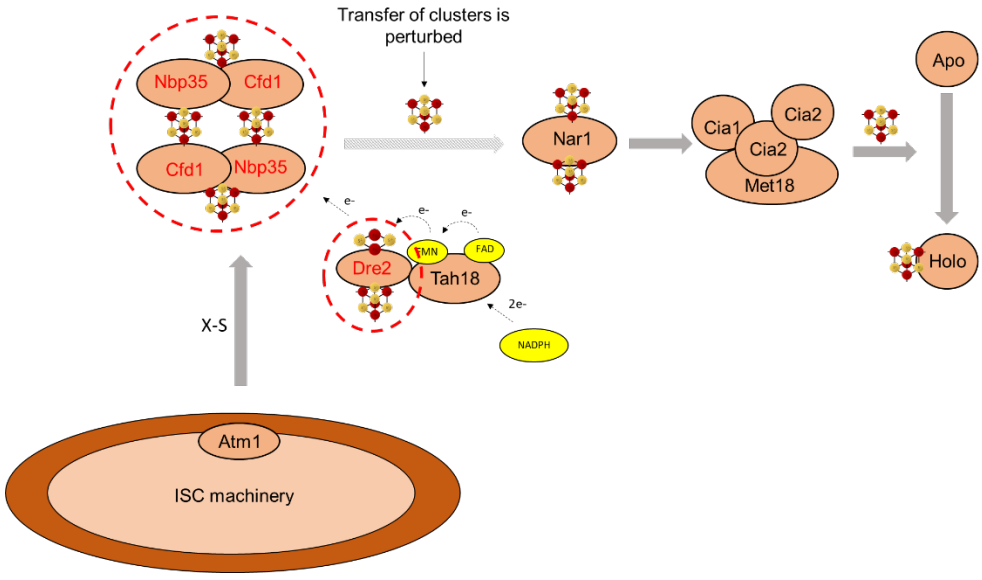

Figure 42. Schematic of the depleted 'early' CIA pathway. The investigation studied three single Nbp35, Cfd1 and Dre2 mutants which are coloured red and surrounded by a dashed box.

After normalising for the protein concentration (mg/mL) in each sample, the data demonstrated that both Nbp35 and Cfd1 mutants had a statistically significant ($p<0.05$) decrease in aconitase activity compared to the wildtype control (WT), **figures 43-44**. These data calculated 26% and 7% of the aconitase activity of wildtype, in Nbp35 (**Figure 43**) and Cfd1 (**Figure 44**) mutants, respectively. A direct comparison between aconitase maturation in Nbp35 and Cfd1 was avoided due to the differing levels of depletion between mutants. Roy et al., (2003) also demonstrated a similar (10%) percentage decrease compared to wildtype using a depleted Cfd1 yeast mutant, suggesting that the method used was fit for purpose.

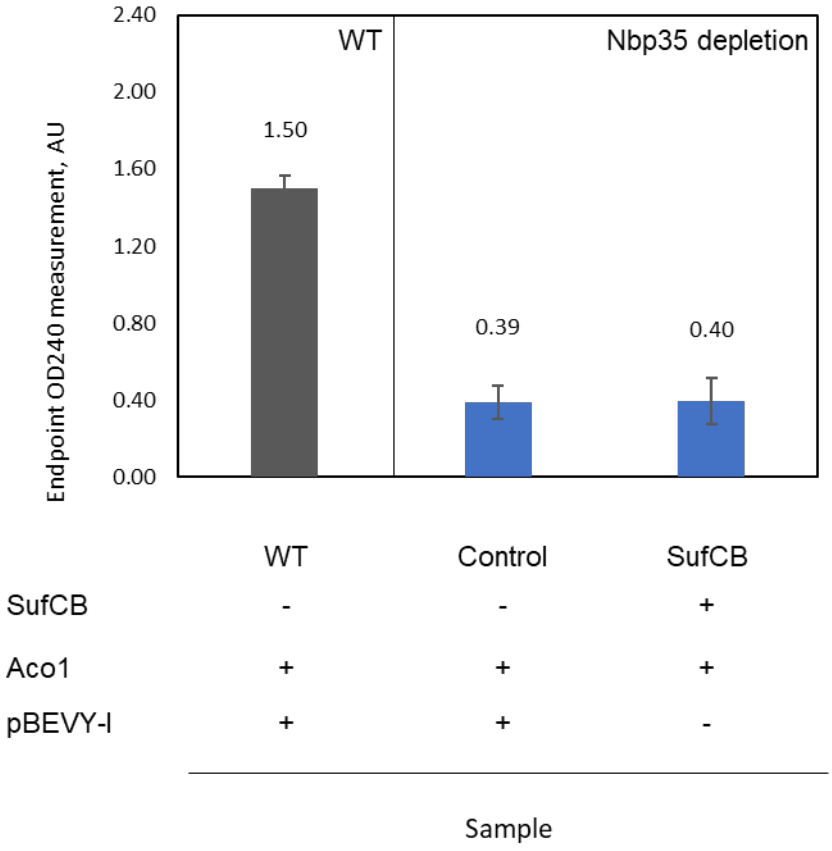

Figure 43. Activity of aconitase in Nbp35 mutants. Total aconitase activity in Nbp35 mutants expressing SufCB or empty vector. Control using wildtype expressing aconitase (WT). Activity was determined by monitoring the endpoint absorbance at 240nm and then normalising to protein input using a quantitative Bradford assay. Significance was determined by one-way ANOVA followed by Tukey's HSD, n=4 error is SEM.

For the Nbp35 mutant, expression of SufCB conferred a very small but insignificant ($p>0.05$) decrease in aconitase activity from 0.397 ± 0.120 AU to 0.389 ± 0.085 AU (**Figure 43)**. Indicating that the two proteins may co-operate for efficient iron-sulfur assembly.

In comparison, the aconitase activity in Cfd1 mutants showed a statistically significant ($p<0.05$) increase upon introduction of SufCB (**Figure 44**). Aconitase activity in the Cfd1 mutant rose from 0.095 ± 0.032 AU to 0.258 ± 0.018 AU when SufCB was present.

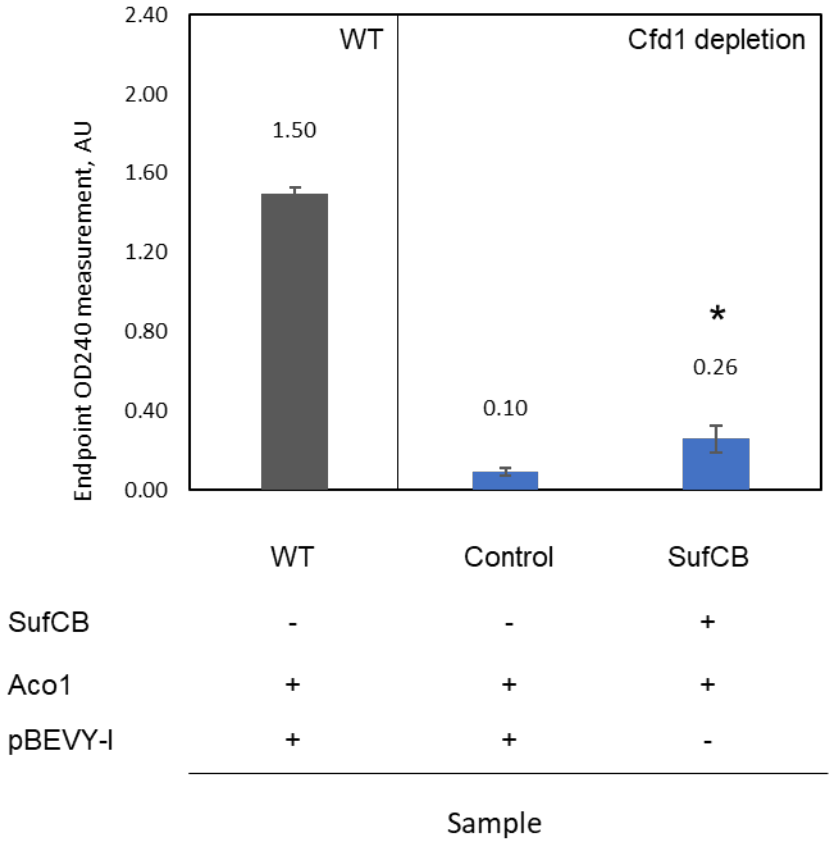

Figure 44. Activity of aconitase in Cfd1 mutants. Total aconitase activity in Cfd1 mutant is rescued by expressing SufCB. Control using wildtype expressing aconitase (WT). Activity was determined by monitoring the endpoint absorbance at OD_{240nm} and then normalising to protein input using a quantitative Bradford assay. Significance was determined by one-way ANOVA followed by Tukey's HSD, data at n=4, error is SEM.

Chapter 5.2 (**Figure 35**) demonstrated a significant reduction in growth rate resulting from expressing SufCB in a Dre2 mutant. In addition to this, we have also shown that aconitase activity is lowered in a Dre2 mutant expressing SufCB. Aconitase activity dropped significantly ($p<0.01$) upon introduction of SufCB from 0.101 ± 0.0065 AU in controls to 0.046 ± 0.006 AU, reflecting an average drop of 45% as a result of expressing SufCB (**Figure 45**).

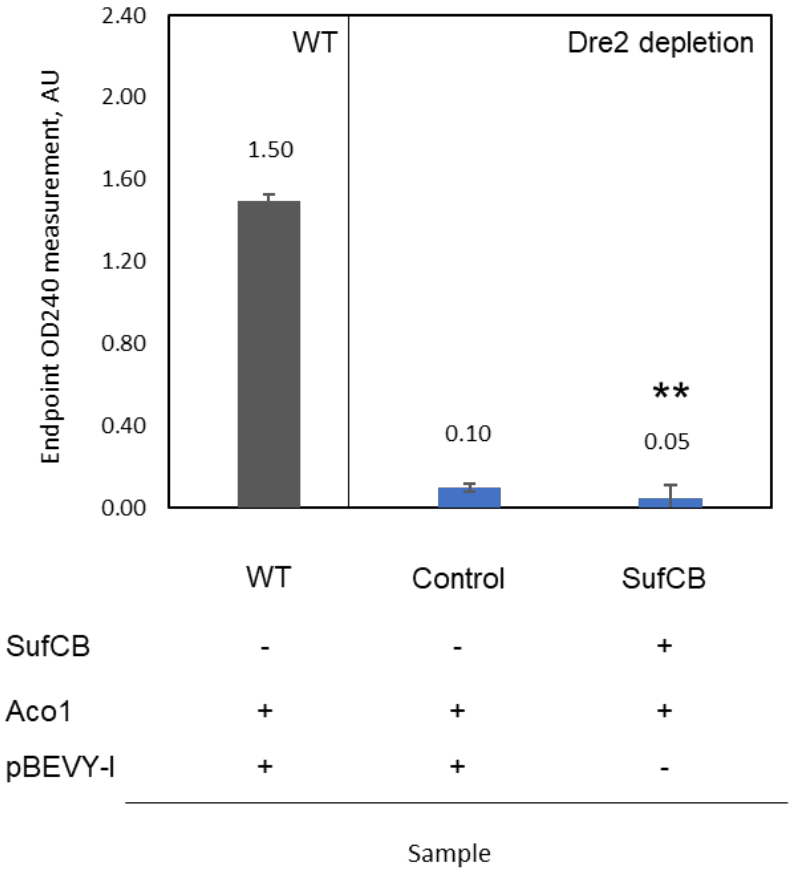

Figure 45. Activity of aconitase in Dre2 mutants. Total aconitase activity in a Dre2 mutant is severely disrupted upon expression of SufCB. Control using wildtype expressing aconitase (WT). Activity was determined by monitoring the endpoint absorbance at 240nm and then normalising to protein input using a quantitative Bradford assay. Significance was determined by one-way ANOVA followed by Tukey's HSD, data at n=4, error is SEM.

5.6 Identifying physical interactions between SufCB and the CIA machinery

By assaying the genetic interactions between SufCB and the CIA machinery, we have given evidence to suggest that SufCB is a 'Cfd1-like' protein.

We next assayed whether SufCB interacts with Cfd1's partner, Nbp35. To perform these experiments, we used an HA-tagged SufCB (C-terminal) and commercially available anti-HA magnetic beads (Pierce, UK) which could be purified from lysates via magnetic rack (Fisher, UK). Lysates of cells containing either tagged SufCB or controls (no SufCB) were prepared by harvesting 250 mL of exponentially (OD_{600nm} of ~1) growing shake flask cultures before cells were chemically disrupted under non-denaturing conditions (YPER). Five 2 mL washes in a bespoke wash buffer (250 mM Tris Base, 100 mM NaCl, 2.5 mM $MgCl_2$ and 2 mM β-mercaptoethanol pH 7.2) was used to remove non-specific contaminants. It was unknown how strongly SufCB may interact with any proteins and so each was fraction was saved for later analysis. We also found that stringent washing steps were required to remove non-specific iron-binding proteins which may interact with the magnetic beads. Although this standard buffer was routinely used, pilot experiments were also performed using high salt (2 M NaCl) and chelating (0.5 M EDTA) protein buffers in order to investigate how these conditions may alter the protein binding by SufCB. Despite this, we were unable to conclusively demonstrate that these buffers altered the binding of SufCB to candidate proteins.

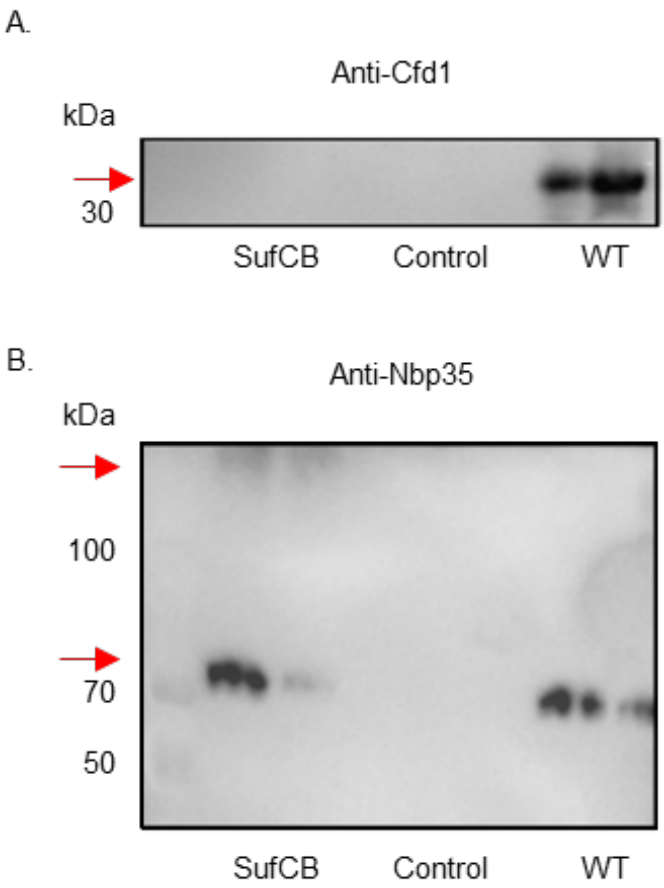

Figure 46. Western blot to identify physical interactions of SufCB with early CIA scaffolds. A) Anti-Cfd1 (31 kDa) shows no physical interaction. B) Anti-Nbp35, SufCB interacts with dimeric Nbp35 protein (70 kDa). 14 µL and 7 µL loading pattern was used for each sample, gels were cropped to the molecular weights of the target proteins. Lysates containing SufCB are indicated by SUFCB or control. 10 µL of BioRad dual colour protein marker was used to confirm the molecular weight of proteins.

An anti-Cfd1 (R. Lill) western blot showed no bands matching the molecular weight of Cfd1, indicating that SufCB did not strongly bind to the Cfd1 protein (31 kDa) in yeast (**Figure 46A**). Anti-Nbp35 antibodies (anti-rabbit, R. Lill), however consistently detected a band matching the weight of dimeric Nbp35 (red arrow, ~70 kDa). In addition, **Figure 46B** also contains a higher molecular weight band which was detected by the anti-Nbp35 antibodies. Although we were unable to identify the nature of this species by further analytics (UHPLC). The samples represented here were generated from three 2mL washes, which suggested that SufCB and Nbp35 form a stable complex. Wildtype controls (WT) were also loaded to confirm that the antibodies used could bind to their target proteins.

Our co-immunoprecipitation experiments demonstrate that SufCB interacts with the core CIA scaffold, Nbp35 in its dimeric (70 kDa) form but not Cfd1 and supports previous genetic data that SufCB is a Cfd1-like protein.

5.7 Purification of SufCB from *S. cerevisiae* lysates

Having demonstrated that SufCB interacts with the yeast iron-sulfur assembly machinery, we next attempted to demonstrate that SufCB is itself an iron-sulfur protein and by doing so this could help to elucidate the mechanism of SufCB, in particular as both Cfd1 and Nbp35 have their own conserved iron-sulfur clusters (Bastow et al., 2017; Stehling et al., 2018).

We used immobilised metal affinity chromatography (IMAC) to purify a tagged (6xHis) SufCB protein from yeast lysates prepared from 5L exponentially growing (OD_{600nm} ~1.2) SufCB-expressing yeast cultures. To perform this, empty PD10 columns (GE Healthcare, UK) were loaded with 5mL of fast chelating sepharose (GE Healthcare, UK), washed and then charged with 0.2M nickel chloride to yield a Ni^{2+}-NTA resin which the his-tagged SufCB protein could bind to and be eluted from. These experiments also served as a comparison to the previously published data produced by Tsaousis et al., (2012) in which SufCB purified from *E. coli* cells was found to contain a [4Fe4S] cluster by UV/Vis spectrophotometry and EPR. In this study, we asked whether SufCB produced by yeast could also bind an iron-sulfur cluster.

First, the SufCB ORF was re-cloned into pBEVY-u with oligonucleotides designed to incorporate a C-terminal 6xhis tag which enabled us to use Ni-affinity chromatography in order to purify the protein from crude yeast lysates. Initially, we performed pilot experiments using exponentially grown cultures at 1L scale and confirmed that SufCB could be purified (0.4 mg/mL) using a harsh denaturing elution buffer (300 mM NaCl, 100 mM Tris-HCl, 5% v/v Glycerol, 100 mM EDTA, pH7.5) which contained 100 mM EDTA (**Appendix 22**). Once we had demonstrated that denatured SufCB could be purified using Ni-NTA, we then replaced EDTA (100 mM) with imidazole (250 mM) in the elution buffer (300 mM NaCl, 100 mM Tris-HCl, 5% v/v Glycerol, 250 mM Imidazole, pH7.5) and increased the culture volume to 5L, which yielded higher concentrations of SufCB protein to 4.7 mg/mL Routinely, 10% v/v acrylamide gels were used to confirm the successful purification of SufCB, in which we saw a faint band at 77 kDa by Coomassie staining and anti-SufCB western blots (**Figure 46**).

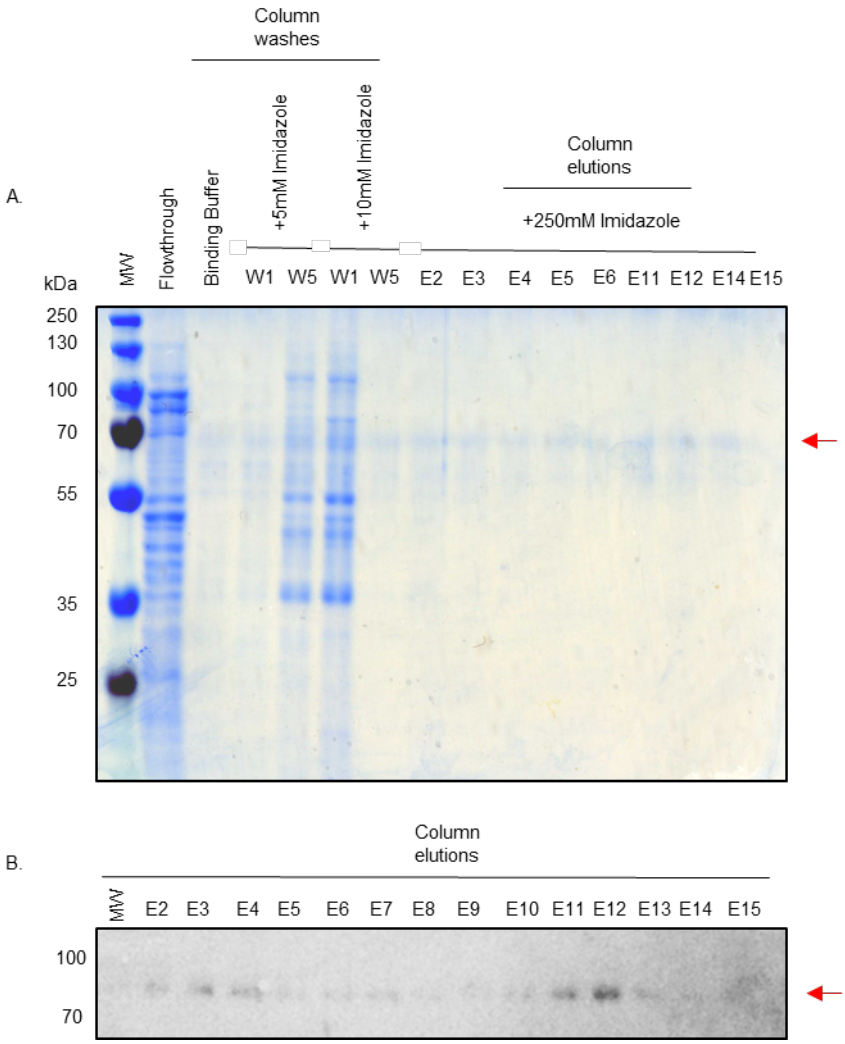

Figure 47. Successful EDTA free aerobic purification of his-tagged SufCB protein using IMAC. A) Coomassie staining of SDS-PAGE gel showing wash steps and elution containing visible full-length protein. B) Anti-western SufCB western blot of elution fractions only showing presence of full length SufCB protein (red arrow) isolated from cell-free lysate. 10 µL loaded per well, samples were analysed immediately after elution from the column. Bands on the lower half of the gel were attributed to non-specific signal and commonly seen. Red arrow indicates the purified SufCB monomer in both gels.

Figure 47 demonstrates the successful purification of tagged SufCB from yeast cell-free lysates. The yield of total protein produced during this purification is summarised in **Table 42,** below. An estimated total protein concentration (mg/mL) for each elution fraction was quantified by UV-spectroscopy in a UV-cuvette at $OD_{280\ nm}$ (1 cm pathlength) to 28.43 mg/mL. This value was then converted using the Beer-Lambert law, to give a SufCB concentration of 4.7 mg/mL. Conversion of total protein to (absorbance at $OD_{280\ nm}$) was calculated using the extinction coefficient of non-reduced SufCB, which equals 51,435 mol^{-1}/cm^{-1} and Beer's Law. However, we continually observed that a fraction of all protein samples aggregated despite boiling and reduction using strong reducing agent DTT at 100 mM (**Figure 47**). Fractions were then buffer exchanged using a prepacked PD10 to remove urea and imidazole into iron-sulfur reconstitution buffer (300 mM NaCl, 100 mM Tris-HCl, 10% v/v Glycerol, pH8.0). Aggregation was a prominent issue throughout purification. As buffer exchanging SufCB from a high-salt (NaCl, 300 mM) into a low salt (50 mM) buffer greatly decreased protein recovery from a desalting PD10 column.

Table 42. His-tagged SufCB elution fractions. The protein content of each fraction was quantified at OD_{280nm} and used to calculate protein concentrations in both mg./mL and µM.

Elution	A280	Total Protein (mg/mL)	SufCB (mg/mL)
#1	0.007	0.072	0.011
#2	0.280	2.080	0.438
#3	0.116	1.160	0.182
#4	0.154	1.540	0.241
#5	0.103	1.030	0.161
#6	0.010	0.100	0.016
#7	0.145	1.450	0.227
#8	0.211	2.110	0.330
#9	0.011	0.110	0.016
#10	0.010	0.100	0.017
#11	0.683	6.830	1.070
#12	1.231	12.31	1.930
#13	0.020	0.200	0.031
#14	0.030	0.300	0.047
Total Pooled (mg/mL)		28.43	4.723
Concentration (µM)		-	61.3

5.7.1 Reconstitution reaction with purified SufCB

SufCB fractions were concentrated using Amicon® Ultra-15 spin-concentrators according to manufacturer's instructions (Merck, UK). Once concentrated, SufCB samples were then incubated with sources of either iron (III) or sulfide (L-cysteine), a reducing agent (DTT) and a cysteine desulfurase (NifS) in iron-sulfur reconstitution buffer (300 mM NaCl, 100 mM Tris-HCl, 10% v/v Glycerol, pH 7.5). A four-fold molar excess of salt to SufCB was used to drive a reaction which favoured the assembly of a [4Fe4S] cluster on SufCB, as observed by Tsaousis et al., (2012). Cysteine desulfurase, NifS (1 µL), was added last and used to initiate the reaction. Exact concentrations of each reactant required were determined by troubleshooting against the appearance of iron-sulfide aggregates.

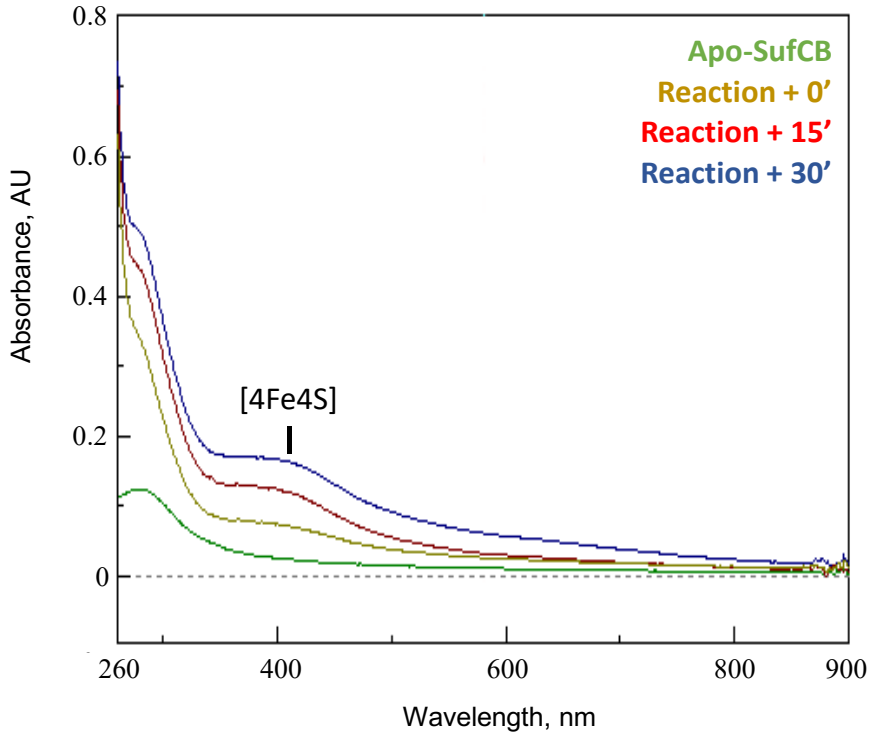

Figure 48. Wavelength scanning (260-900nm) of SufCB protein incubated with excess iron and sulfide salts under reducing conditions. Figure shows the gradual appearance of a shoulder at 300-420nm. Reaction performed in an anaerobic workstation; time points were taken every 15 minutes.

A pronounced shoulder at $OD_{400\text{-}450nm}$ suggested that a [4Fe4S] cluster had begun to form on SufCB **(Figure 48)**, which if followed over time appeared outwards at a slight angle in line with other descriptions of reconstitution reactions (Bastow et al., 2017; Crack et al., 2014b). The ratio of absorbances at OD_{280nm} and shoulder peak ($OD_{400\text{-}450nm}$) was also roughly 2:1, also indicative of a successful cluster reconstitution (advice from J. C. Crack). The reaction also gradually became yellow brown over time and finally black.

The reaction proceeded until a black iron sulfide precipitate began to appear in the cuvette, indicating that the reaction had finished. Before spectroscopy was performed the reaction was syringe filtered through a 0.22 μM PES filter. The rate of the appearance of this precipitate is also dependent upon an accurate quantification of SufCB protein, which was achieved by quantifying the sample absorbance at OD_{280nm}. In addition, this fact also gave an indication that the initial desalting step during preparation for reconstitution had removed enough urea for SufCB protein to refold enough to potentially accommodate an iron-sulfur cluster.

We next sought to investigate whether reconstituted SufCB could pass through a desalting PD10 column (GE Healthcare, UK). Desalting effectively removes all other contaminants which interfere with the wavelength scan. In addition to removing contaminants, this step also indicates whether the possible SufCB-bound cofactor is tightly associated with the protein, giving strength to the argument that SufCB contains a cofactor. Again, we followed colour as a rough guide to track reconstituted SufCB protein as it eluted from the PD10 column, gold-yellow fractions were analysed further, the gradual appearance of darker fractions indicate contaminants from the reconstitution reaction were discarded.

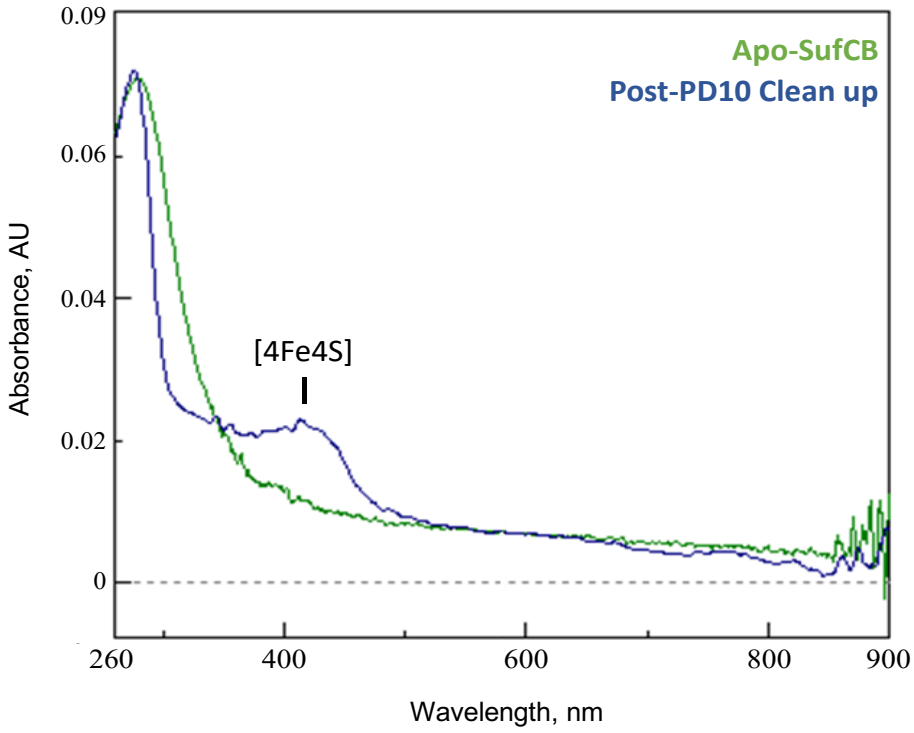

Figure 49. UV/Vis Spectrum of purified reconstituted and desalted SufCB protein compared to apo-protein. Absorbance (Y), arbitrary units (AU), wavelength (X), nm. Range: 260 – 900 nm. Plot shows the persistence of an absorbance region around 380-450nm, indicating tight attachment of a chemical species to SufCB.

The most coloured eluates (500 µL) from the desalting step were then analysed by spectroscopy using a JASCO spectrophotometer and a minimal volume sealable anaerobic UV-cuvette. **Figure 49** shows the spectrum (260-900 nm) of desalted SufCB eluate (**Figure 49, blue trace**) from the PD10 column. The persistence of the shoulder previously seen at $OD_{380\text{-}450nm}$ during reconstitution suggests that a chemical species is tightly associated with the SufCB protein, following incubation with sources of iron and sulfide under reducing conditions. Conversely, apo-SufCB (non-reconstituted) doesn't show a shoulder at this wavelength **(Figure 49, green trace)**. In addition, no other shoulders can be seen on desalted SufCB protein.

5.7.2 Purification of SufCB under non-denaturing conditions

Figure 48 shows that a chemical species tightly associated with isolated SufCB protein following a reconstitution reaction. Next, we anaerobically purify SufCB under non-denaturing conditions, i.e. without urea, to yield folded SufCB. The spectrum of this isolated protein was then compared with the denaturing purification in **Figure 50.** All steps herein, including lysis, were performed within an anaerobic workstation (<2ppm [O_2], Belle Technology) under a blanket of nitrogen and forming gas (BOC, UK). Lysis buffer was degassed for 1 hour with nitrogen and placed within the anaerobic workstation prior to use.

Following lysis, 50 mL of brown yeast lysate containing tagged-SufCB was loaded onto a HiTrap nickel column and purified using an Akta prime at a flow rate of 1 mL/min, conductance and OD_{280nm} was measured to monitor flow of protein through the column. A visibly brown band could be seen moving through the HiTrap matrix. Flowthrough was retained for analysis (**RT, Figure 50**). Once all sample had been loaded, proteins were eluted by inverting the column and adding 500uµµ of elution buffer via 3 mL syringe. Eluate was harvested in 500 µL Eppendorf tubes and an aliquot (10 µL) of each fraction was immediately analysed by SDS-PAGE (10% v/v) to confirm the presence of SufCB protein.

Figure 50 shows a band matching SufCB (77 kDa) had been isolated from the yeast lysate, indicating successful purification under anaerobic conditions.

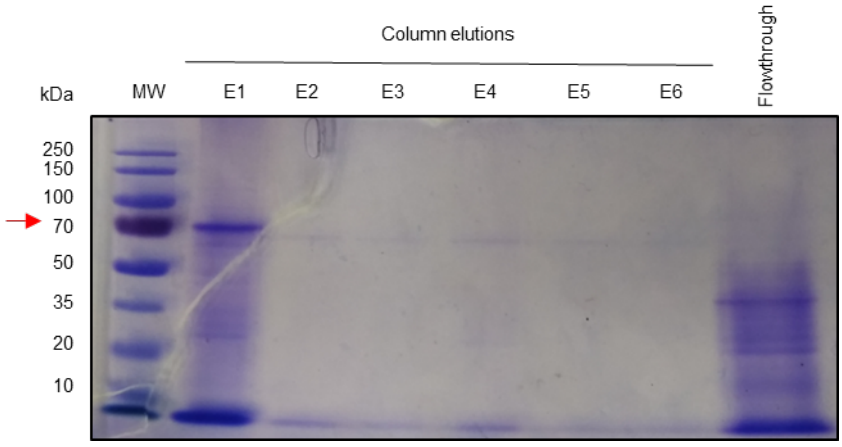

Figure 50. Coomassie staining of native SufCB purification as isolated. 10 µL of each eluate was loaded onto a 10% w/v acrylamide gel and stained with Coomassie blue. Elution fractions are designated E1 – E6. Unbound host proteins which ran freely through the Ni^{2+} column was analysed and was designated 'RT'.

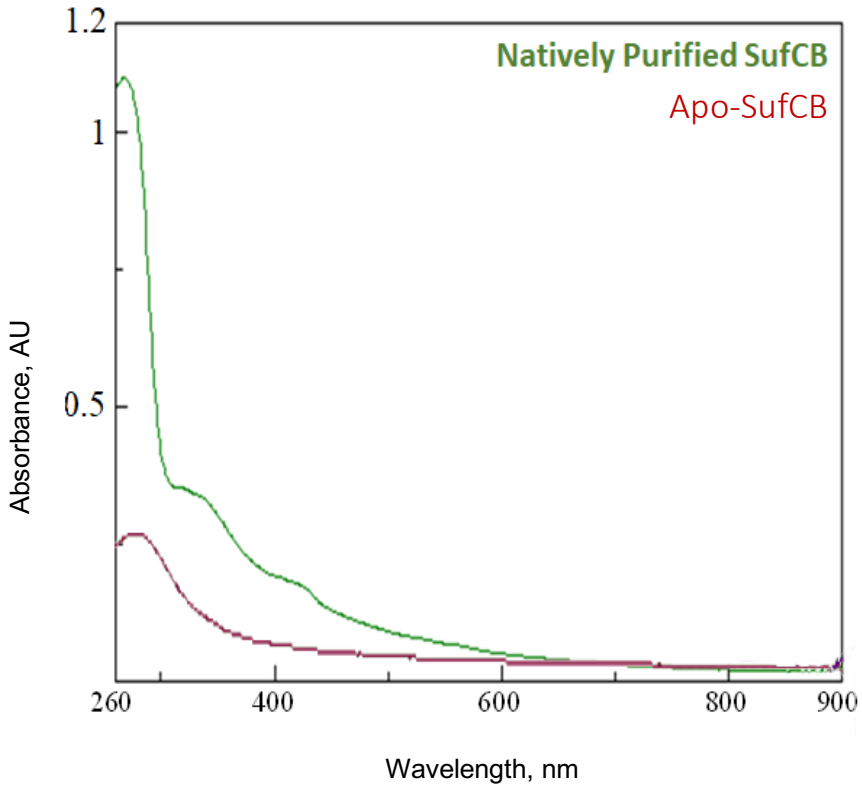

Figure 51. UV/Vis Spectrum of natively purified SufCB protein compared to apo-protein. Absorbance (Y), arbitrary units (AU), wavelength (X), nm. Range: 260 – 900nm. The reaction was performed in a reduced volume (1mL) anaerobically sealed cuvette.

We next transferred the eluate, which was found to contain a band matching the weight of the SufCB protein (**Figure 50, E1**), into a sealable minimal volume (1 mL) anaerobic cuvette. Wavelength scanning between 260-900 nm (**Figure 51**) showed a minimal shoulder at $OD_{400\text{-}450nm}$ which is largely obscured by a much larger absorbance at $OD_{300\text{-}380nm}$ (**Figure 51, green trace**). Again, apo-SufCB control showed no absorbance peaks at any wavelength other than peptide bonds at 280 nm (**Figure 51, red trace**). **Figure 50**, however, demonstrates that the sample was impure and thus the unusual shoulder at OD_{330nm} could be a contaminating protein. Low protein yield prevented us from probing this further by LC/MS or broad-range circular dichroism.

5.8 Summary of results.

The aim of this research chapter was to identify a mechanism for how SufCB is able to produce the phenotypes presented in chapter 4.

v. To probe genetic interactions between SufCB and the mitochondrial and cytosolic iron-sulfur pathways.

Searching for growth rate complementation in various CIA mutants demonstrated that SufCB had mixed effects. We found the growth rates of Atm1 and Nfs1 mutants were significantly increased when expressing SufCB. Counter to this, we also found that the growth and, in some cases, iron-sulfur biogenesis of Bol3 and Dre2 mutants were lowered by expressing SufCB, suggesting that expressing the SufCB protein (or recombinant proteins) is dependent on these proteins.

vi. To replace the yeast CIA machinery with SufCB.

SufCB was able to rescue lethality resulting from a Cfd1 deletion. Despite this, the mutants were still sick showing a significantly decreased growth rate compared to parental strain in both rich YPD and minimal uracil drop-out media, as SufCB was introduced on pBEVY-u. This growth rate could be significantly improved upon after supplementation with 0.5 mg/L iron (II) salts, although not back to the wildtype growth rate. The same supplementation did not rescue the growth rate of a negative control mutant, which contained Cfd1. This indicates that although Cfd1 can be replaced by SufCB, the cell still lacks iron, potentially as a substrate for iron-sulfur assembly.

vii. To perform candidate co-immunoprecipitation experiments to identify protein-partners of SufCB in yeast.

SufCB also appeared to interact with Cfd1's cognate partner protein, Nbp35 which resolved as a dimer, suggesting SufCB specifically interacts with dimeric Nbp35. This reflects the predicted CIA system in *Blastocystis*. These data also reinforce claims made throughout that low SufCB expression is seen due to complex formation with endogenous machinery, a SufCB-Nbp35 dimeric complex would be 154 kDa as monomeric SufCB and 220 kDa as SufCB dimer complexed with Nbp35 dimer. Dimeric Nbp35 has previously been detected by SDS-PAGE, demonstrating that the protein can survive reduction (Camire et al., 2015). By expressing the aconitase construct in CIA mutants we have demonstrated significantly reduced aconitase activity in all mutants tested. Introduction of SufCB into these mutants was able to restore aconitase activity in a Cfd1 mutant, but not in a Nbp35 mutant indicating the above finding is true that SufCB is a Cfd1-like protein and exerts its pro-maturation effect by interacting with Nbp35 scaffold in the early stages of the CIA pathway.

viii. To purify SufCB and investigate its chemical properties.

Finally, we were able to purify SufCB from yeast and indicate some chemical properties. His-tagged SufCB can be purified on a Ni^{2+}NTA column from actively growing yeast and give reasonable yields (0.4 – 4.7 mg/mL) in cultures of 1-5 litres. The yield of SufCB protein from yeast was increased roughly 2-fold with the addition of 8 M urea. Spectroscopy shows SufCB has a spectral signature similar to that of a [4Fe4S] protein when reconstituted with 4-fold molar excess ferric (III) ammonium citrate, L-cysteine and catalysed by NifS. Importantly, this cluster also persists on SufCB after desalting with PD10 column, indicating a prosthetic group on the protein. By using UV/Vis spectroscopy, we also made the comparison between a natively purified and denatured, reconstituted SufCB protein. Data showed a very similar spectral signature between as isolated to reconstituted protein, with a minor absorbance peak at $OD_{400\text{-}420nm}$, suggesting a cofactor. In addition, another shoulder at OD_{330nm} is seen which may indicate another unidentified SufCB-cofactor. In conclusion our purification data gives the first indication that SufCB may itself be an iron-sulfur cluster protein, but this requires further conclusive work.

Conclusions

In this chapter we attempted to identify a mechanism of SufCB in yeast cells. Our data demonstrated that SufCB acts as a Cfd1-like protein, by functionally replacing Cfd1 and physically interacting with Nbp35. In addition we have also demonstrated the unexpected finding that SufCB expression challenges the current model of iron-sulfur biogenesis in yeast by enabling cytosolic iron-sulfur assembly that is independent of the mitochondrial apparatus (Kispal et al., 1999). The chapter also described a protocol to isolate the SufCB protein using affinity (Ni^{2+}-NTA) chromatography under both denaturing (plus 8 M urea) and native (without 8 M urea) conditions. Purification and biophysical experiments demonstrated that the SufCB protein may also contain an iron-sulfur cluster, which would be in line with previous descriptions of the protein (Tsaousis et al., 2012). However, further work will be required to fully optimise and confirm that purified SufCB contains an iron-sulfur cluster.

Discussion

6.1 Summary of results

At the beginning of this project, we proposed that a new expression platform is needed which is specialised towards the maturation of iron-sulfur cluster enzymes. In the three research chapters of this thesis we have demonstrated that the specialised protozoan chaperone, SufCB is able to be accommodated and translated by *S. cerevisiae* (yeast) cells and this expression does improve iron-sulfur cluster biogenesis by interacting with the iron-sulfur assembly machinery.

6.2 SufCB and iron-sulfur enzymes.

With an increasing population, comes the mounting sense of urgency to search for alternative, 'greener' platforms to produce raw materials (Gartland and Gartland, 2018). The development of cell factories currently offer 'greener' means to produce biofuels, pharmaceuticals and raw chemicals and have the potential to increase the availability of resources to a more wide-spread target market (Gartland and Gartland, 2018; Verstraete, 2002). Of these, yeast-based technologies which express iron-sulfur enzymes have already demonstrated to have the potential to revolutionise several high-impact processes (Lopez-Torrejon et al., 2016). One commonly reported pitfall however, is an extreme sensitivity of iron-sulfur enzymes to oxygen and this issue has necessitated the development of costly oxygen-free or cloning processes (Lopez-Torrejon et al., 2016; Raj et al., 2018; Takahashi and Nakamura, 1999). In chapter 4, we have demonstrated that the expression of a single ORF, SufCB, was sufficient to significant increase the abundance and activities of several iron-sulfur enzymes in the baker's yeast *Saccharomyces cerevisiae*.

The pathways responsible for assembling iron-sulfur clusters in yeast cells are well known and consist of several compartmentalised mitochondrial and cytosolic factors which carefully assemble and then deliver clusters into their recipient apo-proteins (Kispal et al., 1999; Netz et al., 2007). We found that the expression of several GFP-tagged iron-sulfur proteins were significantly upregulated in SufCB-expressing yeast and, where possible this could also be correlated to a significantly increased activity in those respective enzymes. We also successfully demonstrated that the activity of the recombinant [4Fe4S] enzyme, aconitase, could be significantly upregulated in SufCB cells. Interestingly, we found that this wasn't the case for the recombinant [2Fe2S] enzyme, CMAH, which suggests that SufCB and or the CIA favours the maturation of [4Fe4S] enzymes, which has previously been suggested (Sharma et al., 2010). Collating this data, we found that SufCB-expression generally conveyed a reproducible 2-fold increase in the maturation of iron-sulfur enzymes in yeast. As to the usefulness of our system, we demonstrated that the enzyme, Bio2 was significantly upregulated, as well as, Ecm17. The latter of which is involved in biofilm formation in *Candida albicans* and therefore SufCB expressing cells with increased Ecm17 activity could also be used to study the functions and phenotypes associated with the overexpression of this enzyme (Li et al., 2013).

The observation that SufCB expression correlated with a 2-fold increase in the apparent maturation of iron-sulfur enzymes also raises interesting questions as to the status of iron-sulfur assembly *in vivo*. We propose that the action of SufCB aligns with a recently reported study in which the iron-sulfur cluster of ferredoxin was demonstrated to influence folding (Lei et al., 2017). It may similarly be that the augmentation of iron-sulfur biogenesis by SufCB, stabilises the 'folding' iron-sulfur enzymes, preventing their degradation (Lei et al., 2017). Yeast are known to degrade misfolded proteins via ER associated pathways (e.g. ERAD) and therefore it may be that the increased binding of clusters alleviates the number of misfolded proteins that would otherwise be degraded (Hwang and Qi, 2018; Sun and Brodsky, 2018). This has the net effect of increasing the abundance of functionally active iron-sulfur enzymes in SufCB cells which, and in some cases (Leu1, Ecm17, Bio2) is able to reach significance over controls.

Alternative proposals to explain this phenomenon include a SufCB-dependent repair mechanism in which SufCB facilitates the repair of oxidatively damaged clusters. Previous authors have demonstrated that oxidatively damaged iron-sulfur enzymes remain in an 'inactivated' apo-state until their clusters are 'repaired' by protein-dependent (e.g. Grx, MitoNEET) mechanisms (Djaman et al., 2004; Golinelli-Cohen et al., 2016). Although such repair mechanisms have been demonstrated in a variety of organisms (Boutigny et al., 2013; Golinelli-Cohen et al., 2016; Zhang et al., 2013), it seems unlikely that the observed two-fold increase in iron-sulfur enzymes could be due to this mechanism as this would require that, at any time, roughly 50% of total translated protein (e.g. Leu1) is in a damaged, apo-state. If true, this would account for an extreme waste of the cell's resources as 50% of all energy invested in translating a particular protein would be wasted and furthermore, this would potentiate iron-related toxicity (e.g. via Fenton reaction) resulting from cluster breakdown (Imlay, 2006; Kafri et al., 2016). Whilst there is also an argument that the transcription of mRNAs encoding iron-sulfur enzymes is upregulated in SufCB yeast, whilst we didn't probe this directly via qPCR or transcriptomics, the finding that the maturation of a recombinant aconitase was also significantly bolstered argues against this explanation, as aconitase was expressed ectopically under a constitutive promoter and therefore without transcriptional control.

The question is therefore posed as to why is the SufCB protein is lacking in the yeast (and higher eukaryotic) iron-sulfur assembly pathways, especially given the range of positive phenotype that come with its expression. SufCB is predicted to have arisen via lateral gene transfer (LGT) of an ancient minimal *suf* operon (*sufBCD*) into the genome of an ancestor of *Blastocystis* before being fused into a single ORF (Tsaousis et al., 2012). We propose that this was due to the observation that SufCB yeast cells harboured a hyperphysiological requirement for iron-uptake. This was shown using Ftr1 import (Δ*ftr1*) mutants led to a significant reduction in cellular fitness, which could be rescued by iron-supplementation of the growth media. From this finding, we propose that SufCB cells have an increased requirement for iron than non-SufCB expressing cells and this may have selected against SufCB in aerobic eukaryotes where excess iron may readily react in the aerobic cytosol, culminating in oxidative stress, and potentially cell death (Imlay, 2006). This may also

explain why SUF machinery is repressed, under unstressed conditions, by Fur in bacteria (Mettert and Kiley, 2014). We propose that this phenotype was due to the constitutive expression of SufCB. As the yeast-expressed SufCB was constitutive, the actions of SufCB (increased assembly of iron-sulfur clusters) as would also require the cell to provide the materials (iron) for increased assembly, this would quickly depleted yeast's iron-stores, resulting in an increased requirement for adequate iron-uptake. Typically, genes are expressed under the control of genetic elements which regulate their expression to meet the various needs of the cell, SufCB expressing yeast therefore have no means of balancing the expression of SufCB to the cell's capacity to the supply materials for cluster assembly (Nachin et al., 2001). A caveat to this is the assumption that the concentration of the active, folded SufCB protein directly related to transcriptional output from the SufCB-ADH1 fusion, which would be interesting to study further.

A final observation from our data suggested that SufCB could only affect the maturation of non-essential iron-sulfur proteins. Essential proteins are required for the viability of yeast cells (Zhao et al., 2019), and the overexpression of essential proteins (Rad2, Rli1) has been demonstrated to have toxic effects on the cell (Dong et al., 2004; Yu et al., 2011). This may suggest that essential proteins are physically unable to be overexpressed by the cell, as this would cause a detriment. Regulatory methods for this could be rapid turnover or even death for those cells which do overexpress the proteins, leaving those which do not. This would give the appearance that the proteins are at normal levels of expression. However, as in the case for Rli1, only the tagged Rli1 (Rli1-FLAG) was found to be toxic when overexpressed in wildtype yeast, as our essential proteins were GFP-tagged, this have similar effects and confound our results. It may also be argued that some iron-sulfur enzymes (XPD) have been found to receive their clusters at specific points in the CIA pathway (Odermatt and Gari, 2017)**,** and given that knowledge of the CIA pathway is still unravelling, this may occur at a point where SufCB does not interact. It must be said however that this is a purely cell biology interest, as our system is intended as a platform for recombinant protein expression and these are non-essential.

In conclusion, we have demonstrated that the interactions between SufCB and iron-sulfur enzymes is positive, resulting in numerous significant increases in abundances and activities, which can be used to overexpress both recombinant and endogenous iron-sulfur enzymes. Our data also provides circumstantial evidence to strengthen pre-existing paradigms ranging from protein folding to universal cell biology of yeast. Further investigations should be targetted towards developing an understanding the expression of SufCB in *Blastocystis* cells. The results of this study could then inform the optimal expression construct for recombinant SufCB.

6.3 SufCB is a Cfd1-like protein

Our third aim was to identify a mechanism for SufCB in yeast which may provide an explanation as to how the protein is able to convey the effects discussed in 6.2. Technology to genetically manipulate *Blastocystis* has only recently been described and because of this, an understanding of the SufCB protein in *Blastocystis* (and other protists) is limited (Li et al., 2019). Studies so far have demonstrated that in *Blastocystis*, SufCB is a cytosolic protein, proposed to function alongside a minimalised CIA pathway, under the control of an oxygen-responsive transcriptional framework (Tsaousis et al., 2012, 2014). Much like *Blastocystis,* iimmunofluorescence studies in yeast, also demonstrated that recombinant SufCB localises to the cytosol, suggesting that it, too, may function alongside the yeast CIA pathway (Tsaousis et al., 2012). Our genetic experiments uncovered a wealth of data suggesting many strong genetic interactions which appeared to be focused in the early CIA pathway. Comparing the two yeast and Blastocystis CIA pathways, we found that unlike yeast *Blastocystis* cells do not encode a Cfd1, which led us to hypothesise that SufCB may have evolved to replace the function of Cfd1 in its native system (Tsaousis et al., 2014).

To this end, we used tetrad dissection and discovered that SufCB expression could rescue an otherwise lethal Cfd1 deletion, suggesting that our hypothesis was correct. At the sequence level, the two proteins (SufCB and Cfd1) do not significantly align and SufCB does not contain Cfd1's conserved FxCPxC motif, nor is it a deviated P-loop NTPase, which suggested that the observed replacement may not be due to a direct complementation of Cfd1's function (Stehling et al., 2018). To this end, we found that SufCB did co-immunoprecipitate with Cfd1's partner protein, Nbp35. It therefore may be that SufCB is able to rescue a Cfd1 deletion by interacting with Nbp35 in a similar fashion to Cfd1.

It has been shown that both Cfd1, Nbp35 and the Nbp35-Cfd1 tetramer exhibit markedly different affinities for nucleotide hydrolysis (Camire et al., 2015; Stehling et al., 2018). Stehling et al., (2018) also demonstrated that Cfd1 and Nbp35 have different affinities for nucleotide triphosphates. Cfd1 preferentially binds GTP whilst Nbp35 preferentially binds ATP which possibly alludes to a diverged relevance for the ATPase activities in both proteins (Stehling et al., 2018). For Cfd1, it has also been demonstrated that the protein's ATPase activity is required to transfer the newly assembled Nbp35-Cfd1-bound cluster to the rest of the CIA machinery (Pallesen et al., 2013).

In our data, this suggests that SufCB, as an ATPase itself (Tsaousis et al., 2012), could potentially replace the absent ATPase activity of Cfd1 and facilitate transfer of clusters in a SufCB-Nbp35 complex. This could also explain why the rescued Δ*cfd1;*+SufCB cells were still slow growing as SufCB did not completely complement Cfd1's function. Therefore, we propose that the general requirement for an ATPase to aid or regulate Nbp35 could explain why SufCB is able to rescue Cfd1 knockouts, despite no significant sequence similarity between the two proteins. In a wider context, it may be such that the CIA system presented in *Blastocystis* represents an ancient form of the CIA pathway, where cluster transfer from the ancient Nbp35 scaffold required less regulation in an anaerobic cytosol (Pallesen et al., 2013; Tsaousis et al., 2014). The accumulation of oxygen may

then have dictated that cluster transfer from Nbp35 had to be more heavily regulated in order to mitigate oxidative stress from the Fenton reaction with iron, could lead to cell death (Imlay, 2006; Stehling et al., 2018).

It has been hypothesised that the gain of Cfd1 enabled organisms to more efficiently and safely utilise pools of iron via the iron-sensing function of aconitase (Pallesen et al., 2013). Aligning with this, we found that the slow growth of the Cfd1 deletions could be significantly stimulated when grown in media that had been supplemented with iron salts. As controls did not show a similar stimulation, this suggests that a function of Cfd1 may be to mobilise iron to the CIA machinery, and more importantly, this is not complemented by SufCB.

Data from this chapter also demonstrated that SufCB yeast cells require wildtype levels Dre2. A highly conserved protein, Dre2 functions within the CIA machinery alongside oxidoreductase Tah18 and both are required to assemble the iron-sulfur clusters on the Nbp35-Cfd1 heterotetramer (Netz et al., 2016). Electron transport is a common requirement for all iron-sulfur pathways identified to date and may facilitate the reduction of sulfide, iron or iron-sulfur clusters (reductive coupling) (Chandramouli et al., 2007; Webert et al., 2014). Introducing SufCB into Dre2 mutants consistently resulted in deleterious phenotypes in both growth rate and the maturation of the [4Fe4S] enzyme, aconitase. Notably, we found no decrease in the growth rate of wildtype yeast cells expressing SufCB and no other mutant behaved quite so extremely. This suggests that an aspect of Dre2 is required to accommodate SufCB's activity within the CIA pathway. Studies in *Arabidopsis* demonstrated that in the absence of Cfd1, Dre2 physically interacts with Nbp35, however, this has yet to be shown in *S. cerevisiae* (Bastow et al., 2017). As we showed that SufCB is able to physically interact with homodimeric Nbp35, it is predicted that Dre2 is required in some way to aid this 'unnatural' Nbp35-SufCB complex to efficiently assemble or transfer its iron-sulfur clusters. There is also the possibility that Dre2 is required for the general expression of recombinant proteins. This could be a route for further investigation, particularly due to the intimacy between the CIA machinery and protein translation via Rli1 (Kispal et al., 2005).

Purification of the SufCB protein from yeast found that the purified protein may be able to bind an iron-sulfur cluster when incubated with excess iron and sulfide. Although our results from these experiments cannot conclude definitively that SufCB is an iron-sulfur protein, both chemically reconstituted and natively purified proteins do show similar spectral fingerprints to a [4Fe4S] protein. Whilst our experimental data lacked the high-resolution required to definitively demonstrate that SufCB contains an iron-sulfur cluster. Alignments of the SufCB protein sequence reveals a short, heavily conserved C-terminal region that is consistent with the iron-binding residues on the SufB protein (**Figure 52**) (Yuda et al., 2017).

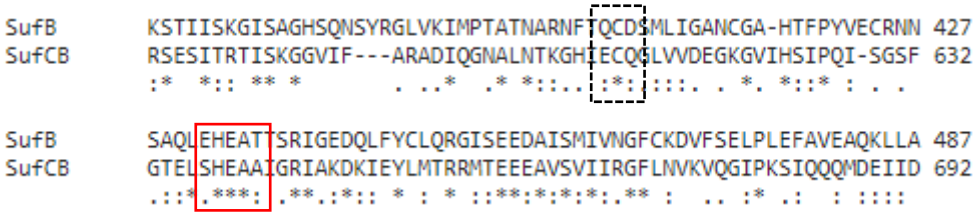

Figure 52. Pairwise sequence alignment of the *Blastocystis* SufCB and SufB of *E. coli***.** Alignment shows the conserved C-terminal iron-binding region (red box) and sulfide trafficking residues (black dashed box). Sequences were obtained from UniProt, uniprot.org and A. Tsaousis for SufB (*E. coli*) and SufCB, respectively. Asterisks indicate conserved amino acids.

The presence of this motif coupled with the findings presented in Tsaousis et al., (2012) suggests that SufCB can bind an iron-sulfur cluster *in vivo*. Our experimental design however was unable to identify whether the bound cofactor is an iron-sulfur cluster, or an iron contamination bound to SufCB during reconstitution. Whilst, it is tempting to lean towards the conclusion that SufCB does bind an iron-sulfur cluster, further work will be required using more detailed techniques (e.g. EPR, ESI-MS) in order to fully elucidate the chemical properties of the purified SufCB protein. It would also be interesting to determine whether SufCB is homodimeric in the yeast system as described by Tsaousis et al., (2012).

In summary, our cell biology data suggest that SufCB functions within the cytosolic iron-sulfur assembly pathway as a Cfd1-like protein. In addition, the interactions also suggest dependency on a function of Dre2 (likely electron transport) in order for yeast cells to express SufCB. **Figure 52** illustrates our findings and graphically compares the wildtype CIA machinery (**Figure 53A**) to the CIA machinery as predicted in SufCB cells (**Figure 53B**). SufCB interacts with Nbp35 which is predicted to form a Nbp35-SufCB heterotetramer, similar to the heterotetrameric Nbp35-Cfd1 complex. Although our investigations were unable to identify the exact stoichiometry of the SufCB-Nbp35 complex, we predicted that SufCB forms a complex with similar stoichiometry to Nbp35-Cfd1. The combination of Nbp35-Cfd1 and Nbp35-SufCB complexes provides one more route to assemble iron-sulfur clusters for the CIA pathway, and therefore results in the observed increases in maturation of iron-sulfur enzymes (**Figure 53B**). It may however also prove to be that Nbp35-SufCB form a more tight (solvent occluding) complex than Nbp35-Cfd1, especially as the interaction between Nbp35 and SufCB was found to be strong as seen by dense anti-Nbp35 signals on western blots. This could mean that the Nbp35-SufCB complex is more efficient at assembling clusters than the natural Nbp35-Cfd1 complex. Further work on the Nbp35-SufCB complex should enlighten this area, in particular whether *Blastocystis* Nbp35 also complexes with SufCB, as our work in yeast suggests that it should.

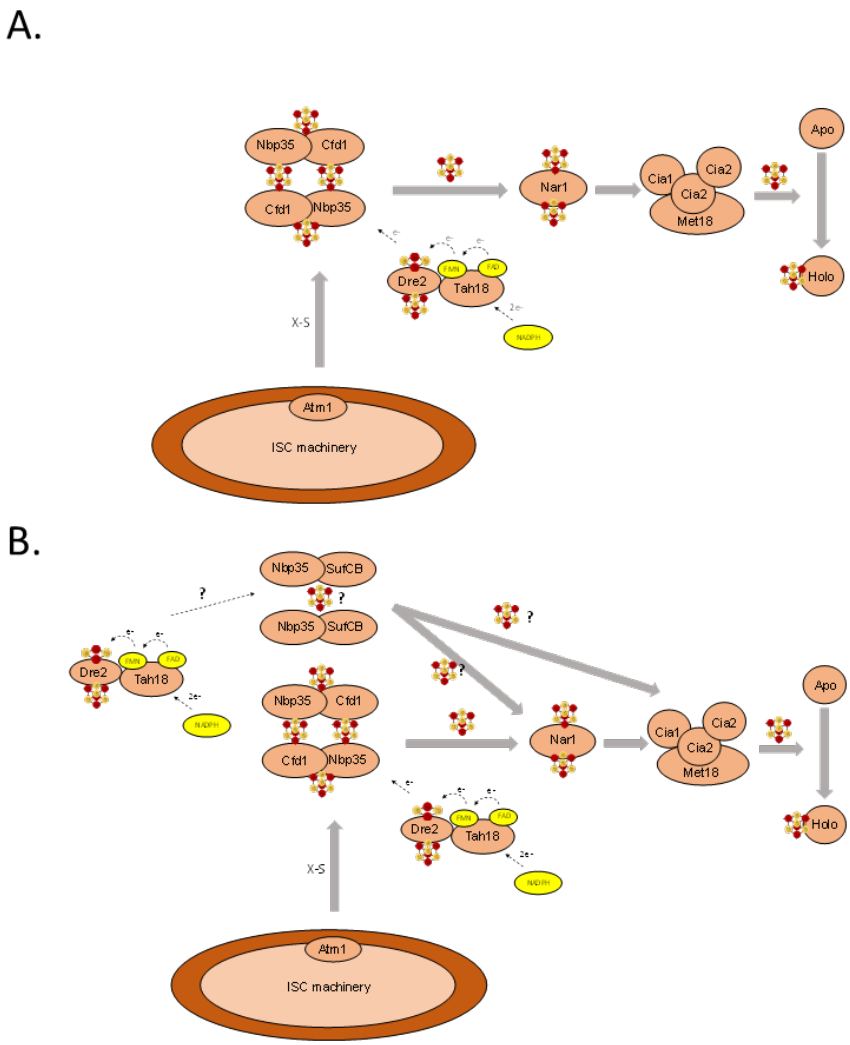

Figure 53. Illustration of CIA pathways in *S. cerevisiae* cells. A) The current CIA pathway as described in yeast. B) The CIA pathway as predicted to exist in SufCB-expressing *S. cerevisiae,* where an additional Nbp35-SufCB complex can facilitate iron-sulfur cluster assembly. Predictions are based upon experimental data. Grey arrows indicate the progression of iron-sulfur assembly, e- = electrons. NADPH/FAD/FMN cofactors are shown in yellow. X-S is the unknown exported molecule.

6.4 Mitochondrial iron-sulfur enzymes

Our work on aim number three also spawned an unexpected finding that SufCB-expression rendered the cytosolic pathway independent of Nfs1. Nfs1 is classically thought of as an essential component of iron-sulfur assembly which produces the exported X-S molecule (Kispal et al., 1999). Although there are several arguments as to the identity of X-S serves as the only known source of sulfide in cytosolic iron-sulfur assembly and this renders the CIA apparatus completely dependent upon mitochondria cluster assembly (Kispal et al., 1999; Schaedler et al., 2014). Unexpectedly, we discovered that SufCB cells were able to mature cytosolic iron-sulfur clusters in mutants which lack functional mitochondria. The same mutants were also able to grow on media which selected for respiratory competence, indicating that the mitochondria are restored in SufCB cells. Our localisation experiments demonstrated that SufCB primarily localises to the cytosol of yeast, however, we could not use fractionation followed by western blotting to confirm purely cytosolic localisation due to the scarcity of the protein detection by ECL. Nonetheless no fluorescent signal from SufCB co-localised with MitoTracker dye, suggesting that our approach was accurate enough to state cytosolic localisation.

We, therefore, ask the question as to how a cytosolic protein is able to overcome Nfs1 depletion and restore respiratory capacity in yeast. Communication between the mitochondrial and cytosolic iron-sulfur pathways has been described in yeast by Bedekovics et al., (2011) and in *Cryptococcus neoformans* (Do et al., 2016). These authors demonstrated that the mitochondrial iron-sulfur apparatus (including Nfs1) is indirectly upregulated by increases in the cytosolic concentration of Leu1 via its transcriptional activator Leu3. This mechanism ensures that the mitochondria efficiently produce enough X-S for use by the CIA pathway (Bedekovics et al., 2011). Therefore, it may be that increasing Leu1 concentrations (as seen in chapter 4) could result in upregulated mitochondrial biogenesis. Interestingly, natively purified SufCB protein showed a strong UV/Vis absorbance at ~OD_{330nm}. It is tempting to speculate that this could originate from a persulfide moiety attached to the protein (Cavallini et al., 1970), and thus represent the site of a forming iron-sulfur cluster, although further work will be required to fully unravel this. However, SufB's essential sulfide trafficking residue (cys 358), is conserved on the primary sequence of SufCB (**Figure 52**) and this, in theory, may enable SufCB to complement Nfs1 mutants by acting as a source of sulfide in the absence of efficient Nfs1. Notably, one of the SufCBs of *Pygsuia* is mitochondrial and appears to have replaced the classical housekeeping ISC pathway, suggesting that replacement of the classic mitochondrial pathways by SufCB is possible (Stairs et al., 2014).

Our results also demonstrated that the mitochondrial Bol homologue (Bol3), was required for SufCB to not be detrimental to the cell. Compared to controls, Δ*bol3* mutants which expressed SufCB presented with slow growth, respiratory incompetence and sensitivity to both oxidative stress and iron-chelation. Although its exact function is unknown, Bol proteins are found throughout nature, and Bol3 is required to transfer [4Fe4S] clusters from Isa1 to recipient apo-proteins. The maturation of Ecm17 in Δ*bol3* was only slightly decreased by the introduction of SufCB, however, this defect became clear when iron was sequestered from the media by 0.5 mM ferrozine, suggesting the

deleterious effects of SufCB expression in Δ*bol3* cells is linked to defective iron-homeostasis, which we showed is altered in SufCB-expressing yeast.

6.5 Concluding remarks

The budding yeast, *Saccharomyces cerevisiae* is an excellent tool for biotechnology (Huang et al., 2014). As a single-celled eukaryote with fast doubling times, no endotoxins and no requirement for antibiotic selection, microbial cell factories based upon yeast cells, boast a wide repertoire of applications (Čiplys et al., 2011; Lopez-Torrejon et al., 2016; Luo et al., 2019; Martínez-Alcántar et al., 2019; Raj et al., 2018)..

Collectively, the three aims of this work have expanded upon the current utility of yeast by developing a simple microbial cell factory which consistently overexpressed a range of recombinant and endogenous iron-sulfur enzymes. Attesting to the commercial utility of this system we also demonstrated overexpression of the protein Bio2 by SufCB yeast and patents to increase the activity of this enzyme have been filed (Shiuan, 2006) In addition to this, we have also demonstrated several novel findings in regard to the role of Cfd1 and SufCB in yeast and *Blastocystis*, respectively.

This work also opens many possibilities for future opportunities to further explore yeast expressed SufCB proteins. In particular, exploring the effect of other protozoan SufCBs (e.g. *Pygsuia* mitochondrial and cytosolic variants), codon-optimised *Blastocystis* SufCB, and expression conditions (e.g. expression via low copy plasmids). Although we were unable to demonstrate here, it would also be of interest to introduce published, recombinant, iron-sulfur enzymes, enoate reductase or nitrogenase (Lopez-Torrejon et al., 2016; Raj et al., 2018).

Bibliography

Albrecht, A.G., Netz, D.J.A., Miethke, M., et al. (2010). SufU is an essential iron-sulfur cluster scaffold protein in Bacillus subtilis. J. Bacteriol. *192*, 1643–1651.

Alhebshi, A., Sideri, T.C., Holland, S.L., et al. (2012). The essential iron-sulfur protein Rli1 is an important target accounting for inhibition of cell growth by reactive oxygen species. Mol. Biol. Cell *23*, 3582–3590.

Amorim Franco, T.M., and Blanchard, J.S. (2017). Bacterial Branched-Chain Amino Acid Biosynthesis: Structures, Mechanisms, and Drugability. Biochemistry *56*, 5849–5865.

Andreini, C., Bertini, I., Cavallaro, G., et al. (2008). Metal ions in biological catalysis: From enzyme databases to general principles. J. Biol. Inorg. Chem. *13*, 1205–1218.

Ardabilygazir, A., Afshariyamchlou, S., Mir, D., et al. (2018). Effect of High-dose Biotin on Thyroid Function Tests: Case Report and Literature Review. Cureus *10*, 1–5.

Atlas, R.M., and Hazen, T.C. (2011). Oil biodegradation and bioremediation: A tale of the two worst spills in U.S. history. Environ. Sci. Technol. *45*, 6709–6715.

Bai, Y., Chen, T., Happe, T., et al. (2018). Iron-sulphur cluster biogenesis: Via the SUF pathway. Metallomics *10*, 1038–1052.

Bailey, T.L., Boden, M., Buske, F.A., et al. (2009). MEME Suite: Tools for motif discovery and searching. Nucleic Acids Res. *37*, 202–208.

Balk, J., Aguilar Netz, D.J., Tepper, K., et al. (2005). The Essential WD40 Protein Cia1 Is Involved in a Late Step of Cytosolic and Nuclear Iron-Sulfur Protein Assembly. Mol. Cell. Biol. *25*, 10833–10841.

Bandyopadhyay, S., Chandramouli, K., and Johnson, M.K. (2008). Iron-sulfur cluster biosynthesis. Biochem. Soc. Trans. *36*, 1112–1119.

Bastow, E.L., Bych, K., Crack, J.C., et al. (2017). NBP35 interacts with DRE2 in the maturation of cytosolic iron-sulphur proteins in Arabidopsis thaliana. Plant J. *89*, 590–600.

Bedekovics, T., Li, H., Gajdos, G.B., et al. (2011). Bedekovics et al. 2011 - Leucine Biosynthesis Regulates Cytoplasmic Iron-Sulfur Enzyme Biogenesis in an Atm1p-independent Manner.pdf. J. Biol. Chem. *286*, 40878–40888.

Berlow, R.B., Dyson, H.J., and Wright, P.E. (2018). Expanding the Paradigm: Intrinsically Disordered Proteins and Allosteric Regulation. J. Mol. Biol. *430*, 2309–2320.

Bernard, D.G., Netz, D.J.A., Lagny, T.J., et al. (2013). Requirements of the cytosolic ironsulfur cluster assembly pathway in Arabidopsis. Philos. Trans. R. Soc. B Biol. Sci. *368*.

Bhatia, S.C., and Bhatia, S.C. (2019). Bioethics and biotechnology. Food Biotechnol. 379–389.

Blanc, B., Clemancey, M., Latour, J., et al. (2014). Molecular Investigation of Iron − Sulfur Cluster Assembly Scaffolds under Stress. Biochemistry *4*, 7867–7869.

Boutigny, S., Saini, A., Baidoo, E.E.K., et al. (2013). Physical and functional interactions of a monothiol glutaredoxin and an iron sulfur cluster carrier protein with the sulfur-donating radical S-adenosyl-L-methionine enzyme MiaB. J. Biol. Chem. *288*, 14200–14211.

Boyd, E.S., Thomas, K.M., Dai, Y., et al. (2014). Interplay between Oxygen and Fe-S Cluster Biogenesis: Insights from the Suf Pathway. Biochemistry *53*, 5834–5847.

Braymer, J.J., and Winge, D.R. (2018). Sulfur from Within: Cytosolic tRNA Thiouridinylation. Cell Chem. Biol. *25*, 645–647.

Braymer, J.J., Lill, R., and Marburg, P. (2017). Iron-Sulfur Cluster Biogenesis and Trafficking in Mitochondria. J. Biol. Chem. *292*, 12754–127.

Breslow, D.K., Cameron, D.M., Collins, S.R., et al. (2008). A comprehensive strategy enabling high-resolution functional analysis of the yeast genome. Nat Methods *5*, 711–718.

Brown, N.M., Kennedy, M.C., Antholine, W.E., et al. (2002). Detection of a [3Fe-4S] Cluster Intermediate of Cytosolic Aconitase in Yeast Expressing Iron Regulatory Protein 1: INSIGHTS INTO THE MECHANISM OF Fe-S CLUSTER CYCLING. J. Biol. Chem. *277*, 7246–7254.

Brychkova, G., Yarmolinsky, D., Ventura, Y., et al. (2012). A novel in-gel assay and an improved kinetic assay for determining in vitro sulfite reductase activity in plants. Plant Cell Physiol. *53*, 1507–1516.

Bud, R. (1989). History of Biotechnology. Nature *337*, 10–11.

Bych, K., Netz, D.J.A., Vigani, G., et al. (2008). The essential cytosolic iron-sulfur protein Nbp35 acts without Cfd1 partner in the green lineage. J. Biol. Chem. *283*, 35797–35804.

Cai, K., and Markley, J.L. (2018). NMR as a tool to investigate the processes of mitochondrial and cytosolic iron-sulfur cluster biosynthesis. Molecules *23*, 2213.

Camire, E.J., Grossman, J.D., Thole, G.J., et al. (2015). The yeast Nbp35-Cfd1 cytosolic iron-sulfur cluster scaffold is an ATPase. J. Biol. Chem. *290*, 23793–23802.

Capozzi, F., Ciurli, S., and Luchinat, C. (1998). Coordination sphere versus protein environment as determinants of electronic and functional properties of iron-sulfur proteins. Met. Sites Proteins Model. Redox Centers *90*, 127–160.

Castro, L., Rodriguez, M., and Radi, R. (1994). Aconitase is readily inactivated by peroxynitrite, but not by its precursor, nitric oxide. J. Biol. Chem. *269*, 29409–29415.

Cavallini, D., Federici, G., Barboni, E., et al. (1970). Formation of persulfide groups in alkaline treated insulin. FEBS Lett. *10*, 125–128.

Chaban, V. V., and Prezhdo, O. V. (2016). The Haber Process made efficient by hydroxylated graphene. J. Phys. Chem. Lett. *7*, 2622–2626.

Chahal, H.K., and Wayne Outten, F. (2012). Separate Fe-S Scaffold And Carrier Functions For SufB2C2 And SufA During In Vitro Maturation of [2Fe-2S] Fdx. J. Inorg. Biochem. *16*, 126–134.

Chahal, H.K., Dai, Y., Saini, A., et al. (2009). The SufBCD Fe-S scaffold complex interacts with sufa for Fe-s cluster transfer. Biochemistry *48*, 10644–10653.

Chandramouli, K., Unciuleac, M.C., Naik, S., et al. (2007). Formation and properties of [4Fe-4S] clusters on the IscU scaffold protein. Biochemistry *46*, 6804–6811.

Child, S.A., Bradley, J.M.M., Pukala, T.L., et al. (2018). Electron transfer ferredoxins with unusual cluster binding motifs support secondary metabolism in many bacteria. Chem. Sci. *9*, 7948–7957.

Choi, H.J., Kim, S.J., Mukhopadhyay, P., et al. (2001). Structural basis of the redox switch in the OxyR transcription factor. Cell *105*, 103–113.

Christman, M.F., Storz, G., and Ames, B.N. (1989). OxyR, a positive regulator of hydrogen peroxide-inducible genes in Escherichia coli and Salmonella typhimurium, is homologous to a family of bacterial regulatory proteins. Proc. Natl. Acad. Sci. U. S. A. *86*, 3484–3488.

Čiplys, E., Samuel, D., Juozapaitis, M., et al. (2011). Overexpression of human virus surface glycoprotein precursors induces cytosolic unfolded protein response in Saccharomyces cerevisiae. Microb. Cell Fact. *10*, 1–18.

Couturier, J., Wu, H., Dhalleine, T., et al. (2014). Monothiol Glutaredoxin – BolA Interactions : Redox Control of Arabidopsis thaliana BolA2 and SufE1. Mol Plant *7*, 187–205.

Crack, J.C., Green, J., Thomson, A.J., et al. (2014a). Iron-sulfur clusters as biological sensors: the chemistry of reactions with molecular oxygen and nitric oxide. Acc. Chem. Res. *47*, 3196–3205.

Crack, J.C., Green, J., Thomson, A.J., et al. (2014b). Techniques for the Production, Isolation, and Analysis of Iron–Sulfur Proteins. Metalloproteins *1122*, 33–48.

Crack, J.C., Thomson, A.J., and Le Brun, N.E. (2017). Mass spectrometric identification of intermediates in the O 2 -driven [4Fe-4S] to [2Fe-2S] cluster conversion in FNR. Proc. Natl. Acad. Sci. *114*, E3215–E3223.

Dai, Y., Kim, D., Dong, G., et al. (2015). SufE D74R Substitution alters active site loop dynamics to further enhance SufE interaction with the SufS Cysteine desulfurase. Biochemistry *54*, 4824–4833.

Degli Esposti, M., Ballester, F., Solaini, G., et al. (1987). The circular-dichroic properties of the “Rieske” iron-sulphur protein in the mitochondrial ubiquinol:cytochrome c reductase. Biochem. J. *241*, 285–290.

Diaz, Y., Gonzalez, A., Lopez, A., et al. (2009). Anti-ganglioside anti-idiotypic monoclonal antibody-based cancer vaccine induces apoptosis and antiangiogenic effect in a metastatic lung carcinoma. Cancer Immunol. Immunother. *58*, 1117–1128.

Djaman, O., Outten, F.W., and Imlay, J.A. (2004). Repair of oxidized iron-sulfur clusters in Escherichia coli. J. Biol. Chem. *279*, 44590–44599.

Do, E., Hu, G., Oliveira, D., et al. (2016). Leu1 plays a role in iron metabolism and is required for virulence in Cryptococcus neoformans. Fungal Genet. Biol. *February*, 11–19.

Dong, J., Lai, R., Nielsen, K., et al. (2004). The essential ATP-binding cassette protein RLI1 functions in translation by promoting preinitiation complex assembly. J. Biol. Chem. *279*, 42157–42168.

Dosztányi, Z., Csizmok, V., Tompa, P., et al. (2005). IUPred: Web server for the prediction of intrinsically unstructured regions of proteins based on estimated energy content. Bioinformatics *21*, 3433–3434.

Duquenne, P., Marchand, G., and Duchaine, C. (2013). Measurement of endotoxins in bioaerosols at workplace: A critical review. Ann. Occup. Hyg. *57*, 137–172.

Edelstein, A., Amodaj, N., Hoover, K., et al. (2010). Computer control of microscopes using manager. Curr. Protoc. Mol. Biol. 1–17.

Ermakova, M., Lopez-Calcagno, P.E., Raines, C.A., et al. (2019). Overexpression of the Rieske FeS protein of the Cytochrome b6f complex increases C4 photosynthesis in Setaria viridis. Commun. Biol. *2*, 1–12.

Fernandez, A., Scott, R., and Berry, R.S. (2004). The nonconserved wrapping of conserved protein folds reveals a trend toward increasing connectivity in proteomic networks. Proc. Natl. Acad. Sci. *101*, 2823–2827.

Fujishiro, T., Terahata, T., Kunichika, K., et al. (2017). Zinc-Ligand Swapping Mediated Complex

Formation and Sulfur Transfer between SufS and SufU for Iron-Sulfur Cluster Biogenesis in Bacillus subtilis. J. Am. Chem. Soc. *139*, 18464–18467.

Gaensly, F., Picheth, G., Brand, D., et al. (2014). The uptake of different iron salts by the yeast Saccharomyces cerevisiae. Brazilian J. Microbiol. *45*, 491–494.

Gakh, Smith IV, D.Y., and Isaya, G. (2008). Assembly of the iron-binding protein frataxin in Saccharomyces cerevisiae responds to dynamic changes in mitochondrial iron influx and stress level. J. Biol. Chem. *283*, 31500–31510.

Garland, S.A., Hoff, K., Vickery, L.E., et al. (1999). Saccharomyces cerevisiae ISU1 and ISU2: Members of a well-conserved gene family for iron-sulfur cluster assembly. J. Mol. Biol. *294*, 897–907.

Gartland, K.M.A., and Gartland, J.S. (2018). Contributions of biotechnology to meeting future food and environmental security needs. EuroBiotech J. *2*, 2–9.

Goffeau, A., Barrell, G., Bussey, H., et al. (1996). Life with 6000 genes. Science (80-.). *274*, 546–567.

Golinelli-Cohen, M.P., Lescop, E., Mons, C., et al. (2016). Redox control of the human iron-sulfur repair protein MitoNEET activity via its iron-sulfur cluster. J. Biol. Chem. *291*, 7583–7593.

Grossman, J.D., Camire, E.J., and Perlstein, D.L. (2018). Approaches to Interrogate the Role of Nucleotide Hydrolysis by Metal Trafficking NTPases: The Nbp35-Cfd1 Iron-Sulfur Cluster Scaffold as a Case Study (Elsevier Inc.).

Hausmann, A., Aguilar Netz, D.J., Balk, J., et al. (2005). The eukaryotic P loop NTPase Nbp35: An essential component of the cytosolic and nuclear iron-sulfur protein assembly machinery. Proc. Natl. Acad. Sci. *102*, 3266–3271.

Hawkes, T.R.R., Cox, J.M.M., Fraser, S., et al. (1993). A Herbicidal Inhibitor of Isopropylmalate Isomerase. Zeitschrift Fur Naturforsch. C - A J. Biosci. *48*, 364–368.

Health and Safety Executive (1998). Compressed Air Safety. *39*, 1–50.

Hirabayashi, K., Yuda, E., Tanaka, N., et al. (2015). Functional dynamics revealed by the structure of the SufBCD Complex, a novel ATP-binding cassette (ABC) protein that serves as a scaffold for iron-sulfur cluster biogenesis.

Huang, M., Bao, J., and Nielsen, J. (2014). Biopharmaceutical protein production by Saccharomyces cerevisiae : current state and future prospects. Pharm. Bioprocess. *2*, 167–182.

Huang, M., Bao, J., Hallström, B.M., et al. (2017). Efficient protein production by yeast requires global tuning of metabolism. Nat. Commun. *8*.

Huh, W.K., Huh, W.K., Falvo, J. V., et al. (2003). Global analysis of protein localization in budding yeast. Nature *425*, 686–691.

Hwang, J., and Qi, L. (2018). Quality Control in the Endoplasmic Reticulum: Crosstalk between ERAD and UPR pathways. Trends Biochem. Sci. *43*, 593–605.

Imlay, J.A. (2006). Iron-sulphur clusters and the problem with oxygen. Mol. Microbiol. *59*, 1073–1082.

Ito, H., Fukuda, Y., Murata, K., et al. (1983). Transformation of intact yeast cells treated with alkali cations. J. Bacteriol. *153*, 163–168.

Ito, S., Tan, L.J., Andoh, D., et al. (2010). MMXD, a TFIIH-Independent XPD-MMS19 Protein

Complex Involved in Chromosome Segregation. Mol. Cell *39*, 632–640.

Johnson, M., Zaretskaya, I., Raytselis, Y., et al. (2008). NCBI BLAST: a better web interface. Nucleic Acids Res. *36*, 5–9.

Jugder, B.E., Payne, K.A.P., Fisher, K., et al. (2018). Heterologous Production and Purification of a Functional Chloroform Reductive Dehalogenase. ACS Chem. Biol. *13*, 548–552.

Kafri, M., Metzl-Raz, E., Jona, G., et al. (2016). The Cost of Protein Production. Cell Rep. *14*, 22–31.

Kim, H., Yoo, S.J., and Kang, H.A. (2015). Yeast synthetic biology for the production of recombinant therapeutic proteins. FEMS Yeast Res. *15*, 1–16.

Kispal, G., Csere, P., Guiard, B., et al. (1997). The ABC transport Atm1p is required for mitochondrial iron homeostasis. FEBS Lett. *418*, 346–350.

Kispal, G., Csere, P., Prohl, C., et al. (1999). The mitochondrial proteins Atm1p and Nfs1p are essential for biogenesis of cytosolic Fe/S proteins. EMBO J. *18*, 3981–3989.

Kispal, G., Sipos, K., Lange, H., et al. (2005). Biogenesis of cytosolic ribosomes requires the essential iron–sulphur protein Rli1p and mitochondria. EMBO J. *24*, 589–598.

Kitaoka, S., Wada, K., Hasegawa, Y., et al. (2006). Crystal structure of Escherichia coli SufC, an ABC-type ATPase component of the SUF iron-sulfur cluster assembly machinery. FEBS Lett. *580*, 137–143.

Kudhair, B.K., Hounslow, A.M., Rolfe, M.D., et al. (2017). Structure of a Wbl protein and implications for NO sensing by M. tuberculosis. Nat. Commun. *8*, 1–12.

Kumar, A., Agarwal, S., Heyman, J.A., et al. (2002). Subcellular localization of the yeast proteome. Genes Dev. *16*, 707–719.

De La Rosa, M.B., and Nelson, S.W. (2011). An interaction between the walker A and D-loop motifs is critical to ATP hydrolysis and cooperativity in bacteriophage T4 Rad50. J. Biol. Chem. *286*, 26258–26266.

Labrada, M., Dorvignit, D., Hevia, G., et al. (2018). GM3(Neu5Gc) ganglioside: an evolution fixed neoantigen for cancer immunotherapy. Semin. Oncol. *45*, 41–51.

Layer, G., Gaddam, S.A., Ayala-Castro, C.N., et al. (2007). SufE Transfers Sulfur from SufS to SufB for Iron-Sulfur Cluster Assembly. J. Biol. Chem. *282*, 13342–13350.

Lee, K.C., Yeo, W.S., and Roe, J.H. (2008). Oxidant-responsive induction of the suf operon, encoding a Fe-S assembly system, through Fur and IscR in Escherichia coli. J. Bacteriol. *190*, 8244–8247.

Leger, M.M., Eme, L., Hug, L.A., et al. (2016). Novel Hydrogenosomes in the Microaerophilic Jakobid Stygiella incarcerata. Mol. Biol. Evol. *33*, 2318–2336.

Lei, H., Guo, Y., Hu, X., et al. (2017). Reversible unfolding and folding of the metalloprotein ferredoxin revealed by single-molecule atomic force microscopy. J. Am. Chem. Soc. *139*, 1538–1544.

Leidgens, S., de Smet, S., and Foury, F. (2009). Frataxin interacts with Isu1 through a conserved tryptophan in its β-sheet. Hum. Mol. Genet. *19*, 276–286.

Li, J., and Cowan, J.A. (2015). Glutathione-Coordinated [2Fe-2S] Cluster: A Viable Physiological substrate for Mitochondrial ABCB7 Transport. Chem. Commun. *33*, 839–841.

Li, D.D., Wang, Y., Dai, B. Di, et al. (2013). ECM17-dependent methionine/cysteine biosynthesis contributes to biofilm formation in Candida albicans. Fungal Genet. Biol. *51*, 50–59.

Li, F.J., Tsaousis, A.D., Purton, T., et al. (2019). Successful Genetic Transfection of the Colonic Protistan Parasite Blastocystis for Reliable Expression of Ectopic Genes. Sci. Rep. *9*, 1–11.

Li, X.-X., Liu, Q., Liu, X.-M., et al. (2016). Using synthetic biology to increase nitrogenase activity. Microb. Cell Fact. *15*, 43.

Lill, R., Dutkiewicz, R., Elsässer, H.P., et al. (2006). Mechanisms of iron-sulfur protein maturation in mitochondria, cytosol and nucleus of eukaryotes. Biochim. Biophys. Acta - Mol. Cell Res. *1763*, 652–667.

Lill, R., Hoffmann, B., Molik, S., et al. (2012). The role of mitochondria in cellular iron-sulfur protein biogenesis and iron metabolism. Biochim. Biophys. Acta - Mol. Cell Res. *1823*, 1491–1508.

Lloyd, S.J., Lauble, H., Prasad, G.S., et al. (2008). The mechanism of aconitase: 1.8 Å resolution crystal structure of the S642A:citrate complex. Protein Sci. *8*, 2655–2662.

Loiseau, L., Ollagnier-de-Choudens, S., Nachin, L., et al. (2003). Biogenesis of Fe-S cluster by the bacterial suf system. SufS and SufE form a new type of cysteine desulfurase. J. Biol. Chem. *278*, 38352–38359.

Loiseau, L., Gerez, C., Bekker, M., et al. (2007). ErpA, an iron-sulfur (Fe-S) protein of the A-type essential for respiratory metabolism in Escherichia coli. Proc. Natl. Acad. Sci. U. S. A. *104*, 13626–13631.

Lopez-Torrejon, G., Jimenez-Vicente, E., Buesa, J.M., et al. (2016). Expression of a functional oxygen-labile nitrogenase component in the mitochondrial matrix of aerobically grown yeast. Nat. Commun. *7*, 11426.

Luo, X., Reiter, M.A., d'Espaux, L., et al. (2019). Complete biosynthesis of cannabinoids and their unnatural analogues in yeast. Nature *567*, 123–126.

Macomber, L., and Imlay, J.A. (2009). The iron-sulfur clusters of dehydratases are primary intracellular targets of copper toxicity. Proc. Natl. Acad. Sci. U. S. A. *106*, 8344–8349.

Magalhães, P.O., Lopes, A.M., Mazzola, P.G., et al. (2011). Methods of Endotoxin Removal from Biological Preparations : A Review. J. Pharm. Sci. *10*, 1–15.

Magnuson, J.K., Romine, M.F., Burris, D.R., et al. (2000). Trichloroethene reductive dehalogenase from Dehalococcoides ethenogenes: Sequence of tceA and substrate range characterization. Appl. Environ. Microbiol. *66*, 5141–5147.

Maio, N., and Rouault, T.A. (2015). Iron-sulfur cluster biogenesis in mammalian cells: New insights into the molecular mechanisms of cluster delivery. Biochim. Biophys. Acta - Mol. Cell Res. *1853*, 1493–1512.

Martínez-Alcántar, L., Madrigal, A., Sánchez-Briones, L., et al. (2019). Over-expression of Isu1p and Jac1p increases the ethanol tolerance and yield by superoxide and iron homeostasis mechanism in an engineered Saccharomyces cerevisiae yeast. J. Ind. Microbiol. Biotechnol. *46*, 925–936.

Martínez-Pastor, M.T., Perea-García, A., and Puig, S. (2017). Mechanisms of iron sensing and regulation in the yeast Saccharomyces cerevisiae. World J. Microbiol. Biotechnol. *33*, 1–9.

Mashruwala, A.A., Bhatt, S., Poudel, S., et al. (2016). The DUF59 Containing Protein SufT Is Involved in the Maturation of Iron-Sulfur (FeS) Proteins during Conditions of High FeS Cofactor

Demand in Staphylococcus aureus. PLoS Genet. *12*, 1–39.

Masse, E., Vanderpool, C., and Gottesman, S. (2005). Effect of RhyB Small RNA on Global Iron Use in Escherichia coli. *187*, 3–10.

Mettert, E.L., and Kiley, P.J. (2014). Coordinate regulation of the Suf and Isc Fe-S cluster biogenesis pathways by IscR is essential for viability of Escherichia coli. J. Bacteriol. *196*, 4315–4323.

Mettert, E.L., Outten, F.W., Wanta, B., et al. (2008). The impact of O(2) on the Fe-S cluster biogenesis requirements of Escherichia coli FNR. J. Mol. Biol. *384*, 798–811.

Mihara, H., Kurihara, T., Yoshimura, T., et al. (2000). Kinetic and mutational studies of three NifS homologs from Escherichia coli: Mechanistic difference between L-cysteine desulfurase and L-selenocysteine lyase reactions. J. Biochem. *127*, 559–567.

Miller, C.A., Martinat, M.A., and Hyman, L.E. (1998). Assessment of aryl hydrocarbon receptor complex interactions using pBEVY plasmids: expressionvectors with bi-directional promoters for use in Saccharomyces cerevisiae. Nucleic Acids Res. *26*, 3577–3583.

Moiseeva, T.N., Gamper, A.M., Hood, B.L., et al. (2016). Human DNA polymerase ε is phosphorylated at serine-1940 after DNA damage and interacts with the iron-sulfur complex chaperones CIAO1 and MMS19. DNA Repair (Amst). *43*, 9–17.

Nachin, L., El Hassouni, M., Loiseau, L., et al. (2001). SoxR-dependent response to oxidative stress and virulence of Erwinia chrysanthemi: The key role of SufC, an orphan ABC ATPase. Mol. Microbiol. *39*, 960–972.

Nachin, L., Loiseau, L., Barras, Â., et al. (2003). SufC : an unorthodox cytoplasmic ABC/ATPase required for [Fe-S] biogenesis under oxidative stress. EMBO J. *22*, 427–437.

Narahari, J., Ma, R., Wang, M., et al. (2000). The aconitase function of iron regulatory protein 1: Genetic studies in yeast implicate its role in iron-mediated redox regulation. J. Biol. Chem. *275*, 16227–16234.

Narayana Murthy, M., Ollagnier-de-choudens, S., Sanakis, Y., et al. (2007). Characterization of Arabidopsis thaliana SufE2 and SufE3: functions in chloroplast iron-sulfur cluster assembly and Nad synthesis. J Biol Chem. *282*, 18254–18264.

Netz, D.J.A., Stümpfig, M., Doré, C., et al. (2010). Tah18 transfers electrons to Dre2 in cytosolic iron-sulfur protein biogenesis. Nat. Chem. Biol. *6*, 758–765.

Netz, D.J.A., Pierik, A.J., Stümpfig, M., et al. (2012). A bridging [4Fe-4S] cluster and nucleotide binding are essential for function of the Cfd1-Nbp35 complex as a scaffold in iron-sulfur protein maturation. J. Biol. Chem. *287*, 12365–12378.

Netz, D.J.A., Mascarenhas, J., Stehling, O., et al. (2014). Maturation of cytosolic and nuclear iron-sulfur proteins. Trends Cell Biol. *24*, 303–312.

Netz, D.J.A., Genau, H.M., Weiler, B.D., et al. (2016). The conserved Dre2 uses essential [2Fe-2S] and [4Fe-4S] clusters for function in cytosolic iron-sulfur protein assembly. Biochem. J. *473*, 2073–2085.

Netz, D.J.A.A., Pierik, A.J., Stümpfig, M., et al. (2007). The Cfd1–Nbp35 complex acts as a scaffold for iron-sulfur protein assembly in the yeast cytosol. Nat. Chem. Biol. *3*, 278–286.

Nevoigt, E., and Stahl, U. (1997). Osmoregulation and glycerol metabolism in the yeast Saccharomyces cerevisiae. FEMS Microbiol. Rev. *21*, 231–241.

Nielsen, J. (2013). Production of biopharmaceutical proteins by yeast. Bioengineered *4*, 207–211.

Nishimura, A., Kawahara, N., and Takagi, H. (2013). The flavoprotein Tah18-dependent NO synthesis confers high-temperature stress tolerance on yeast cells. Biochem. Biophys. Res. Commun. *430*, 137–143.

Odermatt, D.C., and Gari, K. (2017). The CIA Targeting Complex Is Highly Regulated and Provides Two Distinct Binding Sites for Client Iron-Sulfur Proteins. Cell Rep. *18*, 1434–1443.

Outten, F.W., Djaman, O., and Storz, G. (2004). A suf operon requirement for Fe-S cluster assembly during iron starvation in Escherichia coli. Mol. Microbiol. *52*, 861–872.

Pallesen, L.J., Solodovnikova, N., Sharma, A.K., et al. (2013). Interaction with Cfd1 increases the kinetic lability of FeS on the Nbp35 scaffold. J. Biol. Chem. *288*, 23358–23367.

Pardoux, R., Fiévet, A., Carreira, C., et al. (2019). The bacterial MrpORP is a novel Mrp/NBP35 protein involved in iron-sulfur biogenesis. Sci. Rep. *9*, 1–13.

Patzer, S.I., and Hantke, K. (1999). Sufs is a nifs-like protein, and sufd is necessary for stability of the [2fe-2s] fhuf protein in escherichia coli. J. Bacteriol. *181*, 3307–3309.

Paul, V.D., Mühlenhoff, U., Stümpfig, M., et al. (2015). The deca-GX $_3$ proteins Yae1-Lto1 function as adaptors recruiting the ABC protein Rli1 for iron-sulfur cluster insertion. Elife *4*, 1–23.

Pearce, O.M.T., and Varki, A. (2010). Chemo-enzymatic synthesis of the carbohydrate antigen N-glycolylneuraminic acid from glucose. Carbohydr. Res. *345*, 1225–1229.

Pérard, J., and Ollagnier de Choudens, S. (2018). Iron–sulfur clusters biogenesis by the SUF machinery: close to the molecular mechanism understanding. J. Biol. Inorg. Chem. *23*, 581–596.

Peri, S., Kulkarni, A., Feyertag, F., et al. (2018). Phylogenetic distribution of CMP-Neu5Ac hydroxylase (CMAH), the enzyme synthetizing the proinflammatory human xenoantigen Neu5Gc. Genome Biol. Evol. *10*, 207–219.

Petrovic, A., Davis, C.T., Rangachari, K., et al. (2008). Hydrodynamic characterization of the SufBC and SufCD complexes and their interaction with fluorescent adenosine nucleotides. Protein Sci. *17*, 1264–1274.

Peubez, I., Chaudet, N., Mignon, C., et al. (2010). Antibiotic-free selection in E. coli: new considerations for optimal design and improved production. Microb. Cell Fact. *9*, 1–10.

Prakash, L., and Prakash, S. (1977). Isolation and characterization of MMS-sensitive mutants of Saccharomyces cerevisiae. Genetics *86*, 33–35.

Pronk, J.T. (2002). Auxotrophic Yeast Strains in Fundamental and Applied Research. Appl. Environ. Microbiol. *68*, 2095–2100.

Queimado, L., Rao, M., Schultz, R.A., et al. (2001). Cloning the human and mouse MMS19 genes and functional complementation of a yeast mms19 deletion mutant. Nucleic Acids Res. *29*, 1884–1891.

Raj, K., Partow, S., Correia, K., et al. (2018). Biocatalytic production of adipic acid from glucose using engineered Saccharomyces cerevisiae. Metab. Eng. Commun. *6*, 28–32.

Reiser, J., and Käppeli, O. (1989). Developments in biotechnology. Experientia *45*, 1013.

Ro, D.K., Paradise, E.M., Quellet, M., et al. (2006). Production of the antimalarial drug precursor artemisinic acid in engineered yeast. Nature *440*, 940–943.

Rocha, A.G., Knight, S.A.B., Pandey, A., et al. (2018). Cysteine desulfurase is regulated by

phosphorylation of Nfs1 in yeast mitochondria. Mitochondrion *40*, 29–41.

Roy, A., Solodovnikova, N., Nicholson, T., et al. (2003). A novel eukaryotic factor for cytosolic Fe-S cluster assembly. EMBO J. *22*, 4826–4835.

Rudolf, J., Makrantoni, V., Ingledew, W.J., et al. (2006). The DNA Repair Helicases XPD and FancJ Have Essential Iron-Sulfur Domains. Mol. Cell *23*, 801–808.

Saini, A., Mapolelo, D.T., Chahal, H.K., et al. (2010). SufD and SufC ATPase activity are required for iron acquisition during in vivo Fe-S cluster formation on SufB. Biochemistry *49*, 9402–9412.

Savojardo, C., Martelli, P.L., Fariselli, P., et al. (2018). BUSCA : an integrative web server to predict subcellular localization of proteins. *46*, 459–466.

Schaedler, T.A., Thornton, J.D., Kruse, I., et al. (2014). A conserved mitochondrial ATP-binding cassette transporter exports glutathione polysulfide for cytosolic metal cofactor assembly. J. Biol. Chem. *289*, 23264–23274.

Schindelin, J., Arganda-Carrera, I., Frise, E., et al. (2009). Fiji - an Open platform for biological image analysis. Nat. Methods *9*, 241.

Schlesier, J., Rohde, M., Gerhardt, S., et al. (2016). A Conformational Switch Triggers Nitrogenase Protection from Oxygen Damage by Shethna Protein II (FeSII). J. Am. Chem. Soc. *138*, 239–247.

Schonauer, M.S., Kastaniotis, A.J., Kursu, V.A.S., et al. (2009). Lipoic acid synthesis and attachment in yeast mitochondria. J. Biol. Chem. *284*, 23234–23242.

Schwenkert, S., Netz, D.J. a, Frazzon, J., et al. (2010). Chloroplast HCF101 is a scaffold protein for [4Fe-4S] cluster assembly. Biochem. J. *425*, 207–214.

Seguin, A., Bayot, A., Dancis, A., et al. (2009). Overexpression of the yeast frataxin homolog (Yfh1): Contrasting effects on iron-sulfur cluster assembly, heme synthesis and resistance to oxidative stress. Mitochondrion *9*, 130–138.

Selbach, B.P., Pradhan, P.K., Santos, P.C. Dos, et al. (2013). Protected sulfur transfer reactions by the Escherichia coli Suf system. Biochemistry *52*, 4089–4096.

Sharma, A.K., Pallesen, L.J., Spang, R.J., et al. (2010). Cytosolic iron-sulfur cluster assembly (CIA) system: Factors, mechanism, and relevance to cellular iron regulation. J. Biol. Chem. *285*, 26745–26751.

Shepard, E.M., Boyd, E.S., Broderick, J.B., et al. (2011). Biosynthesis of complex iron-sulfur enzymes. Curr. Opin. Chem. Biol. *15*, 319–327.

Shiuan, D. (2006). Methods for preparing yeast with improved biotin productivity using integrating plasmids encoding biotin synthase.

Simossis, V.A., and Heringa, J. (2005). PRALINE: A multiple sequence alignment toolbox that integrates homology-extended and secondary structure information. Nucleic Acids Res. *33*, 289–294.

Singh, A., Dikhit, M., and Zanello, P. (2006). Assembly , Activation , and Trafficking of the Fet3p □ Ftr1p High Affinity Iron Permease Complex in Saccharomyces cerevisiae. 34–46.

Soler, N., Delagoutte, E., Miron, S., et al. (2011). Interaction between the reductase Tah18 and highly conserved Fe-S containing Dre2 C-terminus is essential for yeast viability. Mol. Microbiol. *82*, 54–67.

Sousa, F.L., Preiner, M., and Martin, W.F. (2018). Native metals, electron bifurcation, and CO2

reduction in early biochemical evolution. Curr. Opin. Microbiol. *43*, 77–83.

Srinivasan, V., Netz, D.J.A., Webert, H., et al. (2007). Structure of the Yeast WD40 Domain Protein Cia1, a Component Acting Late in Iron-Sulfur Protein Biogenesis. Structure *15*, 1246–1257.

Stairs, C.W., Eme, L., Brown, M.W., et al. (2014). A SUF Fe-S cluster biogenesis system in the mitochondrion-related organelles of the anaerobic protist Pygsuia. Curr. Biol. *24*, 1176–1186.

Stehling, O., Vashisht, A. a, Mascarenhas, J., et al. (2012). Metabolism and Genomic Integrity. *337*, 195–199.

Stehling, O., Wilbrecht, C., and Lill, R. (2014). Mitochondrial iron-sulfur protein biogenesis and human disease. Biochimie *100*, 61–77.

Stehling, O., Jeoung, J.H., Freibert, S.A., et al. (2018). Function and crystal structure of the dimeric P-loop ATPase CFD1 coordinating an exposed [4Fe-4S] cluster for transfer to apoproteins. Proc. Natl. Acad. Sci. U. S. A. *115*, E9085–E9094.

Sun, Z., and Brodsky, J.L. (2018). The degradation pathway of a model misfolded protein is determined by aggregation propensity. Mol. Biol. Cell *29*, 1422–1434.

Sydor, T., Schaffer, S., and Boles, E. (2010). Considerable Increase in Resveratrol Production by Recombinant Industrial Yeast Strains with Use of Rich Medium. Appl. Environ. Microbiol. *76*, 3361–3363.

Takahashi, and Nakamura (1999). Functional assignment of the ORF2-iscS-iscU-iscA-hscB-hscA-fdx-ORF3 gene cluster involved in the assembly of Fe-S clusters in Escherichia coli. J. Biochem. *126*, 917–926.

Takahashi, Y., and Tokumoto, U. (2002). A Third Bacterial System for the Assembly of Iron-Sulfur Clusters with Homologs in Archaea and Plastids. J. Biol. Chem. *277*, 28380–28383.

Takahashi, T., Kawagishi, S., Funahashi, H., et al. (2015). Production and Purification of Secretory Simian Cytidine Monophosphate-N-acetylneuraminic Acid Hydroxylase Using Baculovirus-Protein Expression System. Biol. Pharm. Bull. *38*, 1220–1226.

Thim, L., Hansen, M.T., Norris, K., et al. (1986). Secretion and processing of insulin precursors in yeast. Proc. Natl. Acad. Sci. U. S. A. *83*, 6766–6770.

Tian, T., He, H., and Liu, X.Q. (2014). The SufBCD protein complex is the scaffold for iron-sulfur cluster assembly in Thermus thermophiles HB8. Biochem. Biophys. Res. Commun. *443*, 376–381.

Tsaousis, A.D., Ollagnier de Choudens, S., Gentekaki, E., et al. (2012). Evolution of Fe/S cluster biogenesis in the anaerobic parasite Blastocystis. Proc. Natl. Acad. Sci. *109*, 10426–10431.

Tsaousis, A.D., Gentekaki, E., Eme, L., et al. (2014). Evolution of the Cytosolic Iron-Sulfur Cluster Assembly Machinery in Blastocystis Species and Other Microbial Eukaryotes. Eukaryot. Cell *13*, 143–153.

Tsaousis, A.D., Hamblin, K.A., Elliott, C.R., et al. (2018). The Human Gut Colonizer Blastocystis Respires Using Complex II and Alternative Oxidase to Buffer Transient Oxygen Fluctuations in the Gut. Front. Cell. Infect. Microbiol. *8*, 371.

Tsujimoto, R., Kotani, H., Yokomizo, K., et al. (2018). Functional expression of an oxygen-labile nitrogenase in an oxygenic photosynthetic organism. Sci. Rep. *8*, 1–10.

Upadhyay, A.S., Stehling, O., Panayiotou, C., et al. (2017). Cellular requirements for iron-sulfur cluster insertion into the antiviral radical SAM protein viperin. J. Biol. Chem. *292*, 13879–13889.

Urzica, E., Pierik, A.J., Mühlenhoff, U., et al. (2009). Crucial role of conserved cysteine residues in the assembly of two iron-sulfur clusters on the CIA protein Nar1. Biochemistry *48*, 4946–4958.

Uzarska, M.A., Dutkiewicz, R., Freibert, S.-A.S.-A., et al. (2013). The mitochondrial Hsp70 chaperone Ssq1 facilitates Fe/S cluster transfer from Isu1 to Grx5 by complex formation. Mol. Biol. Cell *24*, 1830–1841.

Uzarska, M.A., Nasta, V., Weiler, B.D., et al. (2016). Mitochondrial Bol1 and Bol3 function as assembly factors for specific iron-sulfur proteins. Elife *5*, 1–25.

Vaccaro, B.J., Clarkson, S.M., Holden, J.F., et al. (2017). Biological iron-sulfur storage in a thioferrate-protein nanoparticle. Nat. Commun. *8*, 1–9.

Verstraete, W. (2002). Environmental biotechnology for sustainability. J. Biotechnol. *94*, 93–100.

Vinella, D., Loiseau, L., de Choudens, S.O., et al. (2013). In vivo [Fe-S] cluster acquisition by IscR and NsrR, two stress regulators in Escherichia coli. Mol. Microbiol. *87*, 493–508.

Vitale, G., Fabre, E., and Hurt, E. (1996). NBP35 encodes an essential and evolutionary conserved protein in Saccharomyces cerevisiae with homology to a superfamily of bacterial ATPases. Gene *178*, 97–106.

Vo, A. T., Fleischman, N.M., Froehlich, M.J., et al. (2017). Identifying the Protein Interactions of the Cytosolic Iron-Sulfur Cluster Targeting Complex Essential for Its Assembly and Recognition of Apo-Targets. Biochemistry *57*, 1–30.

Vo, A.T., Fleischman, N.M., Marquez, M.D., et al. (2017). Defining the domains of Cia2 required for its essential function in vivo and in vitro. Metallomics *9*, 1645–1654.

Wachterhauser, G. (1988). Before Enzymes and Templates: Theory of Surface Metabolism. Microbiol. Rev. *52*, 452–484.

Wada, K., Hasegawa, Y., Gong, Z., et al. (2005). Crystal structure of Escherichia coli SufA involved in biosynthesis of iron-sulfur clusters: Implications for a functional dimer. FEBS Lett. *579*, 6543–6548.

Wang, M.S., Hoegler, K.J., and Hecht, M.H. (2019). Unevolved De Novo Proteins Have Innate Tendencies to Bind Transition Metals. Life *9*, 1–15.

Wang, X., Li, Q., Yuan, W., et al. (2016). The cytosolic Fe-S cluster assembly component MET18 is required for the full enzymatic activity of ROS1 in active DNA demethylation. Sci. Rep. *6*, 1–15.

Webert, H., Freibert, S.-A., Gallo, A., et al. (2014). Functional reconstitution of mitochondrial Fe/S cluster synthesis on Isu1 reveals the involvement of ferredoxin. Nat. Commun. *5*, 5013.

Van Wietmarschen, N., Moradian, A., Morin, G.B., et al. (2012). The mammalian proteins MMS19, MIP18, and ANT2 are involved in cytoplasmic iron-sulfur cluster protein assembly. J. Biol. Chem. *287*, 43351–43358.

Williams, C.A., Hoffman, R.M., Kronfeld, D.S., et al. (2002). Lipoic Acid as an Antioxidant in Mature Thoroughbred Geldings: A Preliminary Study. J. Nutr. *132*, 1628S-1631S.

Winzeler, E.A., Shoemaker, D.D., Astromoff, A., et al. (1999). Functional characterization of the Saccharomyces cerevisiae genome by gene deletion and parallel analysis. Science (80-.). *285*, 901–906.

Wollenberg, M., Berndt, C., Bill, E., et al. (2003). A dimer of the FeS cluster biosynthesis protein IscA from cyanobacteria binds a [2Fe2S] cluster between two protomers and transfers it to [2Fe2S]

and [4Fe4S] apo proteins. Eur. J. Biochem. *270*, 1662–1671.

Wollers, S., Layer, G., Garcia-Serres, R., et al. (2010). Iron-Sulfur (Fe-S) Cluster Assembly: THE SufBCD COMPLEX IS A NEW TYPE OF Fe-S SCAFFOLD WITH A FLAVIN REDOX COFACTOR. J. Biol. Chem. *285*, 23331–23341.

Wright, P.E., and Dyson, H.J. (2015). Intrinsically Disordered Proteins in Cellular Signaling and Regulation. Nat Rev Mol Cell Biol *16*, 18–29.

Wu, G., Mansy, S.S., Wu, S.P., et al. (2002). Characterization of an iron-sulfur cluster assembly protein (ISU1) from Schizosaccharomyces pombe. Biochemistry *41*, 5024–5032.

Yu, S.L., Kang, M.S., Kim, H.Y., et al. (2011). Restoration of proliferation ability with increased genomic instability from Rad2p-induced mitotic catastrophe in Saccharomyces cerevisiae. Mol. Cell. Toxicol. *7*, 195–206.

Yücesoy, M., and Marol, S. (2003). Performance of CHROMAGAR candida and BIGGY agar for identification of yeast species. Ann. Clin. Microbiol. Antimicrob. *2*, 1–7.

Yuda, E., Tanaka, N., Fujishiro, T., et al. (2017). Mapping the key residues of SufB and SufD essential for biosynthesis of iron-sulfur clusters. Sci. Rep. *7*, 1–12.

Zaugg, S., Rieske, J., Hansen, R., et al. (1964). Studies on the Electron Transfer System. J. Biol. Chem. *239*, 1676–1681.

Zhai, C., Li, Y., Mascarenhas, C., et al. (2014). The function of ORAOV1/LTO1, a gene that is overexpressed frequently in cancer: essential roles in the function and biogenesis of the ribosome. Oncogene *33*, 484–494.

Zhang, B., Bandyopadhyay, S., Shakamuri, P., et al. (2013). Monothiol glutaredoxins can bind linear [Fe3S4]+ and [Fe4S4]2+ clusters in addition to [Fe2S2]2+ clusters: spectroscopic characterization and functional implications. J. Am. Chem. Soc. *135*, 15153–15164.

Zhang, Y., Lyver, E.R., Nakamaru-Ogiso, E., et al. (2008). Dre2, a Conserved Eukaryotic Fe/S Cluster Protein, Functions in Cytosolic Fe/S Protein Biogenesis. Mol. Cell. Biol. *28*, 5569–5582.

Zhao, B., Zhao, Y., Zhang, X., et al. (2019). An iteration method for identifying yeast essential proteins from heterogeneous network. BMC Bioinformatics *20*, 1–13.

Zhao, W., Fang, B.X., Niu, Y.J., et al. (2014). Nar1 deficiency results in shortened lifespan and sensitivity to paraquat that is rescued by increased expression of mitochondrial superoxide dismutase. Mech. Ageing Dev. *138*, 53–58.

Zheng, M., Wang, X., Templeton, L.J., et al. (2001). DNA Microarray-Mediated Transcriptional Pro ling of the. J. Bacteriol. *183*, 4562–4570.

Appendix

>Blastocystis_ST1
MAQPILNVIDLHVEIAGKEVLKGVNLCIYPGETHILFGPNGSGKSTLIKTIIGLSECKVTQGSIFFLGDVT
NKTISERSIMGMGMLFQSPPEIEGLPLKRLVTTAFEQCDEKYMKEMSATTTMTDYLDRDLNVGFSGGERKR
CEAFQLLLQKPVLSMLDEPESGVDLESVRVLGKALSALQDRDVNGIRSATIIITHTGSILQYMHGTQAHVL
IDGRMVCTGDEEVFFDIIQKNGFNYFRNVSCNGRCDTCPEKERHTIIHQELESKRSAKLDAFLNSSSQPVS
QPNGCVNNQANTHMEEEPKTGSLLAAVEGIADDSFLTETTTTAVQAPQQGGVVKVDVTDTDVYGGEYRQRD
QVVEEYESFEDGIEVLCLAKALEKYPWIREKYMWRAMSPDKDEITRAVAKNDKTSPTGYVIIAHPGAKSVN
PINSQLIMENNKIQYVHNILISMPGSCLTVASLCTYHCGQKDHHDYIVGGQHYGVSEFFVEKDSELCFSMI
HTWCNSYIVWPRSAAVVEENGVFYSNYVCLEPVVKVQMCPVADLRGRNAVKFSAVLLAKEGTTLDVGSRAL
LNAEGARSESITRTISKGGVIFARADIQGNALNTKGHIECQGLVVDEGKGVIHSIPQISGSFGTELSHEAA
IGRIAKDKIEYLMTRRMTEEEAVSVIIRGFLNVKVQGIPKSIQQQMDEIIDQASKEGF

>Stygiellai
MKRTKVITTGLLVHDLHVEVHGREILHGVNLEIHPGETHVLLGPNGCGKSTLLSAIMGFGDFTVTKGNIFY
NGRDITKQSIDARARLGIGVMYQKAPSISGLKLRRLLSAIAPSESEERMEEMASSTNVGKLLMRDVNHGFS
GGEVKRSELMQLLCQHPTLVMCDEPESGVDLENISLVGKTIEKLVKRTPETCGLIITHSGNVLDYMKGVDN
GHIMIDGHLQCQGNPRSLLSTIRRFGFDGCVMCARDPSHPKSCATMDIEETPVVLLPPTFEDDFRELVEIT
ARTQSEADKETKSTKNGKMGEPAPRTKKVAPSCSTGPANINEGGRVVISDIMDDDPLDVTETLNYLQVDDR
IVQTLSPIVSGIEVLSLENALEKYSWIKERIFWNVVPMGKDEVTRYVALHEETDKRGYVIIAHEGVDSGDV
PVRVALQLEDMEIQHVHNIIVAKKGSRLHVVSSCSCSQSSAGAHYGVTEFWVEEDAHLSNTMIHKWCDKSI
VYPRSATIVEKNGVFLSNYVSTNAVKTIQSYPVAYLNGEGAVARFNSVIVAPKGALIDTGSRAILGALHTR
AEMVSRMLTFGGKIIARAHIIGAKKDTYGHIECQGLVLHDTGGIHAIPEVEGIVEGSELSHEAAVGKIARE
KIEYVMSRGLTEEQAIGTVIRGFVDVDMKGIPASLQKEIHEVVEVAAMGF

>Blastocystis_ST4

MSQRRKAWRSLIIEPILEVKDLHVEIAGKEVLKGITMSIYPGETHILFGPNGSGKSTFIKTLMGLSDCKVT
QGSITFLGKDVTYSPVSDRSVMGMGMLFQNPPEIDGLPLNRLISHAFADNDKEYIDAVKKTTTMEDHWDRD
LNVGFSGGERKRCEALQLLLQKPVLSMLDEPESGVDLQSVRVLGRALSALQDREVNGVHSATIIITHTGSI
LDYMHGTVAHVLVDGYIACTGDEQVFFNMIAEEGFDYFRNLVCNKDCCHCPEQEKHGMVKHRICACKDVKK
PASLLDAFMTSSTKEQQLSLMEEEPLQVETPVKTLLDNVSSVSDDAFLEGDQVKVNVKEENKKVMVDTNEV
DVYGGAYRQRDQVVEEFESYDDGIEVLSLHKYMWRALDSEKDEVTRAVAENDKKDPTGYVIIAHPGAKSKH
PVNSQLIMENNQMQYVHNLLISMPGSQLTVASTCTYHCGSKDNHEYIVGGKHYGVSEFYVEKDSDGAIVED
NGVFYSNYVCLEPVIKVQMCPVADLRGENSVAKFSSVLLAKEGTVLDIGSRALLKGKGSRSESITRTISKG
GEIYARADIQGFGENTKGHIECQGLVVNEGKGVIHSIPQISGGYGTELSHEAAIGKIAKDKIEYLMTRRMT
EDEAISVIIRGFLNVKVQGIPRSIQAQMDEIIEQASKEGF

>Proteromonas_lac

MGLSGYKITKGKIYFMGEDITEMSISDRANLGMGIMFQKAPSIQGLKLKTLVKTAFGKNKDDIDINNASEQ
SNMKEFLERDVNVGFSGGEMKRCEILQLNLQDPEFIMLDEPESGVDLENMKLVGDSIRNIIHRSEKSRSAL
VITHTGHILSYLKASISHIMLNGRINECGDASECLKVIQESGYEECLKRLGGIYDKDSKLIDVGNHVDKIS
NVCKDCSYGNNLDKMCRCGKYPGKMCLCKQNGGNSKDHVCQCSLSKNKIENKTTITDNKSKKVTINLLEDD
LDRPPSISDINSLESLPEIKTKEIEKVKVSLEDPSLFNGEYKQINNDLVSTIDSNEEGIEILKLAEAIKKY
PDFKEKYLWRNISFDKDDYTKAVYEHEKTIYNGYVIIAHEGAKNLKPVKAQLLMEQISIQYVHNILIAEKG
SCLSVSSFCGYCNKRDEDVLPDGFNGQHYGISEFYVEEDAQLSFSMIHNYCLNYTIYPRSASRVEKNGTFI
SSYVCLDPVNKVQMNPTAFLVGENAIARFSSILVSHEGGVLDIGSTAFLQAPGTSSESVTRALTKGGTIIA
KGRMVSESVKTTAHIECQGMVLKKGIIRSIPEIEGGYDCELSHEAAVGKIAQEKVDYLMSRGIKEEDAVSI
IIRGFLDVKIKGIPPMLQEEIDYVMEEAAKGF

Appendix 1. FASTA sequences of the SufCB proteins provided by A. Tsaousis.

>Pygsuia_mito

MLRALTRNFSFIKGASAITPRFAPSFSQTRRLSSLNYHAFSPKENDELLVLDNLHVAIEGEEILQGIDLLI
RRGENHVILGPNGCGKTTLFSAIMGLDKCKITNGRIIFRNHDVTRAPIYERSRLGLGMMFQKPPAVHGLKL
GKFLGAANPAIDDEHLREHCGITHMGDFLDRDLNAGFSGGETKRSELLQLLSQEPQLALLDEPESGVDLEN
IGLLGKGIKELFAGHDFSCGGLVITHTGLILEHIPNAVGHIMLDGKFRCTGNPVRMLQNIGESGYEHCITC
PKDPSVRGFDAKSAKPLVLGTIEPPSEEEEKQKKDTVFSTGFVPCLVDVPEHPEKGVMHVGHHSGAYLQVN
QDVDCSVSLREGLEVVSLDRALEEHPYLREKYLWKAVNADQDENTKIVADYEKSGAYRGYVIIAREGCNID
EPVDAALLLEKGISAQYVHNLIIAEKGSKLHIASTCAGCKPKTTESHTAADSTHFGISEFFVEDDATLTFS
MIHTFLDDYKIFPRSAAVVGNRGLFFSNYVCLQAPKAIQMYPKATLAGDDAIARFNTVLVASPGSLFDVGS
RAILQGKRSRAEMVSRIISTGGKVIARGHCQGVNPDSRGHIECQGLILGDGTIHAIPEIEGTVEGTELSHE
AAVGKIAKEKLEYLMARGLSEEEATAVIVRGFLDVRMDDVPDELRAKMNAVIDAAAGGM

>Pygsuia_cyto

MVYKDQKVLLSIENLHVSAGKKEILRGVDLTILEGEVHVLLGPNGSGKSTLLGAIMGFSQYQITKGRILFR
GEDITQWSIDQRAKLGLGLMFQRPPHVNGLHLSKLLEAANPTKEFTRAVEFTNMIEFQDRDVNVGFSGGET
KRSELLQLLVQQPSMVLLDEPESGVDLENIVPLGKGCKQLLENSKLNGGLVITHTGHILDFVHTDKAHIMF
KGRIHCQGDPMLLLQHIRTNGYKGCFDCHTMESVQSPLPADIEDVQESGSYQVKKSALDSEVLVFENNNLV
SMKGGKLALEDQDDPSVQRNTNSVTSVNSGIVKLDLEDDELSINGLASSSGRYQQFDQEVSFSTSATPGLE
VLNLQDALTKYHWIERDYLWKCVKPDQDANTTIVKDYEDAGGFRGYVIIAHENCKLQS
PVDAALLMGGKQNQFVHNLLIARPGSELHVISSCKDCHKHGEDPELVTHYGISEFFVDENAKLSFTMVHSF
CEKYTVYPRSASLVKANGVFLSNYCCLSPVGKVQMYPKAILDGANATARFSSVVIAYPGSLIDFGSRALLN
HPNTRAEMVSRIISKGGKVYARGHIVGAVNETRGHIECQGLVLSGNIHAIPEIEGQVEGTELSHEAAVGKI
AREKLEYVMARGLSEAEAVSVIIQGFLDVKIKGMPPKLQAYIDSVVSKAATGFC

Appendix 2. FASTA sequences of the SufCB proteins provided from A. Tsaousis, part 2.

Blastocystis Nand II

Blastocystis subtype 4

Proteromonas lacerate

Pygsuia biforma cytosolic variant

Pygsuia biforma mitochondrial variant

Stygiella incarcerata

Appendix 3. Sequence identity (%) matrix of each SufCB primary sequence. Data was obtained fm a pairwise sequence alignment. Clustal O (1.2.4) was used on default settings, https://www.ebi.ac.uk/Tools/msa/clustalo/.

Protein	Percentage identity, %					
Blastocystis Nand II	100.00	71.95	45.25	42.81	43.19	42.90
Blastocystis subtype 4	71.95	100.00	43.90	41.32	42.17	41.56
Proteromonas lacertae	45.25	43.90	100.00	41.73	42.14	45.81
Stygiella incarcerata	42.81	41.32	41.73	100.00	46.95	48.03
Pygsuia mSufCB	43.19	42.17	42.14	46.95	100.00	52.63
Pygsuia cySufCB	42.90	41.56	45.81	48.03	52.63	100.00

.

Appendix 4. Similarity of SufCB to SufC of *E. coli*. Data was obtained from NCBI Blast P suite, using default settings.

	Similarity to SufC		
Protein	Identity (%)	Positives (%)	E-value
SufC	100%	100%	0
Blastocystis Nand II	39%	60%	$4x10^{-46}$
Blastocystis subtype 4	37%	56%	$4x10^{-46}$
Proteromonas lacertae	36&	54%-	$3x10^{-54}$
Pygsuia biforma (cytosolic variant)	35%	55%	$3x10^{-32}$
Pygsuia biforma (mitochondrial variant)	36%	56%	$2x10^{-46}$
Stygiella incarcerata	31%	54%	$1x10^{-36}$

Appendix 5. Similarity of SufCB to SufB of *E. coli.* Data was obtained from NCBI Blast P suite, using default settings.

	Similarity to SufB		
Protein	Identity (%)	Positives (%)	E-value
SufB	100%	100%	0
Blastocystis Nand II	26%	47%	$4x10^{-15}$
Blastocystis subtype 4	23%	45%	$4x10^{-15}$
Proteromonas lacertae	23%	42%	$3x10^{-17}$
Pygsuia biforma (cytosolic variant)	23%	41%	$2x10^{-22}$
Pygsuia biforma (mitochondrial variant)	22%	39%	$1x10^{-15}$
Stygiella incarcerata	21%	43%	$2x10^{-13}$

List of domain hits

Name	Accession	Description	Interval	E-value
[+] ABC_FeS_Assembly	cd03217	ABC-type transport system involved in Fe-S cluster assembly, ATPase component; Biosynthesis of ...	6-237	1.48e-81
[+] SufC	COG0396	Fe-S cluster assembly ATPase SufC [Posttranslational modification, protein turnover, ...	5-248	3.87e-79
[+] sufC	TIGR01978	FeS assembly ATPase SufC; SufC is part of the SUF system, shown in E. coli to consist of six ...	6-240	7.73e-68
[+] ycf16	CHL00131	sulfate ABC transporter protein; Validated	1-242	6.36e-53
[+] SufB	COG0719	Fe-S cluster assembly scaffold protein SufB [Posttranslational modification, protein turnover, ...	357-680	2.02e-49
[+] UPF0051	pfam01458	Uncharacterized protein family (UPF0051);	441-671	1.67e-43
[+] sufB	TIGR01980	FeS assembly protein SufB; This protein, SufB, forms a cytosolic complex SufBCD. This complex ...	366-691	1.00e-27
[+] ABC_tran	pfam00005	ABC transporter; ABC transporters for a large family of proteins responsible for translocation ...	21-162	5.78e-25
[+] ycf24	CHL00085	putative ABC transporter	542-671	8.63e-08
[+] AAA	smart00382	ATPases associated with a variety of cellular activities; AAA - ATPases associated with a ...	30-67	2.70e-03

Appendix 6. The superfamilies which significantly align to the Blastocystis SufCB protein. Graphic was sourced from NCBI P blast suite.

```
#
#
#  Percent Identity  Matrix - created by Clustal2.1
#
#

     1: BNbp35      100.00   47.49   49.24
     2: Nbp35        47.49  100.00   53.82
     3: AtNbp35      49.24   53.82  100.00
```

Appendix 7. Percent identity matrix between Blastocystis, Arabidopsis and yeast Nbp35 proteins. Moderate sequence conservation (>47%) can be seen between each protein.

```
Met18       -MTPDELNSA------VVTFMANLNIDDSKANETASTVTDSIVHRSIKLLEVVVALKDYF      53
HsMet18     -MAAAAAVEAAAPMGALWGLVHDFVVGQ--QEGPADQVAADVKSGNYTVLQVVEALGSSL      57
MmMet18     MAAATGLEEAVAPMGALCGLVQDFVMGQ--QEGPADQVAADVKSGGYTVLQVVEALGSSL      58
              :     .*      :  :: :: :.:   :  *. *: .:   . .:*:** ** . :

Met18       LSENEVERKKALTCLTTILAKTPKDHLSKNECSVIFQFYQSKLDDQAL-AKEVLEGFAAL      112
HsMet18     ENPEPRTRARAIQLLSQVLLHC-HTLLLEKEVVHLILFYENRLKDHHLVIPSVLQGLKAL      116
MmMet18     ENAEPRTRARGAQLLSQVLLQC-HSLLSEKEVVHLILFYENRLKDHHLVVPSVLQGLRAL      117
             . :   * :.   *: :* :  :  * ::*   :: **:.:*.*: *   .**:*: **

Met18       APMKYVSINEIAQLLRLLLDNYQQGQHLASTRLWPFKILRKIFDRFFVNGSSTEQVKRIN      172
HsMet18     SLCVALPPGLAVSVLKAIFQEVHVQSLPQVDRHTVYNI----ITNFM--RTREEELKSLG      170
MmMet18     SMSVALPPGLAVSVLKAIFQEVHVQSLLQVDRHTVFSI----ITNFM--RSREEELKGLG      171
            :    :  .  ..:*: :::: :  .     *   :.*    : .*:   :  *::* :.

Met18       DLFIETFLHVANGEKDPRNLLLSFALNKSITSSLQNVENFKEDLFDVLFCYFPITFKPPK      232
HsMet18     ADFTFGFIQVMDGEKDPRNLLVAFRIVHDLISRDYSLGPFVEELFEVTSCYFPIDFTPPP      230
MmMet18     ADFTFGFIQVMDGEKDPRNLLLAFRIVHDLISKDYSLGPFVEELFEVTSCYFPIDFTPPP      231
              *   *:** :*********::* : :.: *   .:  * *:**:*  ***** *.**

Met18       HDPYKISNQDLKTALRSAITATPLFAEDAYSNLLDKLTASSPVVKNDTLLTLLECVRKFG      292
HsMet18     NDPHGIQREDLILSLRAVLASTPRFAEFLLPLLIEKVDSEVLSAKLDSLQTLNACCAVYG      290
MmMet18     NDPYGIQREDLILSLRAVLASTPRFAEFLLPLLIEKVDSEILSAKLDSLQTLNACCAVYG      291
            :**: *..:**  :**:.:::** ***     *::*: :.   .* *:* **  *   :*

Met18       GSSILENWTLLWNALKFEIMQNSEGNENTLLNPYNKDQQSDDVGQYTNYDACLKIINLMA      352
HsMet18     QKELKDFLPSLWASIRREVFQTASERV-----------EAEGLAALHSLTACLSRSVLRA      339
MmMet18     QKELKDFLPSLWASIRREVFQTASERV-----------EAEGLAALHSLTACLSCSVLRA      340
             ..: :    ** ::: *::*.:. .            :::.:.   .  ***.   * *

Met18       LQLYNFDKVSFEKFFTHVLDELKPNFKYEKDLK---QTCQILSAIGSGNVEIFNKVISST      409
HsMet18     DA-----EDLLDSFLSNILQDCRHHL-CEPDMKLVWPSAKLLQAAAGASARACDSVTSNV      393
MmMet18     DA-----EDLLGSFLSNILQDCRHHL-CEPDMKLVWPSAKLLQAAAGASARACEHLTSNV      394
                   :  : .*:::*:: : ::  * *:*    :.::*.* ......  : : *..

Met18       FPLFLINTSE----VAKLKLLIMNFSFFVDSYIDLFGRTSKESLGTPVPNNKMAEYKDEI      465
HsMet18     LPLLLEQFHKHSQSSQRRTILEMLLGFL-----KLQQKWSYE----DKDQRPLNGFKDQL      444
MmMet18     LPLLLEQFHKHSQSNQRRTILEMILGFL-----KLQQKWSYE----DRDERPLSSFKDQL      445
            :**:* :  :      : .:* * :.*:     .*  : * *       :. :  :**::

Met18       IMILSMALTRSSKA--EVTIRTLSVIQFTKMIKMKGFLTPEEVSLIIQY-FTEEILTDNN      522
HsMet18     CSLVFMALTDPSTQLQLVGIRTLTVLG-----AQPDLLSYEDLELAVGHLYRLSFLKEDS      499
MmMet18     CSLVFMALTDPSTQLQLVGIRTLTVLG-----AQPGLLSAEDLELAVGHLYRLTFLEEDS      500
              :: ****  *.    * ****.*:         .:*: *::.* : : :   :* ::.

Met18       KNIYYACLEGLKTISEIYEDLVFEISLKKLLDLLPDCFEEKIRVNDEENIH------IET      576
HsMet18     QSCRVAALEASGTLAALYPVAFSSHLVPKLA--------EELRVGESNLTNGDEPTQCSR      551
MmMet18     QSCRVAALEASGTLATLYPGAFSRHLLPKLA--------EELHKGESDVARADGPTKCSR      552
            :.   *.**.  *:: :*   .    : **         *::: .:.:  .       .

Met18       ILKI--ILDFTTSRHILVKESITFLATKL----------------------NRVA-KISK      611
HsMet18     HLCCLQALSAVSTHPSIVKETLPLLLQHLWQVNRGNMVAQSSDVIAVCQSLRQMAEKCQQ      611
MmMet18     HFRCLQALSAVSTHPSIVKETLPLLLQHLCQANKGNMVTESSEVVAVCQSLQQVAEKCQQ      612
             :     *. .:::  :***:: :*  :*                      .::* * .:

Met18       SREYCFLLIST-IYSLFNNNNQNENVLNEEDALALKNAIEP----KLFEIITQESAIVSD      666
HsMet18     DPESCWYFHQTAIPCLLALAVQA-SMPEKEPSVLRKVLLEDEVLAAMVSVIGTATTHLSP      670
MmMet18     DPESYWYFHKTAVPCLFALAVQA-SMPEKESSVLRKVLLEDEVLAALASVIGTATTHLSP      671
            . *  : : .* : .*:    *  .: ::* ::  *  :*      : .:*   :: :*

Met18       N---------YNLTLLSNVLFFTNLKIPQAAHQEELDRYNELFISEGKIRILD-------      710
HsMet18     ELAAQSVTHIVPLFLDGNVSFLPENSFPS-----RFQPFQDG--SSGQRRLIALLMAFVC      723
MmMet18     ELAAQSVTCIVPLFLDGNTSFLPENSFPD-----QFQPFQDG--SSGQRRLVALLTAFVC      724
            :           * * .*. *: : .:*.     .:: :::   *.*: *::

Met18       -------TPNVLAISYAKILSALNKNCQFPQKFTVLFGTVQLLKKHAPRMTETEKLGYLE      763
HsMet18     SLPRNVEIPQLNQLMRELLELSCCHSCPFSSTAAAK-CFAGLLNKHPAGQQLDE---FLQ      779
MmMet18     SLPRNVEIPQLNRLMRELLKQSCGHSCPFSSTAATK-CFAGLLNKQPPGQQLEE---FLQ      780
                    *::  :    :  :  :.* * .. :.    . **:*:       *   :*:
```

```
Met18       LLLVLSNKFVSEKDVIGLFDWKDLSVINLEVMVWLTKGLIMQNSLESSEIAKKFIDLLSN      823
HsMet18     ----LAVD----KVEAG-LGSGPCRSQAFTLLLWVTKALVLRYHPLSSCLTARLMGLLSD      830
MmMet18     ----LAVG----TVEAG-LASESSRDQAFTLLLWVTKALVLRYHPLSACLTTRLMGLLSD      831
                *:      .   * :         : :::*:**.*:::    *: :: :::.***:

Met18       EEIGSLVSKLFEVFVMDISSLKKFKGISWNNNVKILYKQKFFGDIFQTLVSNYKNTVDMT      883
HsMet18     PELGPAAADGFSLLMSDCTDVLTR---AGHAEVRIMFRQRFFTDNVPALVQGFHAA-PQD      886
MmMet18     PELGCAAADGFSLLMSDCTDVLTR---AGHADVRIMFRQRFFTDNVPALVQGFHAA-PQD      887
             *:*  .:. *.::: * :.: .    : : :*:*:::*:** * . :**..:: :

Met18       IKCNYLTALSLVLKHTPSQSVGPFINDLFPLLLQALDMPDPEVRVSALETLKDTTDKHHT      943
HsMet18     VKPNYLKGLSHVLNRLPKPVLLPELPTLLSLLLEALSCPDCVVQLSTLSCLQPLLLEAPQ      946
MmMet18     VKPNYLKGLSHVLNRLPKPVLLPELPTLLSLLLEALSCPDSVVQLSTLSCLQPLLLEAPQ      947
            :* ***..** **:: *.  : * :  *: ***:**. **  *::*:*. *:    :

Met18       LITEHVSTIVPLLLSLSLPHKYNSVSVRLIALQLLEMITTVVPLNYCLSYQDDVLSALIP      1003
HsMet18     VMSLHVDTLVTKFLNLSSS---PSMAVRIAALQCMHAL-TRLPTPVLLPYKPQVIRALAK      1002
MmMet18     IMSLHVDTLVTKFLNLSSS---YSMAVRIAALQCMHAL-TRLPTSVLLPYKSQVIRALAK      1003
            ::: **.*:*  :*.**      *::**: *** :. : * :*    * *: :*: **

Met18       VLSDKKRIIRKQCVDTRQVYYELGQIPFE*     1032
HsMet18     PLDDKKRLVRKEAVSARGEWFLLGSPGS--     1030
MmMet18     PLDDKKRLVRKEAVSARGEWFLLGSPGS--     1031
             *.****::**:.*.:*  :: **.
```

Appendix 8. Full pairwise sequence alignment of the Met18 proteins from yeast, human and mouse. Alignment was performed in Clustal Omega using default settings.

actcccgggATGGCGCAGCCTATTTTGAACGTTATTGATCTCCATGTTGAAATCGCCGGCAAGGAAGTGCTCAAGGGAGTCAACCTGTGCATTTACC
CTGGGGAAACACACATTCTCTTCGGCCCCAACGGCTCCGGAAAGAGCACGTTGATCAAGACGATCATCGGCCTTAGCGAGTGCAAGGTGACACA
GGGATCCATTTTCTTCCTCGGCGAGGACGTCACGAATAAGACCATTTCGGAGCGCTCCATCATGGGCATGGGAATGCTCTTCCAGAGTCCTCCCGA
GATTGAGGGACTGCCGCTGAAGAGACTCGTCACGACGGCGTTCGAGCAGTGCGACGAGAAATACATGAAGGAAATGAGTGCAACCACCACAAT
GACCGATTACCTGGATCGCGACCTGAACGTCGGCTTTTCCGGTGGTGAGCGCAAGCGCTGCGAGGCCTTCCAGCTGCTGCTCCAGAAGCCCGTG
CTCTCCATGCTGGACGAGCCGGAGAGCGGCGTTGATCTGGAATCGGTGCGCGTGCTGGGCAAGGCGCTGTCTGCCCTGCAGGACCGCGACGTC
AACGGCATCCGCTCCGCCACCATCATCATCACGCACACGGGCAGCATCCTGCAGTACATGCATGGAACGCAGGCGCACGTGCTGATCGACGGGCG
CATGGTCTGCACGGGCGACGAGGAGGTGTTCTTCGACATCATTCAGAAGAACGGCTTCAACTATTTCCGCAACGTCTCCTGCAACGGCCGGTGCG
ACACCTGCCCCGAGAAGGAGCGTCACACCATCATCCACCAGGAGCTGGAGAGCAAGCGCTCCGCCAAGCTCGACGCCTTCCTGAACAGTTCCTC
TCAGCCTGTCAGCCAACCCAATGGGTGTGTGAACAATCAGGCAAACACCCACATGGAGGAGGAGCCGAAGACGGGATCGCTGCTGGCAGCGGT
GGAGGGCATCGCGGATGACTCCTTCCTGACGGAGACGACGACGACGGCCGTGCAGGCACCGCAGCAGGGCGGCGTGGTGAAGGTCGACGTGA
CGGACACGGACGTGTACGGCGGCGAGTACCGGCAGCGCGACCAGGTGGTGGAGGAGTACGAGTCGTTCGAGGACGGCATCGAGGTGCTGTGC
CTCGCCAAGGCGCTGGAGAAGTACCCGTGGATCCGCGAGAAGTACATGTGGCGCGCCATGTCCCCCGACAAGGACGAGATCACGCGCGCCGTG
GCGAAGAACGACAAGACGAGTCCGACGGGCTACGTGATCATCGCCCACCCCGGCGCGAAGTCGGTGAACCCGATCAACAGCCAGCTGATCATG
GAGAACAACAAGATCCAGTACGTGCACAACATCCTCATCTCCATGCCCGGCTCCTGTCTGACCGTCGCCTCGCTCTGCACCTACCACTGCGGCCAG
AAGGACCACCACGACTACATCGTCGGCGGGCAGCACTACGGCGTGTCCGAGTTCTTCGTGGAGAAGGACTCGGAGCTCTGCTTCTCGATGATTC
ACACGTGGTGCAACTCCTACATCGTGTGGCCGCGCTCCGCCGCCGTCGTGGAGGAGAACGGCGTGTTCTACTCCAACTACGTGTGTTTGGAGCCC
GTGGTCAAGGTCCAGATGTGCCCCGTGGCCGACCTGCGCGGGCGCAACGCCGTGGCGAAGTTCAGCGCGGTGCTGCTGGCGAAGGAGGGCAC
GACGCTGGACGTGGGGTCGCGCGCGTTGCTGAATGCCGAGGGTGCGCGCAGCGAGAGCATCACGCGCACCATCTCGAAGGGTGGCGTGATCTT
CGCGCGCGCGGACATCCAGGGCAACGCGCTGAACACGAAGGGACACATCGAGTGCCAGGGTCTGGTGGTGGACGAGGGTAAGGGCGTGATCC
ACTCGATTCCGCAGATCTCGGGCAGCTTCGGCACGGAGCTGAGCCACGAGGCGGCGATCGGCCGGATCGCGAAGGACAAGATCGAGTACCTGA
TGACGCGCCGCATGACGGAGGAGGAGGCAGTGTCGGTGATCATCCGCGGTTTCCTGAACGTGAAGGTGCAGGGCATTCCGAAGTCGATCCAGC
AGCAGATGGACGAGATCATCGACCAGGCGAGCAAGGAGGGGTTCTGAgaattcgacacttct

Appendix 9. Demonstrating the sequence of the SufCB ORF in pBEVY-u. Start and stop codons are in bold, red. Restriction enzyme sites for *Xma I* and *EcoR I* are underlined, the ORF is capitalised.

Appendix 10. Localisation prediction of each SufCB using BUSCA server, set to fungi localisation parameters. Scores column indicate localisation likelihood, e.g. 0.7 = 70%. GOterms also given with each organelle predicted organelle.

Accession	GOids	GOterms	Score
Blastocystis_ST1	GO:0005737	C:cytoplasm	0.7
Blastocystis_ST4	GO:0005737	C:cytoplasm	0.6
Proteromonas_lac	GO:0005737	C:cytoplasm	0.7
Pygsuia_cyto	GO:0005737	C:cytoplasm	1
Pygsuia_mito	GO:0005739	C:mitochondrion	0.85
Stygiellai	GO:0005737	C:cytoplasm	1

SufCB's from the following organisms (in order):

Blastocystis Nand II

Blastocystis subtype 4

Proteromonas lacerate

Pygsuia biforma cytosolic variant

Pygsuia biforma mitochondrial variant

Stygiella incarcerata

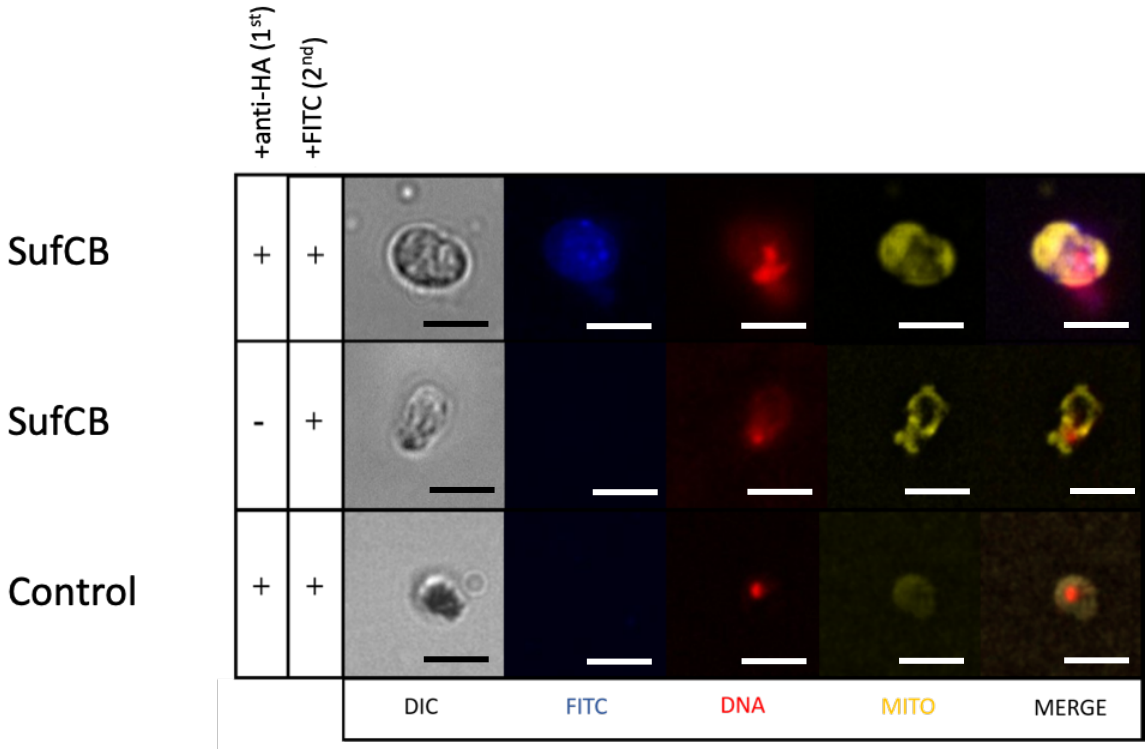

Appendix 11. Immunofluorescence (single cells) of SufCB and controls. In addition to non-SufCB expressing yeast, a control without primary antibody was also used to determine that the FITC signal originated from specific SufCB-antibody interactions. Scale bars at 4 microns.

Appendix 12. The growth rates of SufCB cells under various stressors compared to controls. No significant difference could be seen between any stress.

		Sample	Specific growth rate, Gens/Hr
No stress		SufCB	0.36±0.007
		Control	0.37±0.002
Hydrogen peroxide	0,5 mM	SufCB	0.338±0.006
	0.5 mM	Control	0.355±0.008
	1 mM	SufCB	0.285±0.022
	1 mM	Control	0.107±0.045
	2 mM	SufCB	0.069±0.040
	2 mM	Control	0.059±0.002
Copper chloride	1 mM	SufCB	0.176±0.003
	1 mM	Control	0.122±0.003
	2 mM	SufCB	0.005±0.006
	2 mM	Control	0.003±0.011

Appendix 13. Stop-codon readthrough data for Rli1 function. No difference (p=0.128) can be seen between the stop codon readthrough of SufCB or control cells under exposure to 1 mM hydrogen peroxide. Stdev = standard deviation, SEM = standard error of the mean. Readthrough was unchanged between SufCB and controls (p>0.05).

	Mean	Stdev	SEM
SufCB	0.002379702	0.001153809	0.000364866
SufCB + 1mM H2O2	0.002115478	0.000780248	0.000246736
Control	0.001640933	0.000430744	0.000136213
Control + 1mM H2O2	0.001696132	0.00057277	0.000181126

A full breakdown of this data is in. The iron-sulfur enzymes found to be significantly upregulated in SufCB-cells are underlined. By comparing the percentage fluorescence values of GFP-tagged iron-sulfur enzymes via FACs, we have demonstrated that the expression of SufCB elicited significant abundance changes in several iron-sulfur enzymes throughout yeast cells.

Appendix 14. Relative fold change between SufCB (+) and control (-) cells. Data is with the standard error of the mean (SEM). Presence of SufCB is indicated by a (+), control strains with empty vector only are indicated by (-). All data is background (e.g. autofluorescence) corrected using a non-fluorescent control. Data is n=4, duplicate and 30,000 events were taken per replicate, ± is standard error of the mean (SEM).

Protein	SufCB	Percentage fluorescence, %	Average fold change
Non-fluorescing control	-	0.54	NA
Act1	+	17.37	0.96±0.049
	-	18.08	
Leu1	+	7.64	2.06±0.110
	-	3.70	
Ecm17	+	10.97	1.93±0.2218
	-	5.68	
Ntg2	+	31.036	1.31±0.070
	-	23.58	
Elp3	+	22.30	1.42±0.128
	-	15.60	
Rli1	+	52.51	0.90±0.011
	-	57.76	
Pol2	+	8.02	0.79±0.082
	-	10.04	
Nbp35	+	8.25	0.71±0.044
	-	4.118	
Rad3	+	5.92	0.53±0.014
	-	11.03	
Bio2	+	10.30	2.55±0.074
	-	4.02	
Lip5	+	43.56	0.87±0.037
	-	61.60	
Sdh2	+	23.96	1.38±0.060
	-	17.252	

actcccgggATGGCGCAGCCTATTTTGAACGTTATTGATCTCCATGTTGAAATCGCCGGCAAGGAAGTGCTCAAGGGAGTCAACCTGTGCATTTACC
CTGGGGAAACACACATTCTCTTCGGCCCCAACGGCTCCGGAAAGAGCACGTTGATCAAGACGATCATCGGCCTTAGCGAGTGCAAGGTGACACA
GGGATCCATTTTCTTCCTCGGCGAGGACGTCACGAATAAGACCATTTCGGAGCGCTCCATCATGGGCATGGGAATGCTCTTCCAGAGTCCTCCCGA
GATTGAGGGACTGCCGCTGAAGAGACTCGTCACGACGGCGTTCGAGCAGTGCGACGAGAAATACATGAAGGAAATGAGTGCAACCACCACAAT
GACCGATTACCTGGATCGCGACCTGAACGTCGGCTTTTCCGGTGGTGAGCGCAAGCGCTGCGAGGCCTTCCAGCTGCTGCTCCAGAAGCCCGTG
CTCTCCATGCTGGACGAGCCGGAGAGCGGCGTTGATCTGGAATCGGTGCGCGTGCTGGGCAAGGCGCTGTCTGCCCTGCAGGACCGCGACGTC
AACGGCATCCGCTCCGCCACCATCATCATCACGCACACGGGCAGCATCCTGCAGTACATGCATGGAACGCAGGCGCACGTGCTGATCGACGGGCG
CATGGTCTGCACGGGCGACGAGGAGGTGTTCTTCGACATCATTCAGAAGAACGGCTTCAACTATTTCCGCAACGTCTCCTGCAACGGCCGGTGCG
ACACCTGCCCCGAGAAGGAGCGTCACACCATCATCCACCAGGAGCTGGAGAGCAAGCGCTCCGCCAAGCTCGACGCCTTCCTGAACAGTTCCTC
TCAGCCTGTCAGCCAACCCAATGGGTGTGTGAACAATCAGGCAAACACCCACATGGAGGAGGAGCCGAAGACGGGATCGCTGCTGGCAGCGGT
GGAGGGCATCGCGGATGACTCCTTCCTGACGGAGACGACGACGACGGCCGTGCAGGCACCGCAGCAGGGCGGCGTGGTGAAGGTCGACGTGA
CGGACACGGACGTGTACGGCGGCGAGTACCGGCAGCGCGACCAGGTGGTGGAGGAGTACGAGTCGTTCGAGGACGGCATCGAGGTGCTGTGC
CTCGCCAAGGCGCTGGAGAAGTACCCGTGGATCCGCGAGAAGTACATGTGGCGCGCCATGTCCCCCGACAAGGACGAGATCACGCGCGCCGTG
GCGAAGAACGACAAGACGAGTCCGACGGGCTACGTGATCATCGCCCACCCCGGCGCGAAGTCGGTGAACCCGATCAACAGCCAGCTGATCATG
GAGAACAACAAGATCCAGTACGTGCACAACATCCTCATCTCCATGCCCGGCTCCTGTCTGACCGTCGCCTCGCTCTGCACCTACCACTGCGGCCAG
AAGGACCACCACGACTACATCGTCGGCGGGCAGCACTACGGCGTGTCCGAGTTCTTCGTGGAGAAGGACTCGGAGCTCTGCTTCTCGATGATTC
ACACGTGGTGCAACTCCTACATCGTGTGGCCGCGCTCCGCCGCCGTCGTGGAGGAGAACGGCGTGTTCTACTCCAACTACGTGTGTTTGGAGCCC
GTGGTCAAGGTCCAGATGTGCCCCGTGGCCGACCTGCGCGGGCGCAACGCCGTGGCGAAGTTCAGCGCGGTGCTGCTGGCGAAGGAGGGCAC
GACGCTGGACGTGGGGTCGCGCGCGTTGCTGAATGCCGAGGGTGCGCGCAGCGAGAGCATCACGCGCACCATCTCGAAGGGTGGCGTGATCTT
CGCGCGCGCGGACATCCAGGGCAACGCGCTGAACACGAAGGGACACATCGAGTGCCAGGGTCTGGTGGTGGACGAGGGTAAGGGCGTGATCC
ACTCGATTCCGCAGATCTCGGGCAGCTTCGGCACGGAGCTGAGCCACGAGGCGGCGATCGGCCGGATCGCGAAGGACAAGATCGAGTACCTGA
TGACGCGCCGCATGACGGAGGAGGAGGCAGTGTCGGTGATCATCCGCGGTTTCCTGAACGTGAAGGTGCAGGGCATTCCGAAGTCGATCCAGC
AGCAGATGGACGAGATCATCGACCAGGCGAGCAAGGAGGGGTTC**TACCCATACGATGTTCCAGATTACGCT**TGAgaattcgacacttct

Appendix 15. Demonstrating the sequence of the SufCB-HA tagged ORF in pBEVY-u. Start and stop codons are in bold, red. Restriction enzyme sites for *Xma I* and *EcoR I* are underlined, the ORF is capitalised. HA tag is bold, underlined.

actcccgggATGGCGCAGCCTATTTTGAACGTTATTGATCTCCATGTTGAAATCGCCGGCAAGGAAGTGCTCAAGGGAGTCAACCTGTGCATTTACC
CTGGGGAAACACACATTCTCTTCGGCCCCAACGGCTCCGGAAAGAGCACGTTGATCAAGACGATCATCGGCCTTAGCGAGTGCAAGGTGACACA
GGGATCCATTTTCTTCCTCGGCGAGGACGTCACGAATAAGACCATTTCGGAGCGCTCCATCATGGGCATGGGAATGCTCTTCCAGAGTCCTCCCGA
GATTGAGGGACTGCCGCTGAAGAGACTCGTCACGACGGCGTTCGAGCAGTGCGACGAGAAATACATGAAGGAAATGAGTGCAACCACCACAAT
GACCGATTACCTGGATCGCGACCTGAACGTCGGCTTTTCCGGTGGTGAGCGCAAGCGCTGCGAGGCCTTCCAGCTGCTGCTCCAGAAGCCCGTG
CTCTCCATGCTGGACGAGCCGGAGAGCGGCGTTGATCTGGAATCGGTGCGCGTGCTGGGCAAGGCGCTGTCTGCCCTGCAGGACCGCGACGTC
AACGGCATCCGCTCCGCCACCATCATCATCACGCACACGGGCAGCATCCTGCAGTACATGCATGGAACGCAGGCGCACGTGCTGATCGACGGGCG
CATGGTCTGCACGGGCGACGAGGAGGTGTTCTTCGACATCATTCAGAAGAACGGCTTCAACTATTTCCGCAACGTCTCCTGCAACGGCCGGTGCG
ACACCTGCCCCGAGAAGGAGCGTCACACCATCATCCACCAGGAGCTGGAGAGCAAGCGCTCCGCCAAGCTCGACGCCTTCCTGAACAGTTCCTC
TCAGCCTGTCAGCCAACCCAATGGGTGTGTGAACAATCAGGCAAACACCCACATGGAGGAGGAGCCGAAGACGGGATCGCTGCTGGCAGCGGT
GGAGGGCATCGCGGATGACTCCTTCCTGACGGAGACGACGACGACGGCCGTGCAGGCACCGCAGCAGGGCGGCGTGGTGAAGGTCGACGTGA
CGGACACGGACGTGTACGGCGGCGAGTACCGGCAGCGCGACCAGGTGGTGGAGGAGTACGAGTCGTTCGAGGACGGCATCGAGGTGCTGTGC
CTCGCCAAGGCGCTGGAGAAGTACCCGTGGATCCGCGAGAAGTACATGTGGCGCGCCATGTCCCCCGACAAGGACGAGATCACGCGCGCCGTG
GCGAAGAACGACAAGACGAGTCCGACGGGCTACGTGATCATCGCCCACCCCGGCGCGAAGTCGGTGAACCCGATCAACAGCCAGCTGATCATG
GAGAACAACAAGATCCAGTACGTGCACAACATCCTCATCTCCATGCCCGGCTCCTGTCTGACCGTCGCCTCGCTCTGCACCTACCACTGCGGCCAG
AAGGACCACCACGACTACATCGTCGGCGGGCAGCACTACGGCGTGTCCGAGTTCTTCGTGGAGAAGGACTCGGAGCTCTGCTTCTCGATGATTC
ACACGTGGTGCAACTCCTACATCGTGTGGCCGCGCTCCGCCGCCGTCGTGGAGGAGAACGGCGTGTTCTACTCCAACTACGTGTGTTTGGAGCCC
GTGGTCAAGGTCCAGATGTGCCCCGTGGCCGACCTGCGCGGGCGCAACGCCGTGGCGAAGTTCAGCGCGGTGCTGCTGGCGAAGGAGGGCAC
GACGCTGGACGTGGGGTCGCGCGCGTTGCTGAATGCCGAGGGTGCGCGCAGCGAGAGCATCACGCGCACCATCTCGAAGGGTGGCGTGATCTT
CGCGCGCGCGGACATCCAGGGCAACGCGCTGAACACGAAGGGACACATCGAGTGCCAGGGTCTGGTGGTGGACGAGGGTAAGGGCGTGATCC
ACTCGATTCCGCAGATCTCGGGCAGCTTCGGCACGGAGCTGAGCCACGAGGCGGCGATCGGCCGGATCGCGAAGGACAAGATCGAGTACCTGA
TGACGCGCCGCATGACGGAGGAGGAGGCAGTGTCGGTGATCATCCGCGGTTTCCTGAACGTGAAGGTGCAGGGCATTCCGAAGTCGATCCAGC
AGCAGATGGACGAGATCATCGACCAGGCGAGCAAGGAGGGGTTC**CATCATCATCATCATCATTGA**gaattcgacacttct

Appendix 16. Demonstrating the sequence of the SufCB-6xhis tagged ORF in pBEVY-u. T Start and stop codons are in bold, red. Restriction enzyme sites for *Xma I* and *EcoR I* are underlined, the ORF is capitalised. His tag is bold, underlined.

A pBEVY construct containing HA-tagged SufCB was first produced by appended codons for an HA tag onto the C-terminus of SufCB by Taq PCR. After ligation and amplification in *E. coli*, the newly made construct was digested with the original Xma1 and EcoR1 restriction enzymes in the same manner as Chapter 3 and Chapter 5. A western blot with Anti-HA antibody then confirmed the expression of HA-tagged SufCB in 10 µL yeast protein extracts analysed on a 10% SDS-PAGE gel.

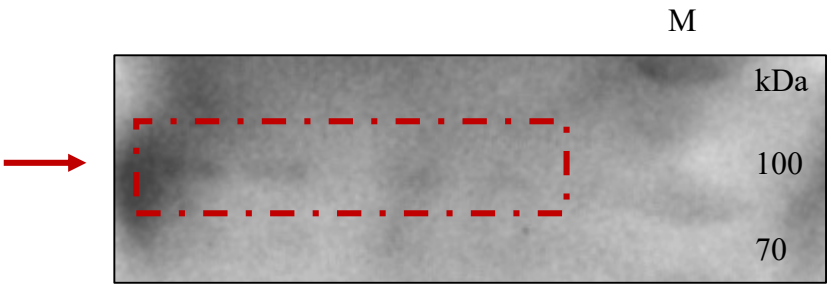

Appendix 17. Visualising the expression of HA-tagged SufCB protein (red dashed box) using anti-HA antibodies. The protein migrated to the expected size. M = marker, 10 µL of ladder used.

cctgcaggtcgacATGAACCGGTAGAACGCCTAGTACATCAACTCCTACGGGGGCAACTCCTTTATTCACTCGAGGTGTAGTCACAGTTTGGAG
TACTGTCGGACCTTCCAGAACGGTCATAGGTCGAACTGGACCTGAAAGTAAACACCAAACTCCAAAAGACCTTATTACTATCACATAGCAAG
AACGGGACACTCGGGGTCCCGTAGACGTAAGAGTGGTCCCTCTATAAGTTCACCCTAGTGTGGGTAGGGTTGGTCCAATGACGCCACTTAC
GCGAGCATCGAGAGCCGGTCCTGCCGAAACTAAGGGTCGTCCTTTCCCGGGAATCGACGGGTCAGAGCCCTCGACGGACGTGGCATGAG
AAACGGTCGGTCTTGCTAGTCCCCTTCCGGACGGACGACCATGGCGAGTCGTCGTAGTTTGTGTAGTTCCTAAAGGGGTCTTCCGTCTACC
TATCAGACACCACGGACGAACAAGTTTTTAGACAAATTGTTCGCTTACAACCGTTTACAAGGGGCACGGTACTGCCGCAGTAATGGAGCCG
CCCTCGGTATCCTCAACTTAAGAGCACCTCAATCCGGAGACAATCAATTCATCGCTCGTCGTCCTGACAAAGAACGTTATAAAGGTCGACCC
CTCTACACCAGTCAACAATGGCTTAGAGGGTTTAAATCGTCGTGTATCCGTAGGTGATATCTAAATCCCCCGACTTCTAGGTTTCAGTCCAAA
AGTTTCTTACCACCACTAAACTATATGCATCTAAACCTTAAGGTCTTTTTGTCGAATAGACTACCCCAACGATTCCGTAAGGTCGAAAGTAAG
TGTCAGAGATAAAAGACTATCTGAAGGAATTTGTAGGGGCCCTACTGTATGACTGCGAGGTGACGGACCTAGAGCAGAGATCAGCCGGTC
TATAGAAAGTCTTTATGGACGACAGGGAAACGTAAATGAGGGTTACCGAGAAAGAGTTTCAGCTAAGACTACCAAGGTCGTTAACGTATAC
GATAATGATTCCCCCCTCTCCGATTTATCAACCGGGCCCACAACCCCACTTGAGCTGGAAGTTTTAAGGACAAAGGTCTATCATGAGGTTGT
CGATGTTCCAGAGGGACACACTACCGAAGATGGTGTCCAAGTCCATTTCCGGGTGACAACGGTTACGTCCAGTACGTCGGTATCGGGTGG
TGCAGTTTGGGTTCGACTCTGTCTATTCCGTACTGAGGCGAAAGAACATCCATCATCCACTGGTGCGGTGAGGGTCCTCTGTCCGATCAAA
ACTACATTCCGTAGTGCAAGTCCGGTCGTAGGTGTCGAAAGAAACGATTGTTAGGACGGGGATTGTAGTGTCTGCCTAATGACCACAAACA
CGTCGATCATTACCGTCGTTACTGGTGTCTTGGTACTCGTTCCCACTTAAGTCACAATAGTATCTATTTCCAGAATACCAGTAATACTACAAGTC
CTCGTTGAACCTTAGGAAATTTAGGAACGAACCGAGGTTCCGTCGAGAGTTTCAGGAAAAAGTACAGCCTGTGTCGTTGAAACAGGACTC
CGGAAAACCCAGGTGATGTCGTTCCGTGATGACAAAAGTTTAGATTAAGGTGTTGGACCCACTTCAGACCCAGAACTCTTCCCAGTAACTT
TAGAGCTTTGTAAGGATGTCGGACTTCTATAAAAAATTATATGAAATTAAAAAGAAGTAGTGCTGGACAAACGTGGTCCATGCACTATGATT
GAAGTAGTTGACCCTTTTTCCGTCGTCAACGAGGCATGAGACCTGTGTACAATCGTTAGCATCGAGCCAGTCGTTACCTGTTGACCCGATGA
GGTCCGGGCTTCTTGAGCTGTTTAAACGGGTGATGGGGTTGGACCGCCTCCACGAACCATTACCACTCGTGCTACAGTCACCTACAATGGT
CTCCCACCCCGAAGGGGTAGTCGGACATCGGTTAGTGGACTCCTTCGTGGTATGACTAACCGACTGGGTCGTACTGTCGAAGACGAAGTTA
TGGTGGCTGTGGGGTTGGTTCTTACGGGTTCGGTAGTTAGTACCATCACACGCTCAGACACGGGTGCTCCGACAGACCCATTATTATAGGT
AGGACTAGTTTATGGTGAGAACGGTTTATAAGGTTTAAGTGGACCACCTACTAAGGACTCGGTCCCCCTTATTAGGCGTACAACACTTTTCG
GACCCTTGGGGTGAAATTTTTAAGTTTAGCGAGAGATAAAGAAAGTTTAAGGTCCAGAACTAAGAAGACATTTGACAGACGGGAAGACA
ACTTTAGTTGGACCTACCTTACTAGATAATGTTCTAGTCGTCCCGTCTGTCCCAAATAAAAGAGACCTAGAGGAGGATTGAAAAAGTGTCGT
AGTGCGTAACGTCGTTTCAGTTGGTGTCGCCCGTGTGGGCATTTCAGGACGTCCTACTGTGCTCGTCCGAATTTACCGTGAAGATACAAGA
ACACGACGCACTGTAAGGTTACATCTTATAAAAGTTATAGGACAAAGAAGTGGTTTTTGAGTAGTGTTAAGGCTTACCGACGAAGGTCTTCT
TGAGACTAGCTTTTACCATTCGCGGGTATAGAACTTAGGAGGTTAAATAAGTTTAACTTCTTAAAGAAAGGACCAACATGTCCTAGGTTACC
GAGTCGTTCCACACGCTTACCCAACGAGTAtctagaggatc

Appendix 18. Sequence of aconitase construct in pBEVY-I. Start and stop codons are in bold, red. Restriction enzyme sites for *Sal I* and *Xba I* are underlined, the ORF is capitalised.

agctgcctaggATGATGGACAGGAAACAGACAGCTGAGACCCTGCTGACCCTGTCTCCTGCTGAAGTTGCCAACCTCAAGG
AAGGGATCAATTTTTTTCGAAATAAGACTACTGGGAAAGAGTACATTTTATACAAGGAGAAGGACCATCTAAAGGCATGC
AAGAACCTCTGCAAGCACCAGGGAGGCCTGTTCATGAAAGACATCGAGGATTTAGATGGAAGGTCCGTTAAATGCACAA
AGCACAACTGGAAGTTAGACGTGAGCACCATGAAATATATCAACCCTCCAGGGAGCTTCTGTCAAGACGAGCTCGTTATT
GAAATGGATGAAAACAATGGGCTTTCCCTGGTAGAACTGAACCCTCCTAACCCCTGGGACTCTGATCCCAGGTCTCCTGA
AGAATTAGCTTTTGGGGAAGTACAGATAACATATCTCACTCATGCCTGCATGGACCTCAAGTTGGGAGACAAGCGAATGG
TATTTGACCCTTGGTTAATTGGCCCTGCTTTTGCCCGAGGATGGTGGTTGCTACATGAGCCTCCATCTGACTGGTTGGAGA
GGCTGTGCAAAGCAGACCTCATTTATATCAGCCACATGCACTCAGACCACCTGAGCTACCCTACCCTGAAGCAGCTTTCCC
AGAGACGACCAGACATTCCCATTTATGTTGGCGACACAGAAAGGCCTGTGTTTTGGAACCTGGATCAGAGTGGCGTCGG
GTTAACTAACATCAACGTGGTTCCATTTGGAATATGGCAACAGGTAGACAAAAGTCTGCGGTTCATGATCTTGATGGACGG
CGTTCATCCTGAGATGGACACATGCATTATCGTGGAGTACAAAGGTCATAAAATACTCAACACAGTGGACTGCACCAGACC
CAATGGGGGAAGGCTTCCTGAGAAAGTTGCTCTAATGATGAGTGATTTCGCAGGAGGTGCATCAGGCTTTCCAATGACTT
TCAGTGGTGGAAAATTTACTGAGGAATGGAAAGCCCAGTTCATTAAGGCTGAAAGAAGAAAGCTTCTGAATTACAAAGC
TCAGCTGGTGAAGGACCTGCAGCCCCGAATCTACTGTCCGTTTGCTGGGTACTTTGTGGAGTCTCACCCATCTGACAAGT
ACATTAAGGAAACAAACACCAAAAATGACCCAAATCAGCTCAACAATCTTATCAGGAAAAACTCTGACGTGGTGACATGG
ACCCCACGACCTGGCGCTGTCCTCGACCTTGGCAGGATGCTGAAGGACCCAACAGACAGCAAGGGCATTGTGGAGCCT
CCAGAGGGGACAAAGATTTACAAGGATTCCTGGGACTTTGGCCCGTACCTGGAGATCTTGAATTCTGCTGTCAGAGATG
AAATCTTCTGTCATTCATCCTGGATTAAAGAGTACTTCACGTGGGCTGGATTTAAGAATTACAACCTGGTGGTCAGGATGA
TTGAAACAGATGAAGATTTCAGCCCTTTTCCTGGAGGGTACGACTATCTGGTGGACTTTCTAGATTTATCCTTTCCGAAAG
AAAGACCCAGCCGGGAGCATCCTTATGAAGAAATCCATAGCCGGGTGGATGTCATCAGGTACGTGGTGAAGAACGGCCT
GCTGTGGGATGATCTGTATATTGGATTCCAGACCCGATTGCTGCGGGACCCTGATATATACCATCATCTGTTTTGGAATCATT
TTCAGATAAAACTCCCTCTAACACCACCCAACTGGAAGTCGTTCCTAATGCACTGTGATTACCCATACGATGTTCCAGATTA
CGCTTAGcagctggacg

Appendix 19. The sequence of the CMAH construct in pBEVY-I. Start and stop codons are in bold, red. Restriction enzyme sites for *BamH I* and *Sal I* are underlined, the ORF is capitalised. HA tag is bold underlined.

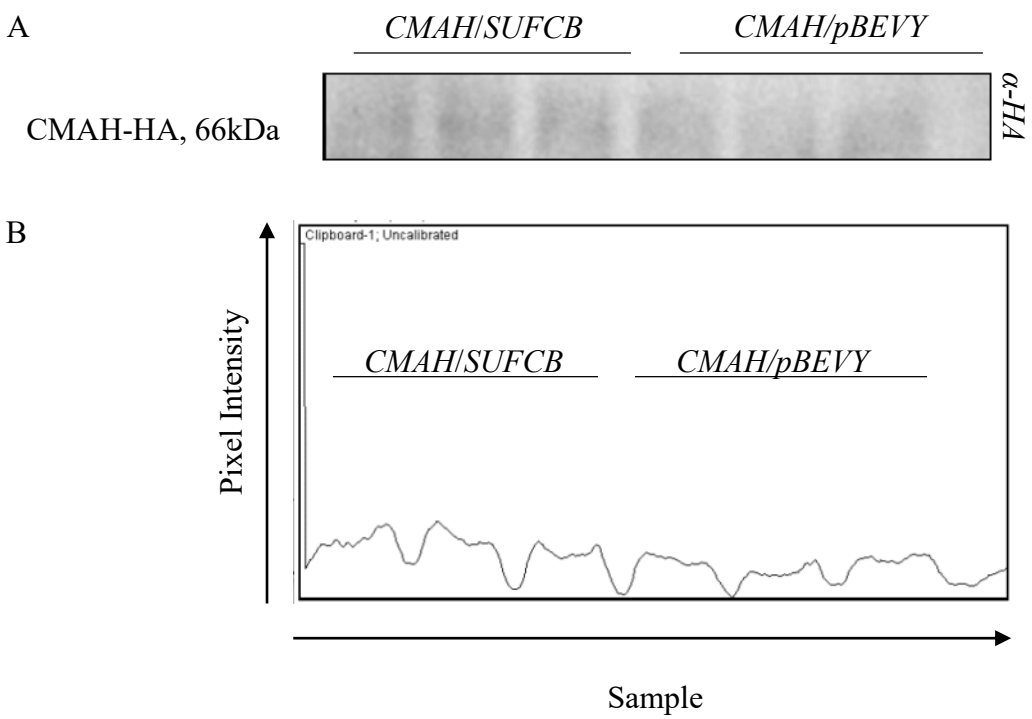

Appendix 20. Western blot and Densitometry of CMAH Band expressed in both SUFCB and negative controls. A) Anti-HA western blot (1:1000) as visualised by ECL. B) Coomassie loading control of total protein extracts. B) Plot of pixel intensity using g Fiji image analysis.

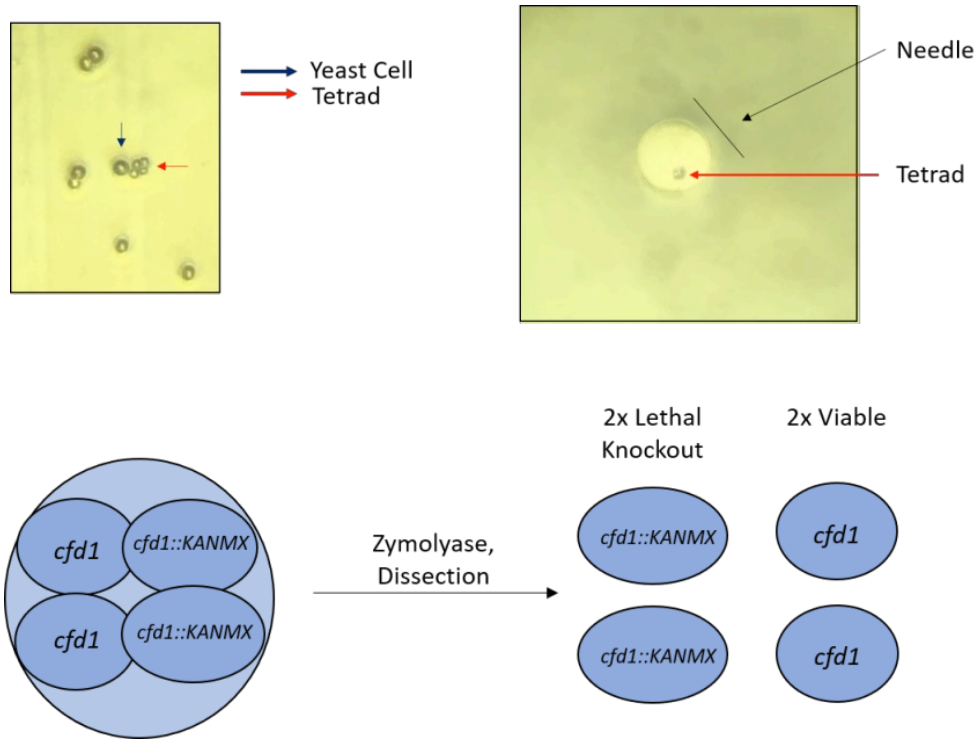

Appendix 21. Microscope image of yeast tetrads and cartoon illustrating geneticin selection of positive clones (*cfd1* knockouts).

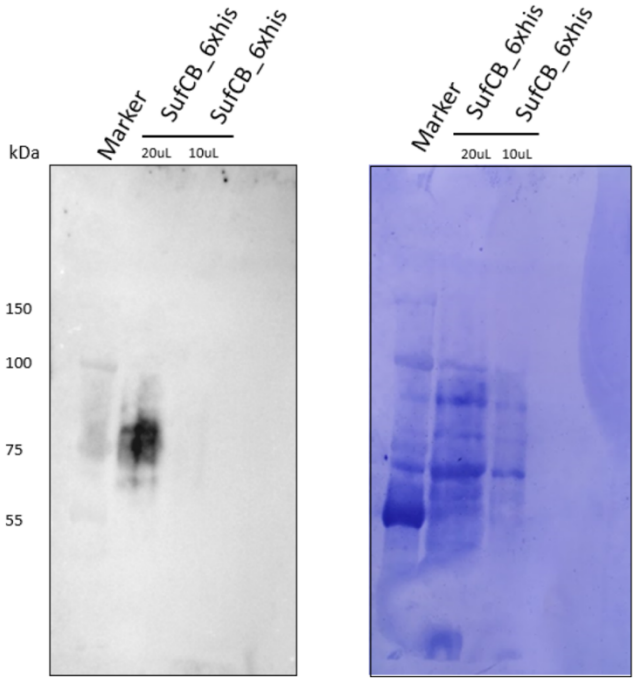

Appendix 22. Purification of SufCB using EDTA, western blot (anti-SufCB, left) and commassie stained PVDF membrane (post-transfer, right).

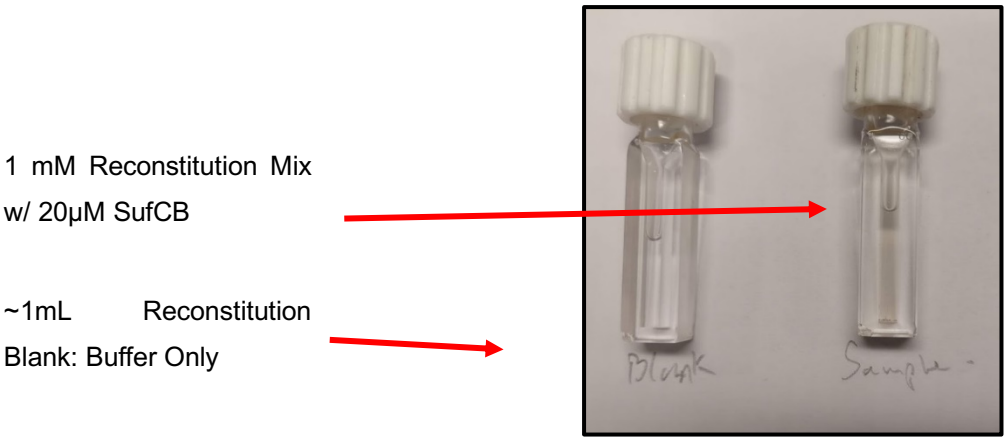

Appendix 23. Image showing golden yellow colour of the reconstituted SufCB protein, post PD10. Mix w/ 20 μM SufCB = Mix with 20 μM SufCB.

Percent Identity Matrix - created by Clustal2.1

1: NUBP1	100.00	53.07	49.25	43.93
2: Nbp35	53.07	100.00	47.35	44.07
3: NUBP2	49.25	47.35	100.00	50.18
4: Cfd1	43.93	44.07	50.18	100.00

Appendix 25. Percentage identity matrix (Clustal O) between Nbp35 and Cfd1 homologues. High sequence similarity exists between all four proteins (>43%).

```
NUBP1      KVKLPIIGVVENMSGFICPKCKKESQIFPPTTGGAELMCQDLEVPLLGRVPLDPLIGKNC 277
Nbp35      KAGINILGLVENMSGFVCPNCKGESQIFKATTGGGEALCKELGIKFLGSVPLDPRIGKSC 295
NUBP2      KTGLRVMGIVENMSGFTCPHCTECTSVFS--RGGGEELAQLAGVPFLGSVPLDPALMRTL 236
Cfd1       KVDLKILGIIENMSGFVCPHCAECTNIFS--SGGGKRLSEQFSVPYLGNVPIDPKFVEMI 241
           *. : ::*::******** **:*   :.:*    **.: :.:   :  ** **:** : .
```

Appendix 24. Pairwise sequence alignment of Nbp35 and Cfd1 homologues from yeast to humans (NUBP1 and NUBP2). The black box demonstrates the conserved FxCPxC cluster binding site.